

https://dspace.org/

Plagioclase compositions in the upper zone of the bushveld complex

Lum, Jullieta Enone

2011-07-07
http://hdl.handle.net/10539/10270

Downloaded from a DSpace repository. https://dspace.org/

Plagioclase Compositions in the Upper Zone of the Bushveld Complex

By
Jullieta Enone Lum

Submitted in fulfillment of the requirements for the degree of Master of Science, in the Department of Geosciences, University of the Witwatersrand, Johannesburg, South Africa

March 2011

Declaration

I declare that this dissertation is my own, unaided work. It is being submitted for the Degree of Master in Science in the University of the Witwatersrand, Johannesburg. It has not been submitted before for any degree or examination in any other University.

Signed:

Jullieta Enone Lum
School of Geosciences
University of the Witwatersrand
Johannesburg

March 2011

Abstract

The approximately 2 km thick Upper Zone of the Rustenburg Layered Suite represents a series of differentiated rocks with the appearance of magnetite, olivine and apatite in that order, as cumulus phases in the stratigraphy. Plagioclase is the dominant cumulus mineral throughout the sequence; hence its composition provides a continuous record of differentiation. 126 plagioclase mineral separates have been obtained and analyzed from bore core drilled through the Upper Zone. Anorthite content decreases from An_{60} close to the base of the Upper Zone to An_{30} at the top. Six reversals were identified in a previous study occurring over a vertical interval of 16 to 69 m and in which the An increases upward by 3 to 6%. A detailed examination of one prominent reversal in the present study shows that the reversal is gradual. Sr in plagioclase concentrations increase erratically upward from about 400 ppm to 800 ppm. Ba contents in plagioclase vary irregularly between 200 and 500 ppm throughout the lower 1.5 km of stratigraphy and only increase to about 700 ppm towards the top of the sequence. The reversals which are observed in the An content are not observed in the Ba and Sr contents of plagioclase. Data for Sr and Ba in plagioclase exist for the Skaergaard intrusion and have not been quantitatively modeled before. Hence, Rayleigh fractionation models are developed to quantitatively model both intrusions. For the Skaergaard intrusion, Sr in plagioclase increases slowly from 400 at the base to about 600 ppm at 80% crystallized. It then increases rapidly to 1300 ppm at the end of crystallization. Ba varies erratically between 79 ppm and 200 ppm until 90% of crystallization from where its concentration increases to over 600 ppm at the end of crystallization.

The most simplistic model for the evolution of such trace elements in a layered intrusion is to assume a homogenous magma chamber crystallizing a mineral assemblage in constant proportions, with constant partition coefficients and with a constant proportion of trapped liquid so that bulk D is constant throughout crystallization. However, these assumptions are totally inappropriate for natural situations because mineral assemblages, their proportions, trapped liquid fractions and partition coefficients change as magmas fractionate. It therefore becomes necessary to subdivide the crystallization into a very

large number of small Rayleigh fractionation stages, and change any or all of these four variables at each stage.

For the Skaergaard intrusion, the following variables are used. Values for F are estimated from the percentage of crystallization of the entire intrusion which is then subdivided into 100 small stages of fractionation. Observed plagioclase mode and trapped liquid fractions are set to change from 55 to 33% and 45 to 4% upwards respectively so that cumulus plagioclase mode can be calculated. Utilizing the conventional Rayleigh modeling by calculating a starting liquid content from $D=C_M/C_L$ and applying the Rayleigh Law to the section does not fit typical parental magma compositions and observed data for plagioclase. Consequently, a value for the Skaergaard parental magma within the range of typical Ba contents of starting liquid is then used to model the section and allowance is made for the trapped liquid shift (TLS) effect. The Ba content of calculated re-equilibrated plagioclase differs by a factor of 3 from the calculated original cumulus plagioclase content. Incorporation of the TLS effect produces the observed range of values for Ba in plagioclase. In all the models, a constant D_{Ba} of 0.4 is used throughout fractionation because the model is relatively insensitive to changing D_{Ba} in plagioclase. Sr which is compatible into plagioclase has a smaller TLS effect, thus the model is more sensitive to variations in D_{Sr} in plagioclase. The best fit with the observed data is obtained if D_{Sr} in plagioclase is varied smoothly from 1.7 at the start of fractionation to 1.9 at the end.

In the case of the Upper Zone of the Bushveld Complex, values for F, D_{Ba} in plagioclase, plagioclase mode and TL fraction are used to set up a calculation similar to the Skaergaard intrusion. A constant D_{Ba} in plagioclase of 0.4, D_{Sr} in plagioclase from 1.5 to 2.1, observed plagioclase mode from 65 to 45% and a constant proportion of trapped liquid of 10% are used. Different starting liquid compositions are then tried until values are obtained for which Ba and Sr contents of calculated re-equilibrated plagioclase are in agreement with analytical data. Based on modeling of the Upper Zone of the Bushveld Complex, Ba contents of calculated re-equilibrated plagioclase also differ significantly from respective original cumulus contents due to the TLS effect. Therefore, applying the

model to the Upper Zone of the Bushveld Complex validates the importance of allowing for the TLS effect. The computed liquid contents at the base of the UZ are 273 and 325 ppm for Sr and Ba respectively. In view of the reversals in mineral composition and small scale variations in the Sr and Ba contents of plagioclase, various magmatic processes such as magma addition and internal overturn which have been proposed to occur in the Upper Zone are inferred to be possible. There are a number of uncertainties with the modeling, hence none of these processes can be conclusively ruled out.

Acknowledgements

I am greatly indebted to my supervisor, Prof. R. Grant Cawthorn for initiating this project and for his invaluable support and guidance. I acknowledge funding received from the platinum companies; Anglo Platinum, Impala Platinum and Lonplats.

I would like to thank Prof. Lewis Ashwal for academic discussions on various aspects of this project. For technical support I would like to thank Prof. Allan Wilson and Sharon Turner for laboratory assistance on XRF work and Alex Mathebula who made my thin sections. Most sincere thanks to many friends for the assistance they have given me especially my office mate Anika Solanki, Stefanie Weise and Silindilile Wela. Thanks also to Marina Yudovskavia for being there to discuss ideas and for motivation. I also acknowledge the encouragement and unfailing support from my family here and in Cameroon.

Table of Contents

Declaration ii

Abstract iii

Acknowledgements vi

Table of Contents vii

List of Figures xi

List of Tables xiii

Chapter 1- Introduction 1

1.1. The Bushveld Complex 2

1.2. Boundary between the Main and Upper Zones 5

1.3. The Geology of the Upper Zone 6

1.4. Models for the Evolution of the Upper Zone 8

Chapter 2- Research Rationale and Methodology 12

2.1. Fractionation in Layered Intrusions 12

2.2. The Skaergaard Intrusion 14

2.3. Justification for selection of samples from the Upper Zone of the Bushveld Complex 16

2.4. Objectives of the Project 19

2.5. Petrographic and Analytical Techniques 20

Chapter 3- Petrography 21

3.1. Introduction 21

3.2. Major Features of the Bierkraal Boreholes 21

3. 3. Inclusions and Composite Grains 25

3.3.1. Apatite 25

3.3.2. Plagioclase 25

3.3.4. Magnetite 25

Chapter 4- Geochemistry 27

4.1. Introduction 27

4.2. Removal of effects of included minerals 28

4.2.1. Apatite 28

4.2.2. Alkali feldspar 35

4.2.3. Quartz 38

4.2.4. Mafic minerals 38

4.3. Major Element Trends 41

4.3.1. Anorthite Content of Plagioclase 43

4.3.2. Summary 50

4.4. Trace Element Geochemistry 51

4.4.1. The Skaergaard Intrusion 51

4.4.2. The Upper Zone, Bushveld Complex 54

4.4.2a. Strontium in plagioclase 54

4.4.2b. Barium in Plagioclase 56

Chapter 5- Development of a Fractionation Model 58

5.1. Introduction 58

5.1.1. Rayleigh Fractional Crystallization 58

5.1.2. The trapped liquid shift (TLS) effect 61

5.2. Modeling barium in plagioclase in the Skaergaard Intrusion 64

5.2.1. Rayleigh Fractionation of Ba contents in plagioclase 65

5.2.1.a Modeling with the starting liquid content (C_o) from the equation $D=C_M/C_L$ 66

5.2.1. b Modeling with the typical Ba content of the Skaergaard parental magma. . 68

5.2.2. Incorporation of the trapped liquid shift (TLS) effect 70

5.3. Lateral Variation in Ba in Plagioclase 76

5.4. Assessment of the effect of variables on fractionation models for the Skaergaard Intrusion 78

5.5. Modeling Strontium in Plagioclase in the Skaergaard Intrusion 83

5.6. Comparison with previously published D values 88

5.7. Summary 91

Chapter 6- Modeling the Crystallization of the Upper Zone of the Bushveld Complex 93

6.1. Introduction 93
6.2. Details of Modeling Procedure 94
6.2.1. Plagioclase proportions 94
6.2.2 Trapped Liquid Fractions (TL%) 95
6.2.3. Fraction of Magma remaining (F) 95
6.2.4. Starting Liquid Compositions (C_O) 97
6.2.5. Build up of the fractionation Model 97
6.3. Barium in plagioclase 98
6.4. Strontium in plagioclase 102
6.5. Relationship to previously published D values and Liquid Contents 106
6.6. Incorporation of lost Magma in the Upper Zone 110
6.7. Possible magmatic processes in the Upper Zone 111
6.7.1. Re-examination of the single magma model 111
6.7.2. The Possibility of fractionation Cycles 112
6.7.3. Magma addition 113
6.7.4. Crystal Settling and Sorting 118
6.7.5. Magma Overturn 119
6.8. Summary 125

Chapter 7- Conclusions 127

7.1. Differentiation Patterns 127
7.2. Rayleigh Fractionation and the trapped liquid shift effect 127
7.3. Partition Coefficients 130
7.4. Calculated Liquid Contents 131
7.6. Magma Chamber Processes 132

References 133

Appendices A – D 141

Appendix A- Analytical Techniques and Standards Used..... 142
Appendix B. Dissolution Experiments 151
Appendix C. Major and Trace Element Compositions..... 167
Appendix D. Variables used in modeling the Upper Zone of the Bushveld Complex and resulting calculated compositions 176

List of Figures

Fig. 1.1 Simplified Geological Map of the Bushveld Complex 3

Fig. 1.2 Stratigraphy of the Eastern and Western limbs of the Bushveld Complex 4

Fig. 1.3 Initial $^{87}Sr/^{86}Sr$ ratio plotted against stratigraphic height in the Upper Main Zone and Main Zone. 9

Fig. 2.1. Mineral compositions in the Bushveld Complex, above the Pyroxenite Marker and the Skaergaard Layered Series 15

Fig. 2.2. Generalized stratigraphic section of the Bushveld Complex and combined Bierkraal drill cores. 18

Fig. 3.1. Microphotographs showing the major cumulus phases in the Upper Zone. 23

Fig. 3.2. Intercumulus minerals 24

Fig. 3.3. Inclusions and composite grains 26

Fig. 4.1 Plot of An content vs. stratigraphic height. An contents are uncorrected for the presence of apatite and show samples that contain apatite. 31

Fig. 4.2 Plots of Sr content vs. height and fraction of magma remaining 33

Fig. 4.3 Sr vs. P_2O_5 contents for samples from 1400 m upward..... 34

Fig. 4.4 Ba vs. P_2O_5 Correlation. 36

Fig. 4.5 Barium contents of plagioclase plotted against height 39

Fig. 4.6 Barium vs. K_2O from analyses. 40

Fig. 4.7 SiO_2, K_2O and P_2O_5 contents from analyses of separates plotted against height. 42

Fig. 4.8 Variation of plagioclase An content with Height in the Bierkraal drill cores. 46

Fig. 4.9 Plot of An content in plagioclase versus height for the biggest reversal..... 48

Fig. 4.10 Plot of An content in plagioclase vs. height for the section in which the second biggest reversal in the data of Tegner et al. occurs. 49

Fig. 4.11 Ba and Sr contents of plagioclase for the Skaergaard Layered Series. 53

Fig. 4.12 Plots of Sr contents of plagioclase for the Upper Zone of the Bushveld Complex. 55

Fig. 4.13 Barium contents of plagioclase plotted against height for the Bushveld Upper Zone. 57

Fig. 5.1 Trapped Liquid Shift effect for barium in plagioclase showing its enormous effect. 72

Fig. 5.2 Trends for barium in the Skaergaard intrusion showing the difference in calculated compositions (liquid, cumulus and re-equilibrated plagioclase)from the three different models. 75

Fig. 5.3. Variation in re-equilibrated plagioclase Ba resulting from varying Trapped Liquid fractions at the same stratigraphic sample..... 77

Fig. 5.4. Relationship between D for Sr and Ba into plagioclase and anorthite content .. 78

Fig. 5.5 Calculated trends for barium in the Skaergaard intrusion from varying different parameters with crystallization. 80

Fig. 5.6 Calculated trends based on Rayleigh fractionation with the Sr content of the Skaergaard parental liquid 87

Fig. 5.7 Sr contents of liquid, cumulus and re-equilibrated plagioclase calculated from D values of Blundy and Wood..... 90

Fig. 6.1 Plots of Ba in liquid, original cumulus and re-equilibrated plagioclase vs. F (fraction of magma remaining) and height 101

Fig. 6.2 Plots of Sr in liquid, original cumulus and re-equilibrated plagioclase vs. F(fraction of magma remaining) and height 104

Fig. 6.3 Plots of Sr in liquid, original cumulus and re-equilibrated plagioclase vs. F(fraction of magma remaining) and height 105

Fig. 6.4 Trends for Sr and Ba contents of liquid, cumulus and re-equilibrated plagioclase for the Bushveld intrusion..... 109

Fig. 6.5 Sr contents of plagioclase across the Lower- Upper Critical Zone boundary... 113

Fig. 6.6 Possible trends in the Ba contents of plagioclase plotted against height and fraction of magma remaining..... 116

Fig. 6.7 Sr and Ba contents of the section over which the largest reversal in plagioclase An occurs in the Upper Zone of the Bushveld Complex 121

Fig. 6.8 Comparison of cycles based on increase in Fe_2O_3 in whole rocks with reversals in plagioclase An content..... 124

List of Tables

Table 4.1. Leached and unleached pairs of samples showing the effect of apatite on the anorthite content of plagioclase 30

Table 4.2.Comparison of anorthite content between samples common to this study and Tegner et al. 44

Table 5.1. Calculated trends based on Rayleigh fractionation, incorporating varying TL and plagioclase mode 67

Table 5.2.Calculated trends based on Rayleigh Fractionation with the typical Ba content of starting liquid 69

Table 5.3.Calculated trends based on Rayleigh fractionation with the typical Ba content of starting liquid and allowing for the trapped liquid shift effect. 73

Table 5.4. Sensitivity of bulk D and Ba content of re-equilibrated plagioclase 82

Table 5.5.Calculated trends using the Sr content of parental liquid from Nielsen (2004) and incorporating the TLS effect. 86

Table 5.6.Variables and resulting Sr contents of plagioclase from modeling with the D values of Blundy and Wood..... 89

Table 6.1.Rock compositions for the nine subzones in the Upper Zone 96

Table 6.2.Data for Sr in plagioclase in the lower part of the Upper Zone of the Bushveld Complex. 122

Chapter 1- Introduction

The study of layered intrusions provides vast information on the processes involved in their formation. These intrusions generally encompass cumulate rocks, made up of cumulus minerals which have equilibrated with intercumulus liquid. A common characteristic of layered intrusions is intense fractionation during crystallization, shown by their rock and mineral assemblages and changes in mineral compositions such as the An content of plagioclase and Mg# of mafic minerals. These parameters serve as useful indicators of differentiation in layered intrusions because they generally decrease significantly and systematically with crystallization.

Trace element contents of minerals can also be used to infer magmatic processes in various systems, including large layered intrusions like the Bushveld Complex and the Skaergaard intrusion. Various experimental investigations have been carried out with these elements, leading to many theories on the behavior of trace elements during magma evolution (e.g. Blundy and Wood, 1991; Blundy, 1997). For layered intrusions which are commonly governed by fractional crystallization, trace element concentrations of minerals and whole rocks ought to change according to variations in partition coefficients, modal proportions and trapped liquid fractions. Based on these parameters, a variety of models have been presented to illustrate the controls on trace element behavior during fractionation. However, certain assumptions are usually incorporated in such modeling, leading to misleading conclusions. It therefore becomes necessary to elucidate the application of models in order to better understand the evolution of these intrusions.

1.1. The Bushveld Complex

According to SACS (1980), the Bushveld Complex is composed of the Rashoop Granophyre suite, the Rooiberg Group volcanic province, the ultramafic to mafic layered rocks of the Rustenburg Layered Suite (RLS), the Lebowa Granite Suite and the mafic sills that intruded the Transvaal Supergroup (Fig. 1.1). For the purpose of this study however, the term "Bushveld Complex" will be used for the ultramafic to mafic layered rocks equivalent to RLS as it is the term most widely used for this section of the complex in the published literature.

The Bushveld Complex outcrops in three provinces in northern South Africa (North-west, Limpopo and Mpumalanga) and is the largest known mafic layered intrusion emplaced into a stable cratonic setting (Wager and Brown, 1968; Cawthorn and Walraven, 1998). An age of 2.06 Ma has been reported (Walraven et al.,1990, Walraven,1997) even though different ages have been suggested for particular layers of the complex (e.g. 2054_1·3 Ma by Scoates and Friedman, 2008 for the Merensky Reef). The Bushveld Complex encompasses a total areal extent of about 66000 km^2 and thickness of about 9 km (Willemse, 1969). Replenishment of the Bushveld Complex occurred intermittently for about 65,000 years (Cawthorn and Walraven, 1998). The Complex is comprised of four exposed limbs; the Western, Eastern, Far Western and Northern limbs (Fig.1.1); the Southeastern Bethal lobe is concealed by younger sediments. The eastern and western limbs are best exposed and dip towards each other.

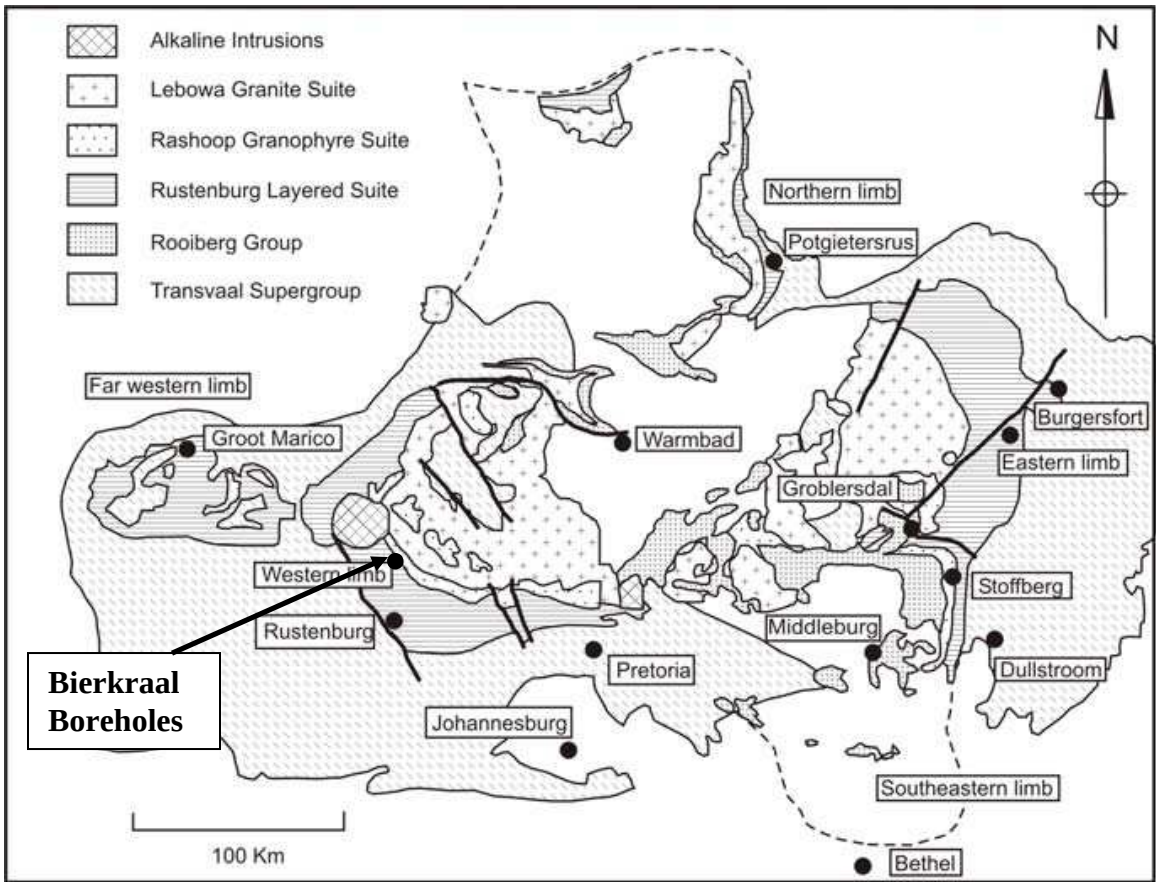


Fig. 1.1 Simplified Geological Map of the Bushveld Complex showing the location of the Bierkraal boreholes (based on Eales and Cawthorn, 1996)

Five major zones define the regional stratigraphy of the Bushveld Complex (Fig. 1. 2); the Marginal Zone, Lower Zone (LZ), Critical Zone (CZ) Main Zone (MZ) and Upper Zone (UZ). These divisions were first proposed by Wager and Brown (1968) based on the appearance and disappearance of cumulus phases in the intrusion, geochemistry and unconformities due to magma recharge; although the exact boundaries of the different zones have been disputed (e.g. Kruger, 1990). The lower part of the stratigraphy has been subject to magma influxes whereas differentiation dominated the upper part. The main magma influxes at the Merensky Reef and below the Pyroxenite Marker represent major unconformities and led to lateral expansion of the magma chamber (Kruger, 2005).

The Marginal zone forms the basal contact of the Bushveld Complex and lacks layering (Eales and Cawthorn, 1996). It is composed of norite and pyroxenite and these rocks

show evidence of crustal assimilation from floor rocks (Cawthorn and Walraven, 1998). The Lower Zone (up to about 1.3 km thick) is composed of harzburgite, dunite, pyroxenite, peridotite and minor norite. It exhibits varying scales of layering from about 1 m to hundreds of meters and is characterized by rocks containing ≥ 95% cumulus orthopyroxene and olivine (Eales and Cawthorn, 1996). The Critical Zone, about 1 km thick, consists of pyroxenite through norite to anorthosite with distinctive chromitite layers and a number of magmatic cycles (Eales and Reynolds, 1986). Overlying the Critical Zone is the Main Zone which is about 4 km thick and is composed of gabbronorite, anorthosite and rare pyroxenite. This succession is followed by a highly differentiated sequence of lithologies which make up the Upper Zone and consist of norite, gabbronorite, ferro-gabbronorite, ferrodiorite, anorthosite, troctolite and titaniferous magnetite.

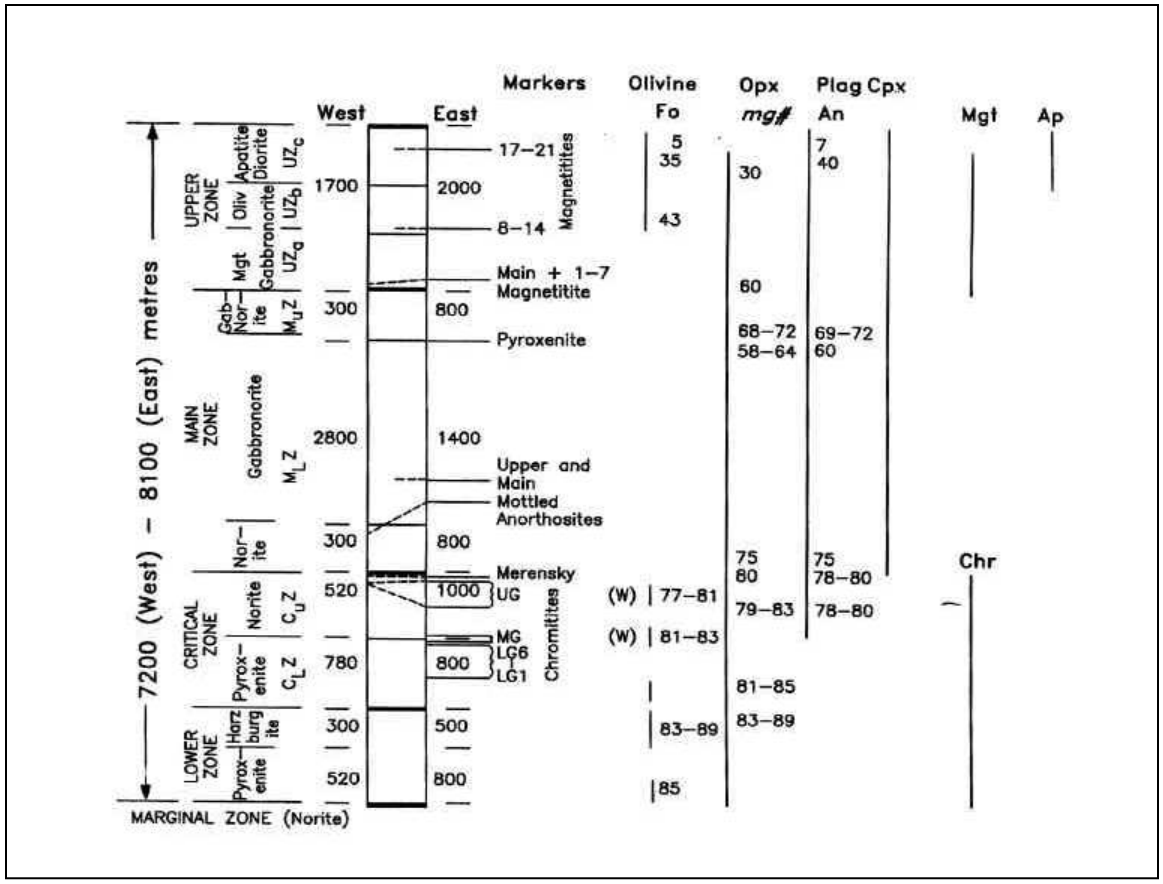


Fig. 1.2 Stratigraphy of the Eastern and Western limbs of the Bushveld Complex showing rock types and appearance of cumulus minerals (Eales and Cawthorn, 1996)

The eastern and western limbs of the Bushveld Complex are quite similar in stratigraphy, exemplified by the occurrence of chromitite and magnetitite layers and the Merensky Reef and Pyroxenite Marker (Px Mk) in both limbs. These similarities and exposure of sections of the Bushveld rocks between the eastern and western limbs have supported lateral continuity of the Bushveld beneath the exposed limbs (Cawthorn et al., 1998; Cawthorn and Webb, 2001)

1.2. Boundary between the Main and Upper Zones

At the level of the PxMk, there are changes in initial $^{87}Sr/^{86}Sr$ ratio (Sharpe, 1985; Kruger et al., 1987; Cawthorn et al., 1991) and prolonged reversals in Mg# and An content of pyroxene and plagioclase respectively (von Gruenewaldt, 1970). Due to the mineralogical, isotopic and chemical differences between the rocks below and above the PxMk and its continuity in both the eastern and western limbs of the Bushveld Complex, this layer was proposed as a boundary between the Upper Zone and the Main Zone (Kruger et al., 1987; Kruger, 1990; Kruger, 2005). However, this principle for delineating the boundary between MZ and UZ has not been extensively applied.

Wager and Brown (1968) suggested the division of layered intrusions based on the appearance and disappearance of cumulus minerals. The Main Magnetitite Layer (MML) has also been used as a boundary between the Main and Upper Zones (Willemse, 19690) and as a subzone boundary in the Upper Zone (von Gruenewaldt, 1973). Molyneux (1974) later subdivided UZ into four subzones based on the distribution and composition of magnetite layers, anorthosite and troctolite. Although the stratigraphic markers such as the PxMk and MML are excellent markers in the field, the cumulus mineralogy is more crucial in delineating boundaries in layered intrusions as it is readily identifiable in the field (Wager and Brown, 1968). The appearance of cumulus magnetite is thus the favored boundary between the Main and Upper Zones and three subzones have been distinguished based on the appearance of cumulus magnetite (UZa), olivine (UZb) and

apatite (UZc) respectively (SACS, 1980). This terminology is therefore used in the present study to mark the base of the Upper Zone (0 m in the stratigraphy)

1.3. The Geology of the Upper Zone

The Upper Zone, approximately 2 km thick, is layered and is the most laterally extensive of the Bushveld Complex (Kruger, 2005). Correlation of lithological units has shown that the thickness and rock successions are not the same in the different limbs (von Gruenewaldt, 1973; Tegner et al., 2006). The UZ is present in four of the five lobes of the Bushveld complex and constitutes most of the rocks in the southern lobe (Kruger, 2005). It is characterized by a highly differentiated progression of norite, gabbronorite, ferro-gabbronorite, ferrodiorite, anorthosite, troctolite, titaniferous magnetite and apatite-rich rocks (Molyneux, 1974; Reynolds, 1985b; Kruger et al., 1987). These lithological units are dominated by plagioclase, titanomagnetite, Fe-rich pyroxenes, Fe-rich olivine, and apatite, which are the main cumulus phases (Wager and Brown; 1968) and rare sulfides (von Gruenewaldt, 1976). Biotite, hornblende, quartz and potassium feldspar occur as intercumulus phases.

The dominant silicate mineral in UZ is plagioclase. According to investigations by Roberts (2005), plagioclase mode decreases from about 60% at the bottom to 45% at the top of the Upper Zone. Plagioclase grains form large tabular crystals and or larger aggregates which are either not zoned or show reverse zoning, constrained to the outermost boundaries (Molyneux, 1974; Harney et al., 1990; Harney et al., 1995). Plagioclase An content decreases fairly regularly upwards with a number of reversals which coincide with other reversals in mineral composition in the sequence (Tegner et al., 2006).

Magnetite occurs both as massive layers, disseminated grains and as magnetitite pipes in UZ and has high Ti content which increases with stratigraphic height (Reynolds, 1985a). The magnetite content of rocks ranges from 5% in silicate rocks up to 100% in

magnetitite layers (Molyneux, 1974). Cumulus magnetite occurs in all the rocks except in some anorthosite layers (Wager and Brown, 1968; von Gruenewaldt, 1976). About 25 separate magnetitite and nelsonite layers occur with varying thicknesses and alternate with anorthosite layers. These magnetitite layers have very sharp footwall contacts and gradational hanging wall contacts with partings and inclusions of silicate rocks.

Cumulus olivine appears in subzone B and changes from Fo_{44} to almost pure fayalite at the top, with reversals that coincide with the reversals in plagioclase An content (Molyneux, 1974; Tegner et al., 2006). Clinopyroxene is the most abundant ferromagnesian mineral present although it is less abundant compared to olivine where both occur. Mg# of clinopyroxene evolves from 74 at the PxMk through 66 at the base of UZa to 5 at the top of UZc and correlates positively with An content of plagioclase (Tegner et al., 2006). Close to the base of UZ, primary orthopyroxene is replaced by inverted pigeonite and is present up to the roof, except in a pyroxenite above MML (Molyneux, 1974). Orthopyroxene content varies up to 35% of the rocks and evolves from En_{72} to En_{22} from the bottom to the top of UZb (von Gruenewaldt, 1973; Molyneux, 1974).

Apatite appears in subzone C of the Bushveld Upper Zone. Its modal abundance generally varies between 4-6 % in the lower part of subzone C and decreases rapidly upwards to 0.5% in the uppermost rocks (von Gruenewaldt, 1973). The average modal abundance is between 2.2 % and 2.4 % (von Gruenewaldt, 1973; Molyneux, 1974). The appearance of apatite at this level (subzone C) in the stratigraphy indicates that the magma had reached saturation in P_2O_5 (Cawthorn and Walsh, 1988). Cumulus olivine and apatite occur intermittently after apatite appears in the Upper Zone (Tegner et al., 2006).

Sulfides are also present in the Upper Zone. Pyrrhotite is most common whereas chalcopyrite, cubanite and sphalerite are minor (Reynolds, 1985a). The sulfides either occur as interstitial to cumulus minerals in anorthosites and magnetite gabbros or as

minute drop-like bodies in the magnetite gabbros and olivine diorites (von Gruenewaldt, 1976).

1.4. Models for the Evolution of the Upper Zone

Various hypotheses have been put forward for the evolution of UZ. The most popular of these is its evolution as a single series without major magma recharge or crustal assimilation. Investigations by von Gruenewaldt (1973) and Molyneux (1974) imply that after the addition of magma at the PxMk, the magma differentiated without any interruption to form the Upper Main and Upper Zone rocks. Data presented by Kruger et al. (1987) indicate that the UZ rocks crystallized from an isotopically homogeneous magma (Fig.1.3) and represent a single differentiated series.

The concentration of incompatible elements can be used to infer the evolution of magmas during fractional crystallization and estimate the trapped liquid content (Cawthorn and Mc Carthy, 1985; Cawthorn et al., 1991; Tegner et al., 2009). In such a study undertaken by Cawthorn and Mc Carthy (1985), incompatible element data showed that the uppermost 500 m of UZ were derived from a single homogeneous magma. A further study of the entire UZ by Cawthorn and Walraven (1998) showed that incompatible element concentrations (Zr) increased exponentially with height due to fractionation without addition of magma. These findings imply that additional internal processes possibly operated within the magma chamber to produce the mineralogical diversity, reversals in mineral composition, and the magnetitite and anorthosite layers in UZ (Kruger, 2005).

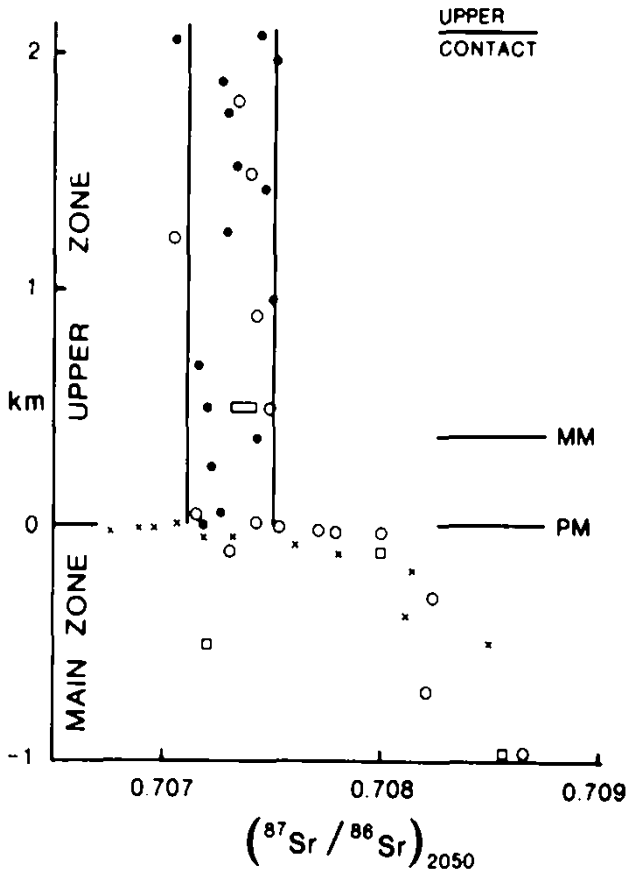


Fig. 1.3 Initial $^{87}Sr/^{86}Sr$ ratio plotted against stratigraphic height in the Upper Main Zone and Main Zone. □ (Hamilton, 1977), o (Sharpe, 1985), x (Kruger et al., 1986) and ● (Kruger et al., 1987)

The absence of rock types associated with quenching in Bushveld rocks and the increase in An and En values in mineral compositions close to the PxMk indicate that addition of magma at the PxMk took place before the resident magma cooled and differentiated considerably and the added magma was hotter and less differentiated (von Gruenewaldt, 1973; Cawthorn et al., 1991). Cawthorn and Walraven (1998) also proposed a model for the crystallization of the entire Bushveld complex. The model shows that even though UZ is about 2.5 km thick, up to 4 km of magma were present in the chamber; signifying a loss of about 1.5 km of magma. Moreover, since Tegner et al (2006) suggest that the magma at the Pyroxenite Marker is a quartz normative Fe-rich tholeiite, one would expect the most evolved UZ rocks to contain significant quartz. The absence of such rocks in UZ suggests that some SiO_2 rich magma escaped from the chamber (Cawthorn and Walraven, 1998). It is now established based on MELTS modeling incorporating the

felsic roof rocks with Upper Zone compositions that 25% of magma escaped from the chamber (Vantongeren et al., 2010).

Different models have been developed for the formation of magnetitite layers in UZ. A review of these models is presented in Tegner et al. (2006) in which bottom crystallization from a stratified magma chamber is proposed as a cause not only for the formation of magnetitite layers but also for the cyclicity and mineralogical breaks in UZ (Tegner et al., 2006). In layered intrusions, crystallization mostly occurs in the lowermost convecting layer (Cawthorn and McCarthy, 1980; Kruger and Smart, 1987). Double diffusive convection probably plays a part in such a process as crystallization of magnetite which is considerably denser than the residual liquid would lead to instability in the magma chamber (Kruger and Smart, 1987). The model implies that the magma at the PxMk underwent Fe enrichment by crystallizing gabbronorite up to UZa. Crystallization of magnetite- and olivine-bearing rocks reduced the magma density causing episodic mixing events in the magma chamber (Tegner et al., 2006). A similar model has also been used to explain the reversals in Cr content of magnetite at the level of MML (Kruger and Smart, 1987). However, after reviewing the different models developed to explain the origin of anorthosite and magnetitite layers, Cawthorn and Ashwal (2009) refuted this model due to the general absence of reversals across magnetitite layers. They proposed crystal settling augmented by changes in pressure to be more reasonable explanations for the Upper Zone paradigm and highlighted the fact that no single mechanism seems to explain the features present in the Bushveld Upper Zone.

Various authors have alternatively suggested that the UZ was recharged with injections of magma during its evolution. This possibility was proposed by Harney et al. (1990) at the level of the MML due to differences in Sr and Sr/Al_2O_3 ratios below and above this layer. Ashwal et al. (2005) also suggested small injections of magma to explain the reversals in mineral composition, regardless of the fact that Sr_o are more or less constant throughout the sequence. The implication is that small injections of magma with Sr_o identical to that in the UZ magma chamber occurred during UZ evolution. However, the possibility of such a process to have occurred is highly implausible visualizing investigations by

Kruger et al. (1987) that UZ crystallized from a homogenized mixture of new and resident magmas at the PxMk. Hence the Sr_o of any magma added during UZ evolution ought to be identical to that of the mixed magma. However, Cawthorn and Ashwal (2009) argued against various possibilities of magma injection which might have occurred in UZ using the An content of plagioclase and density measurements in the various successions.

Chapter 2- Research Rationale and Methodology

2.1. Fractionation in Layered Intrusions

Crucial to the formation of layered intrusions is the evolution of their liquids as well as various magmatic processes involved in their crystallization. These processes have generally been inferred with the use of mineral and whole rock compositions. Mineral compositions commonly record differentiation processes, e.g. compositional zoning, reaction rims and mineral inclusions. These features can either result from basic variations within the system such as temperature and pressure or open system processes such as magma recharge or contamination. Abrupt changes in major element compositions of minerals can be used to infer breaks in differentiation (e.g. the Mg# of mafic minerals and the An# of plagioclase). However, trace element compositions provide more specific emphasis on the evolutionary processes in magma chambers, hence their use in modeling the crystallization of magmas. Plagioclase is an important mineral which has been employed to comprehend magma chamber processes because of its common occurrence as a major crystallizing phase in most layered intrusions. Harney et al. (1990) used plagioclase Sr and An content to show the possibility of a magma mixing event at the level of the Main Magnetitite Layer in the Bushveld Upper Zone. Similarly, Tegner et al. (2006) used plagioclase An content in combination with other mineral and whole rock compositions to model crystallization processes within the Bushveld Upper Main Zone and Upper Zone magma chamber. These and other studies have shown plagioclase compositions to be a representative way to infer trends in the evolution of layered intrusions.

Several authors have used the concept of trace element partitioning to model magmatic systems (e.g. Henderson, 1970; Morse, 1982; Blundy, 1997). In such modeling, the importance of trace element partitioning between simultaneous phases cannot be overemphasized. Likewise the assemblage of rocks produced by any system depends on a combination of factors; the rate of cooling which is a direct consequence of the volume of magma, the composition of the crystallizing magma and the presence of volatile components. These conditions vary for different systems; hence care must be taken in using partition coefficients from one system to another. Many experimental and modeling studies have shown how trace element partition coefficients ought to behave with respect to various parameters. Drake and Weill (1975) have revealed the dependence of D of various elements in plagioclase on changing temperature. Morse (1982) and Blundy and Wood (1991) further depicted the effect of compositional changes on trace element partitioning between plagioclase and silicate melts. Their investigations show that both Sr and Ba partitioning between plagioclase feldspar and melt are chiefly controlled by plagioclase An content, both being more compatible in albitic than anorthositic plagioclase.

The fact that intense fractionation is a common feature of cumulate rocks implies that original liquid compositions are not normally preserved. It has also been shown that the formation of cumulates involves two stages; the cumulus stage in which crystals fractionate and accumulate, followed by the post-cumulus stage which is dominated by the crystallization of intercumulus liquid and consolidation of the cumulus pile (Wager et al., 1960). Therefore, analyses of bulk minerals which are generally thought to be cumulus do not necessarily represent the cumulus phase only, but are a combination of cumulus and intercumulus contributions. During the consolidation stage, modification of initial cumulus compositions of minerals takes place. The Mg # of olivine and pyroxene have been used to show the effect of this modification for situations in which the residual interstitial liquid tends to migrate through the early formed cumulus crystals (Irvine, 1980) and those in which the liquid remains trapped (Barnes, 1986). Barnes specifically identified the change in composition between original cumulus and final re-equilibrated mineral compositions to be the trapped liquid shift (TLS) effect. Investigations by

Cawthorn (1996) further proposed that residual intercumulus liquid in the Bushveld Ccmplex remained trapped during its crystallization, implying that the TLS effect is an important parameter that needs to be considered during modeling.

Incompatible elements generally concentrate in the liquid during fractionation and crystallize at the consolidation stage, hence the concentrations of original cumulus minerals is enormously modified. The implication of this post-cumulus modification is that allowance needs to be made for the crystallization and equilibration of residual intercumulus liquid in modeling the evolution of cumulate rocks. For incompatible elements especially, the difference between original cumulus and re-equilibrated content of minerals ought to be enormous (Cawthorn, 1996). It therefore becomes important to use the principles in such modeling to infer crystallization processes in the Upper Zone for which there is plenty of ongoing debate about its evolution. Various attempts at similar modeling have generally ignored the TLS effect (e.g. Blundy, 1997; McBirney, 2002), and this could lead to misleading and erroneous conclusions especially for the evolution of incompatible elements.

2.2. The Skaergaard Intrusion

In spite of the huge differences in age, size, and shape between the Bushveld and the Skaergaard intrusion, the cumulus mineralogy in their Upper sections is rather similar (Fig. 2.1; Tegner and Cawthorn, 2009). Furthermore, the two intrusions both undergo extreme iron enrichment with a comparatively small degree of plagioclase fractionation, evident from An contents of plagioclase which remain relatively high whereas Mg#s of pyroxenes and olivine change significantly during crystallization (Wager and Brown, 1968; Tegner et al., 2006). Similar to the Bushveld Upper Zone, each of the three series of the Skaergaard intrusion (LS, UBS and MBS) are believed to have formed from a single magma without major addition (Wager and Brown, 1968; Nielsen, 2004).

The similarities between the upper sections of these two intrusions permit useful judgments about the processes involved in the evolution of their magmas. An extra convenience to the present study is the fact that the Skaergaard intrusion has been well documented in terms of mineral proportions and trapped liquid fractions (e.g. Wager and Brown, 1968; Tegner et al., 2009). The starting liquid composition of the Skaergaard intrusion can also be estimated accurately (e.g. Brooks and Nielsen; 1978; Nielsen 2004). Trace element data for plagioclase also exist for the entire Skaergaard intrusion (Jang and Naslund, 2001), hence its crystallization can be constrained and the principles applied to the Bushveld Upper Zone in order to infer the means by which the magma evolved including various cumulus and post-cumulus processes. Hence, in this thesis, the Sr and Ba contents of plagioclase in the Skaergaard and Upper Zone of the Bushveld Complex will be compared and their evolution modeled.

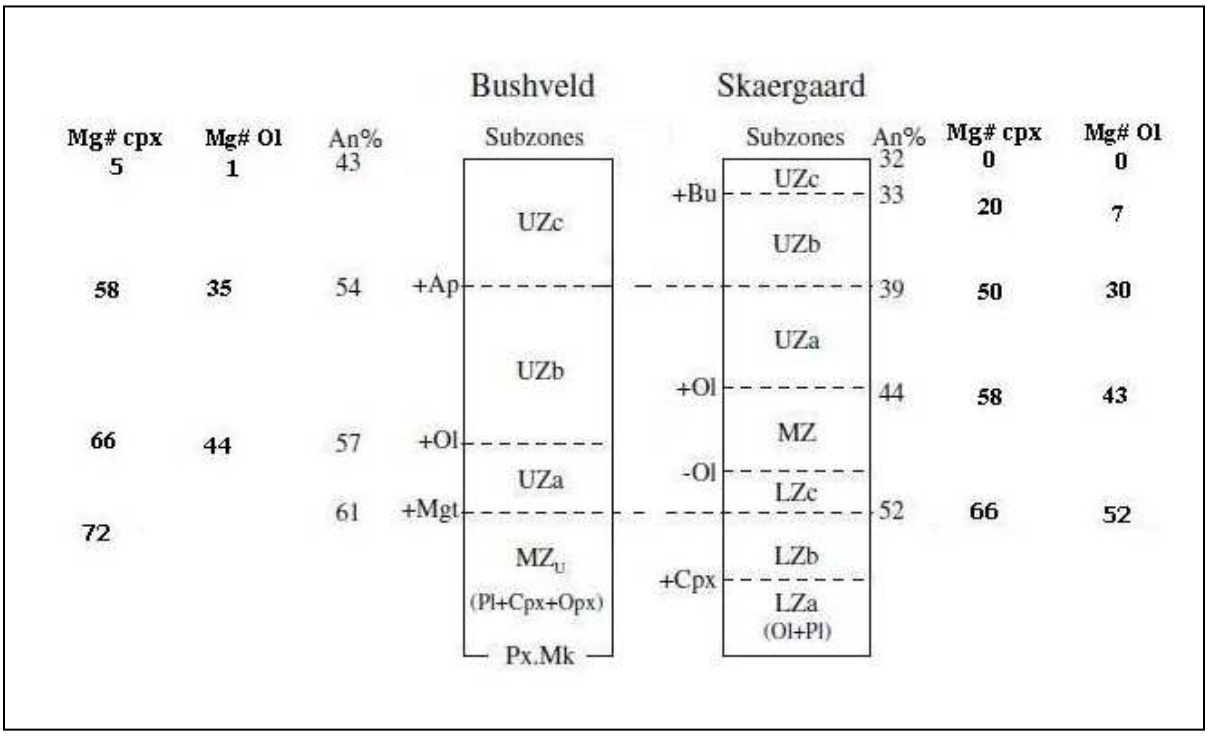


Fig. 2.1. Mineral compositions in the Bushveld Complex, above the Pyroxenite Marker and the Skaergaard Layered Series (Modified after Tegner and Cawthorn, 2009). Data for the Bushveld from Tegner et al. (2006) and for the Skaergaard from Thy et al. (2009)

2.3. Justification for selection of samples from the Upper Zone of the Bushveld Complex

In a bid to obtain a continuous section through the UZ, the Council for Geosciences undertook a drilling programme, in the north east of the Rustenburg Layered Suite in 1974 on the Bierkraal farm (Walravens and Wolmarans, 1979). Three boreholes; BK1, BK2 and BK3 (Fig 2.2) were drilled intersecting different lengths of UZ stratigraphy. Correlation of these boreholes has been provided (Walraven and Wolmarans, 1979; Kruger et al., 1987; Tegner et al., 2006) and borehole depths and intersections have also been presented (Walraven and Wolmarans, 1979; Cawthorn and Walsh, 1988). The combined Bierkraal boreholes provide a continuous section through the entire Upper Zone and material from BK1 and BK3 is used in the present study.

Samples from the Bierkraal cores have been sampled for various projects.
The distribution of Cr in magnetite: Bierkraal samples were originally collected to study the distribution of Cr in magnetite in order to understand crystallization processes within the Upper Zone (Cawthorn and McCarthy, 1980). Hence, mainly magnetite-rich intervals were sampled for the study.

The distribution of apatite: The same samples from the previous study were used to make a preliminary study of the distribution of apatite in UZ (Cawthorn and Walsh, 1988). The highest concentration of apatite occurs in an interval from 1620 m to 1700 m above the base of the Upper Zone (between 1W547 to IW667). Further detailed sampling was then undertaken along this interval as a result of discovering the most enriched part of the bore core. Detailed sampling ought to provide understanding of the mechanism of accumulation of super-cotectic proportions of apatite in the succession (using REE abundances in plagioclase as a tracer).

Sr isotope ratios: A study of the initial Sr isotope ratios was initiated, which required sampling on a more equally spaced basis of the entire section above the Pyroxenite

Marker (Kruger et al., 1987). It was also found that the most dramatic changes in fractionation (especially trace elements) occur at the very end of differentiation (top of Upper Zone). An intriguing aspect of the Sr isotope studies was that there did not appear to be any contamination or assimilation of the felsic overlying roof rocks into the residual evolved magma (Kruger et al., 1987; Tegner et al., 2006). Hence a suite of samples near the top of the mafic phase (IW403 to 1W452, within 50 m from the top) was collected.

Major Element Composition of Minerals: This study was initiated by Tegner et al. (2006) and typical sample intervals were between 20 and 40 m, yielding about 60 samples throughout the entire 1800 m of the Upper Zone. In the modeling by these authors, it was suggested that there were occasional reversals in the An content of plagioclase, but the sample spacing in that study was large, and so the nature of those reversals (sharp or gradual) could not be resolved. More closely spaced samples were taken across the boundary of Unit IV to V of Tegner et al. where the largest reversal in An content was recorded. This interval is from 846 m to 884 m (IW1515-IW1473) above the base of the Upper Zone.

Various aspects of these focused projects are still ongoing. Where sufficient plagioclase could be obtained, these samples were analyzed for all elements. Thus, the distribution of the samples appears rather erratic (some large gaps and some closely spaced sections). However, in many cases, there were only sufficient samples to obtain the trace element abundances for Ba and Sr, which is the main thrust of this thesis. Aspects of the ongoing studies will be referred to here, where relevant.

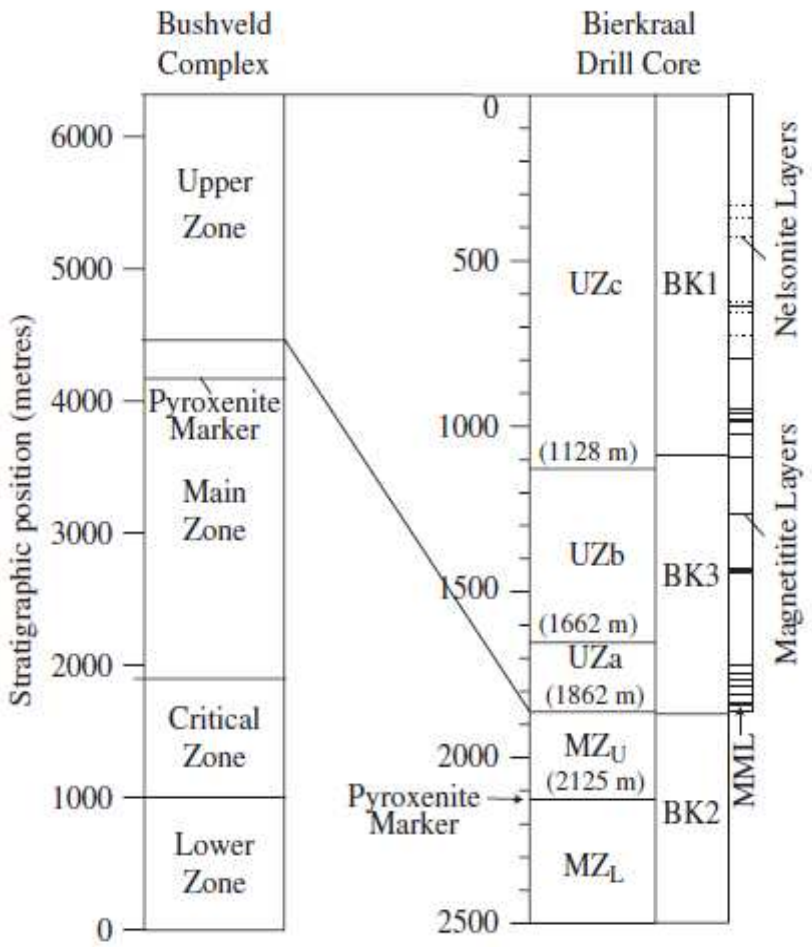


Fig. 2.2. Generalized stratigraphic section of the Bushveld Complex and combined Bierkraal drill cores. Subzones have been divided based on the appearance and disappearance of cumulus minerals (Tegner et al., 2006). BK1 and BK3 samples = 1W and 3W respectively for sample numbers.

The method used in calculating the stratigraphic position of samples assumes that the dip of the layers is 24ºN and the core is vertical (Tegner et al., 2006). The uppermost sample in this study (which represents the top of the intrusion) occurs at 1W 403.4, and is 12 m lower than that of Tegner et al. (2006). 12 m were therefore added to the height of each sample with the purpose of compensating for the difference between the observed roof for this study and Tegner et al. In order to compute the heights of samples, the first appearance of cumulus magnetite was used as the base of UZ. The stratigraphic interval investigated in this study encompasses samples from the heights 9.2 m to 1863 m above the base of UZ.

2.4. Objectives of the Project

The evolution of the Upper Zone of the Bushveld Complex has been the subject of debate for various reasons. Apart from its diverse mineralogy, it contains at least 25 magnetitite layers which are continuous over the eastern and western limbs of the Bushveld Complex. The sequence is also marked by reversals in mineral compositions (Ashwal et al., 2005; Tegner et al., 2006); hence significant magma addition and/or contamination may be suggested. In spite of these aspects, evidence against magma addition or assimilation in the entire 2.1 km of rocks has been presented (Kruger et al., 1987; Tegner et al., 2006); and they suggest internal mechanisms which would explain the evolution of the Upper Zone. Plagioclase is the dominant cumulus mineral throughout the sequence and therefore its composition provides a continuous record of differentiation in the Upper Zone.

This project therefore aims to model the crystallization of the Upper Zone and utilize data from a similar but much better constrained intrusion to develop the model. In doing so, various processes which possibly operated in the Upper Zone are evaluated based on major and trace element contents of plagioclase. Major element data are used to estimate An contents of plagioclase. In order to model the trace element contents, Rayleigh fractionation models are developed and suitable mineral melt partition coefficients utilized to test different hypothetical evolution trends of trace elements in plagioclase. In estimating cumulus and final re-equilibrated compositions of plagioclase, trapped liquid fractions become critical, hence they will be incorporated in order to show the the importance of allowing for the trapped liquid shift effect. These calculations are crucial in constructing the trace element contents of the magma compatible with cumulus and post-cumulus processes in the magma chamber. They also shed light on the possible processes which operated in this part of the complex. This will further test previous hypotheses that have been proposed to understand such processes (e.g. Harney et al., 1995; Tegner et al., 2006; Cawthorn and Ashwal, 2009).

2.5. Petrographic and Analytical Techniques

Each core sample was divided into two in order to make provision for microscopic examination and for geochemical investigations. Thin sections of 20 samples were studied. Plagioclase separates were prepared for all 61 new samples of BK1 core, and combined with 65 (BK1 and BK3 core samples) previously prepared by Prof. Cawthorn. Further details of the separation are presented in appendix A. Each sample was then milled in an electric mortar to the consistency of dust. For each sample, the plagioclase separate was preserved for XRF analyses on pellet (for trace element analyses), XRF on a fusion disc (for major element analyses) and ICP analyses (for additional trace element analyses). Preliminary analytical data indicated a serious problem, namely that many samples included apatite that were enclosed within plagioclase grains and so could not be separated by using dense liquids. Removing this apatite required the development of a leaching method that is described in Appendix B. The most crucial aspect of this leaching process was that it should completely dissolve the apatite, not leaving any possible residue containing of the rare earth elements (which forms part of another study). It should also have no effect on the compositions of the plagioclase. Thereafter, the powders were analyzed for major elements and certain trace elements at the University of the Witwatersrand and the instrument information is also specified in appendix A.

ICP analyses were carried out on a number of samples at the University of Cape Town. Also some duplicate samples were analyzed at SGS laboratories to test for analytical precision. The major elements analyzed for include SiO_2, TiO_2, Al_2O_3, Fe_2O_3, FeO MnO, MgO, CaO, Na_2O, K_2O, P_2O_5 and Loss on Ignition (LOI) while Co, Ni, Cu, Sr, Zr, Nb, Ba, La, Ce, Pr, Nd, Sm, Eu, Gd, Tb, Dy, Ho, Er, Tm, Yb, Lu, Hf, Ta, Pb,Th and U were analyzed as trace elements. Analytical techniques, instrument information and standards used are presented in appendix A.

Chapter 3- Petrography

3.1. Introduction

Detailed petrographic descriptions have been provided for the rocks of the Upper Zone in the eastern Bushveld Complex (Wager & Brown, 1968; von Gruenewaldt, 1973; Molyneux, 1974). In addition, various petrographic aspects in the northern limb have been presented by Ashwal et al. (2005). Due to poor outcrop exposure in the western limb, most investigations have been carried out on drill core material. Coertze (1970) provided petrographic descriptions for the entire western limb, likewise mineralogical and petrographic aspects of the Bierkraal boreholes have been broadly studied by various authors (e.g. Cawthorn and McCarthy, 1985; Reynolds, 1985a; Roberts, 2005; Tegner et al., 2006). Hence, only features of relevance to the present study are highlighted here.

3.2. Major Features of the Bierkraal Boreholes

Rock types intersected in the two boreholes are gabbro, magnetite gabbro, anorthosite, and ferrodiorite. Most samples are relatively fresh whereas a few have suffered some degree of alteration. Bushveld granite occurs from about 380 m (Cawthorn and Walsh, 1988) and above in the core. Anorthosite generally contains about 90% plagioclase with the remaining 10% comprising one or more of the following phases; orthopyroxene, clinopyroxene, magnetite and olivine. Magnetitite layers commonly contain more than 90% magnetite with the remaining portion comprising apatite and plagioclase.

The main cumulus phases in the section are plagioclase, orthopyroxene, clinopyroxene, magnetite, olivine and apatite. Most rocks encountered contain between 60 to 45% plagioclase, except in magnetitite layers in which plagioclase mode is much less. Clearly,

the plagioclase content of anorthosite layers is higher. Plagioclase grains range from euhedral to subhedral and are locally altered to sericite or saussurite (Fig. 3.1a). Olivine appears in UZb and occurs intermittently in the section. It varies from subhedral to anhedral with grain sizes typically between 3 to 5mm (Fig.3.1b). Pyroxenes range in grain shape from euhedral to subhedral and a minor amount is anhedral. Clinopyroxene grains are generally subhedral to anhedral (Fig 3.1c). Disseminated magnetite grains are quite variable in shape and size. They range from subhedral to anhedral (Figs. 3.1d and 3.3d) and occur as composite grains and inclusions with other phases.

The appearance of apatite as a cumulus phase in UZ is detected in samples from the BK1 and the upper part of BK3 (Cawthorn and Walsh, 1988). The occurrence of apatite is important to the present study as it occurs as inclusions in other mineral phases including plagioclase.

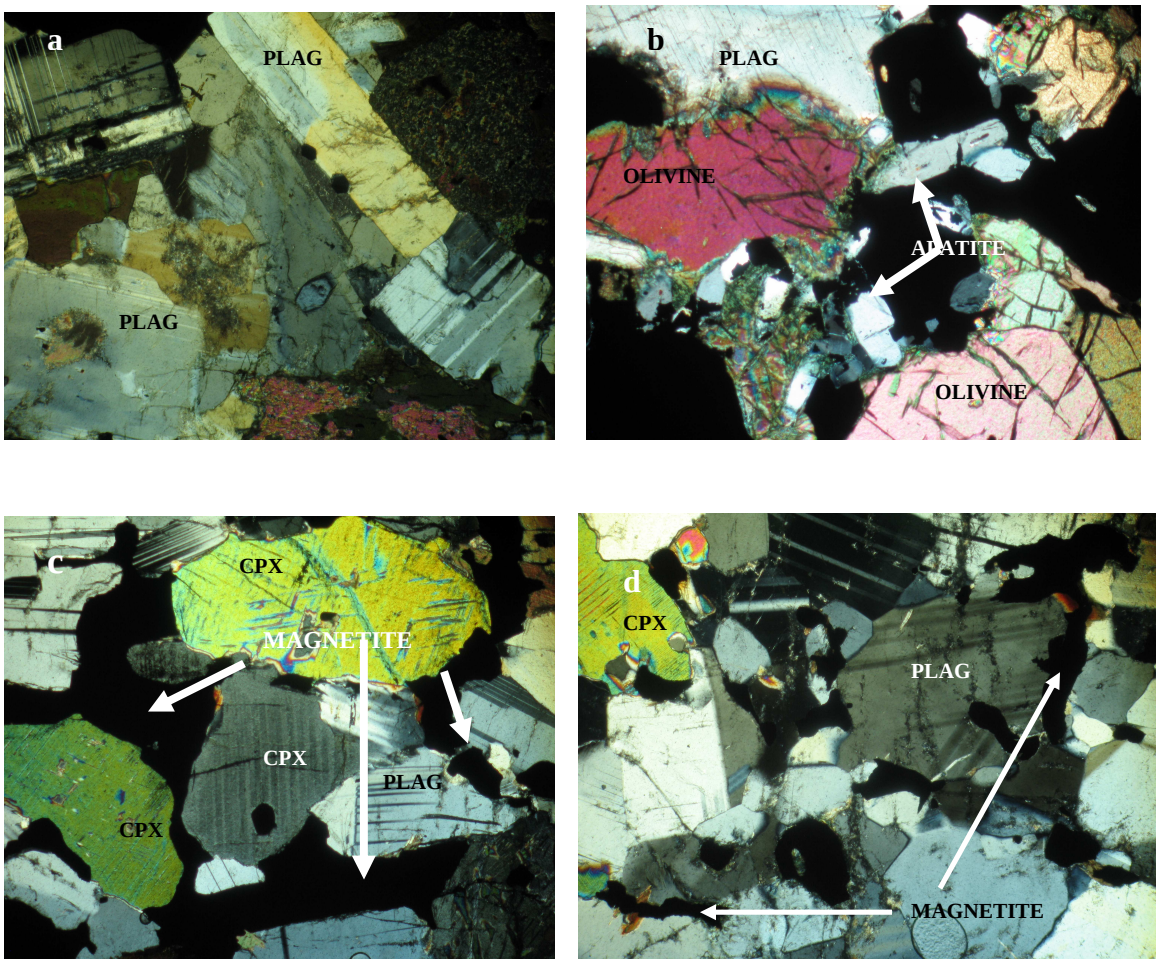


Fig. 3.1. Microphotographs showing the major cumulus phases in the Upper Zone. a.) -1W443.8; Plagioclase grains, some altered to sericite. b.)-1W636.2; Olivine altered along the rims and cracks to bowlingite. c.)-1W1473 Subhedral cpx with anhedral magnetite d.)- 1W1498.7; Cumulus and interstitial magnetite as inclusions and composite grains. All views are taken with a x4 lens under crossed polars, field of view is 3 mm.

The intercumulus phases including alkali feldspar, quartz and hornblende only appear in the uppermost part of BK1, whereas biotite occurs throughout. Hornblende forms a pokilitic texture with plagioclase and clinopyroxene (Fig. 3.2a). Alkali feldspar commonly forms a pokilitic texture, enclosing plagioclase and other minerals (Fig. 3.2b). Quartz is quite minor and is intergranular (3.2c) and biotite is anhedral (Fig. 3.2d)

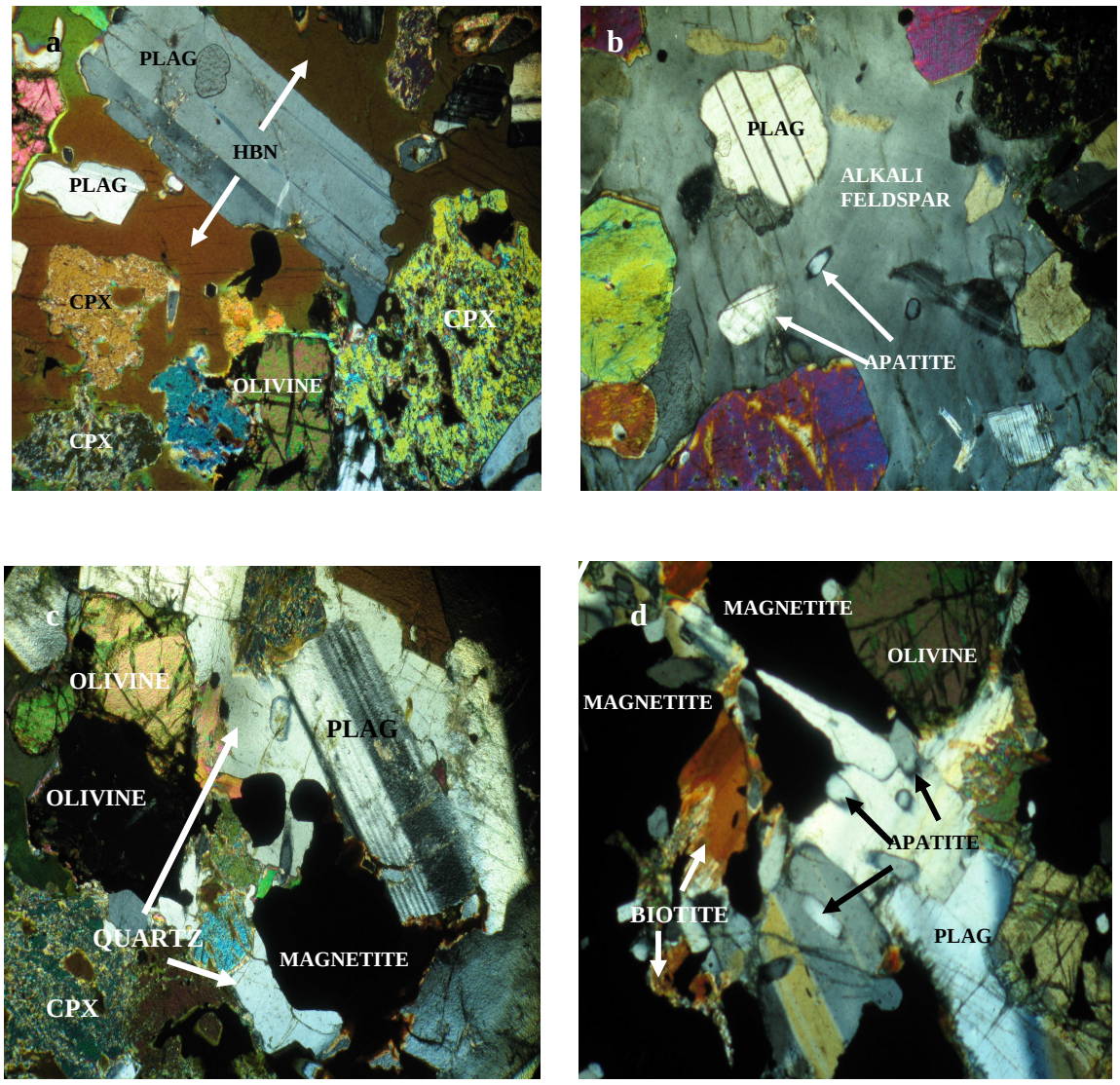


Fig. 3.2. Intercumulus minerals a.)- 1W443.8; Hornblende poikilitic to cpx, plagioclase and magnetite. b.)-1W443.8; Alkali feldspar pokilitic to plagioclase and apatite c.)-1W443.8; Intergranular quartz. d.) -1W636.2; Intercumulus biotite. All views are taken with a x4 lens under crossed polars, field of view is 3 mm.

3. 3. Inclusions and Composite Grains

3.3.1. Apatite

Apatite grains commonly occur as inclusions in other mineral phases (Fig. 3.3a, b and d). The inclusions vary in abundance from sample to sample and are randomly distributed in the cumulus and intercumulus phases. They occur both in the cores and close to the rims of grains, signifying their entrapment at an early stage. Most are unaltered and range in shape from purely hexagonal to elongate but rarely rounded. It was impossible to separate the plagioclase from apatite because apatite grains are often present as inclusions.

3.3.2. Plagioclase

Plagioclase also occurs along the grain boundaries of mafic phases such as olivine and hornblende (Figs 3.3c). The smaller size of plagioclase inclusions compared to the normal sizes which generally occur suggest that inclusions represent plagioclase grains which were not subjected to post-cumulus processes, as they formed earlier.

3.3.4. Magnetite

Magnetite was also encountered occurring as composite grains with and/or inclusions in other phases. In situations in which plagioclase is involved (Fig. 3.3d), magnetic separation was difficult. This shows that magnetite remained a major cumulus phase throughout the crystallization of UZ.

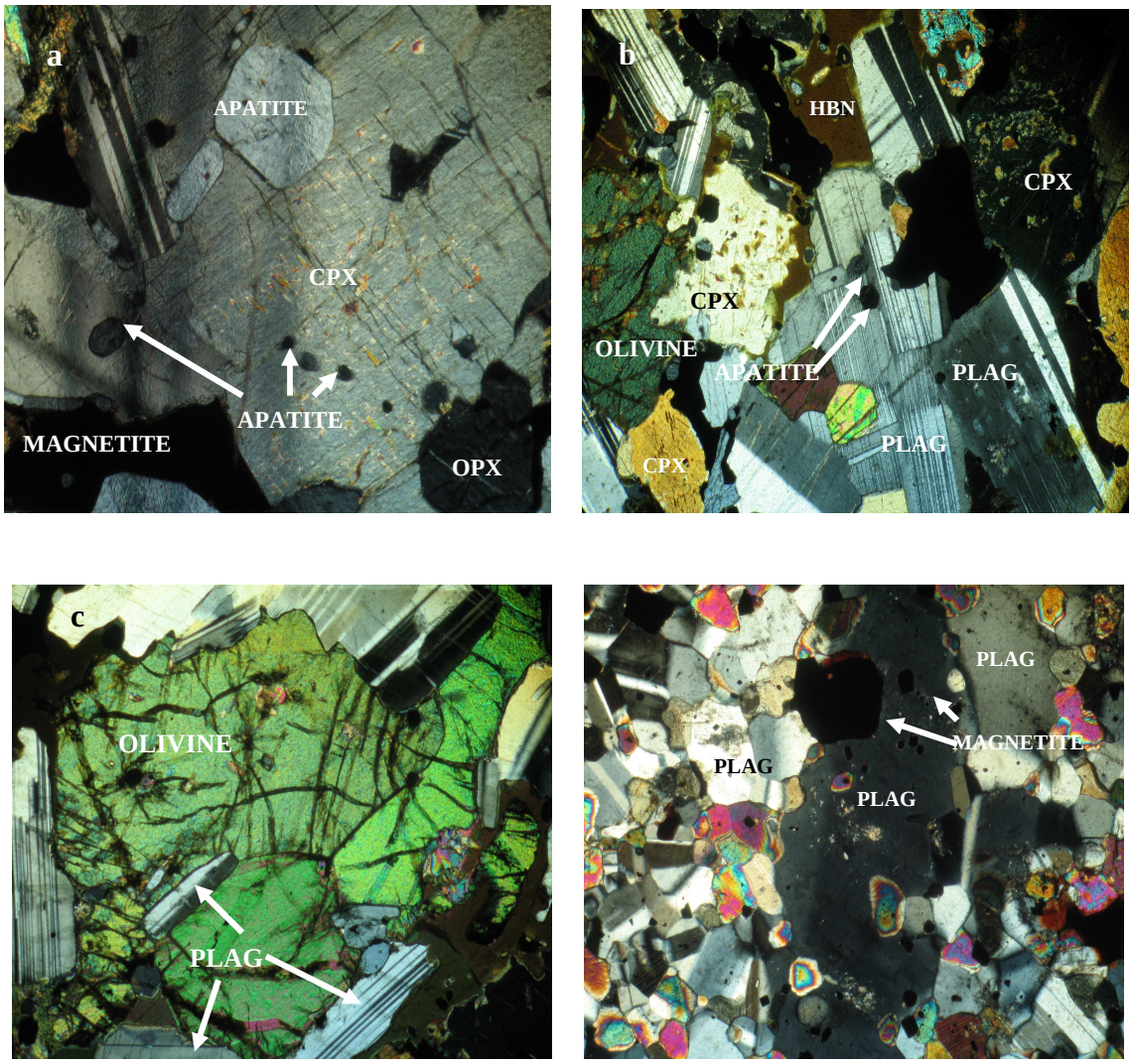


Fig. 3.3. Inclusions and composite grains a.)-1W604.5; apatite included in cpx b.)-1W545.7 apatite included in plagioclase c.)-1W545.7 plagioclase on grain boundary of olivine d.) Subhedral plagioclase and disseminated magnetite grains.

Chapter 4- Geochemistry

4.1. Introduction

This chapter presents major and trace element data for plagioclase separates from BK1 and BK3 together with trace element data for the Layered Series of the Skaergaard intrusion. It is emphasized here that the plagioclase compositions presented are bulk analyses of the mineral hence they represent some contribution from both cumulus and intercumulus compositions. The chemical composition of plagioclase is reflected in the SiO_2, CaO, Na_2O, K_2O and Al_2O_3. These components have been used to calculate anorthite content using the mineral structural formula (An = Ca / (Ca + Na) * 100). Major element data are presented in appendix C and show that some portions within the stratigraphy (hundreds of meters) were not analyzed. Therefore, microprobe data for plagioclase for the entire UZ available from a previous study (Tegner et al., 2006) have been integrated with the current data. Tegner et al. used a JEOL 8600 electron microprobe at the University of Aarhus, Denmark to obtain the plagioclase compositions and analytical techniques are presented in the study. The stratigraphic section from Tegner et al. (2006) is composed of the interval between 20 m and 1855.4 m. All height in meters are quoted relative to the base of the Upper Zone. Some samples are common to both studies and comparisons have been made based on results of these samples.

XRF analyses on pellets were initially employed to obtain trace elements of plagioclase for samples in the present study. Results for Sr, Ba, K and P were obtained from these analyses and the K_2O and P_2O_5 contents were computed. These results served as a guide in identifying samples that required leaching and in selecting samples for further XRF and ICP analyses and for various corrections which are discussed later in this chapter. In order to evaluate the representativeness and reproducibility of the data, multiple pellets were prepared from the powdered plagioclase of one sample (1W649). The results for these XRF analyses on pellets are presented in appendix C and show little variation in the Sr, Ba, K_2O and P_2O_5 contents of plagioclase. This is shown by a mean and standard

deviation of 538 ± 2.2, 608 ± 7.2 0.84 ± 0 and 1.25 ± 0.2 respectively on the 3 powders from sample 1W649. The minute variation indicates that the crushing and milling process employed to make XRF pellets adequately homogenizes the material. From these results, samples were leached where necessary and then chosen for XRF analyses on a fusion disc and ICP analyses, presented in appendix C. Duplicate samples which were analyzed for major elements at SGS laboratories as a further test of reproducibility are also presented in appendix C.

4.2. Removal of effects of included minerals

Results of analyses show that some separates contain various proportions of apatite and/or alkali feldspar as well as quartz and mafic minerals. The non-magnetic minerals report with the non-magnetic fraction during magnetic separation because it is not possible to separate them magnetically from plagioclase; hence their presence affects analytical data. The presence of mafic minerals indicate inclusions or unseparated fragments of these minerlals with the non-magnetic fraction. It therefore becomes important to correct for the effects of these minerals either by developing suitable calculations to correct for their presence, using leaching techniques to dissolve the fractions of these minerals or excluding data for which corrections are too large or unconstrained.

4.2.1. Apatite

Apatite occurs within plagioclase grains in mineral separates taken from the interval in which apatite is present. Apatite is present as a cumulus phase at 777 m in UZ based on the increase in P_2O_5 and REE contents and it then occurs irregularly from this level upwards (Cawthorn and Walsh, 1988). Samples are shown in appendix C that, based on their high P content, contain apatite which introduces an error in the calculation of the An content (Fig. 4.1). The analyses reported for Sr also represent Sr contents for plagioclase with variable proportions of apatite. Ba does not concentrate apatite, but the presence of apatite would dilute the Ba contents from analyses, hence a correction needs to be made for this effect.

The problem of the presence of apatite was addressed by two means; leaching samples in citric acid in order for the apatite fraction to dissolve and calculating out the fraction of apatite. Samples which reported P_2O_5 contents >0.1% in XRF analyses (on pellet) were selected for correction. The remaining samples with 0 to 0.1% P_2O_5 obviously have no apatite and did not need correction.

A dissolution technique had to be developed in order to completely dissolve the apatite out of the separates, not leaving any residue of the rare earth elements and not affecting the compositions of plagioclase. Hence preliminary dissolution experiments were carried out (reported in Appendix B) to ensure complete apatite removal and that there was no effect on plagioclase compositions before samples were leached in citric acid. A number of samples were then leached in citric acid in order to dissolve the apatite present. After leaching, the residual powders of samples were again analyzed with their unleached counterparts to ascertain the success of apatite removal. Results of major element analyses indicated that apatite was totally leached out of the separates. This was indicated by the absence of P_2O_5 and reduction in CaO in leached separates. However, comparison of trace element data for leached and unleached samples show that the Sr and Ba contents of plagioclase were dissolved alongside the apatite proportion. Thus this method could not be used as a quantitative means of removing apatite for Sr and Ba.

The calculation technique was developed to estimate the amount of apatite present in samples which were not selected for leaching in citric acid. For samples that had been leached, their compositions were compared with the results of the removal by calculation to confirm that both methods gave the same result for the An, Sr and Ba contents. It is emphasized that because the leaching method dissolved the Sr and Ba contents of plagioclase, only the calculation method was used to correct for these elements. The data presented and interpreted for Sr and Ba therefore utilized the calculation technique. The calculation procedures developed are presented below.

4.2.1. a. Calculation for the An content

Fig. 4.1 shows An contents calculated from raw analytical data and the samples which contain apatite. The technique involves calculating out the effect of apatite based on stoichiometry of apatite and analyses. The procedure is as follows. The CaO and P_2O_5 contents of apatite are taken to be 56% and 44% respectively. Hence in order to remove apatite from the plagioclase analyses, an amount equal to % P_2O_5 in the analyses * (55/44) is subtracted from the CaO content of the analyses. The resultant amount then needs to be renormalized to the original total before the removal of apatite, as it affects the absolute concentrations of the major oxides.

Table 4.1 shows selected samples and their compositions before apatite removal (by leaching or calculation), after samples were leached in citric acid and after calculating out the fraction of apatite based on apatite stoichiometry and the original analyses. The similarity in CaO and An% from the two techniques implies that using both methods to correct for the presence of apatite is accurate.

Table 4.1. Leached and unleached pairs of samples showing the effect of apatite on the anorthite content of plagioclase

Height (m)	Sample #	CaO[a]	P_2O_5[a]	An %[a]	CaO[b]	P_2O_5[b]	An %[b]	CaO[c]	P_2O_5[c]	An %[c]
1827.7	1W440.5P	7.2	0.6	39.3	6.5	0.0	36.7	6.5	0.0	36.7
1823.5	1W445.15P	8.6	0.4	42.4	8.2	0.0	41.1	8.3	0.0	41.2
1654.7	1W629.9P	15.0	4.5	61.0	10.2	0.0	48.8	10.0	0.0	49.8
884.6	1W1473P	11.0	0.2	53.3	10.7	0.0	52.7	10.4	0.0	52.5

[a] compositions from analyses of plagioclase separates

[b] compositions after the effect of apatite has been calculated out

[c] compositions from analyses after apatite has been leached out of plagioclase

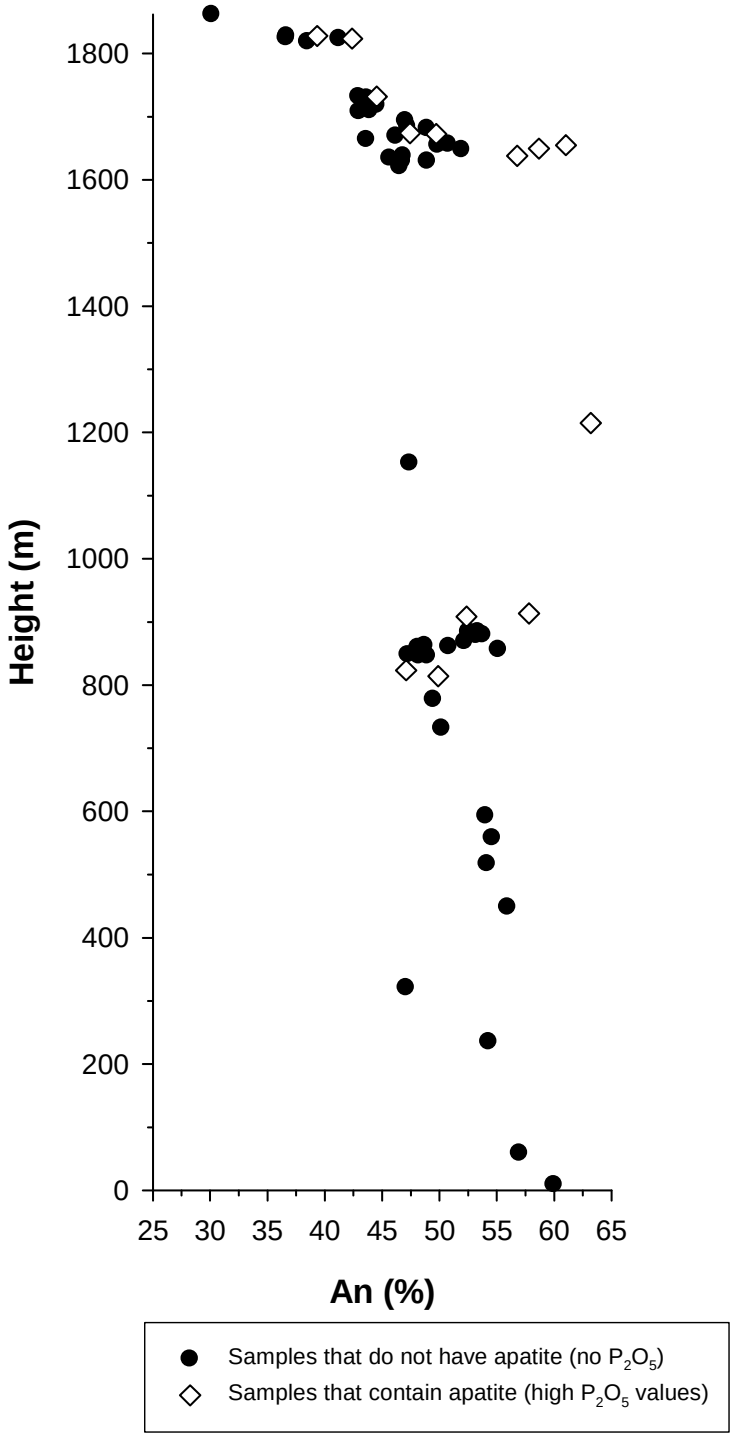


Fig. 4.1 Plot of An content vs. stratigraphic height. An contents are uncorrected for the presence of apatite and show samples that contain apatite.

4.2.1. b. Calculation for strontium

The Sr contents plotted in Fig. 4.2 show the samples which contain apatite; hence a correction has to be made for its presence. The calculation is done as follows. Fig. 4.3 shows the Sr and P_2O_5 of the composite samples from 1400 m upward, which includes the apatite-bearing interval. A best fit line is drawn through all the sample data points with more than 0.1% P_2O_5. Extrapolation to 44% P_2O_5 (composition of apatite) yields a value of 400 ppm Sr and is assumed to be constant

The amount of Sr that will contribute to the composite sample = (%P_2O_5 from analyses* 400)/44. This amount is subtracted from the composite sample.

Then the % plagioclase in the composite sample = 100- (wt% P_2O_5 from analyses*100)/44.

Sr in pure plagioclase = (Sr left after apatite removal * 100)/ % plagioclase in the composite sample. This calculation was applied to the samples containing apatite in the sequence in order to obtain the Sr content of pure plagioclase (Appendix C).

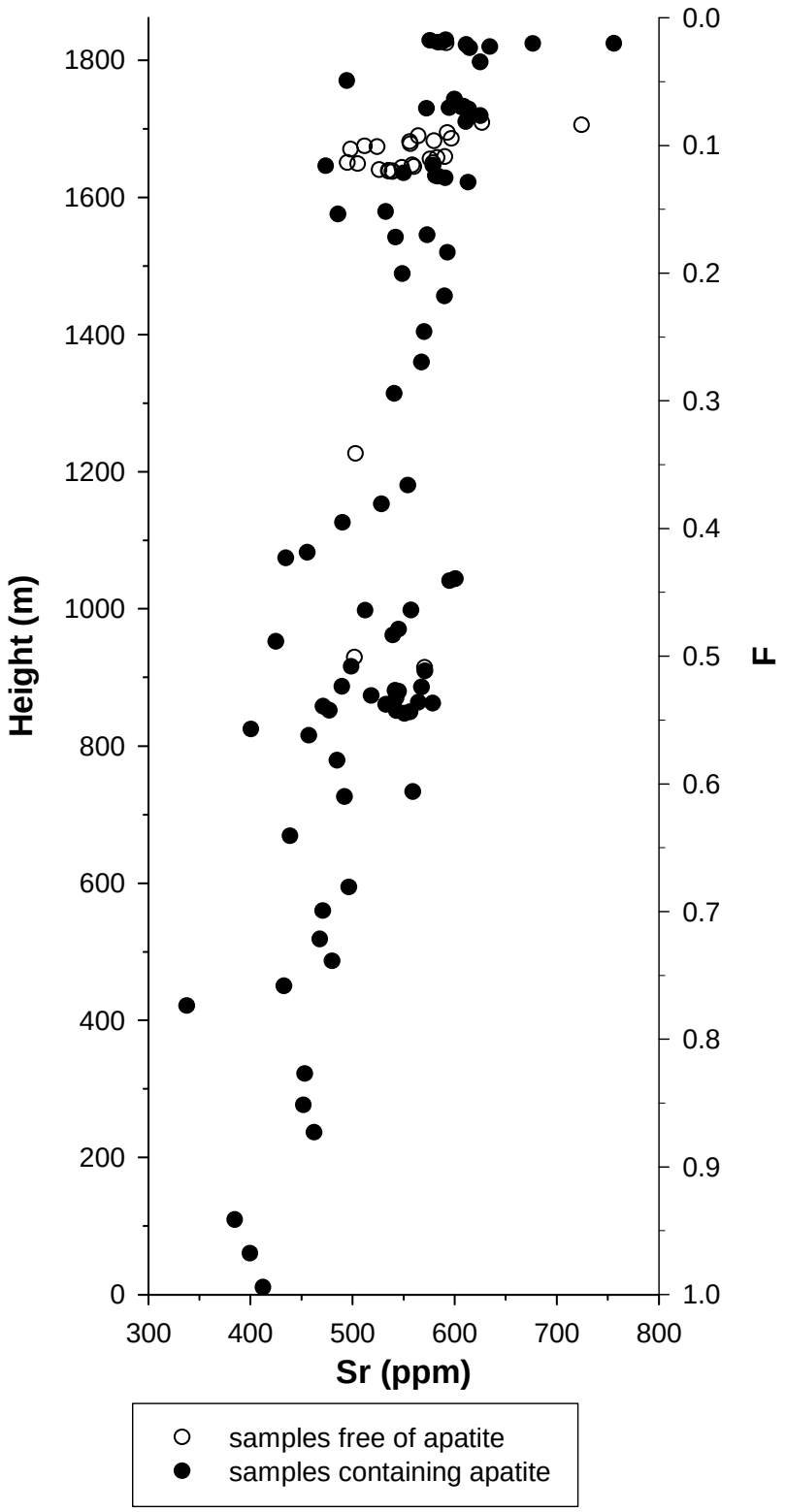


Fig. 4.2 Plots of Sr content vs. height and fraction of magma remaining showing the samples which contain apatite. Data are not corrected for the presence of apatite.

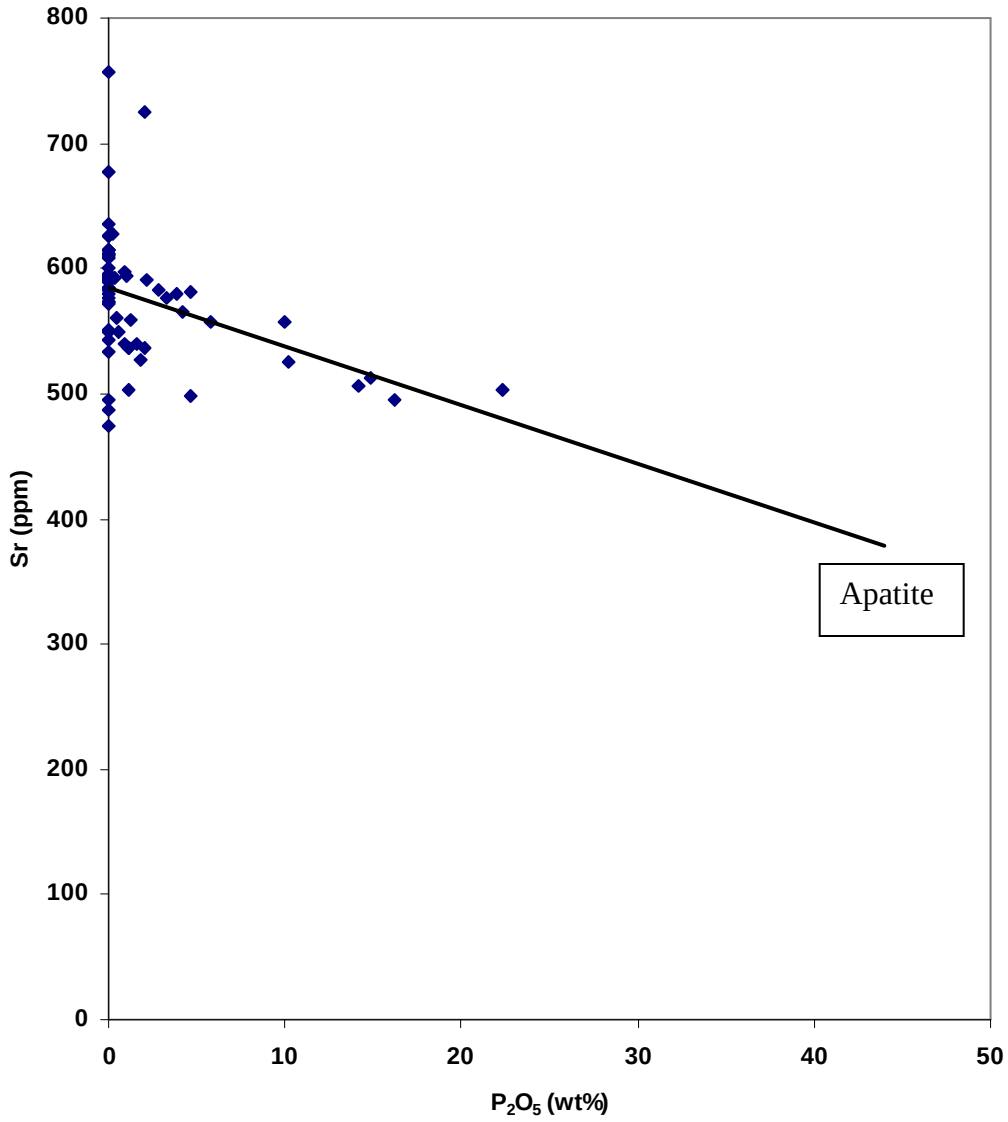


Fig. 4.3 Sr vs. P_2O_5 contents for samples from 1400 m upward (which include the apatite-bearing interval) showing how a calculation can be made to correct for the presence of apatite.

4.2.1. c. Calculation for barium

Barium does not concentrate in apatite; hence it is necessary to correct for the amount of barium that is decreased by the presence of apatite in the separate. Fig. 4.4 shows the Ba and P_2O_5 contents of samples within the apatite bearing interval. A best fit line drawn through all data points approximating to the composition of apatite (44% P_2O_5) leads to 0 ppm Ba. Thus the presence of apatite in the plagioclase separates within the apatite bearing interval would dilute the amount of Ba from analyses, thereby reporting values which are low. This problem was resolved by adjusting Ba contents as follows. Fig 4.4 shows that pure apatite should have 0ppm Ba. Pure apatite also contains 44% P_2O_5

Therefore, the % plagioclase in the composite sample = (100- %P_2O_5 from analyses*44)/100)

Hence Ba in pure plagioclase = Ba from analyses* (100/ % plagioclase in the composite sample).

This calculation leads to a small increase in the corrected Ba content of pure plagioclase compared to the analytical data for composites with apatite inclusions (Appendix C).

Comparison of the data in appendix C (for uncorrected vs. corrected Sr and Ba) shows that the calculations make a trivial difference to the data, but is included to demonstrate the principle which can be applied to any other element (e.g. REE) in apatite. For the reason that the effect of apatite on the Sr and Ba in plagioclase is small, there is no significant difference in concentrations in the section with abundant apatite (1620 m to 1700 m) which was studied in detail.

4.2.2. Alkali feldspar

Alkali feldspar is present in rocks from 1693 m to the top of the borehole. For the reason that alkali feldspar cannot be magnetically separated from plagioclase, it reports with the plagioclase fraction during separation. Plagioclase commonly contains about 0.4% K_2O and alkali feldspar typically contains about 8% K_2O. Most samples in the present study contain less than 0.5% K_2O (similar to probe data of Tegner et al., 2006) and therefore have no alkali feldspar. However, K_2O contents increase up to 1.1% from 1693 m upward (Appendix C) indicating the presence of significant alkali feldspar in the feldspar separates. It is therefore necessary to infer the effect its presence will have on the Sr and Ba contents from analyses.

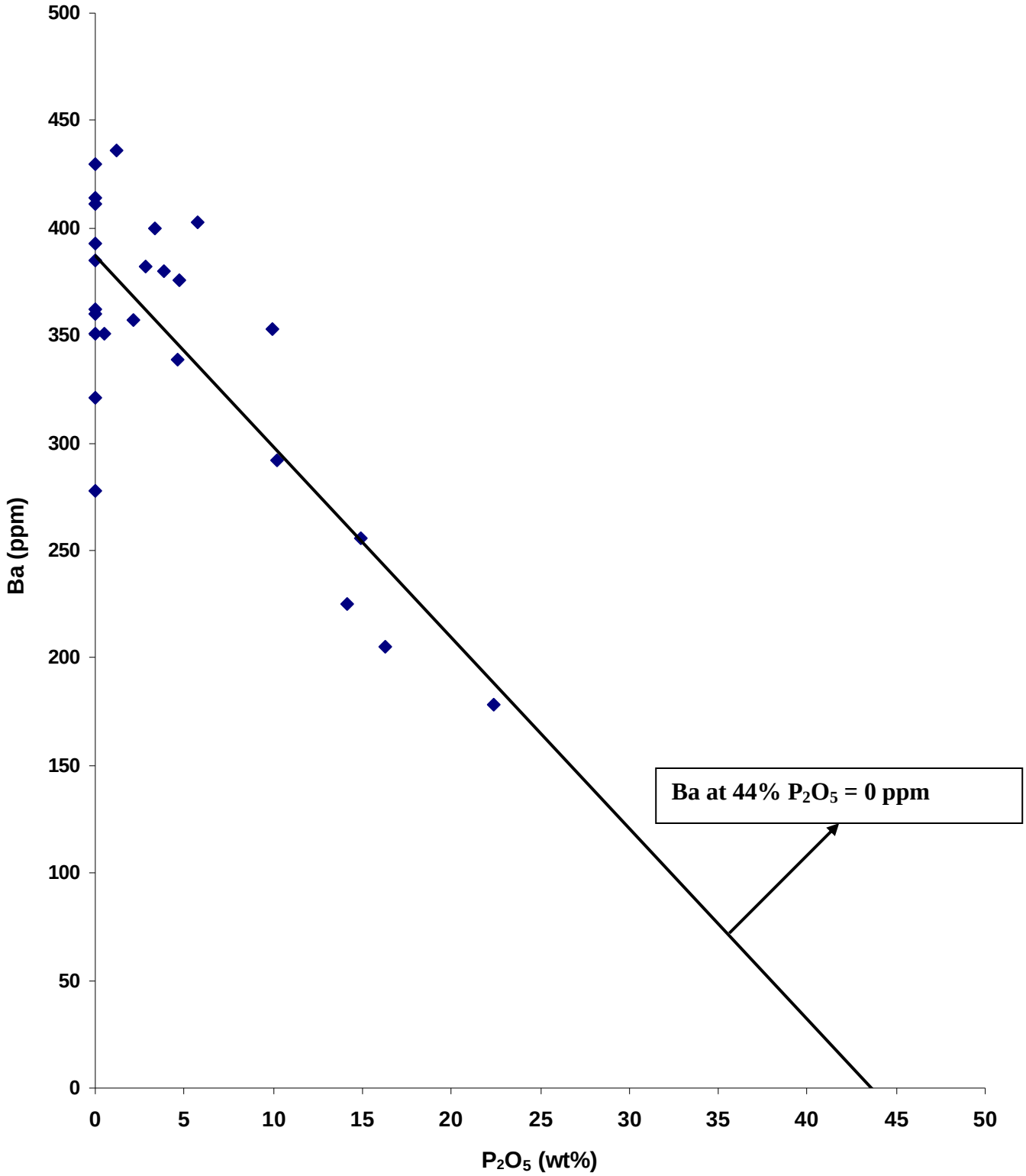


Fig. 4.4 Ba vs. P_2O_5 Correlation. Extrapolation to the P_2O_5 concentration of apatite shows that apatite does not concentrate Ba.

4.2.2. a. Strontium

Sr concentrates in alkali feldspar which is present in samples from 1693 m upward. Therefore, it is necessary to investigate the effect alkali feldspar would have on the Sr contents from analyses. However, D for Sr into alkali feldspar is about the same as into plagioclase (Rollinson, 1993). Therefore, the presence of alkali feldspar will not affect the Sr contents of plagioclase.

4.2.2. b. Barium

Fig. 4.5 illustrates the plot of Ba vs. height, showing the samples which contain alkali feldspar. The plot of Ba vs. K_2O for samples with K_2O contents > 0.4 (Fig. 4.6) shows that samples with high Ba contents also have high K_2O contents indicating that these samples contain alkali feldspar with high Ba contents. D for Ba into alkali feldspar ranges between 4 and 11 and varies between 0.2-0.5 for plagioclase (Rollinson, 1993). Hence Ba has a higher affinity for alkali feldspar than for plagioclase. Therefore, the Ba contents reported from this level upwards represent Ba contents of plagioclase with varying proportions of alkali feldspar. An attempt was made to calculate Ba in alkali feldspar as follows:

The correlation in Fig. 4.6 shows that pure alkali feldspar ought to have about 11000 ppm Ba. If plagioclase contains 0.4% K_2O and the composite sample reports 1.1% K_2O from analyses, therefore, alkali feldspar would contain 0.7% K_2O.

Ba in the composite sample = (0.7 * 11000)/8 = 963 ppm

Ba left after alkali feldspar removal = 1342-963 = 379 ppm

% plagioclase in the composite sample = 100-(0.7*100/8) = 91%%

Ba in pure plagioclase = (379*100)/91 = 416 ppm.

Therefore, out of 1342 ppm Ba from analyses of the separate, 926 ppm represents the amount that concentrates in alkali feldspar and only 416 concentrates in pure plagioclase. The calculation shows that the effect of alkali feldspar on the Ba contents is enormous and would lead to huge reduction in the Ba contents reported from analyses. Hence the effect is too big to calculate out. For this reason, modeling for Ba is stopped at the level where alkali feldspar appears, at 1693 m.

4.2.3. Quartz

Six samples contain quartz based on their high SiO_2 contents (Fig. 4.7a). An increase of 3 to 5% SiO_2 for five samples would indicate 9-12% quartz. The one sample with 20% excess SiO_2 would contain 33% quartz. However, the presence of quartz will not affect the An content. For the five samples, Ba and Sr are increased to allow for this dilution of quartz. The other sample is excluded from all subsequent modeling.

4.2.4. Mafic minerals

The FeO (total) contents of mineral separates are commonly 0.1 to 0.3% greater than values yielded by electron microprobe (Tegner et al., 2006). Six samples had higher values and suggest that the mineral separates contain inclusions of, or unseparated fragments of mafic minerals. The FeO (total) contents of clinopyroxene, orthopyroxene, olivine and magnetite are 30%, 50%, 70% and 80%; so there may be a few mafics in these separates. The presence of clinopyroxene may have a small effect on the calculated An content, but other minerals will not affect the An content. The presence of mafic minerals will also not affect the Sr and Ba contents from analyses because these elements are essentially being excluded from the mafic phases.

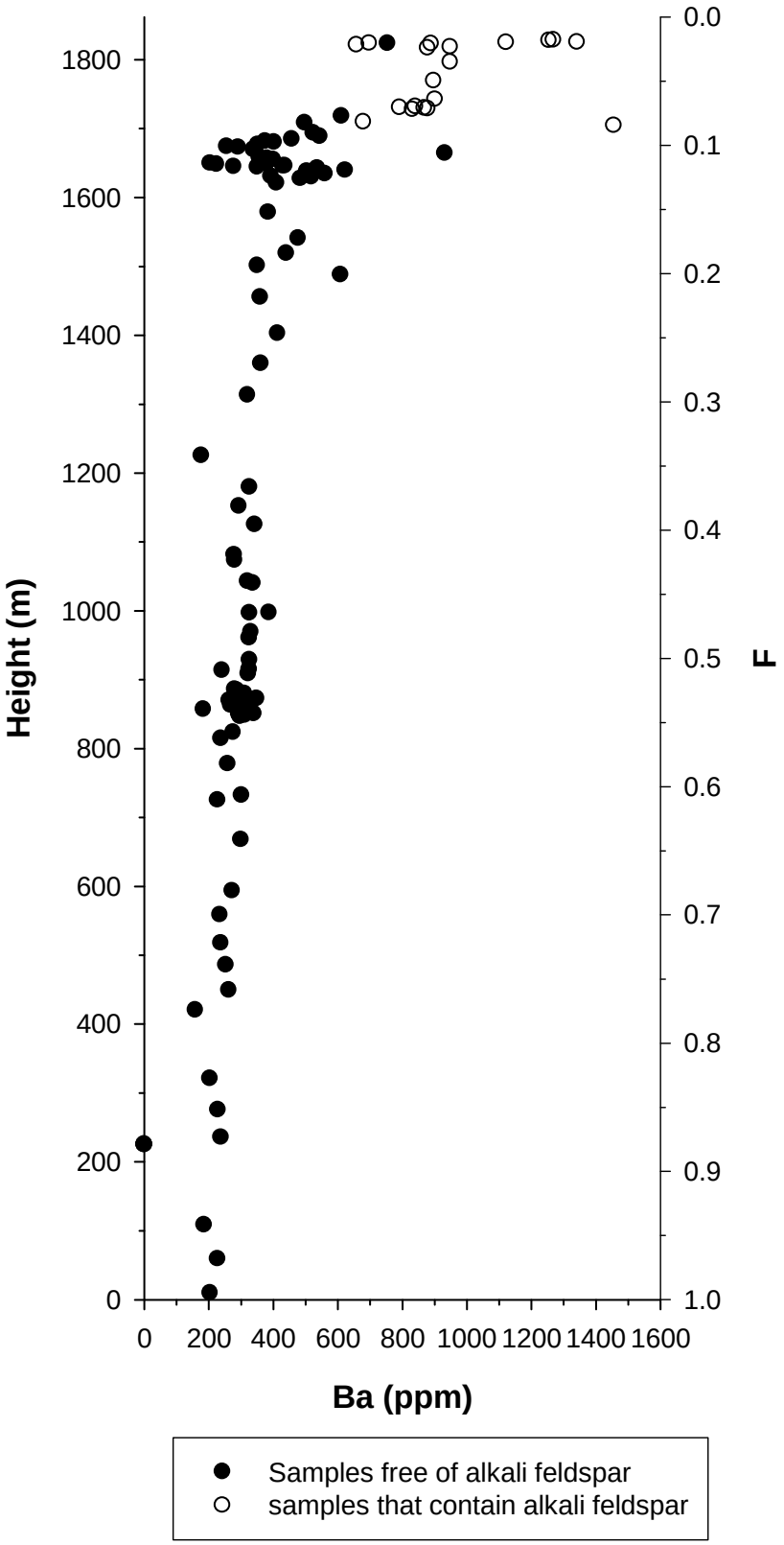


Fig. 4.5 Barium contents of plagioclase plotted against height for the Bushveld Upper Zone showing samples which are rich in alkali feldspar.

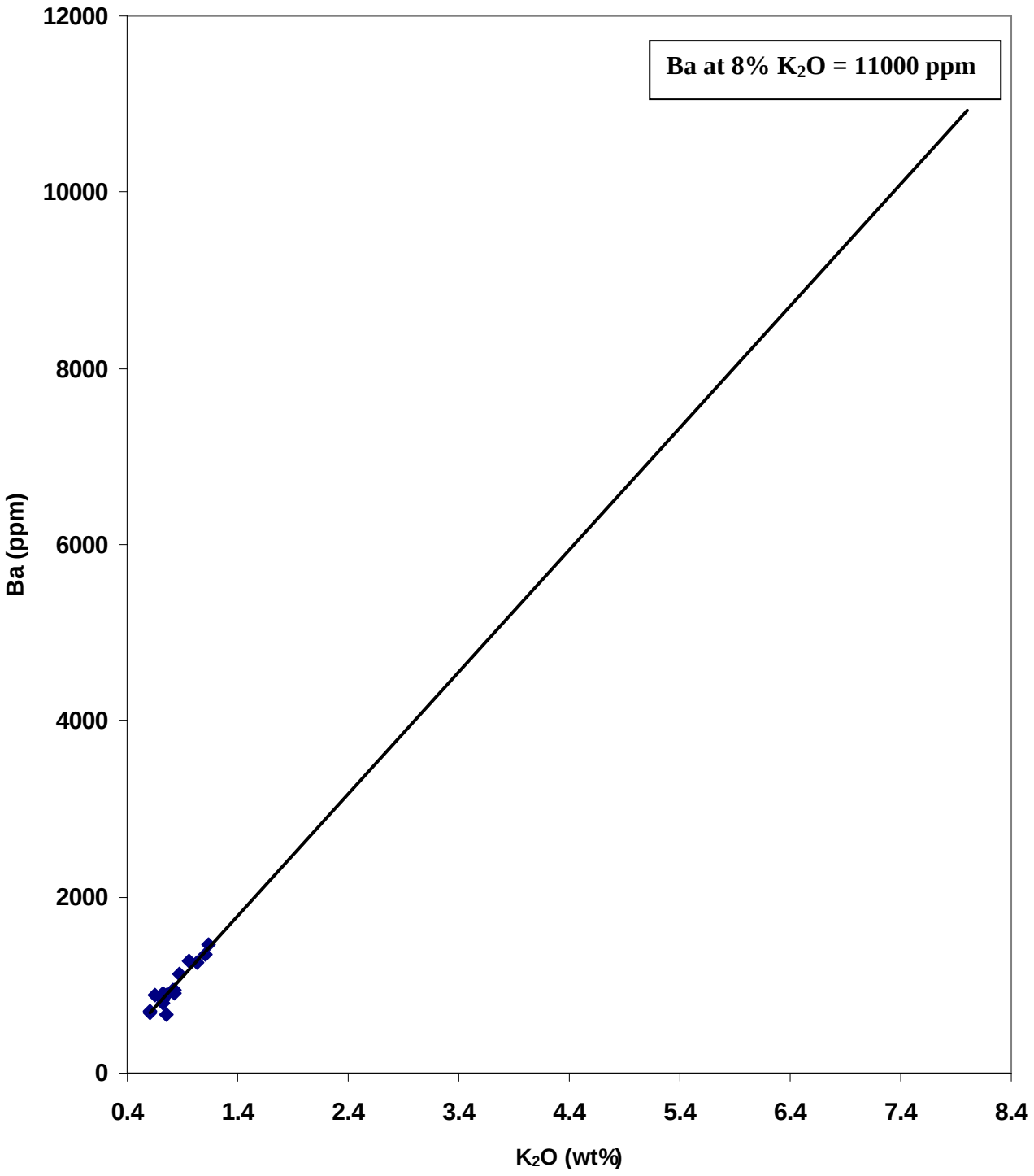


Fig. 4.6 Barium vs. K_2O from analyses. Samples which report high K_2O also have high Ba values hence contain significant alkali feldspar.

4.3. Major Element Trends

Results of major elements are presented in appendix C.

SiO_2 contents are generally between 53-60% (Fig. 4.7a). However, six samples at the top of the sequence have anomalous SiO_2 contents, signifying the presence of quartz in these samples which again could not be separated.

K_2O contents commonly vary between 0.2% and 0.6% (Fig. 4.7b) from the bottom up to about 1693 m where intercumulus alkali feldspar increases significantly in abundance. As a result, the K_2O contents of the analyses are affected because K_2O is a major constituent of alkali feldspar which cannot be separated from plagioclase magnetically. Thus K_2O contents from this level upwards are higher (up to 1.1%).

P_2O_5 contents are generally below 0.01 % (Fig. 4.7c). However, in samples taken from intervals in which apatite is present, P_2O_5 and CaO contents may be considerably higher.

Leaching and calculation techniques were developed to handle all these complications.

CaO and Al_2O_3 decrease from 12 % to 3.9% and from 28.7 % to 15.8 % respectively from the base to the top of UZ. Na_2O contents vary slightly irregularly from 4.4 % at the base to 7.3 % at the top of UZc.

The SiO_2 contents plotted in Fig. 4.7a are from XRF analyses on a fusion disc and the K_2O and P_2O_5 contents from XRF on pellet. It was felt that greater precision could be obtained, especially for P_2O_5, if analyzed on pressed pellets. Other oxides such as MnO, TiO_2, Cr_2O_3 and NiO have been excluded from the database because they do not concentrate in plagioclase; hence they report very low values.

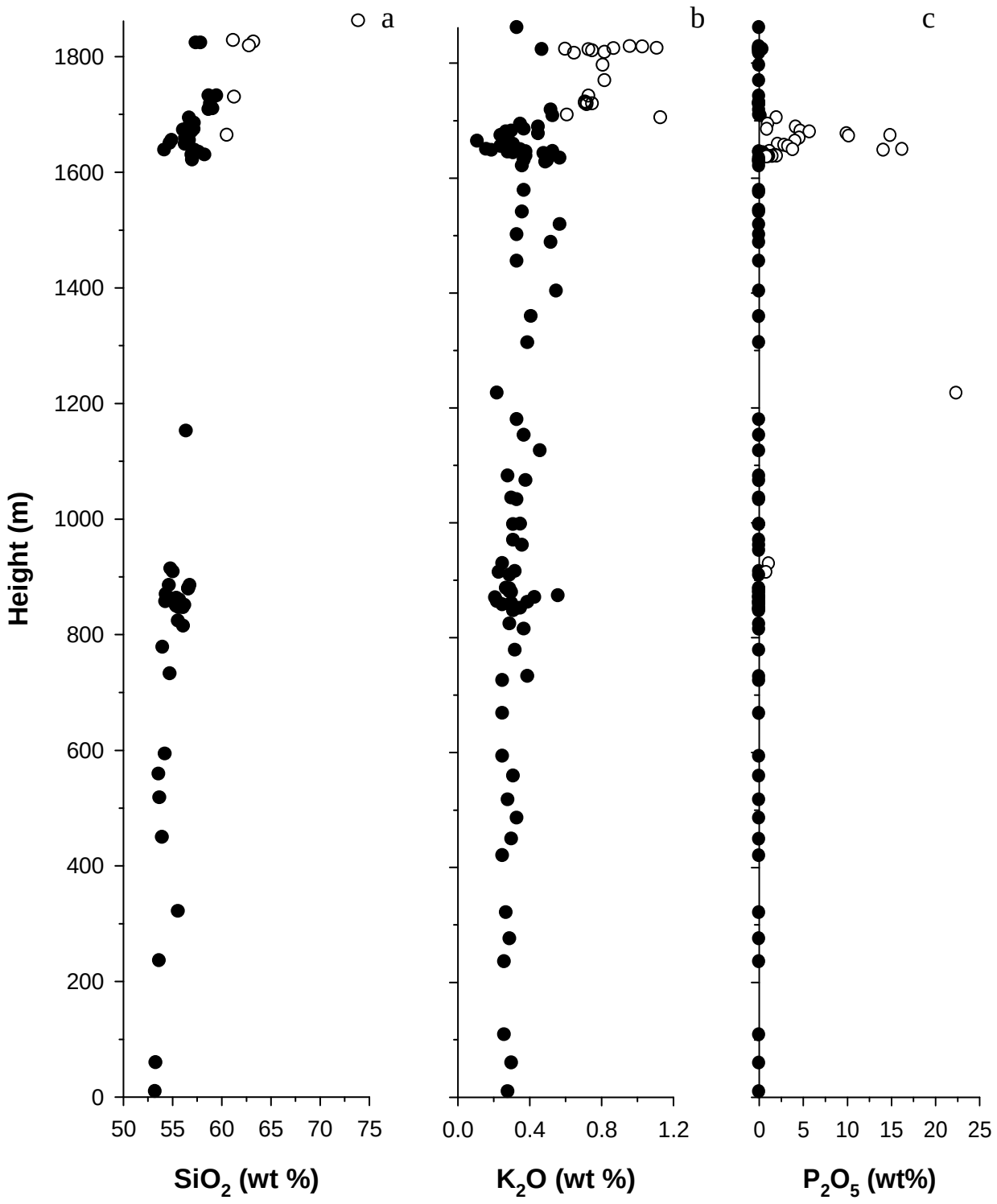


Fig. 4.7 SiO_2, K_2O and P_2O_5 contents from analyses of separates plotted against height. Empty circles are a) samples which contain quartz, b) samples that contain significant alkali feldspar and c.) Samples which contain apatite. The sections in b and c contain more samples than in section a because these plots are created from XRF analyses on pellets in which all samples were analyzed.

4.3.1. Anorthite Content of Plagioclase

After corrections have been made for the presence of apatite either by leaching or calculation or both, variation in An content is considerably reduced and samples plot within the general trends (Fig 4.8).

Plagioclase An contents of Upper Bushveld rocks have been shown to vary between 2 and 7% (Ashwal et al, 2005), 9% and up to 18 % in exceptional instances (Harney et al., 1995) within single thin sections. The large variation within grains suggests that abrupt sample to sample variations in the current dataset are inevitable. The average An contents of most samples have been shown to have a standard deviation of about 2% (Harney et al., 1990; Ashwal et al., 2005), hence only sample to sample changes >2% have been considered significant (Cawthorn and Ashwal, 2009) and the same principle is applied to the present study. Therefore, an analytical uncertainty of ±2 has to be accepted for these data.

Comparing An contents in this study with those of Tegner et al. (2006), the latter are slightly different from those reported here (Table 4.2). Such variations certainly result from a difference in microprobe (Tegner et al., 2006) and XRF (this study) methods used. Whereas the microprobe analyses were only of Ca-rich plagioclase cores, XRF analyses are a combination of cores and rims which could either be Na-rich or Ca-rich depending on the presence of normal or reverse zones (Cawthorn and Ashwal, 2009). If normal zones are present, the XRF method reduces the An content by incorporating a sodic rim. In cases where reverse zones occur, the rim will be Ca-rich. It would be worthwhile to investigate zoning patterns in the entire UZ in order to test this postulate. Furthermore, considering the general variability in UZ plagioclase compositions, only variations in An > 2% can be regarded as being actually different in the two methods used. Two out of 6 samples compared exceed this difference. In most cases, the data of Tegner et al. are greater than this study which may suggest that most grains display normal zoning.

Table 4.2.Comparison of anorthite content between samples common to this study and Tegner et al. (2006)

UZ height(m)	sample #	This study, An(%)	Tegner et al. (2006), An(%)	Difference (%)
9.2	1W1550P	60.0	60.7	0.7
558.4	3W540P	54.6	57.7	3.1
593.1	3W590P	54.0	55.4	1.4
732.0	3W742P	50.2	53.5	3.3
777.7	3W780P	49.5	49.8	0.3
814.2	3W1381.25P	49.9	48.5	-1.4

The An content changes abruptly between closely spaced samples in various sections within the stratigraphic section. For example, between 1672.5 and 1673.8 m, An contents vary by 2.3% (Fig. 4.8; appendix C). However, such variation is expected because of the large variation in An within single thin sections. This variation has been shown to result from the occurrence of reverse zones in plagioclase grains and the existence of low anorthite patches within plagioclase cores (Cawthorn and Ashwal, 2009).

Plagioclase changes in composition from An_{60} close to the base of UZ to An_{30} at the top of UZc (Fig. 4.8). The general up-section decrease in An in the Bushveld Upper Zone has previously been depicted (e.g. Wager and Brown, 1968; von Gruenewaldt, 1973; Molyneux, 1974; Ashwal et al., 2005; Tegner et al., 2006). However, reversals to higher An contents were detected by Tegner et al. (2006) and were used in conjunction with the intermittent occurrence of apatite to subdivide UZ into cycles. One aspect of the present study was focused on investigating the nature of the largest reversal identified in the former study. A total of 9 reversals can be identified by incorporating data from Tegner et al. (2006) with this study. Cycles 1 to 6 on Fig. 4.8 represent the cycles identified based on reversals to higher An content of plagioclase whereas the top three were identified based on the occurrence of apatite. The lowest reversal occurs at the Pyroxenite Marker and is not included in the section investigated in this study.

Close to the base of UZ at 9.3m, the An content decreases from 60.0 to 54.2% at 235 m, and decreases rapidly from this level to 46.4% at 321 m. The change in An of 7.8% over this 86 m interval is large and indicates that this could be an anomalous sample. The An

content then increases to 55.9% at 448.8 m and decreases fairly regularly to 48.2 at 846.2 m. This level marks the start of the biggest reversal which is later described in detail. Within the reversal (846.2 and 875m), the An content increases irregularly to 55.1. It then decreases regularly from 875 m to 46.5 at 1520.7 m. From this level to the top of the borehole (1861.6), then decreases rather erratically to 30%.

The biggest reversal in plagioclase An content encountered by Tegner et al. (2006) was also evident in this study. However, due to the fact that the reversals identified by Tegner et al. were on points analyzed in the stratigraphy, the detailed nature of this reversal (gradual or abrupt) could not be documented in that study. Out of the 6 reversals identified by Tegner et al., this reversal seemed to be the largest and most abrupt as it was perceived to occur only over 16.6 m (853.5 to 870.1 m) with the highest An change at 5.8%, unlike the others which were gradual (with changes in An of 3 to 4%), occurring over vertical distances of 28 to 69 m. However, more detailed sampling over this interval in the present study shows this reversal to occur over about 30 m of stratigraphy (between 846 and 875 m) and involving 11 samples (Fig 4.9). It is emphasized here that the precise start and end of the reversal are only approximate as the nearest sample just below the reversal (at 823 m) occurs 23 m below and that above the reversal occurs 4 m above. Hence, it is possible that the reversal could start below the level at which it is observed to begin or terminate above the level at which it is observed to do so.

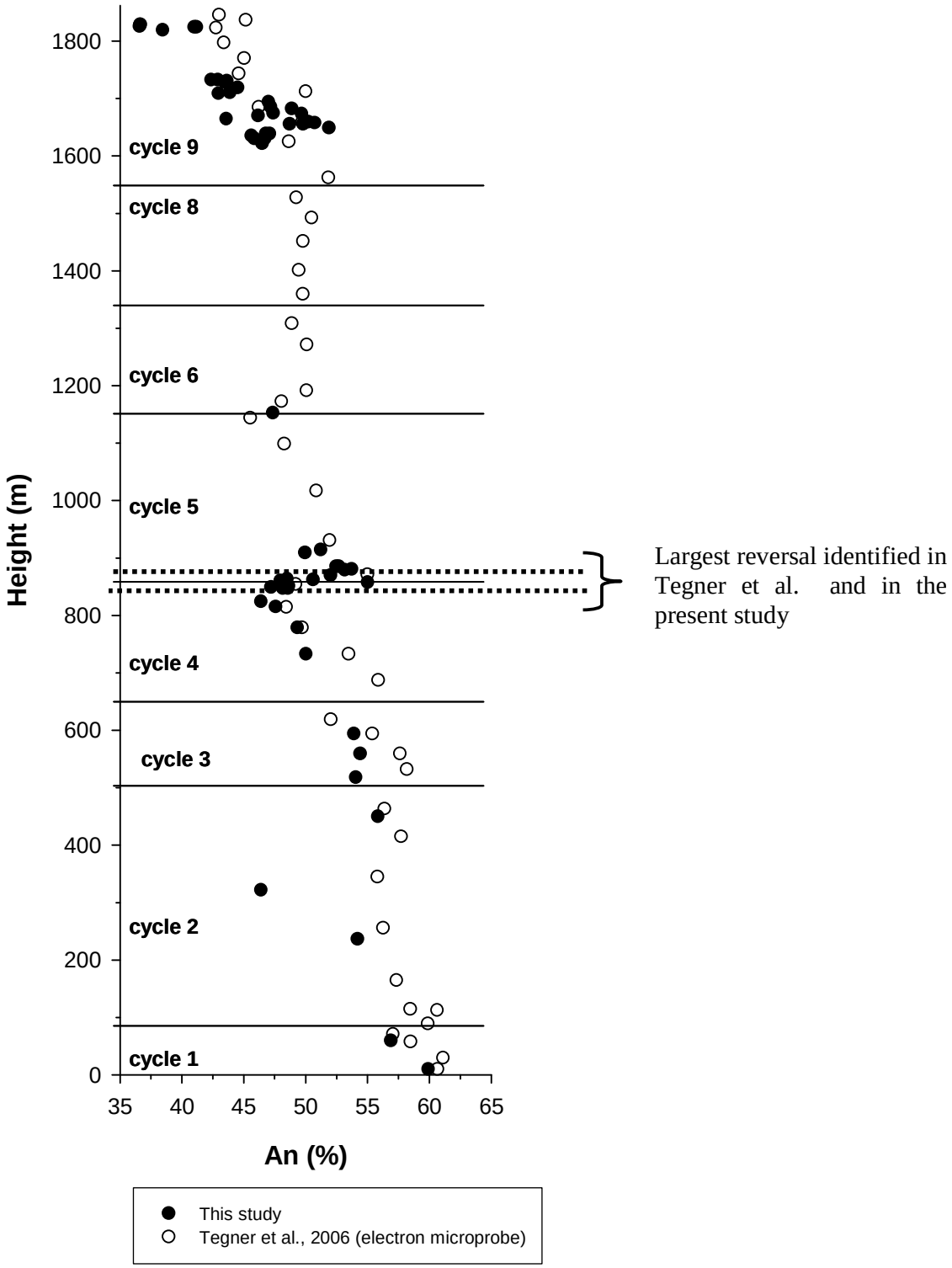


Fig. 4.8 Variation of plagioclase An content with Height in the Bierkraal drill cores. Data have been corrected for the presence of apatite by leaching or calculation and probe data are from Tegner et al. (2006). Location of cycles are from Tegner et al.

The An content increases from 47.3% to 55.1% within the reversal hence showing a total variation of 7.6% (Fig. 4.9a and b). From 846 to 856.7 m, the An increases from 47.3% to 55.1% and then deceases to 48% at 859.3 m where it varies erratically to 53.7% at 879.6 m. The An content at 856.7 m is high as the change in An% between the sample at this level and the nearest sample (6 m below) is 6% An. Fig. 4.9b shows the 820 to 880 m interval. The An varies within the ±2% uncertainty; indicating a slow reversal over the section. One sample plots outside the uncertainty; hence it is probably an anomalous sample.

The second biggest reversal in the data of Tegner et al. was also investigated at 1710 m. The section is shown in Fig. 4.10 and depicts a comparatively short vertical interval of 84 m over which certain remarkable features can be observed with the An variation. Twenty samples were analyzed from this section and show a total variation of 9.5% An. Considering a total change in An content over 1800 m of 30% An, this change is quite dramatic for a 30 m section. Therefore, the section illustrates a fairly rapid change in plagioclase An over a short vertical interval. The An contents plot within the ±2% uncertainty apart from the odd sample at 1663.7 m

Data from Tegner et al. (2006) show that the An content at 1711 m is 50.0%. This value leads to anticipation that there ought to be a reversal at this level since the An content has increased by 3.7% relative to the underlying sample. However, more detailed sampling in the present study suggests that this sample could just be an odd sample because the change in An is not sustained in the overlying samples which occur only within 21 m above it. Hence the reality of this reversal of Tegner et al. could be questioned.

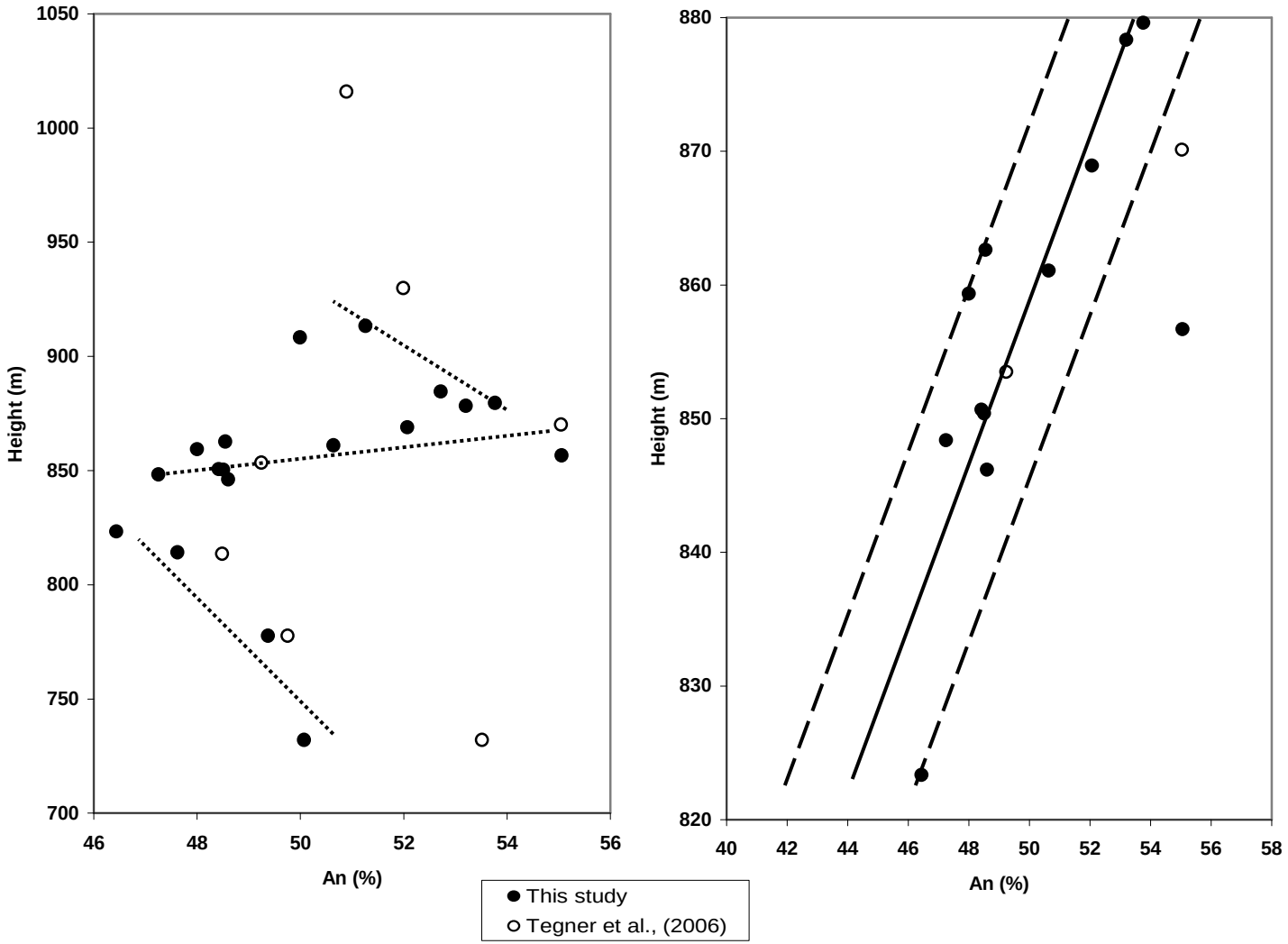


Fig. 4.9 Plot of An content in plagioclase versus height for the biggest reversal a) Section from 700 to 1050 m showing the most prominent reversal in plagioclase An. b) Section from 820 to 880 m; a best fit line (continuous) and 2% An uncertainty (dashed lines) are included.

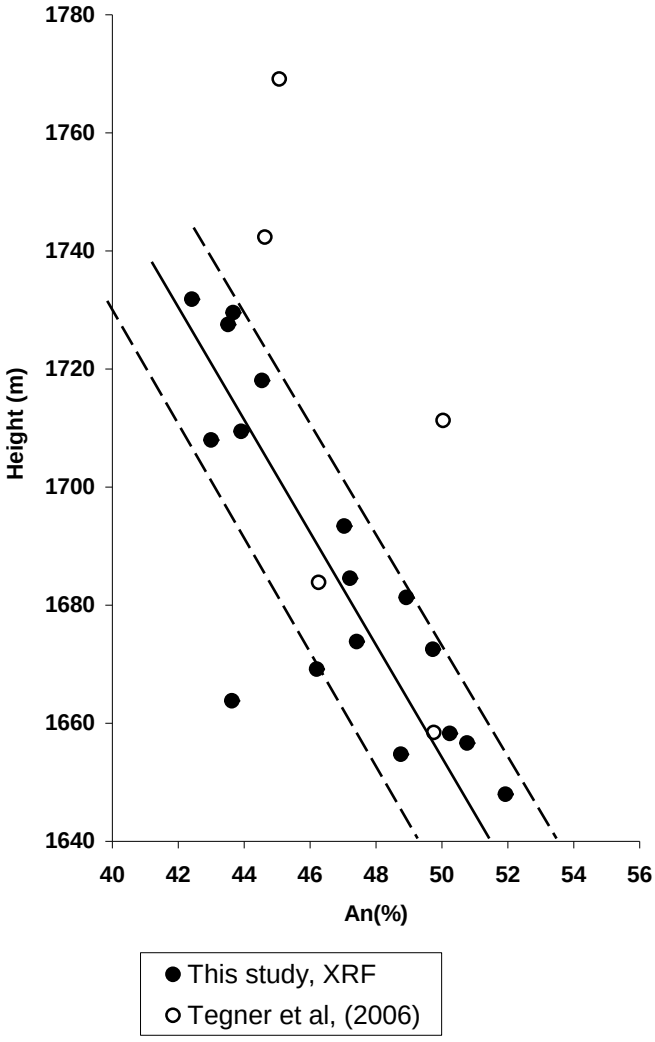


Fig. 4.10 Plot of An content in plagioclase vs. height for the section in which the second biggest reversal in the data of Tegner et al. occurs. The best fit line is indicated with a continuous line and 2% uncertainty on both sides indicated with dashed lines.

4.3.2. Summary

Generally, plagioclase An content in the Bushveld Upper Zone display the following features:

- An overall upward decrease from An_{60} close to the base to An_{30} at the top of the section.
- Reversals in the sequence which can be abrupt or gradual. The biggest reversal identified by Tegner et al. was perceived to be abrupt with a change in An of 5.8% between adjacent samples which were 16.6 m apart. However more detailed sampling in this study indicates that the reversal is gradual and the vertical intervals of reversals identified are only approximate. The reality of one more reversal in the data of Tegner et al. may be questioned.
- Sections showing little upward change in An. For example, within the interval 450 to 600 m, the An only changes by 2% (from 55.9% to 53.9%).
- Sections showing rapid upward decrease in An such as through the depth range 1640 to 1740 m in which the An changes by 9.5% (from 51.9% to 42.4%)
- Isolated anomalously high or low An values also occur in the stratigraphy. Three such samples were identified in the stratigraphy (at 321 m, 856.7 m and 1663.7 m). Trace element contents of these samples will be investigated for possible reasons for the anomalous An values.

4.4. Trace Element Geochemistry

This section presents trace element data for plagioclase separates for the Layered Series of the Skaergaard Intrusion and the Upper Zone of the Bushveld Complex. Trace element data for the Skaergaard intrusion were obtained from a study by Jang and Naslund (2001). For the reason that the Skaergaard intrusion is believed to have crystallized from a single magma injection, it ought to be comparatively simple and straight forward to model. Hence trace element data for this intrusion are utilized to develop and demonstrate the applicability of various fractionation models. Models can then be applied to the more complicated Bushveld Upper Zone in which parental magma compositions are harder to estimate.

Trace element studies were generally focused on Sr and Ba. Sr is strongly included in plagioclase. Even though Ba does not have a high affinity for plagioclase, it is more compatible into plagioclase compared to the other crystallizing phases. Plots comparing the Ba and Sr contents from the two methods (XRF and ICP) are presented in appendix A. Absolute values differ but it is more crucial to compare the relative changes. The linear correlation shows that relative changes in the Sr and Ba contents from the two methods are identical, hence the variation is real. The contents used in modeling are of the XRF because these analyses involved all samples in the stratigraphic section. Extensive use of the Rayleigh Law is made here, which includes the term F - fraction of liquid remaining, and so the graphs include values for F on the vertical axes.

4.4.1. The Skaergaard Intrusion

Sr and Ba trends for plagioclase are plotted in Fig 4.11 (Jang and Naslund, 2001). The fraction of magma remaining was calculated based on the percent crystallized which has been estimated by several authors (Wager and Brown, 1968; Jang and Naslund, 2001; Nielsen, 2004) from the stratigraphic height of samples. The chilled margin is assumed to represent 0% of crystallization, LZa 30% and the Sandwich Horizon 100%. The lowest sample of Jang and Naslund was collected from a height in LZa which corresponds to

36% of crystallization and the highest sample at the Sandwich Horizon. As the present study exploits Rayleigh fractionation models to constrain crystallization processes, this sample defines the base for these calculations and is given the value for F = 1, and the Sandwich Horizon a value of F=0. Multiple samples were taken along strike; these include 6 samples from the lower part of the Middle Zone (at 54% crystallized) and 3 samples from the upper part (at 72% crystallized).

Sr in plagioclase increases slowly from 400 ppm at F = 1 to about 600 ppm at F=0.1. It then increases rapidly to about 1300 ppm at the end of crystallization (Fig. 4.11a). Ba varies erratically between 79 ppm and 200 ppm throughout the sequence until 90% of crystallization (F= 0.1) where its concentration increases to 384 ppm and finally over 600 ppm at the end of crystallization (Fig 4.11b). In Fig 4.11, two y-axes values are shown, one for the entire intrusion (referred to as percent crystallized) and the section that can be modeled (referred to as F).

The general trend in plagioclase Sr and Ba is interrupted by some lateral variation in the contents. At the same stratigraphic heights, plagioclase trace element contents vary widely, e.g. at 54% crystallized, the Ba content of plagioclase varies from 78 to 149 ppm and the Sr content varies from 540 to 590 ppm.

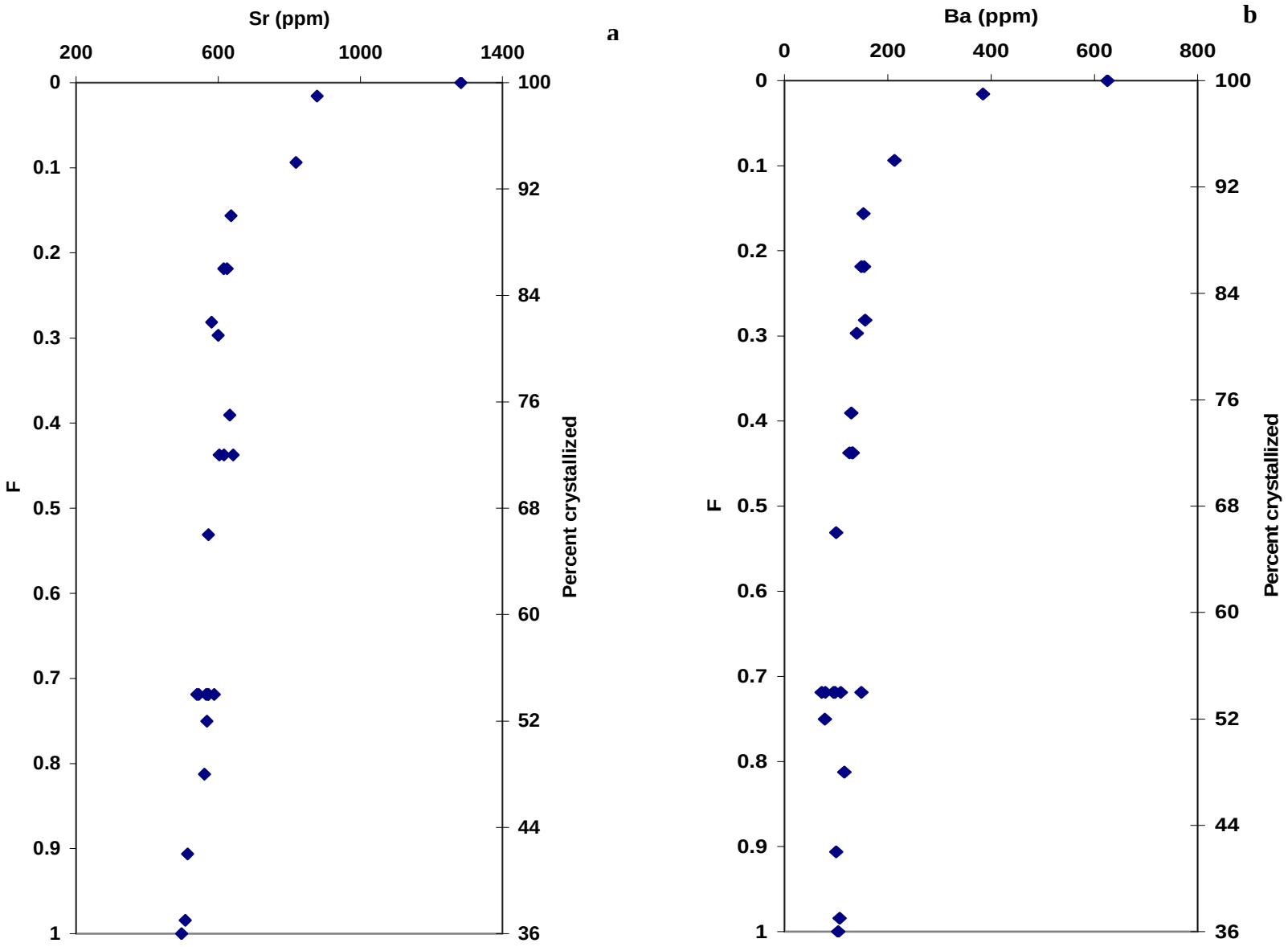


Fig. 4.11 Ba and Sr contents of plagioclase for the Skaergaard Layered Series.

4.4.2. The Upper Zone, Bushveld Complex

Analytical data for trace elements are presented in appendix C. These results are arranged in stratigraphic order. Once all corrections have been applied to the data and all data for which such corrections are too large or unconstrained have been excluded, the variations in Sr and Ba contents of plagioclase can now be presented. Figures 4.12 and 4.13 show these trends and these will be used for subsequent modeling.

4.4.2a. Strontium in plagioclase

About 400 ppm of Sr is present in plagioclase at the base of UZ, and it increases erratically till it attains a two fold increase towards the end of crystallization (Fig. 4.12a); a similar trend portrayed by Sr in plagioclase in the Skaergaard intrusion.

The general trend of plagioclase Sr seems to be interrupted by smaller fractionation cycles (Fig 4.12b). Six of these cycles seem to coincide with the ones identified by Tegner et al. (2006). Sample spacing in their study was however large (average 40 m) compared to the more closely spaced intervals in the present study, hence exact cycle boundaries differ. Smaller sample spacing allows for a more detailed assessment of cycle boundaries. Therefore, vertical intervals over which the cycles occur may differ slightly from those for Tegner et al. (2006). The possibility of these observed “breaks” to be fractionation cycles is further discussed in chapter six in terms of the magma chamber model proposed by Tegner et al.

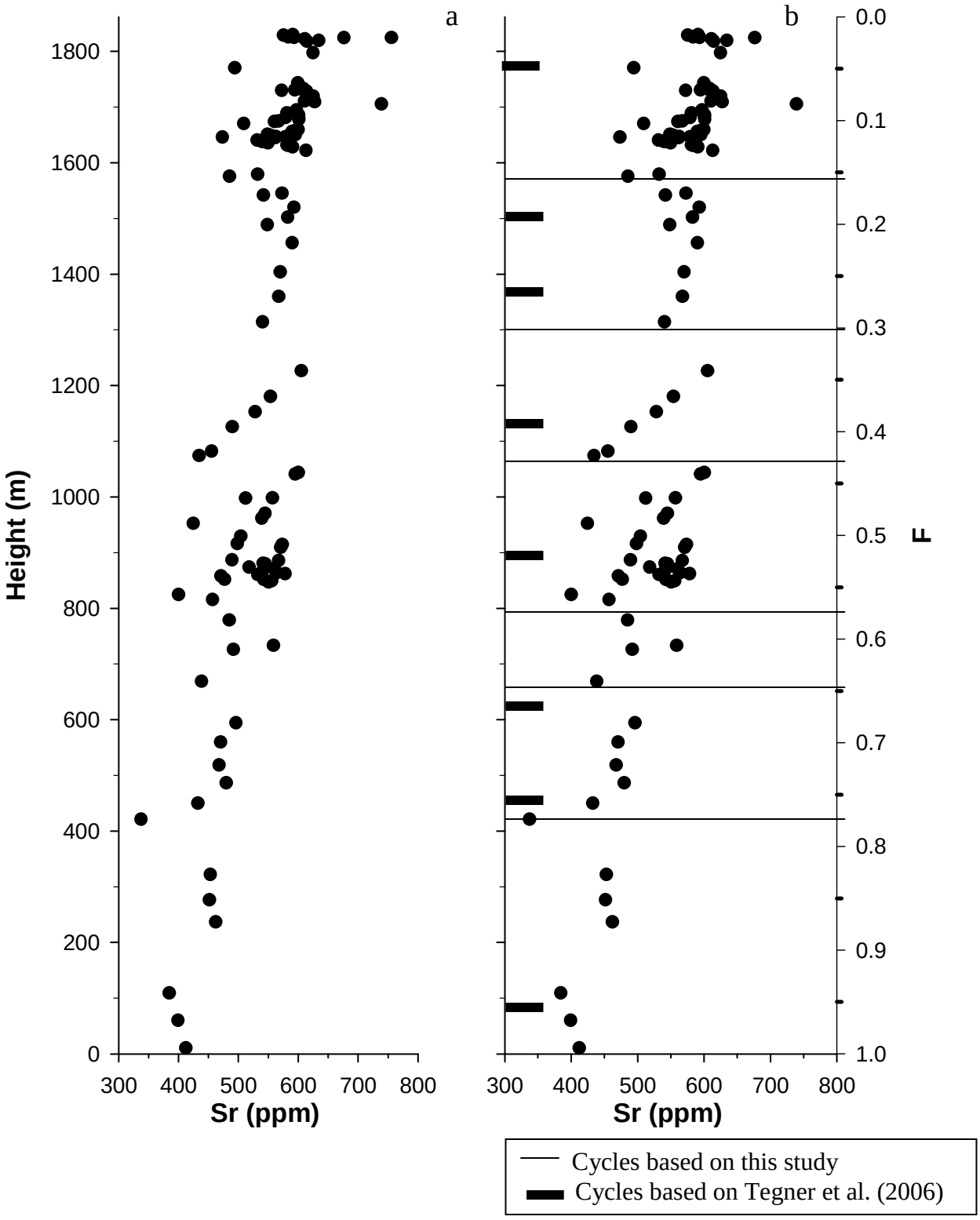


Fig. 4.12 Plots of Sr contents of plagioclase for the Upper Zone of the Bushveld Complex. Data have been corrected for the presence of apatite. Two y-axes values are shown, one for the height relative to the base of the Upper Zone and the section that can be modeled (referred to as F). The section in b includes fractionation cycles for the present study and for Tegner et al.

4.4.2b. Barium in Plagioclase

Ba contents of plagioclase in the Upper Zone are generally higher than the Skaergaard intrusion. However, they also vary irregularly, between 200 ppm to 500 ppm through most of the crystallization interval and only increase markedly after 90% of crystallization, that is at F= 0.15 (Fig. 4.13). There is large variation in the Ba contents of plagioclase between 1600 and 1700 m. Within this interval of 100 m, Ba varies between 300 and 600 ppm. For the reason that alkali feldspar occurs from 1693 m to the top and because its occurrence affects analytical results, only the lower 1693 m of the section were modeled.

The Sr and Ba concentrations of the three samples which reported anomalous An contents were investigated. The sample at 1663.7 m with anomalous An content reports very low Sr values and very high Ba content, hence it was excluded from subsequent models. The other two samples at 856.7 and 321m (with odd An contents) do not report anomalous Sr and Ba contents, hence they were included in the models. One sample containing anomalous Ba contents is present at 950.7 m and does not follow the normal fractionation trend. This sample also has low Sr contents at 426 ppm and was therefore excluded from our dataset as some contamination was suspected to have occurred.

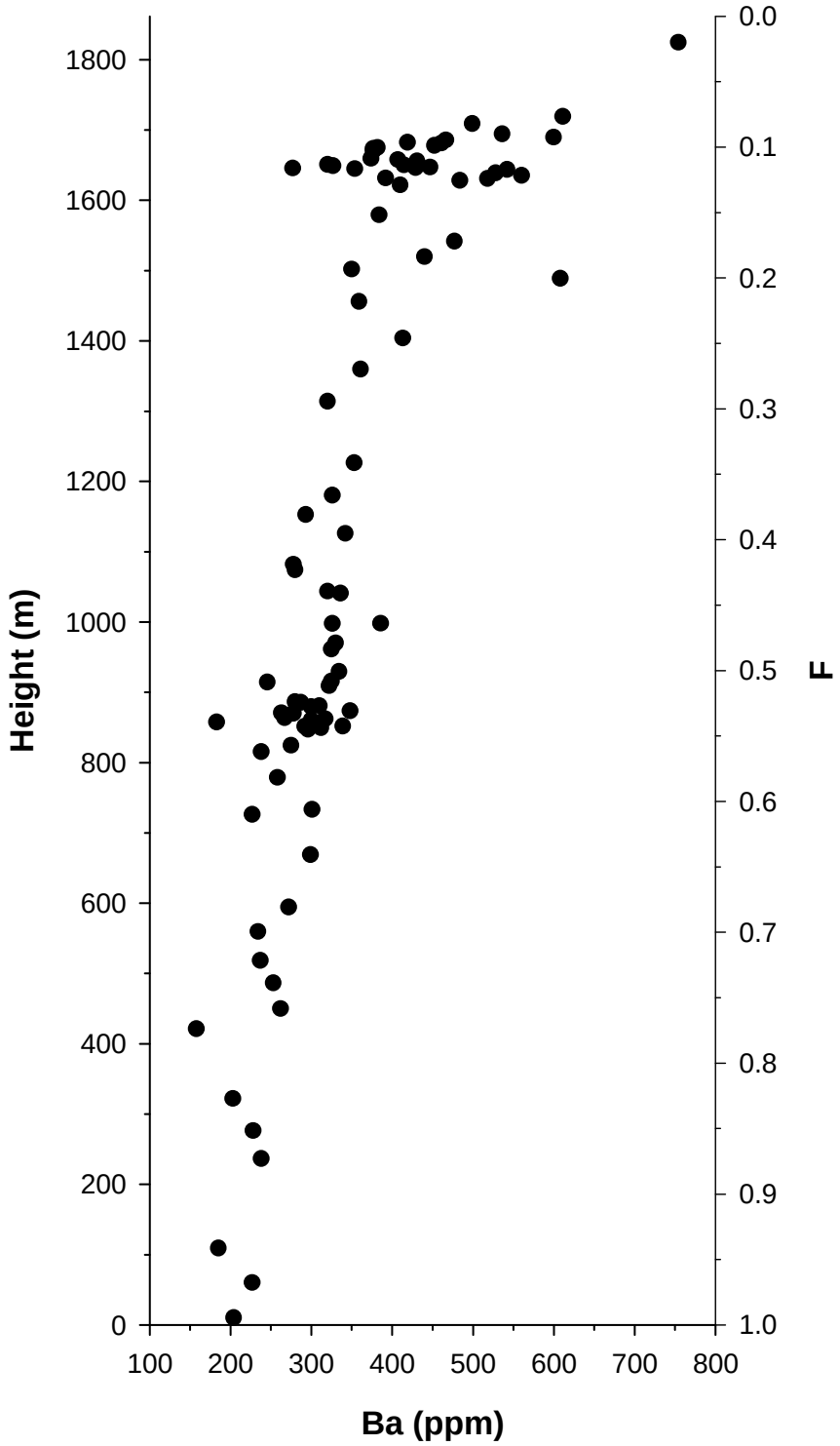


Fig. 4.13 Barium contents of plagioclase plotted against height for the Bushveld Upper Zone. Data exclude samples which contain significant alkali feldspar.

Chapter 5- Development of a Fractionation Model

5.1. Introduction

This section presents the steps involved in building up a model to infer crystallization processes including magma evolution, cumulus and post-cumulus processes within the Upper Zone of the Bushveld Complex . Sr and Ba data for plagioclase in the Skaergaard intrusion are therefore used to test various hypotheses for its evolution. The Skaergaard intrusion crystallized as a single differentiated series and is much more constrained; hence a model can be developed for its evolution and then related to the Bushveld Upper Zone.

5.1.1. Rayleigh Fractional Crystallization

Based on the processes occurring in a particular suite of rocks (e.g. fractional crystallization), trace elements behave in particular predictive ways (Cox et al., 1979). This behavior has been widely explored in igneous petrology and the most popular technique which has been developed to demonstrate the ways in which trace element concentrations are expected to change during fractional crystallization is the Rayleigh Fractionation Equation.

Over the years, the Rayleigh law (Equation 5.1) has proven useful in modeling the behavior of trace elements during fractional crystallization, therefore it ought to be capable of testing whether chemical analyses from a suite of rocks are consistent with the process of fractional crystallization.

$C_L/C_o=F^{(D-1)}$……. …… (5.1)

C_o= concentration of a trace element in the starting liquid

C_L= concentration of a trace element in the residual magma

F= Fraction of magma remaining. F begins at 1, representing the start of crystallization and decreases with increasing crystallization until it reaches zero.

D= The partition Coefficient of a trace element (D), given by Henry's Law

$$D = \frac{\text{Concentration in Mineral}}{\text{Concentration in Liquid}} \quad \ldots\ldots\ldots\

A rock may report modal proportions of 60% plagioclase and 40% mafic minerals. It is assumed in this calculation that 20% of liquid were trapped between the interstices of cumulus minerals during crystallization.

Cumulus plagioclase mode = Modal percent observed in rock – fraction of plagioclase formed from the trapped liquid.

If it is assumed that the trapped liquid crystallizes ½ plagioclase and ½ other minerals, then % cumulus plagioclase = 60- (20 * ½)

= 50%

Bulk D therefore becomes:

$$\text{Bulk D} = \{\{\text{Observed Percent of plagioclase} - (\text{(TL/2)/100})\} * D^{\text{Plagioclase}}\} + \{\{\text{Percent of all other Minerals} - (\text{the fraction that crystallizes from the trapped liquid})\} * D^{\text{All other minerals}} + \{(\text{TL\%/100}) * D^{TL}\} \quad \text{..... (5.4)}$$

For mafic minerals, the fraction that crystallizes from the trapped liquid can also be estimated. For example, in an assemblage consisting of plagioclase, cpx, opx, olivine and magnetite, the TL makes 50% plagioclase. The remaining 50% TL may make 25% cpx, 5% opx, 10% olivine and 10% magnetite.

The bulk D is of high importance in magmatic evolution since it establishes how strongly a particular element is removed from the liquid into the accumulating rock. If the bulk D is >1, the trace element gets depleted in the evolving magma, and hence also in the crystals forming with crystallization and vice versa. The most simplistic model for the evolution of a layered intrusion is to assume a homogenous magma chamber crystallizing a mineral assemblage of constant proportions, with constant partition coefficients and with a constant proportion of trapped liquid so that bulk D is constant throughout crystallization. However, these assumptions are totally invalid for natural situations because mineral assemblages, their proportions, trapped liquid fractions and partitioning change as magmas fractionate. It therefore becomes necessary to subdivide the crystallization into a very large number of small Rayleigh fractionation stages, and change any or all of these four variables at each stage.

5.1.2. The trapped liquid shift (TLS) effect

Subsequent to the accumulation of crystal grains during fractionation, and as post-cumulus processes occur, the composition of minerals is modified. This change in composition is quite significant for incompatible elements which concentrate in melts as crystallization progresses. Previous attempts have been made to quantify the extent of original cumulus modification, stipulating that the liquid remains trapped (e.g. Barnes, 1986; Cawthorn, 1996) and have identified it as the trapped liquid shift effect (Barnes, 1986). However, the TLS effect has been ignored by various authors in attempting to model the crystallization of layered intrusions (e.g. McBirney, 2002) and may lead to erroneous modeling and interpretations especially for incompatible elements.

It has been disputed whether the liquid does necessarily remain "trapped" (Irvine, 1980) particularly in the Merensky Reef of the Bushveld Complex (Mathez 1994) and might tend to migrate upwards making the assumption of trapped liquid crystallization invalid. However, the TLS effect was totally ignored in Mathez' study. Subsequently Cawthorn (1996) showed that incorporating the TLS effect led to changes in mineral composition which were previously attributed to migration of interstitial liquid.

The extent of the TLS effect is dependent on cumulus modes and trapped liquid fractions (Cawthorn, 1996). For example, consider a very simplistic and general situation in which a liquid contains 400 ppm Ba. There may be 50% plagioclase, 20% mafic minerals and 30% trapped liquid at the cumulus stage of crystallization(D_{Ba} into plagioclase is taken as 0.4, D_{Ba} into mafic minerals is taken as 0 and D_{TL} =1).
The original cumulus plagioclase will have (0.4* 400) =160 ppm Ba
In the rock, plagioclase would contribute (160* 50% plagioclase) = 80 ppm Ba
The trapped liquid will contribute (400ppm *30% trapped liquid) = 120 ppm Ba
The mafic minerals contribute 0 ppm Ba
Total Ba in rock = 80+120 =200 ppm

It is assumed that the trapped liquid crystallizes 50% plagioclase and 50% other minerals (with D_{Ba} = 0). Hence, the solidified rock will contain 65% plagioclase in total. It is assumed that diffusion homogenizes the Ba in the plagioclase.
The Ba in the rock must finally be incorporated into the 65% plagioclase. Hence Ba in the re-equilibrated plagioclase =200/.65 = 308 ppm

However, if the cumulus assemblage is 80% plagioclase and only 10% mafic minerals and 10% of trapped liquid, the calculation will yield a different result.
In the rock, plagioclase would contribute (160* 80% plagioclase) = 128 ppm
The trapped liquid will only contribute (400 ppm* 10% trapped liquid) = 40 ppm
Total Ba in rock = 128 + 40 = 168 ppm
At the consolidation stage, in which trapped liquid crystallizes, another 5% of plagioclase is formed increasing plagioclase mode to 85%
Ba in final re-equilibrated plagioclase = 168/.85 = 197 ppm

The above calculation shows that the trapped liquid shift effect is tremendous for an incompatible element such as Ba in plagioclase. This is evident from the significant difference in original cumulus (160 ppm) and re-equilibrated (308 and 197 ppm respectively) plagioclase contents depending on TL% and mode. This is because Ba, being incompatible into plagioclase tends to accumulate in the liquid and only crystallize during the consolidation stage and increase the re-equilibrated concentration. In the initial situation with less plagioclase and more trapped liquid, the enrichment of Ba in the final re-equilibrated plagioclase is much higher than the subsequent situation with a higher proportion of plagioclase and a comparatively minor amount of trapped liquid.

However, the TLS effect is minor for a compatible element such as Sr in plagioclase. In the following example, the effect of trapped liquid crystallization is shown. The Sr content of the liquid is taken as 300 ppm and the TLS effect is modeled for identical conditions as above, that is, 50% plagioclase, 20% mafic minerals (with D_{Sr}=0), 30% trapped liquid; and 80% plagioclase, 10% mafics, 10% TL. D_{Sr} in plagioclase is taken as 1.8 in the calculations.

In the first instance with 50% plagioclase, 20% mafics and 30% TL,
The original cumulus plagioclase will have (1.8* 300) =540 ppm Sr
In the rock, plagioclase would contribute (540* 50% plagioclase) = 270 ppm Sr
The trapped liquid will contribute (300ppm *30% trapped liquid) = 90 ppm Sr
Total Sr in rock = 270+90 =360 ppm
It is assumed that the trapped liquid crystallizes 50% plagioclase and 50% other minerals. Hence, the solidified rock will contain 65% plagioclase in total.
The Sr in the rock must finally be incorporated into the 65% plagioclase. Hence Sr in final re-equilibrated plagioclase =360/.65 = 554 ppm

However, if there is 80% plagioclase and only 10% mafic minerals and 10% of trapped liquid at the cumulus stage, in the rock, plagioclase would contribute up to (540* 80% plagioclase) = 432 ppm
The trapped liquid will only contribute (300 ppm* 10% trapped liquid) = 30 ppm
Total Sr in rock = 432 + 30 = 462 ppm. At the consolidation stage, in which trapped liquid crystallizes, another 5% of plagioclase is formed increasing plagioclase mode to 85%. Sr in final re-equilibrated plagioclase = 462/.85 = 544 ppm

The original cumulus plagioclase contains 540 ppm Sr and the final re-equilibrated contents are 554ppm and 544 ppm Sr in the two illustrations. This difference is extremely small compared to the huge variation between original cumulus and final re-equilibrated in Ba contents of plagioclase.

The change in plagioclase mode initiated during the consolidation stage suggests that trapped liquid crystallization not only changes mineral compositions but also increases mineral proportions. This implies that the mineral proportions observed in a rock are a combination of cumulus and intercumulus contributions and the TLS effect needs to be allowed for in calculating the proportion of plagioclase which actually accumulates during the cumulus stage and the concentration of plagioclase at the cumulus stage.This change in mineral proportion is further depicted in Fig. 5.1.

5.2. Modeling barium in plagioclase in the Skaergaard Intrusion

In this section, a fractionation model is developed which can be generally applied to layered intrusions. This is done by using plagioclase separate data in conjunction with suitable starting liquid compositions, partition coefficients, modal proportions and trapped liquid fractions.

The Ba and Sr concentrations presented by Jang and Naslund (2001) for trace elements in plagioclase in the Skaergaard intrusion and plotted in Fig. 4.11 were not modeled in their study. Data for trace elements in plagioclase were also presented by McBirney (2002) and were modeled but required some unusual D values (D_{Ba} between 0.3- 0.08 and D_{Sr} between 1.2 and 0.5). The purpose of the step-like models presented in this section is to develop a model for the crystallization of the Skaergaard intrusion. The effects of varying Ds, mineral proportions and trapped liquid fractions during fractionation are also explored. Sr and Ba are utilized in modeling because Sr partitions relatively largely into plagioclase, the most abundant cumulus mineral in the Skaergaard intrusion and is essentially excluded from all other minerals (except for Sr into apatite). Ba does not have a high affinity for plagioclase but is least incompatible into plagioclase compared to the other crystallizing phases in the intrusion.

For the purpose of modeling, plagioclase proportions and TL fractions were taken from Tegner et al. (2009). Their study showed plagioclase modes and TL fractions in Skaergaard rocks to change from 55% to 33% and 45% to 4% from bottom to top of the intrusion. However, in order to successfully model the crystallization of the intrusion, the cumulus mode must be estimated.

For example, the rock from the bottom (LZa) has been shown to contain 55% observed plagioclase and to have crystallized with 45% trapped liquid. A reasonable cumulus mode can be estimated from these modal data as follows.

During consolidation which involves the crystallization and equilibration of trapped liquid, the trapped liquid crystallizes 50% plagioclase and 50% other minerals. Therefore, 45% TL would crystallize about 22% plagioclase and 23% mafic minerals.

Thus, the amount of cumulus plagioclase is only 55%-22% = 33% cumulus plagioclase.

For simplicity, a smooth change is assumed for each parameter. As it will be shown in section 5.3, varying D_{Ba} in plagioclase within the range of published values does not have a huge effect on Bulk Ds and modeled concentrations. Therefore a constant D for Ba in plagioclase of 0.4 is used in the first models throughout crystallization. It is emphasized that modeling by means of simplistic Rayleigh fractionation cannot be used for the Skaergaard intrusion because trapped liquid fractions change with crystallization hence bulk D changes as well..

The fraction of magma remaining (F) was calculated from the percentage of crystallization for the entire intrusion, thus providing a means for the intrusion to be divided into small Rayleigh fractionation steps (with F=1 and F= 0 representing the start and the end of crystallization respectively). However, it should be noted that this fraction (F) records progressive changes over considerable distances and there is no proof that samples were collected right up to the extreme differentiates of the intrusion. It is not possible to determine what rocks represent the extreme end of differentiation (that is, when F approaches zero). Also, all Rayleigh fractionation models become asymptotic towards the end and extreme concentrations result, whereas probably other minerals begin to crystallize, changing the bulk D dramatically. Hence, the calculations are terminated at F= 0.09. The magma composition ought to change with crystallization; hence the starting liquid composition of each subsequent step (C_o) would equal the calculated residual liquid composition of the previous step (C_L). At each increment of crystallization, new values for plagioclase mode and TL fraction are incorporated. The results of these calculations are shown in the ensuing tables. No fractionation occurs between the samples taken from the same level of fractionation (e.g. 54% crystallized). Hence F^1 is shown as 1 and C_L and Ba in plagioclase (calculated) do not change.

5.2.1. Rayleigh Fractionation of Ba contents in plagioclase

Based on the Rayleigh model (equation 5.1), Ba contents of plagioclase can be modeled with the following steps.

5.2.1.a Modeling with the starting liquid content (C_o) from the equation $D=C_M/C_L$

Step 1: Ba concentration of the starting Liquid (C_o)

Trace element contents of minerals can be used to calculate the contents of the magma from which the minerals crystallized with the use of partition coefficients. Therefore, if the Ba content of plagioclase at 36% crystallized (taken as F=1 for these calculations) is 104 ppm, the use of equation (5.2) with a partition coefficient of 0.4 (Rollinson, 1993) will result in 260 ppm Ba in the liquid.

Step 2: Bulk partition coefficient:

If plagioclase mode ≈ 55% and trapped liquid 45% at this level (Tegner et al., 2009), this will lead to 33% cumulus plagioclase (for which D_{Ba} in plagioclase ≈ 0.4), 22% mafic minerals (D_{Ba} in mafics = zero) and 45% TL. Since the trapped liquid is assumed equal to the instantaneous magma composition, it is considered as another phase with D_{TL}= 1.

That is, Bulk D = ((33/100) * 0.4) + ((22/100)* 0) + (45/100 *1) = 0.58

Modeling in the present study was commenced at this level, hence F=1. Progressive steps are modeled using F^1 (for each individual step of fractionation), a constant D of 0.4 and variable cumulus plagioclase mode from 33 to 31% and trapped liquid from 45 to 4% from the bottom to top. However, calculated Ba contents of plagioclase increase by a factor of five (from 104 to 559 ppm) from F=1 to F= 0.09 (Table 5.1) whereas analytical data only increase by a factor of 2 (that is, from 104 to 213 ppm) within the same interval. Hence, there are two major contradictions in modeling the crystallization of the Skaergaard intrusion using this method; the calculated starting liquid content (C_o) is more than two times higher than the typical value and modeled Ba contents of plagioclase increase outstandingly contrary to analytical data.

Table 5.1. Calculated trends based on Rayleigh fractionation, incorporating varying TL and plagioclase mode

Zone	% cryst.	F	F^1	Plag mode	TL %	Cumulus Plag mode	Bulk D	$C_{L(}$ppm)	Calc. Ba in Plag. (ppm)	Observed Ba (ppm)
SH	100	0.00	0.00	33	4	31	0.16			625
UZc	99	0.02	0.17	33	4	31	0.17	6235	2494	384
UZc	94	0.09	0.60	35	5	33	0.18	1397	559	213
UZb	90	0.16	0.71	36	7	33	0.20	919	368	153
UZb	86	0.22	1.00	38	9	33	0.22	703	281	154
UZb	86	0.22	0.78	38	9	33	0.22	703	281	149
UZb	82	0.28	0.95	39	12	33	0.25	578	231	156
UZa	81	0.30	0.76	40	13	33	0.26	555	222	140
UZa	75	0.39	0.89	42	18	33	0.31	453	181	129
MZ	72	0.44	1.00	43	20	33	0.33	419	168	126
MZ	72	0.44	1.00	43	20	33	0.33	419	168	132
MZ	72	0.44	0.82	43	20	33	0.33	419	168	131
MZ	66	0.53	0.74	45	26	32	0.39	368	147	100
MZ	54	0.72	1.00	49	34	32	0.47	306	122	79
MZ	54	0.72	1.00	49	34	32	0.47	306	122	98
MZ	54	0.72	1.00	49	34	32	0.47	306	122	72
MZ	54	0.72	1.00	49	34	32	0.47	306	122	109
MZ	54	0.72	1.00	49	34	32	0.47	306	122	95
MZ	54	0.72	0.96	49	34	32	0.47	306	122	149
LZc	52	0.75	0.92	50	35	32	0.48	299	120	78
LZb	48	0.81	0.90	51	38	32	0.50	287	115	116
LZb	42	0.91	0.92	53	41	32	0.54	272	109	100
LZb	37	0.98	0.98	55	44	32	0.57	262	105	107
LZa	36	1.00	1.00	55	45	33	0.58	260	104	104

% crystallized are values given by Jang and Naslund (2001) based on the entire Skaergaard Intrusion

F = Fraction of magma remaining using deepest sample as C_o, F=1

F^1= value of F used for each step

Plag mode and TL% are set to vary smoothly from the start to end of crystallization

Cumulus plag mode: Plagioclase proportion during the cumulus stage and used in calculating the bulk D.

C_L : Ba concentration in the liquid

Calc. Ba in plag: Resultant Ba content of plagioclase calculated from the model

Observed Ba = Ba in plagioclase from analyses of Jang and Naslund (2001)

5.2.1. b Modeling with the typical Ba content of the Skaergaard parental magma.

As previously indicated, various authors have calculated the Ba content of the original Skaergaard magma (C_o) to be between 50 to 90 ppm (e.g. Nielsen, 2004). This amount can be substituted in the Rayleigh law and progressive steps modeled, similar to section 5.1.1.

Step1: Ba concentration of the starting Liquid (C_o)

Based on Rayleigh fractionation, the Ba content of the liquid at LZa (F = 1) ought to be about 100 ppm, taken as C_o as defined here.

Step 2: Bulk Partition coefficient:

Bulk D = ((33/100) * 0.4) + ((22/100)* 0) + (45/100 *1) = 0.58

Step 4: Ba concentration of plagioclase.

Ba content of plagioclase = D(plagioclase) * Ba content of liquid (C_L)

= 0.4 * 100 = 40 ppm Ba

The results obtained from modeling progressive steps are presented in Table 5.2. Calculated Ba content of plagioclase is 40ppm at F = 1. It then attains a five fold increment (215 ppm) at F=0.09.

Table 5.2.Calculated trends based on Rayleigh Fractionation with the typical Ba content of starting liquid

Zone	% cryst	F	F^1	Plag mode	TL %	Cumulus Plag mode	Bulk D	$C_{L(}$ppm)	Calc. Ba in plag. (ppm)	Observed Ba (ppm)
SH	100	0.00	0.00	33	4	31	0.16			625
UZc	99	0.02	0.17	33	4	31	0.17	2398	959	384
UZc	94	0.09	0.60	35	5	33	0.18	537	215	213
UZb	90	0.16	0.71	36	7	33	0.20	354	141	153
UZb	86	0.22	1.00	38	9	33	0.22	270	108	154
UZb	86	0.22	0.78	38	9	33	0.22	270	108	149
UZb	82	0.28	0.95	39	12	33	0.25	222	89	156
UZa	81	0.30	0.76	40	13	33	0.26	214	85	140
UZa	75	0.39	0.89	42	18	33	0.31	174	70	129
MZ	72	0.44	1.00	43	20	33	0.33	161	65	126
MZ	72	0.44	1.00	43	20	33	0.33	161	65	132
MZ	72	0.44	0.82	43	20	33	0.33	161	65	131
MZ	66	0.53	0.74	45	26	32	0.39	142	57	100
MZ	54	0.72	1.00	49	34	32	0.47	118	47	79
MZ	54	0.72	1.00	49	34	32	0.47	118	47	98
MZ	54	0.72	1.00	49	34	32	0.47	118	47	72
MZ	54	0.72	1.00	49	34	32	0.47	118	47	109
MZ	54	0.72	1.00	49	34	32	0.47	118	47	95
MZ	54	0.72	0.96	49	34	32	0.47	118	47	149
LZc	52	0.75	0.92	50	35	32	0.48	115	46	78
LZb	48	0.81	0.90	51	38	32	0.50	110	44	116
LZb	42	0.91	0.92	53	41	32	0.54	105	42	100
LZb	37	0.98	0.98	55	44	32	0.57	101	40	107
LZa	36	1.00	1.00	55	45	33	0.58	100	40	104

Problems with the method

The calculated Ba content of plagioclase at the level of LZa is only 40 ppm compared to 104 ppm from analyses of Jang and Naslund. (2001). Forward modeling of progressive steps using the Rayleigh Law leads to a five fold increment in the calculated Ba content of plagioclase from F=1 to F= 0.09 (that is from 40 to 215 ppm) whereas analytical data only increase by a factor of 2 (Table 5.2). This implies that modeling the intrusion based on Rayleigh fractionation and using the conventional Ba content of liquid also disagrees with analytical data.

5.2.2. Incorporation of the trapped liquid shift (TLS) effect

The trapped liquid shift effect allows for the combination of original cumulus compositions with a composition of the mineral that might form from the intercumulus liquid to calculate re-equilibrated compositions. If the liquid at LZa has 100 ppm Ba (calculated from Nielsen's parental magma), then the original cumulus plagioclase would have 40 ppm Ba. The original cumulus plagioclase refers to the composition of plagioclase when it first crystallized from the liquid whereas the re-equilibrated composition refers to the composition of the plagioclase when it finally crystallizes, that which is now observed in the rock (Cawthorn, 1996).

Step1: Ba concentration of the starting Liquid (C_o)

The Ba content of the liquid at LZa (that is F = 1) is 100 ppm

Step 2. Ba concentration of original cumulus plagioclase

Ba in the original cumulus plagioclase is 40 ppm

Step 3. Ba in rock from intercumulus contribution

This represents the Ba in the whole- rock analysis resulting from the consolidation stage, as the trapped liquid crystallizes. This is given by (Trapped Liquid Fraction/100) * Ba in the liquid

= (45/100) * 100 = 45 ppm

Step 4. Ba in rock from cumulus minerals.

It is assumed that plagioclase is the only cumulus mineral in which Ba is included because even though D_{Ba} in plagioclase is less than unity, D_{Ba} for all other cumulus phases are much less, hence they contribute a very negligible amount to total Ba in the rock and can be ignored.

Hence Ba from cumulus minerals = Ba in cumulus plagioclase * (percent plagioclase in cumulus phase / 100), that is, 40 * (33/100) = 13 ppm

Step 5. Total Ba in rock

This is given by the amount of Ba in rock from cumulus minerals + Ba in rock from intercumulus contribution. This is 45 + 13 = 58 ppm

Step 6. Ba in re-equilibrated plagioclase

At the consolidation stage in which trapped liquid crystallizes, incompatible elements which were formerly concentrated in the melt have to be distributed between the solidified minerals.
The total Ba in rock must finally be incorporated into the 55% plagioclase, because other minerals concentrate essentially no Ba.
That is, 58/ (55/100) =105 ppm Ba in plagioclase). The plagioclase proportion increases from 33 to 55% and the Ba content changes from 40 in the original cumulus plagioclase to 105 ppm in the re-equilibrated plagioclase (Fig. 5.1).

This calculated re-equilibrated Ba composition (105 ppm) of plagioclase is in much better agreement with analyzed data (104 ppm) than values calculated in the previous models. This model depicts two important issues; the original cumulus and re-equilibrated compositions for an incompatible element such as Ba can differ by a factor of nearly three in cumulus and re-equilibrated plagioclase (Fig. 5.1). as the original cumulus plagioclase contains 40 ppm Ba, which increases to 105 ppm Ba at the consolidation stage. This change in composition is due to the trapped liquid shift (TLS) effect. The TLS effect has generally been ignored in studies in which the crystallization of layered intrusions is modeled (e.g. Henderson, 1970; McBirney, 2002; Tegner et al., 2009). However, the enormous difference between original cumulus and final re-equilibrated compositions of Ba imply that the TLS effect must be allowed for in modeling the evolution of layered intrusions.

Forward modeling of progressive steps leads to a three fold increment in Ba in the calculated re-equilibrated plagioclase from F=1 to F=0.1, which is quite similar to the increase in Ba in analyzed plagioclase (Table 5.3; Fig. 5.2c). The model shows that by using the conventional Ba content of starting liquid for the Skaergaard intrusion in the Rayleigh law and allowing for the TLS effect as shown in section 5.2.2, a consistent model can be derived for calculating the change in Ba in plagioclase for the Skaergaard intrusion.

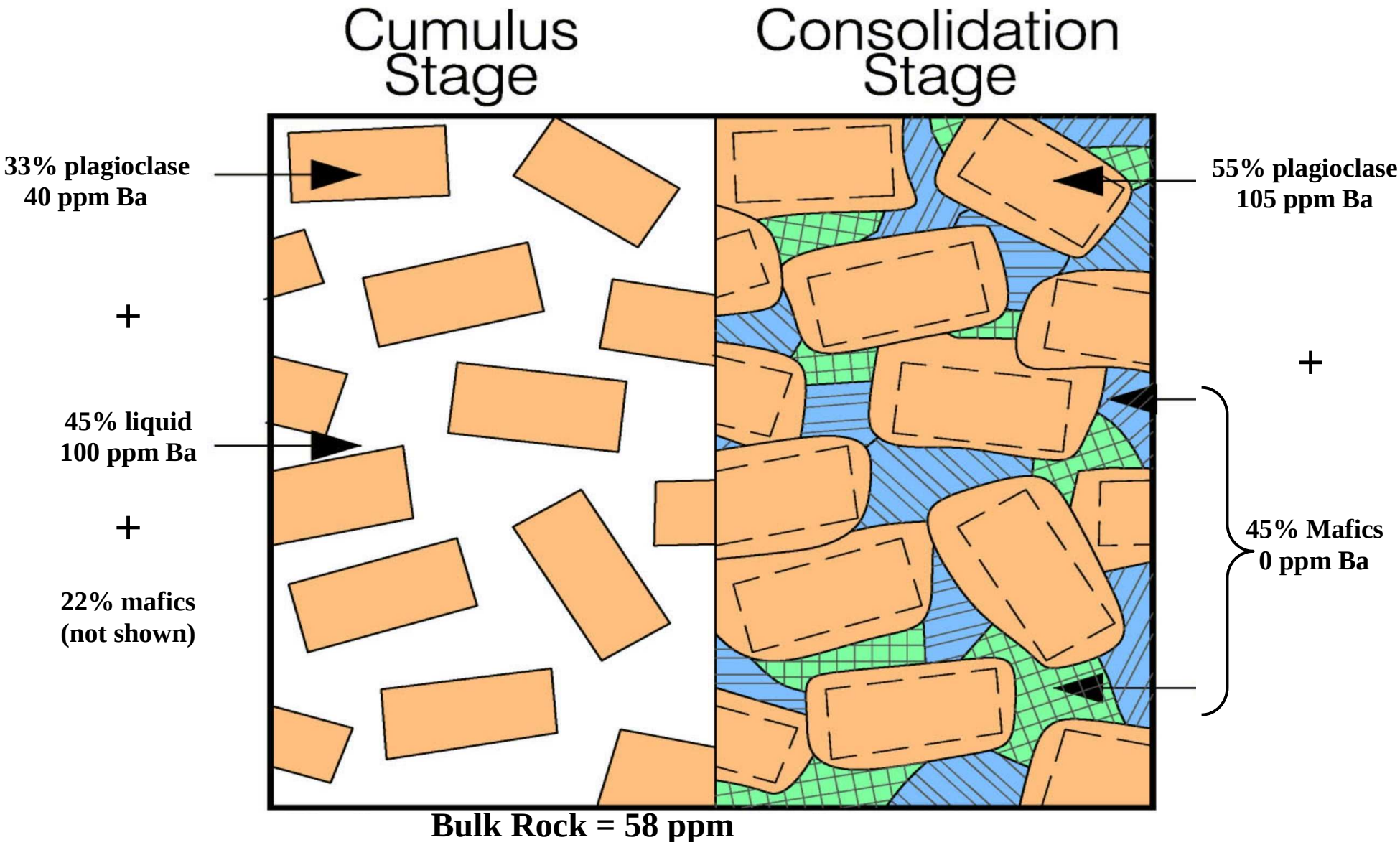


Fig. 5.1 Trapped Liquid Shift effect for barium in plagioclase showing its enormous effect. Original cumulus and re-equilibrated compositions differ by a factor of nearly three.

Table 5.3.Calculated trends based on Rayleigh fractionation with the typical Ba content of starting liquid and allowing for the trapped liquid shift effect.

Zone	% cryst	F	F^1	Plag mode	TL %	Cumulus Plag mode	Bulk D	C_L(ppm)	Ba in cumulus plagioclase (ppm)	Ba in bulk rock	Ba in re-equilibrated plagioclase (ppm)	Observed Ba in plagioclase(ppm) (Jang and Nalund, 2001)
SH	100	0.00	0.00	33	4	31	0.16					625
UZc	99	0.02	0.17	33	4	31	0.17	2398	959	397	1189	384
UZc	94	0.09	0.60	35	5	33	0.18	537	215	97	276	213
UZb	90	0.16	0.71	36	7	33	0.20	354	141	71	196	153
UZb	86	0.22	1.00	38	9	33	0.22	270	108	60	160	154
UZb	86	0.22	0.78	38	9	33	0.22	270	108	60	160	149
UZb	82	0.28	0.95	39	12	33	0.25	222	89	56	143	156
UZa	81	0.30	0.76	40	13	33	0.26	214	85	56	142	140
UZa	75	0.39	0.89	42	18	33	0.31	174	70	54	130	129
MZ	72	0.44	1.00	43	20	33	0.33	161	65	53	125	126
MZ	72	0.44	1.00	43	20	33	0.33	161	65	53	125	132
MZ	72	0.44	0.82	43	20	33	0.33	161	65	53	125	131
MZ	66	0.53	0.74	45	26	32	0.39	142	57	55	123	100
MZ	54	0.72	1.00	49	34	32	0.47	118	47	55	112	79
MZ	54	0.72	1.00	49	34	32	0.47	118	47	55	112	98
MZ	54	0.72	1.00	49	34	32	0.47	118	47	55	112	72
MZ	54	0.72	1.00	49	34	32	0.47	118	47	55	112	109
MZ	54	0.72	1.00	49	34	32	0.47	118	47	55	112	95
MZ	54	0.72	0.96	49	34	32	0.47	118	47	55	112	149
LZc	52	0.75	0.92	50	35	32	0.48	115	46	55	111	78
LZb	48	0.81	0.90	51	38	32	0.50	110	44	56	109	116
LZb	42	0.91	0.92	53	41	32	0.54	105	42	57	107	100
LZb	37	0.98	0.98	55	44	32	0.57	101	40	58	106	107
LZa	36	1.00	1.00	55	45	33	0.58	100	40	58	105	104

Modeling of the Sr and Ba contents of plagioclase of the same section was performed by McBirney (2002). However, some atypical D values were used in modeling based on the view that trace elements in plagioclase do not conform to the process of fractional crystallization. A reassessment of Ba contents of bulk rock and plagioclase quoted in that study indicates that the Ba contents quoted for plagioclase do not agree with Ba contents of bulk rock. For example the average values quoted for Ba in bulk rock and plagioclase for LZa are 62ppm and 3.8 ppm respectively. The lower zone consists of plagioclase (for which $D_{Ba} \approx 0.3\text{-}0.6$), olivine (for which $D_{Ba} \approx 0$), augite (for which $D_{Ba} \approx 0$) and inverted pigeonite (for which $D_{Ba} \approx 0$). If only 3.8 ppm of the total 62 ppm bulk rock Ba concentrates in plagioclase for which D_{Ba} is highest, the rest of the 58 ppm Ba are unlikely to concentrate in any of the remaining three minerals because of the very small affinities for barium.

The erroneous Ba contents of plagioclase led to the use of unusual D values for Ba and Sr in plagioclase. D_{Ba} in plagioclase was shown to decrease uniformly from 0.3 to 0.08 and D_{Sr} in plagioclase to decrease irregularly from 1.2 to 0.5. Basically calculating a bulk D from these D values would lead to anticipation that Ba and Sr contents of plagioclase ought to increase very significantly with crystallization, an expectation which is contrary to the observed Ba and Sr concentrations in plagioclase. Modeling of the section using the Ba contents of plagioclase from Jang and Naslund (2001) with the steps presented in section 5.2.2 shows that the observed Ba contents of plagioclase in the Skaergaard intrusion can be produced by normal fractional crystallization, by using the Rayleigh law and incorporating the trapped liquid shift effect (Fig. 5.1). The Ba contents of plagioclase also agree with bulk rock concentrations. Hence, it is unnecessary to appeal to other processes other than Rayleigh crystal fractionation to explain the observed plagioclase compositions in the Skaergaard intrusion. Subsequent models presented in the present study therefore use the same principles to infer magma chamber processes during fractionation.

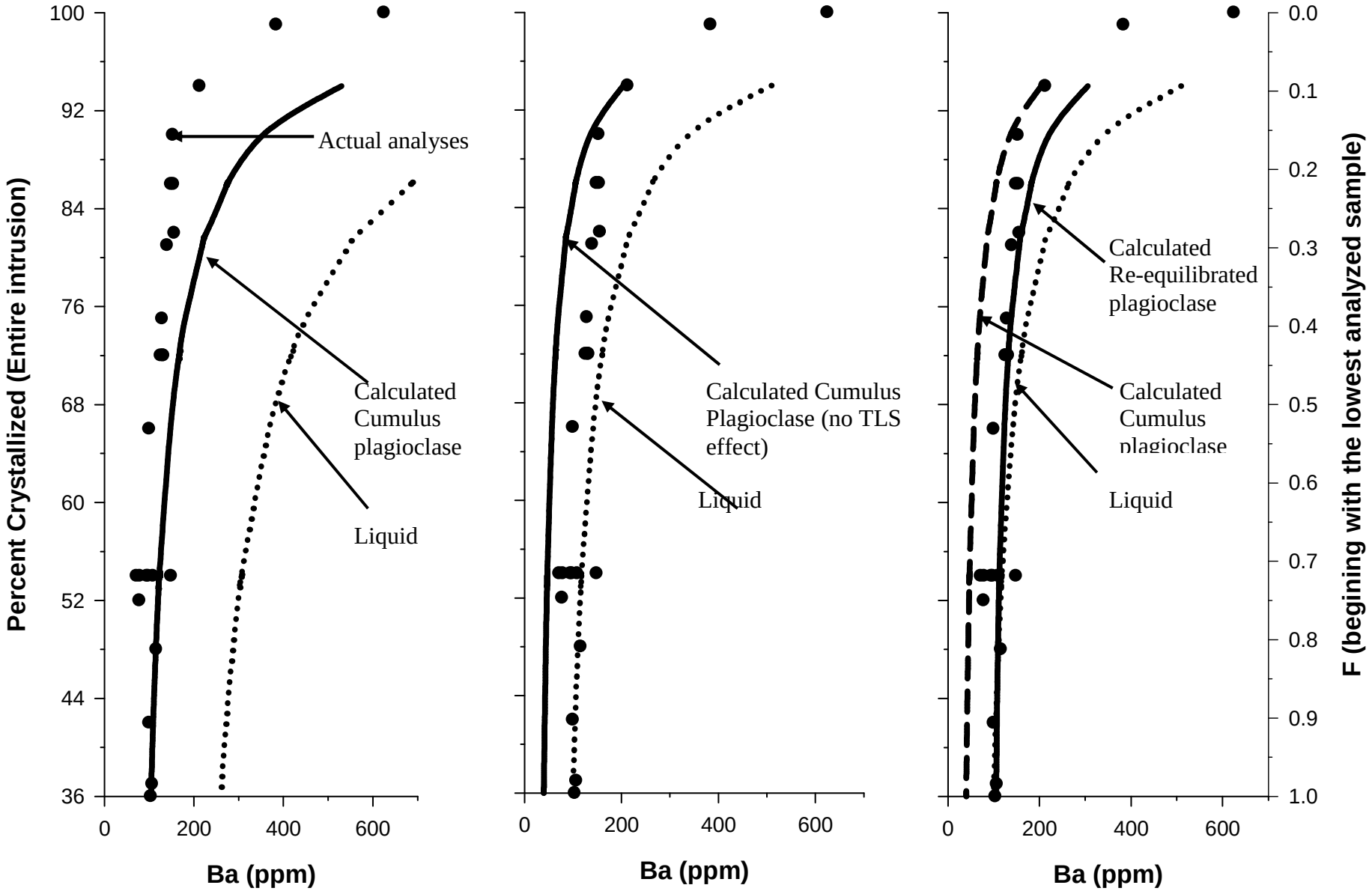


Fig. 5.2 Trends for barium in the Skaergaard intrusion showing the difference in calculated compositions (liquid, cumulus and re-equilibrated plagioclase)from the three different models. a) Compositions modeled as described in section 5.2.1a. b) Modeled as in 5.2.1b and data are from Table 5.2 c) Modeled as described in section 5.2.2.and re-equilibrated plagioclase Ba contents agree a lot better with observed plagioclase Ba.

5.3. Lateral Variation in Ba in Plagioclase

There are huge variations in the Ba content of plagioclase at the same stratigraphic heights (e.g. Ba contents of plagioclase vary from 72 ppm to 149 ppm at F= 0.7). It is not clear how such differences can exist given the conventional modeling (section 5.2.1). An explanation for the lateral variation in the Ba content of plagioclase was also not given in the original paper because the re-equilibration of interstitial liquid (TLS) was ignored. However, modeling in the present study shows that the lateral variation in Ba in plagioclase can be explained by varying contributions of TL fraction and mode to the TLS effect. Investigations by Tegner et al. (2009) concluded that trapped liquid fractions vary rather erratically from 45 to 4% and plagioclase mode decreases regularly from 55 to 33% from the bottom to top of the Skaergaard intrusion. Modeling in this study however assumes a smooth variation in TL fractions from 45% to 4% from bottom to top. The fact that the TLS effect is tremendous for Ba in plagioclase (as shown in Fig. 5.1) indicates that if a TL fraction different from the actual value in a particular layer is used in modeling, modeled plagioclase compositions are likely to differ. Therefore, the model assumes progressive changes over a number of samples and does not reflect the exact trapped liquid fractions involving small distances.

Fig. 5.3 depicts the effect of variation in TL to the re-equilibrated concentration of Ba in plagioclase. It shows the same model presented in section 5.2.2, but different TL fractions have been used at the level where Ba contents vary widely (F=0.7) in order to show the changes which might result if TL fractions varied over small distances. Based on the values used in modeling, the section ought to have crystallized with about 34 % TL. However, TL fractions of 10% and 45% have been incorporated at the same level in order to show the effect of varying TL fractions to the model. It is seen that calculated re-equilibrated plagioclase compositions with the three TL fractions of 10%, 34% and 45% differ considerably, shown by Ba contents of 67 ppm, 112 ppm and 133 ppm respectively. Therefore the variation in TL explains the observed variation in Ba in plagioclase at similar stratigraphic heights.

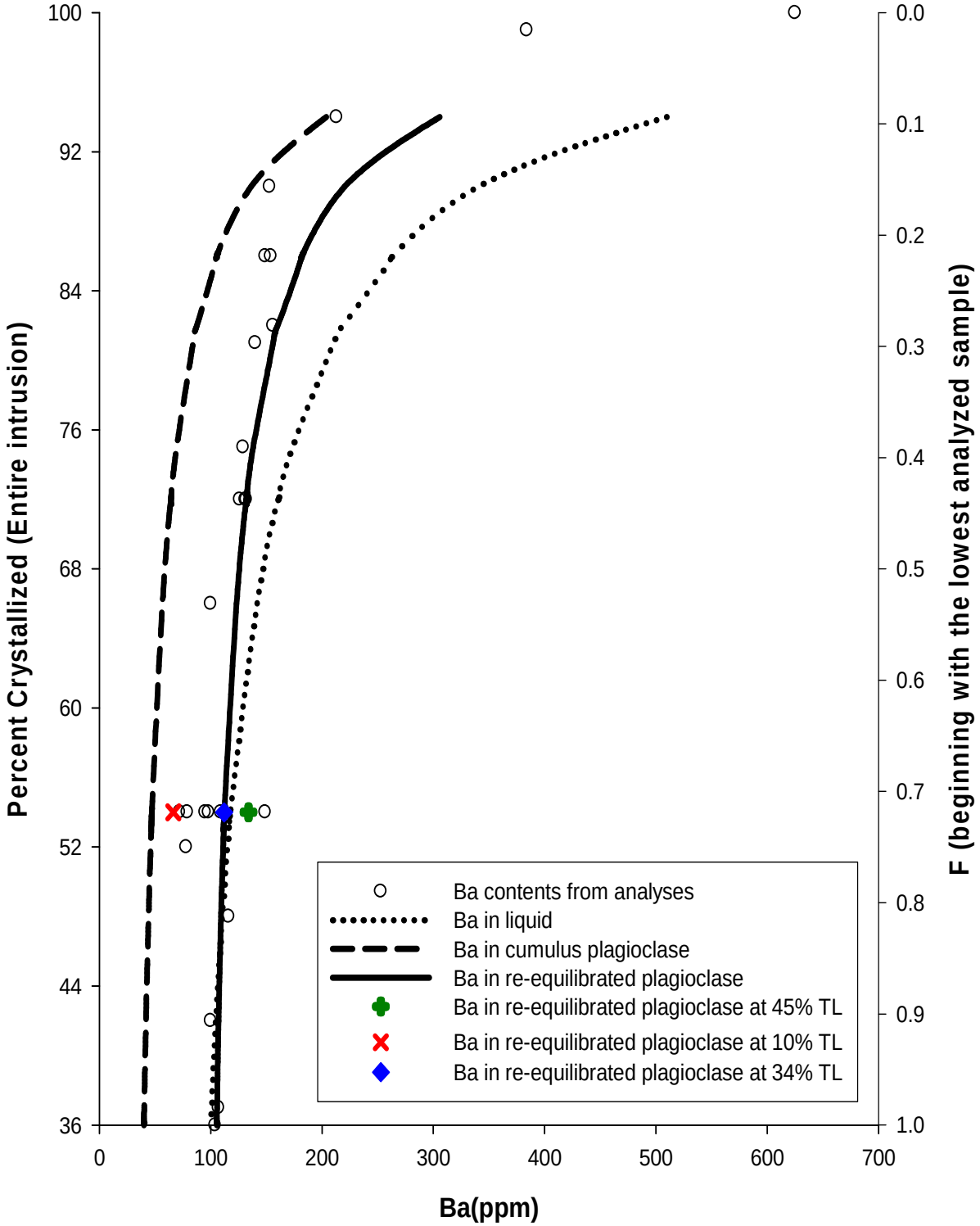


Fig. 5.3. Variation in re-equilibrated plagioclase Ba resulting from varying Trapped Liquid fractions at the same stratigraphic sample

5.4. Assessment of the effect of variables on fractionation models for the Skaergaard Intrusion

Partition Coefficients of trace elements into various mineral phases is expected to change as crystallization progresses. Plagioclase proportions and trapped liquid fractions change with fractionation as well. However, Bedard (2006) studied trace element partitioning in plagioclase of various compositions and showed that the link between D for various trace elements into plagioclase and An content can be very imprecise (Fig. 5.4). Therefore, a realistic range of partition coefficients can be tested in the model in order to check their sensitivity to varying D values. Various numerical models are therefore presented below to show possible fractionation trends and detect the sensitivity of modeled compositions if different parameters are set to vary with crystallization. C_o of Ba is set to 100 ppm for all models. The results are shown in Fig. 5.5 and Table 5.4.

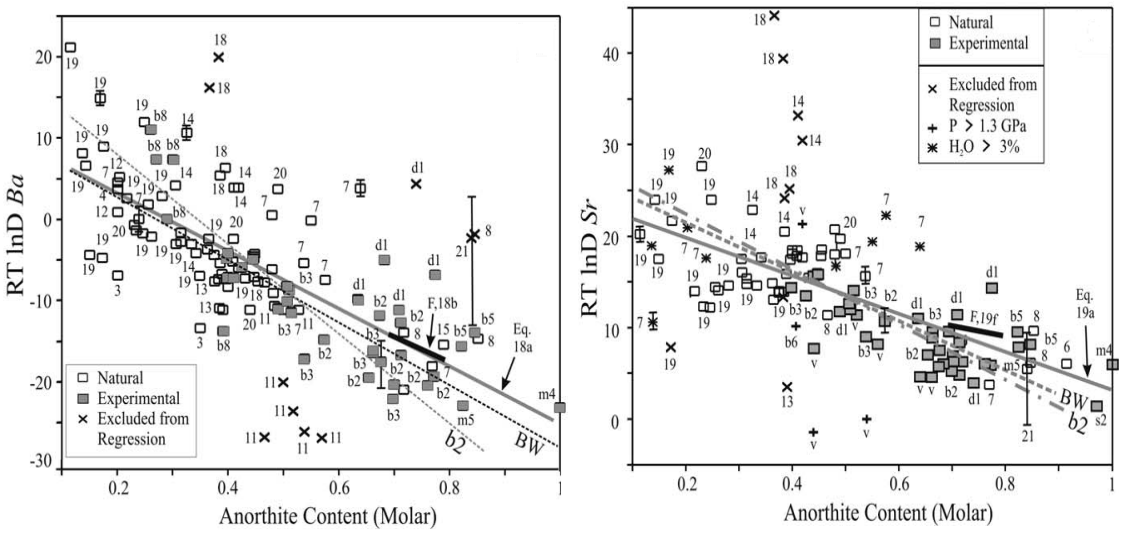


Fig. 5.4. Relationship between D for Sr and Ba into plagioclase and anorthite content (Bedard, 2006)

a. Constant Dplag , plagioclase proportions and trapped liquid fractions

Dplag, plagioclase proportion and trapped liquid fractions were kept constant from the start to end of crystallization. Plagioclase proportion, D_{Ba} in plagioclase and trapped liquid fraction used are 50%, 0.4 and 30% respectively.

b. Varying Dplag, constant trapped liquid and constant plagioclase proportion

D_{Ba} in plagioclase is varied from 0.3 at the bottom to 0.5 at the top. The trapped liquid fraction and plagioclase proportion were kept constant at 30% and 50% respectively.

c. Constant Dplag, constant trapped liquid fraction and varying plagioclase proportion

D_{Ba} in plagioclase and trapped liquid fractions are kept constant at 0.4 and 30% respectively whereas plagioclase proportion is made to change regularly from 55% at LZa to 33% at the top.

d. Constant Dplag, constant plagioclase proportion and varying trapped liquid fraction

In this instance, D_{Ba} in plagioclase and plagioclase proportion are kept constant at 0.4 and 50% respectively, whereas the trapped liquid fraction formulated to change regularly from 45% at the bottom to 5% at the top.

e. Varying Dplag, varying trapped liquid fraction and constant plagioclase proportion

The plagioclase proportion is kept constant at 50% whereas D_{Ba} in plagioclase is made to change from 0.3 at the bottom to 0.5 at the top and the trapped liquid fraction from 45% to 5%.

f. Constant Dplag, varying plagioclase proportion and varying trapped liquid fractions

D_{Ba} in plagioclase is kept constant at 0.4, plagioclase mode and trapped liquid fraction varied from 55% to 33% and 45% to 5% from bottom to top of the intrusion.

g. Varying Dplag, plagioclase proportion and constant trapped liquid fraction.

In this model, D_{Ba} in plagioclase is made to change from 0.3 to 0.5, plagioclase proportion from 55% to 33% whereas the trapped liquid fraction is kept constant at 30%.

h. Varying Dplag, plagioclase proportion and trapped liquid fraction

All three variables are set to change from the bottom to top of the intrusion. Dplag changes from 0.3 to 0.5, plagioclase mode from 55% to 33% and trapped liquid fraction from 45 to 5% respectively.

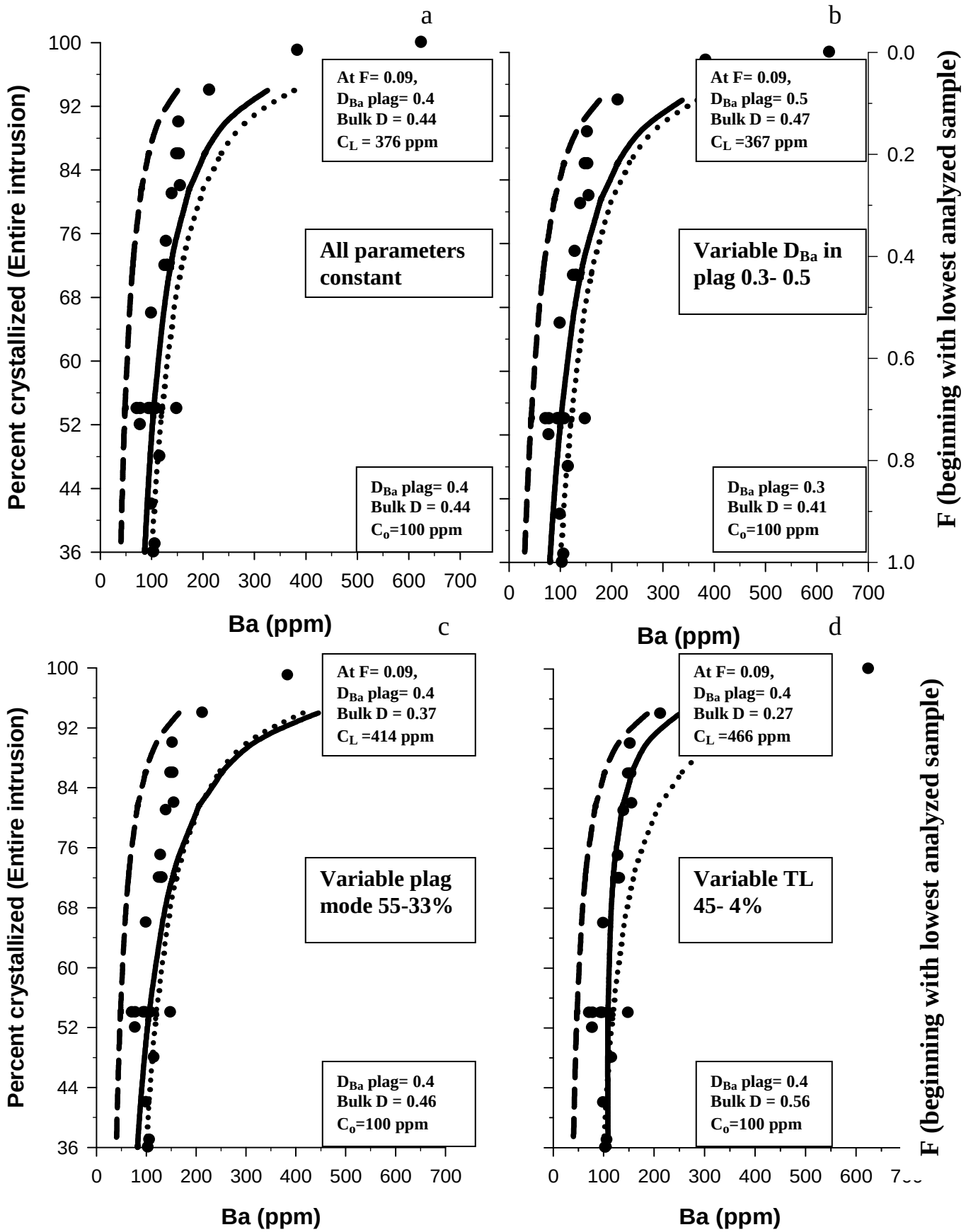


Fig. 5.5 Calculated trends for barium in the Skaergaard intrusion from varying different parameters with crystallization. F values start at LZa; percent crystallized is for entire intrusion from Jang and Naslund (2001) and C_L is the liquid composition at F =0.1. Dotted curves represent Ba in the liquid and solid curves are Ba in the modeled plagioclase, dashed curve in c represents Ba in the original cumulus plagioclase.

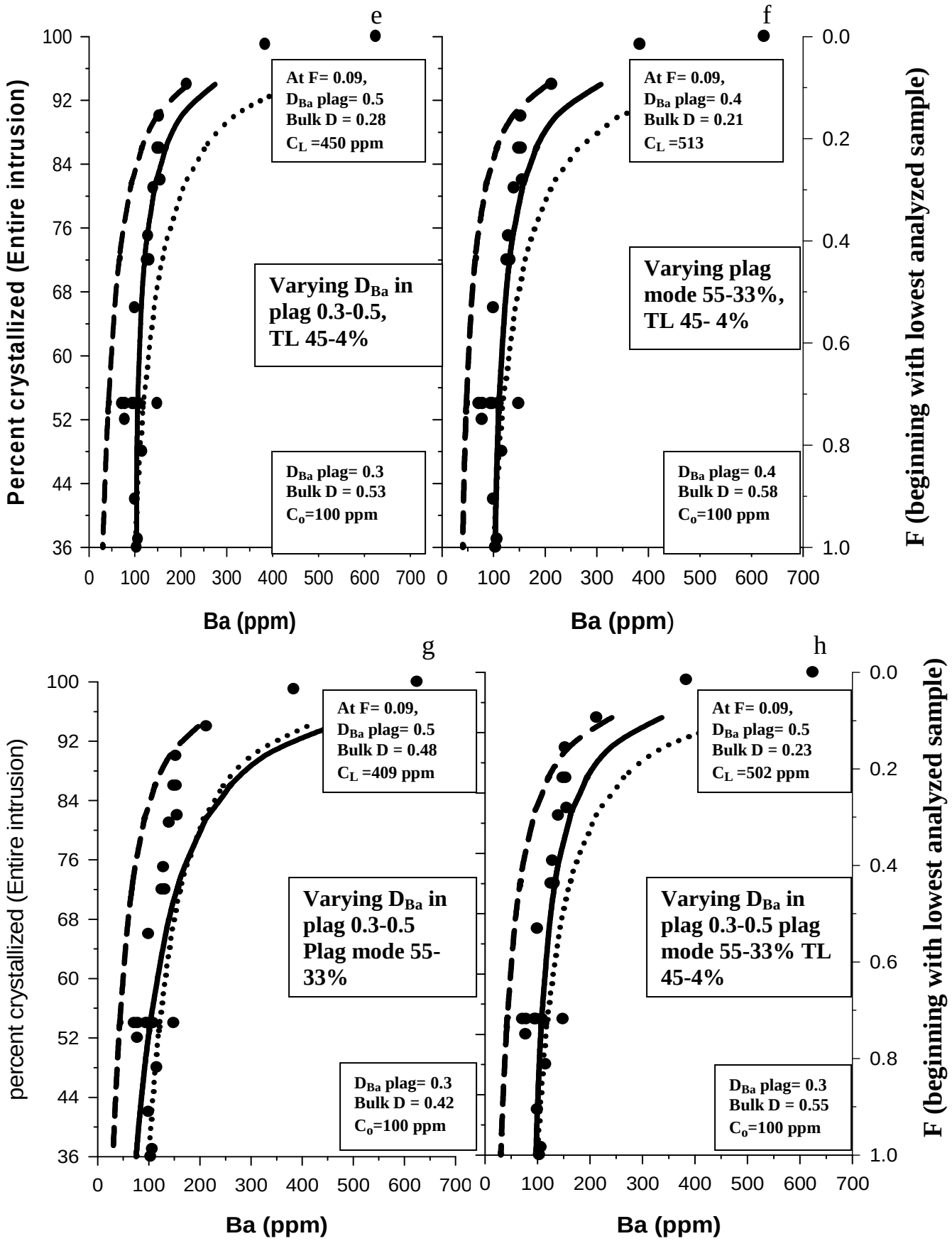


Fig. 5.5. cont. Calculated trends for barium in the Skaergaard intrusion from varying different parameters with crystallization.

All these hypothetical models show that the calculated bulk Ds and final plagioclase compositions are relatively insensitive to variations in D_{Ba} in plagioclase and plagioclase mode. However, they are very sensitive to variations in TL fraction. The varying effects can be seen from the changes which occur in each model in which the trapped liquid fraction is varied (models d, e, f and h in Fig. 5.5 and Table 5.4) compared to the other models in which TL is kept constant. Thus trapped liquid fraction has the most significant effect on the Ba contents of calculated re-equilibrated plagioclase. Hence models d, e, f and h give the best fit to data. In view of the overall insensitivity of the model to changing plagioclase proportions and D_{Ba}, it is more crucial to employ exact TL fractions in modeling the evolution of Ba in plagioclase.

Table 5.4. Sensitivity of bulk D and Ba content of re-equilibrated plagioclase in the model to variations in Dplag, TL fraction and plagioclase mode.

	Variables	**Dplag**	**TL %**	**plag %**	**Bulk D**	**Change in**	**Ba in Re-equilibrated plag (ppm)**	**Change in Re-equilibrated plag (ppm)**
	Value at F=0.09					**Bulk D**		
a	All three parameters constant	0.4	30	50	0.44	N/A	325	N/A
b	Varying Dplag only	0.5	30	50	0.47	0.03	338	13
c	Varying plag % only	0.4	30	35	0.37	-0.07	445	120
d	Varying TL % only	0.4	5	50	0.27	-0.17	250	-75
e	Varying Dplag + TL %	0.5	5	50	0.28	-0.16	275	-50
f	Varying plag % + TL	0.4	5	35	0.21	-0.23	308	-17
g	Varying Dplag + plag %	0.5	30	35	0.48	0.04	458	133
h	Varying all three parameters	0.5	5	35	0.23	-0.21	337	12
	Value at F=1							
a	All three parameters constant	0.4	30	50	0.44	N/A	86	N/A
b	Varying Dplag only	0.3	30	50	0.41	-0.03	80	-6
c	Varying plag % only	0.4	30	55	0.46	0.02	82	-4
d	Varying TL % only	0.4	45	50	0.56	0.12	109	23
e	Varying Dplag + TL %	0.3	45	55	0.53	0.09	104	18
f	Varying plag % + TL	0.4	45	55	0.58	0.14	103	17
g	Varying Dplag + plag %	0.3	30	55	0.42	-0.02	75	-11
h	Varying all three parameters	0.3	45	55	0.55	0.11	97	11

Change in bulk D = change in bulk D relative to simplistic Rayleigh model in which all three parameters are kept constant.

5.5. Modeling Strontium in Plagioclase in the Skaergaard Intrusion

The data presented by Jang and Naslund (2001) show Sr in plagioclase to increase slowly from about 500 ppm at the lowest analyzed sample in LZa (36% crystallized; F=1 in this study) to about 600 ppm at F=0.2. It then increases abruptly to over 1000 ppm at the sandwich horizon (F=0.0). A reasonable fit is also obtained with the Skaergaard data for Sr in plagioclase by using the steps employed in the modeling for Ba (Section 5.2.2). Sr contents of Skaergaard starting liquid proposed by Nielsen (2004) range between 200 and 300 ppm. For the purpose of modeling, 273 ppm Sr was chosen among the values proposed to be used as the starting liquid composition.

Initially, values for D_{Sr} in plagioclase from the literature (e.g. Blundy and Wood, 1991; Rollinson, 1993), generally between 2 and 3 were used to model Sr in plagioclase for the Skaergaard intrusion. However, using these values leads to a bulk D greater than 1 and the calculated Sr content of liquid (and hence calculated re-equilibrated plagioclase) ought to decrease upward. This trend is not observed in the data of Jang and Naslund (2001) and hence smaller D values had to be used. D_{Sr} in plagioclase of 1.7 was therefore chosen for modeling, incorporating F values for the entire intrusion, rather than the lowest analyzed sample.

If D_{Sr} in plagioclase is 1.7, cumulus plagioclase is 33% and TL% is 45%, this will lead to a bulk D of 1.003. A bulk D close to unity (1.002)indicates that the Sr content of liquid at this level would not change significantly after 36% of crystallization (F=1 in this study).

Substituting in equation 5.1 ($C_L/C_o=F^{(D-1)}$), $C_L= 273 * 0.64^{(1.002-1)}$

$$C_L \approx \underline{273 \text{ ppm}}$$

Hence 273 ppm Sr was used for the liquid at 36% crystallized (F=1 for modeling in this study). Modeling for Ba in plagioclase has shown that allowance must be made for the trapped liquid shift effect. Hence the calculations presented below include the TLS effect from the beginning and in the modeling of progressive steps.

Step1: Sr concentration of the starting Liquid (C_o)

The Sr content of liquid at LZa (that is F = 1) is taken to be 273 ppm

Step 2: Bulk Partition coefficient:

In order to obtain the cumulus plagioclase mode, the observed plagioclase is set to change from 55 to 33% and TL from 45% to 5% from bottom to top such that cumulus mode can be calculated.

Cumulus plagioclase mode at the bottom = 55-(45/2) = 33%

Hence Bulk D = ((33/100) * 1.7) + ((22/100)* 0) + (45/100 *1) = 1.002

Step 3. Sr concentration of original cumulus plagioclase

Using equation (5.2), the Sr content of plagioclase = D_{Sr} plagioclase * Sr content of liquid

= 1.7 * 273 = 464 ppm Sr

Step 4. Sr in rock from intercumulus contribution

It represents the Sr present during the consolidation stage, as the trapped liquid crystallizes and it is given by Trapped Liquid Fraction/100 * Sr in the Liquid (C_L)

= (45/100) * 273 = 123 ppm

Step 5 Sr in rock from cumulus minerals.

Sr from cumulus minerals = Sr in cumulus plagioclase * (percent plagioclase in cumulus phase / 100). That is, 464 * (33/100) = 151 ppm

Step 6. Total Sr in rock

The total Sr in the rock is the amount of Sr in rock from cumulus minerals + Sr in rock from intercumulus contribution. This is 123+151 = 274 ppm

Step 7. Sr in final re-equilibrated plagioclase

The total Sr in rock must finally be incorporated into the 55% plagioclase.

That is, 274/(55/100) = 497 ppm Sr in plagioclase

From an original cumulus content of 464 ppm Sr, it has increased to 497 ppm due to TLS effect (Table 5.5; Fig. 5.6), a trivial difference as shown by Cawthorn (1996). Thus the TLS effect that was a dominant parameter for Ba in plagioclase has minimal effect for Sr in plagioclase, and so the following discussion focuses on variable D_{Sr} and plagioclase mode. D_{Sr} in plagioclase was set to change from the start to end of fractionation because

unlike Ba for which TL variation establishes the model fit, Sr in plagioclase is insensitive to TL variation. Cumulus plagioclase mode was also calculated

Cumulus apatite appears in the Middle Zone of the Skaergarrd intrusion and is present till the top reaching 10% mode at its highest. Apatite concentrates Sr, so its contribution was included in bulk D calculations from this level upward. D_{Sr} in apatite of 2 was used for the modeling. However, modeling with or without apatite has a trivial effect to the model because apatite is quite a minor phase.

Table 5.5.Calculated trends using the Sr content of parental liquid from Nielsen (2004) and incorporating the TLS effect.

Zone	% cryst	F	F^1	Plag mode	TL %	D_{Sr} in plag	Cumulus Plag mode	Bulk D	C_L(ppm)	Sr in cumulus plag (ppm)	Sr in re-equilibrated plag (ppm)	Observed Sr in plag(ppm) (Jang and Naslund, 2001)
SH	100	0.00	0.00	33	4	1.9	31	0.648				1283
UZc	99	0.02	0.17	33	4	1.9	31	0.663	831	1577	1582	878
UZc	94	0.09	0.60	35	5	1.9	31	0.683	455	855	859	819
UZb	90	0.16	0.71	36	7	1.9	31	0.751	387	723	728	636
UZb	86	0.22	1.00	38	9	1.9	31	0.805	356	660	666	615
UZb	86	0.22	0.78	38	9	1.9	31	0.805	356	660	666	625
UZb	82	0.28	0.95	39	12	1.8	31	0.880	339	624	633	581
UZa	81	0.30	0.76	40	13	1.8	31	0.741	336	619	628	600
UZa	75	0.39	0.89	42	18	1.8	31	0.777	313	571	583	632
MZ	72	0.44	1.00	43	20	1.8	31	0.793	306	554	567	616
MZ	72	0.44	1.00	43	20	1.8	31	0.793	306	554	567	603
MZ	72	0.44	0.82	43	20	1.8	31	0.793	306	554	567	642
MZ	66	0.53	0.74	45	26	1.8	32	0.830	294	527	544	572
MZ	54	0.72	1.00	49	34	1.8	32	0.900	279	490	513	572
MZ	54	0.72	1.00	49	34	1.8	32	0.900	279	490	513	571
MZ	54	0.72	1.00	49	34	1.8	32	0.900	279	490	513	545
MZ	54	0.72	1.00	49	34	1.8	32	0.900	279	490	513	566
MZ	54	0.72	1.00	49	34	1.8	32	0.900	279	490	513	540
MZ	54	0.72	0.96	49	34	1.8	32	0.900	279	490	513	589
LZc	52	0.75	0.92	50	35	1.8	32	0.910	278	486	510	568
LZb	48	0.81	0.90	51	38	1.7	32	0.933	276	479	506	561
LZb	42	0.91	0.92	53	41	1.7	32	0.968	274	470	500	514
LZb	37	0.98	0.98	55	44	1.7	32	0.997	273	465	498	507
LZa	36	1.00	1.00	55	45	1.7	33	1.002	273	464	497	497

Data for observed Sr in plagioclase are from Jang and Naslund (2001).

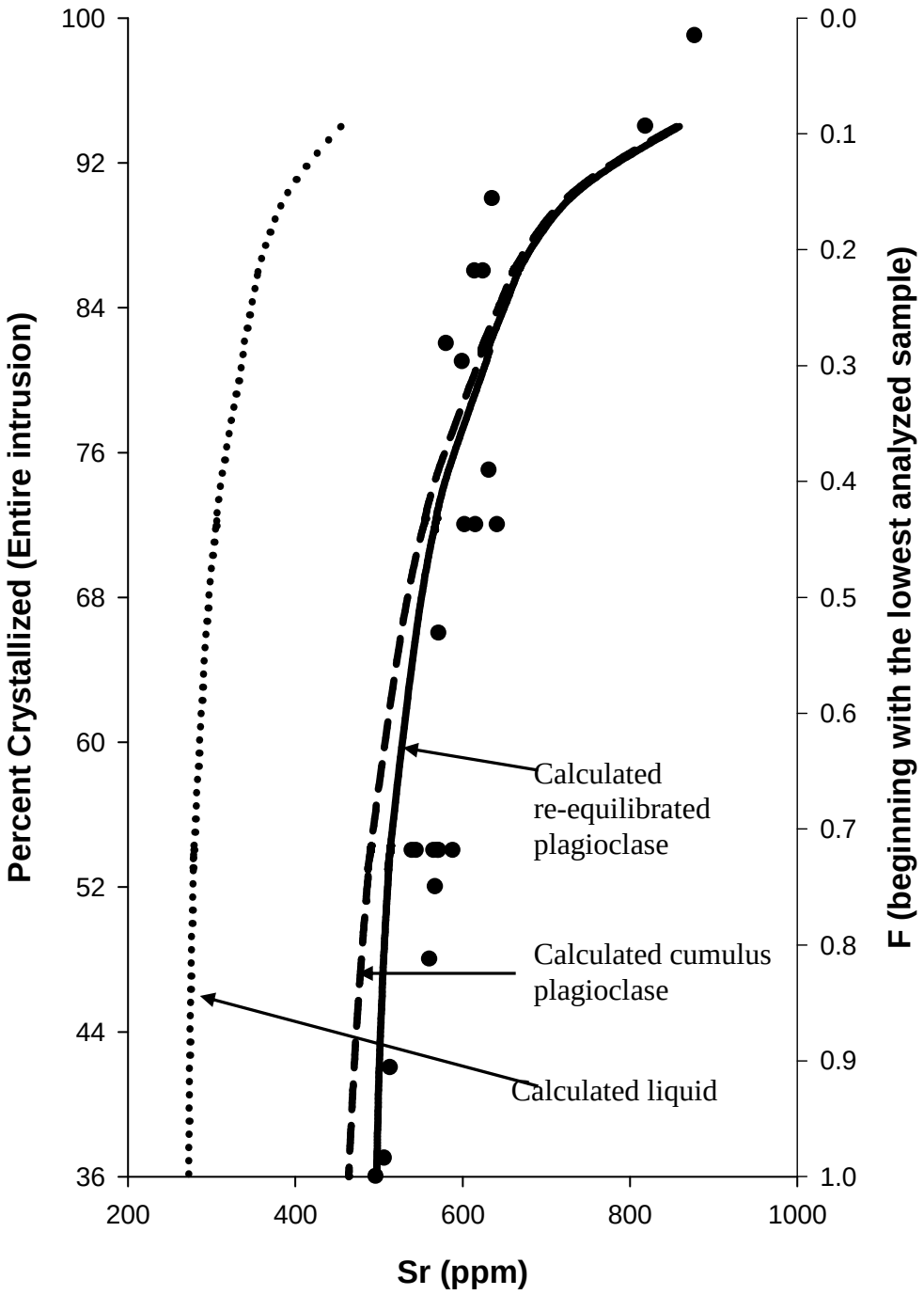


Fig. 5.6 Calculated trends based on Rayleigh fractionation with the Sr content of the Skaergaard parental liquid (Nielson, 2004) and allowing for the trapped liquid shift effect. Solid dots are data from Jang and Naslund (2001).

5.6. Comparison with previously published D values

A number of experiments were carried out by Drake and Weill (1975) to investigate the partitioning of Sr and Ba between plagioclase and liquids. These experiments were done on melts covering the temperature range of crystallization and An contents of layered intrusions spanning through the Skaergaard and Bushveld Complexes. An important conclusion which arose from their study is that plagioclase fractionation ought to deplete residual liquids of Sr and enrich them in Ba for the reason that D_{Sr} in plagioclase is greater than 1 and D_{Ba} in plagioclase is less than 1. However, the importance of using a bulk D rather than a D (for a trace element into a mineral) in modeling was ignored in their study. The present model highlights the contribution of all crystallizing phases including the TL fraction and their effects on the bulk D which should be used in modeling as it determines whether a trace element gets depleted or enriched in the liquid. In the present model, the Sr content of liquid in the Skaergaard intrusion does not decrease with crystallization (as Drake and Weill would postulate) because the bulk D is close to unity.

The model developed for Sr and Ba in the present study can also be compared with the work of Blundy and Wood (1991). The later study investigated the controlling factors on trace element partitioning between plagioclase, hydrothermal fluids and silicate melts and two equations were developed to calculate D values which can be used to model magmatic systems. Their equation for Sr (equation 5.3) is used to calculate the D_{Sr} in plagioclase, which is then used to model the Skaergaard intrusion using the steps shown in section 5.2.2. All parameters used in the equation and the resulting compositions are shown on Table 5.6.

$RT\ln D_{Sr} = 26{,}800 - 26{,}700\ XAn$ ……5.3

where R= A gas constant (8.314KJ-1mol-1), T= temperature in Kelvin and XAn = the anorthite content of plagioclase expressed as a mole fraction

The An contents used to calculate Ds are 70% at F=1 and 30% at F=0 and were obtained from Thy et al. (2009). Values for temperature are 1195^{o}C at F=1 and 950^{o}C at F=0, obtained from Morse et al. (1980). These variables were set to vary smoothly from the start to end of crystallization such that D_{Sr} in plagioclase could be calculated for each step

of fractionation. According to the equation, calculated Ds for Sr ought to vary from 2.3 at the start to 4 at the end of crystallization, hence these values were used to calculate bulk Ds, liquid and plagioclase contents of plagioclase. Plagioclase mode was set to vary from 55 to 33% according data from Tegner et al. (2009). The results of the calculation are also presented in Table 5.6.

Table 5.6.Variables and resulting Sr contents of plagioclase from modeling with the D values of Blundy and Wood (1991)

Temp ^{0}C	An # (%)	Plag mode (%)	cumulus plag mode(%)	D_{Sr}	TL %	Bulk D	C_L (ppm)	Sr in plag^1 (ppm)	Sr in plag ^{2} (ppm)
Value at F=0.009	30	33	31	4	4	1.3	143	549	531
Value at F=1	70	55	33	2.3	45	1.2	273	629	595

Sr in plag^1 = Sr in cumulus plagioclase

Sr in plag^2 = Sr in re-equilibrated plagioclase

A reasonable fit was not obtained compared to analytical data (Fig 5.7). The resulting Bulk D for Sr is close to 1.2 at F=1 and increases above 1 towards F=0.009. This leads to a decrease in the Sr content of liquid and re-equilibrated plagioclase, a variation which is contrary to the Sr contents of plagioclase from analyses. In order to fit the data for Sr in plagioclase, using the Blundy and Wood values of greater than 2 would require decreasing the proportion of plagioclase in the cumulate. Therefore, the D_{Sr} values calculated from equation 5.3 are more than the ones utilized in the fractionation model in this study and do not fit analytical data for Sr in plagioclase.

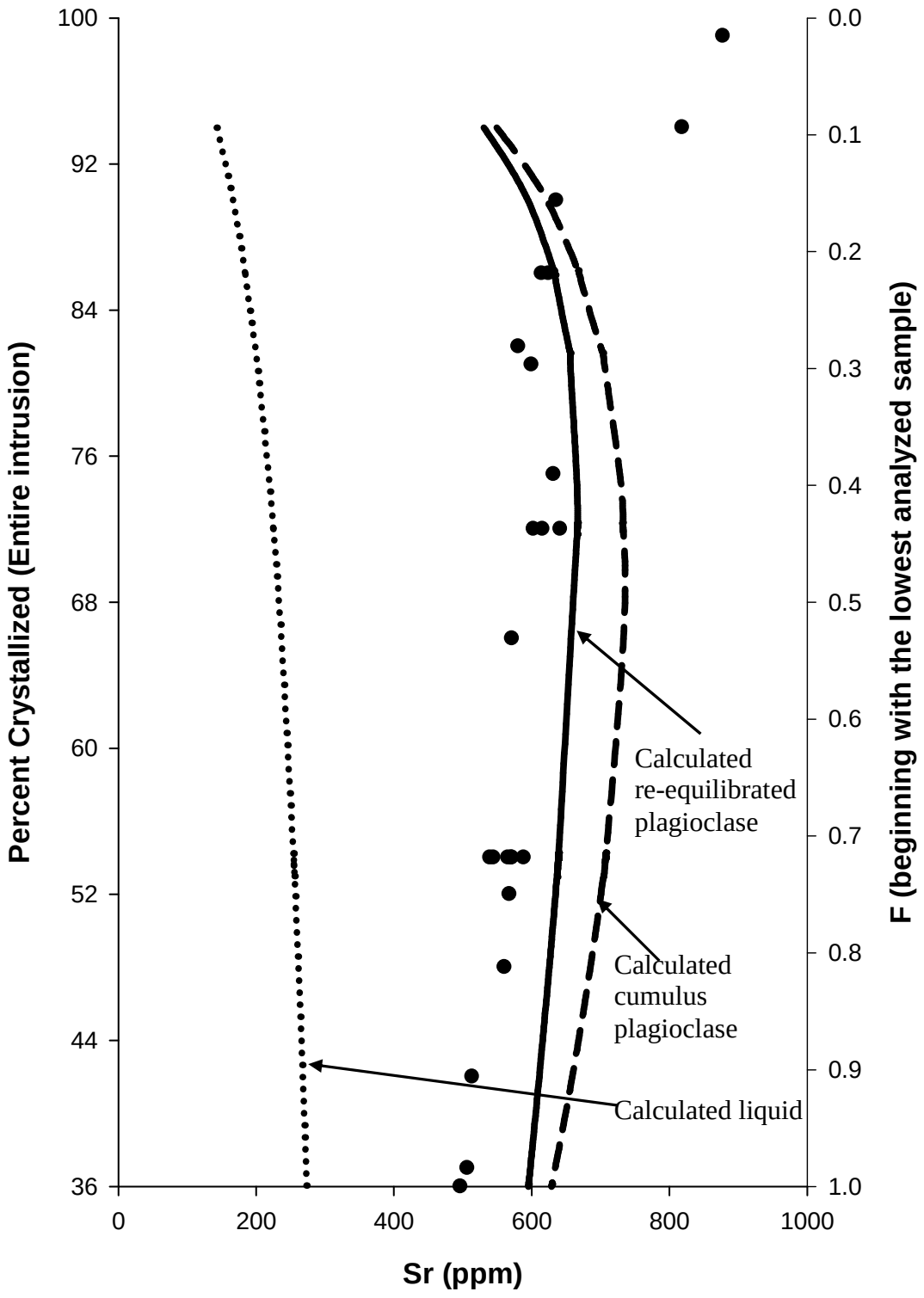


Fig. 5.7 Sr contents of liquid, cumulus and re-equilibrated plagioclase calculated from D values of Blundy and Wood (1991)

5.7. Summary

A fractionation model has been developed to model the crystallization of the Skaergaard intrusion by using the Rayleigh law and allowing for the TLS effect. The following aspects of modeling are emphasized:

- The equation $D = C_M/C_L$, (equation 5.2), should not be used in calculating the liquid content of magmas, as it leads to incorrect values and erroneous interpretations especially for incompatible elements. The shortcomings of using this equation in calculating the liquid composition for an incompatible element such as Ba in plagioclase have been shown in section 5.2.1.
- The importance of using a bulk D, which considers the contribution of all crystallizing mineral phases is highlighted. The bulk D must be of the cumulus minerals and the contribution of the trapped liquid fraction must also be included in calculating the bulk D.
- The most important outcome of modeling Ba in plagioclase for the Skaergaard intrusion is that allowance must be made for the trapped liquid shift effect as it resolved the predicament of previous models. The importance of the trapped liquid shift effect is shown in section 5.2.2. The value of 105 ppm calculated for the re-equilibrated Ba content of plagioclase show that the original cumulus and re-equilibrated concentrations of an incompatible element can differ enormously (Fig. 5.1). This value gives the best agreement with analytical data and modeling of progressive steps fits reasonably well (Fig.5.2c) compared to the other models in which this effect is ignored (Figs. 5.2a and b).
- The Skaergaard intrusion can be modeled as a single magma which differentiated and conforms to Rayleigh fractional crystallization. The model is designed in a way that new magmas can be put in at any level of the calculations simply by manually entering a new set of relevant data at the specified value for F or percent crystallized. The model can therefore be applied to similar intrusions in order to infer magma chamber processes. Modeling requires knowledge of D values, mineral proportions, trapped liquid fractions and values for F.

- The models developed show that for an incompatible element such as Ba in plagioclase, modeling is relatively more sensitive to variations in TL fraction than plagioclase mode and D. Contrarily, for a compatible element such as Sr in plagioclase for which the TLS effect is minimal, modeling is comparatively more sensitive to variable in D and mode.

The principles of modeling will therefore be applied to infer the evolution of the Upper Zone of the Bushveld Complex.

Chapter 6- Modeling the Crystallization of the Upper Zone of the Bushveld Complex

6.1. Introduction

The Upper Zone of the Bushveld Complex may have crystallized from a single magma (Kruger et al., 1987; Tegner et al., 2006) without major magma addition or assimilation based on Sr isotope ratios. This implies that the section can be modeled in a similar way as the Skaergaard intrusion. However, reversals in An content suggest internal overturn, or some other effect or process.

Based on a previous study which proposed that some amount of magma was lost from the UZ magma chamber (Cawthorn and Walraven, 1998), the major element composition of the magma at the base of the Upper Zone was constrained by Tegner et al. (2006); but the trace element contents were not computed in that study. However, Vantongeren et al. (2010) showed that the calculated contents of Tegner et al. are not representative of the primary cumulus minerals above the Px Mk. The composition of the parental magma to the Upper Zone was further constrained based on MELTS modeling, by using the felsic roof rocks to represent the proportion of magma which was proposed to have escaped from the magma chamber. For the reason that the mechanism of magma escape and its quantitative relations to the roof rocks were not indicated, it still remains unclear how the roof rocks might represent a proportion of the residual liquid of the Upper Zone. The present study therefore seeks to model the crystallization of UZ, thereby inferring the Sr and Ba contents of the magma at the base of UZ by careful application of the Rayleigh model and showing the effect of trapped liquid crystallization. These compositions can then be compared with various proposed compositions like the ones proposed by Cawthorn (2006) and Vantongeren et al. (2010) for UZ. If the last major recharge event occurred at the PxMk, the trace element contents of the liquid at the base of UZ ought to have signatures of single magma differentiation, considering that they crystallized from

thorough mixing of new and resident magmas at the PxMk. A separate section is incorporated to demonstrate the possible effect of magma loss from the Upper Zone magma chamber on the model. In addition, various magmatic processes which were proposed are reviewed with reference to current data.

6.2. Details of Modeling Procedure

Critical to the application of Rayleigh fractionation is the estimation of various parameters such as crystallizing mineral proportions, trapped liquid fractions and values for the fraction of liquid remaining (F).

6.2.1. Plagioclase proportions

Of the 116 samples used for this project, whole rock analyses had been conducted on 25 by Roberts, (2005). A summary of the average plagioclase from the subzones delineated shows plagioclase mode to vary from about 60% at the base to 45% at the top of UZ (Table 6.1). However, based on investigations in the eastern Bushveld by Molyneux (1974), plagioclase mode in UZ rocks varies irregularly from 90 to 20%. The huge variation in plagioclase proportion is a consequence of the occurrence of magnetitite and anorthosite layers. However, it should be noted that these values represent the observed plagioclase modes rather than the ones which were instantaneously crystallizing at the cotectic.

A review by Cawthorn and Ashwal (2009) emphasized the fact that the observed modes can differ significantly from the actual crystallizing modes which are controlled by the sequence of appearance of cumulate minerals in their cotectic proportions. The difference in accumulating vs. observed modes results from differential settling and sorting rates of minerals. This process has a very important implication on bulk D calculations for cumulus minerals because the bulk D ought to be calculated from the proportion of cumulus minerals crystallizing from the magma, not the proportion seen in each layer of rock. This effect is emphasized in the Bushveld Upper Zone because unlike the Skaergaard intrusion, observed plagioclase mode varies enormously. Thus if the cumulus plagioclase proportion is calculated from two observed levels containing a magnetitite

(about 20% plagioclase) and an anorthosite (about 90% plagioclase) layer based on the suggested calculation in the previous section, this would still lead to a “false” bulk D because these observed modes differ significantly from the ones which were crystallizing from the magma. Therefore in constructing the model, plagioclase proportions are set to change from 60% at the bottom to 45% at the top according to norm calculations for the nine subzones (Table 6.1) designated by Roberts (2005) such that cumulus proportion can be calculated from this value and the fraction of trapped liquid. These values are similar to the plagioclase proportions used by Tegner et al. (2006) in modeling.

6.2.2 Trapped Liquid Fractions (TL%)

Cawthorn and Walsh (1988) modeled the proportion of trapped liquid in the Upper Zone using phosphorus contents of whole rocks and suggested trapped liquid fractions of about 10% Hence a constant TL fraction of 10% is utilized throughout crystallization.

6.2.3. Fraction of Magma remaining (F)

For the purpose of modeling, the entire sequence is divided into small Rayleigh fractionation steps with the base of the Upper Zone representing the start of crystallization (F=1) and the top representing the end (F=0). The total thickness of the magma chamber is taken to be 1862 m as it is the length of the section starting from the appearance of cumulus magnetite to the level at which the core records the end of the occurrence of mafic rocks. In the modeling, the magma chamber is assumed to be boxed shaped and the sides vertical so that F is directly proportional to the height in meters. The magma chamber can be treated as a sheet in terms of volume and calculating F as it is 200- 300 kms wide. The stratigraphic height of each sample is then used to estimate values for F within the sequence by calculating the vertical distance between adjacent samples relative to the vertical interval to the top such that for each step, F values become extremely close to unity. The last 10% of crystallization is also ignored in interpretations because it is uncertain if the core was drilled into the extreme differentiates of the intrusion. The presence of felsic and granitic intrusions within the upper parts of the core suggest that some portions of the layered rocks might be missing, and so make the calculations inaccurate. Hence the models are terminated at F=0.09.

Table 6.1.Rock compositions for the nine subzones in the Upper Zone, showing normative proportion of minerals (Roberts, 2005)

Subzone	**UZ1**	**UZ2**	**UZ3**	**UZ4**	**UZ5**	**UZ6**	**UZ7**	**UZ8**	**UZ9**
Major oxides (wt(%)									
SiO_2	42.60	41.50	42.90	37.90	40.90	42.80	41.60	42.10	45.20
TiO_2	2.30	3.10	2.70	3.60	2.80	2.40	2.30	2.50	2.00
Al_2O_3	20.70	17.80	18.90	15.30	14.70	15.60	14.60	13.00	11.50
Fe_2O_3	9.28	12.28	9.53	13.00	11.29	10.19	9.83	10.54	9.84
FeO	6.68	8.84	7.71	11.70	11.17	10.09	11.49	13.28	13.28
MnO	0.10	0.10	0.10	0.20	0.30	0.30	0.30	0.40	0.40
MgO	2.50	4.10	3.50	3.50	3.80	2.90	3.10	2.40	2.20
CaO	10.10	8.80	8.90	7.50	8.90	8.40	9.00	8.50	8.50
Na_2O	3.20	3.00	3.70	2.60	2.90	3.10	2.90	2.60	2.30
K_2O	0.40	0.30	0.40	1.20	0.30	0.40	0.30	0.50	1.00
P_2O_5	0.00	0.10	0.10	1.20	1.00	0.30	0.90	0.90	0.80
H_2O	0.00	0.00	0.00	0.00	0.00	0.00	0.00	0.00	0.00
Total	97.86	99.92	98.44	97.70	98.06	96.48	96.32	96.72	97.02
NORM									
Calcite	0.00	0.00	0.00	0.00	0.00	0.00	0.00	0.00	0.00
Chromite	0.00	0.00	0.00	0.00	0.00	0.00	0.00	0.00	0.00
Sulphide	0.00	0.00	0.00	0.00	0.00	0.00	0.00	0.00	0.00
Apatite	0.00	0.22	0.22	2.62	2.18	0.66	1.97	1.97	1.75
Ilmenite	4.38	5.90	5.14	6.85	5.33	4.57	4.38	4.76	3.80
Magnetite	13.48	17.84	13.84	18.89	16.40	14.80	14.27	15.31	14.29
Orthoclase	2.36	1.77	2.36	7.08	1.77	2.36	1.77	2.95	5.90
Albite	26.43	25.36	29.18	21.98	24.52	26.21	24.52	21.98	19.44
Cor	0.00	0.00	0.00	0.00	0.00	0.00	0.00	0.00	0.00
Anorthite	40.90	34.18	33.75	26.50	26.18	27.44	25.91	22.30	18.08
Cpx-Mg	6.36	6.29	6.42	1.56	5.67	5.58	5.11	4.25	5.05
Cpx-Fe	0.88	0.62	1.30	0.81	3.73	4.53	5.64	7.63	11.04
Opx-Mg	0.00	5.99	0.00	4.57	6.80	4.61	5.32	3.99	3.12
Opx-Fe	0.00	0.68	0.00	2.72	5.14	4.29	6.75	8.24	7.83
Ol-Mg	2.28	0.89	3.99	2.37	0.00	0.00	0.00	0.00	0.00
Ol-Fe	0.40	0.11	1.03	1.56	0.00	0.00	0.00	0.00	0.00
Q	0.00	0.00	0.00	0.00	0.18	1.35	0.54	3.21	6.57
Neph	0.34	0.00	1.14	0.00	0.00	0.00	0.00	0.00	0.00
Total	97.80	99.85	98.37	97.52	97.89	96.39	96.17	96.58	96.89
An+Ab	67.33	59.54	62.92	48.49	50.70	53.65	50.42	44.28	37.53
An/An+Ab	60.19	57.41	53.63	54.66	51.64	51.15	51.38	50.36	48.18
Recalculated to 100%									
Plag	70.8	60.6	69.9	51.3	52.8	57.3	53.9	46.9	43.7
Cpx	7.5	7.2	3.2	6.9	9.7	10.3	10.6	13.4	12.9
Opx	0.0	6.8	0.0	7.7	12.4	9.5	12.9	12.9	12.7
Ol	2.8	1.0	5.6	4.2	0.0	0.0	0.0	0.0	0.0
Oxide	18.8	24.2	21.1	27.2	22.6	20.7	19.9	21.3	21.1
Q	0.0	0.0	0.0	0.0	0.2	1.4	0.6	3.4	7.6
Ap	0.0	0.2	0.2	2.8	2.3	0.7	2.1	2.1	2.0
Total	100.0	100.0	100.0	100.0	100.0	100.0	100.0	100.0	100.0

6.2.4. Starting Liquid Compositions (C_O)

Unlike the well-constrained Skaergaard intrusion in which suitable parental magma compositions have been estimated, the starting liquid composition (C_o) of the Upper Zone has not been well constrained. Modeling the Skaergaard intrusion has shown that calculating C_o by using equation 5.2 ($C_{liquid} = C_{mineral} / D$) is highly inaccurate and will definitely lead to erroneous interpretations about magmatic processes especially for an incompatible element such as Ba. The use of this equation also requires that the mineral in question preserve its cumulus composition. However, Fig. 5.1 shows that in layered intrusions, original cumulus compositions are commonly modified by reaction with intercumulus trapped liquid and such a condition is not always attained. Therefore using the principle of Ds in such instances to calculate magma compositions is highly questionable. The lack of a generally accepted estimate for C_o at the level of the Upper Zone also limits direct substitution into the Rayleigh Law as the case of the Skaergaard intrusion.

6.2.5. Build up of the fractionation Model

The model is constructed by incorporating values for F, TL, mineral proportion and trapped liquid fraction, using D values from various studies to build up a calculation similar to that performed in section 5.2.2 for the Skaergaard intrusion. The bulk Ds are calculated based on these values and progressive steps are subsequently modeled. A process of trial and error is then used to obtain values of C_o for Sr and Ba. For Barium, since the Bushveld plagioclase concentration is twice that of Skaergaard, a value of C_o of twice that of Skaergaard is tried initially. However, because the proportion of trapped liquid in the Bushveld Complex is less than the Skaergaard, a revised C_o is selected and tried into the built in calculation until a reasonable fit is obtained. For strontium with a small TLS effect, and with similar plagioclase contents for both the Skaergaard intrusion and the Upper Zone of the Bushveld Complex, a value similar to that of the Skaergaard is used into the calculation and gives reasonable fit. It has also been shown with the Skaergaard model for Ba that varying D in plagioclase within the range of published values with crystallization has a negligible effect on modeled compositions, thus trying to deduce values of D_{Ba} for progressive steps is imprecise. However, the Sr content of

plagioclase is relatively sensitive to variations in D_{Sr} in plagioclase hence this parameter is varied with crystallization. Trapped liquid fractions are then incorporated into the model to obtain re-equilibrated compositions as described in section 5.2.2.

In the following figures, the dotted curves represent liquid compositions; the dashed curves, original cumulus mineral compositions and the solid curves the re-equilibrated compositions of the trace elements. Points on the graphs represent analytical data. Model Dplag, bulk Ds and liquid compositions (C_o) are presented in Appendix D.

6.3. Barium in plagioclase

Ba in plagioclase in the Upper Zone of the Bushveld Complex is generally higher than the Skaergaard intrusion However, it also varies irregularly between 200 and 500 ppm throughout the crystallization sequence until after F=0.15 where it increases significantly. From F=1 to F= 0.15, the general upward rate of change in the Ba contents of observed plagioclase is the same in the Upper Zone of the Bushveld (from 200 to 500 ppm) and in the Skaergaard intrusion (from 100 to 200 ppm). The incoming of alkali feldspar at 1693 m depth (F=0.1) considerably affects analytical results for Ba. All modeling and data interpretation therefore exclude the overlying interval.

The cumulus minerals pyroxene, olivine, magnetite and apatite have a negligible contribution to the calculated bulk D; hence for the purpose of modeling, it is assumed that Ba is perfectly incompatible in these minerals. In the model, D_{Ba} in plagioclase is kept constant at 0.4 as changing D values with crystallization have a negligible effect on the model. The bulk D is < 1 throughout crystallization; therefore Ba in the liquid increases steadily with progressive crystallization (Fig. 6.1a see Appendix D for details of bulk D, liquid, cumulus and final re-equilibrated plagioclase compositions). However, because of the trapped liquid shift effect for Ba, re-equilibrated plagioclase contents remain fairly constant and only increase significantly from F = 0.2 upward, fairly similar to analytical data. However, the Ba content of calculated re-equilibrated plagioclase

between F=0.15 and F=0.10 is higher than the increase in analytical data. A possible explanation for the higher Ba contents of calculated re-equilibrated plagioclase at this level is that more plagioclase could have been crystallizing towards the top of UZ. Hence increasing the plagioclase mode would minimize the increase of Ba in calculated re-equilibrated plagioclase. However, increasing the plagioclase mode towards the top does not agree with modal data from Roberts (2005). There is also wide variation in the observed Ba contents of plagioclase (300- 600ppm) at this level which is difficult to explain by the single magma model.

It has been shown in section 5.1.2 and 5.2.2 that both the TL fraction and plagioclase mode are significant factors that influence the TLS effect. For the Upper Zone of the Bushveld, the consequence of wide variation in plagioclase mode is that an incompatible element such as Ba can vary enormously in plagioclase from plagioclase-rich vs. plagioclase- poor successions (e.g. anorthosite vs. magnetite layer). For example, consider a situation in which an anorthosite ($\geq$ 85% cumulus plagioclase) is directly overlain by a magnetitite layer ($\leq$ 10% cumulus plagioclase), as can occur in the Upper Zone of the Bushveld. The cumulus and trapped liquid (intercumulus) contributions in the two cases would differ significantlt. In this illustration, the Ba content of the liquid is taken as 300 ppm and D_{Ba} in plagioclase is taken as 0.4. D_{Ba} for all other crystallizing minerals is very close to zero and can be ignored.

The anorthosite contains 85% cumulus plagioclase, 5% of other cumulus minerals (with D_{Ba}=0) and 10% trapped liquid which solidifies to produce a further 5% plagioclase, and 5% of other minerals.
The original cumulus plagioclase will have (0.4* 300) =120 ppm Ba
In the rock, plagioclase would contribute (120* 85% plagioclase) = 102 ppm
The trapped liquid will contribute (300ppm *10% trapped liquid) = 30 ppm Ba
Total Ba in rock = 102+30 =132 ppm
The solidified rock will contain 90% plagioclase in total or 85% cumulus plus 5% intercumulus plagioclase.

The Ba in the rock must finally be incorporated into the 90% plagioclase. Hence Ba in final re-equilibrated plagioclase =132/.90 = 147 ppm

In the magnetitite layer, there is only 10% cumulus plagioclase, 80% cumulus magnetite (for which D_{Ba}=0) and 10% trapped liquid which crystallizes to produce an additional 5% plagioclase and 5% other minerals.
Plagioclase would contribute (120* 10% plagioclase) = 12 ppm in the rock
The trapped liquid will contribute (300 ppm* 10% trapped liquid) = 30 ppm
Total Ba in rock = 12 + 30 = 42 ppm
At the consolidation stage, another 5% of plagioclase is formed increasing plagioclase mode to 15%. Ba in final re-equilibrated plagioclase = 42/.15 = 280 ppm

Ba in plagioclase in the magnetitite layer (280 ppm) is about two times higher than that in anorthosite (147 ppm) even though both rocks formed from a liquid with the same Ba content. This is because in the magnetitite layer, there is less cumulus plagioclase. The calculation demonstrates that closely spaced rocks with huge differences in modal proportion can result in different Ba contents in their plagioclase due to differing degrees of cumulus and trapped liquid contributions. It is crucial to consider the TLS effect between magnetite and anorthosite as it explains the general variation in the Ba contents of plagioclase, even though the overall effect on the sense of differentiation is not significant.

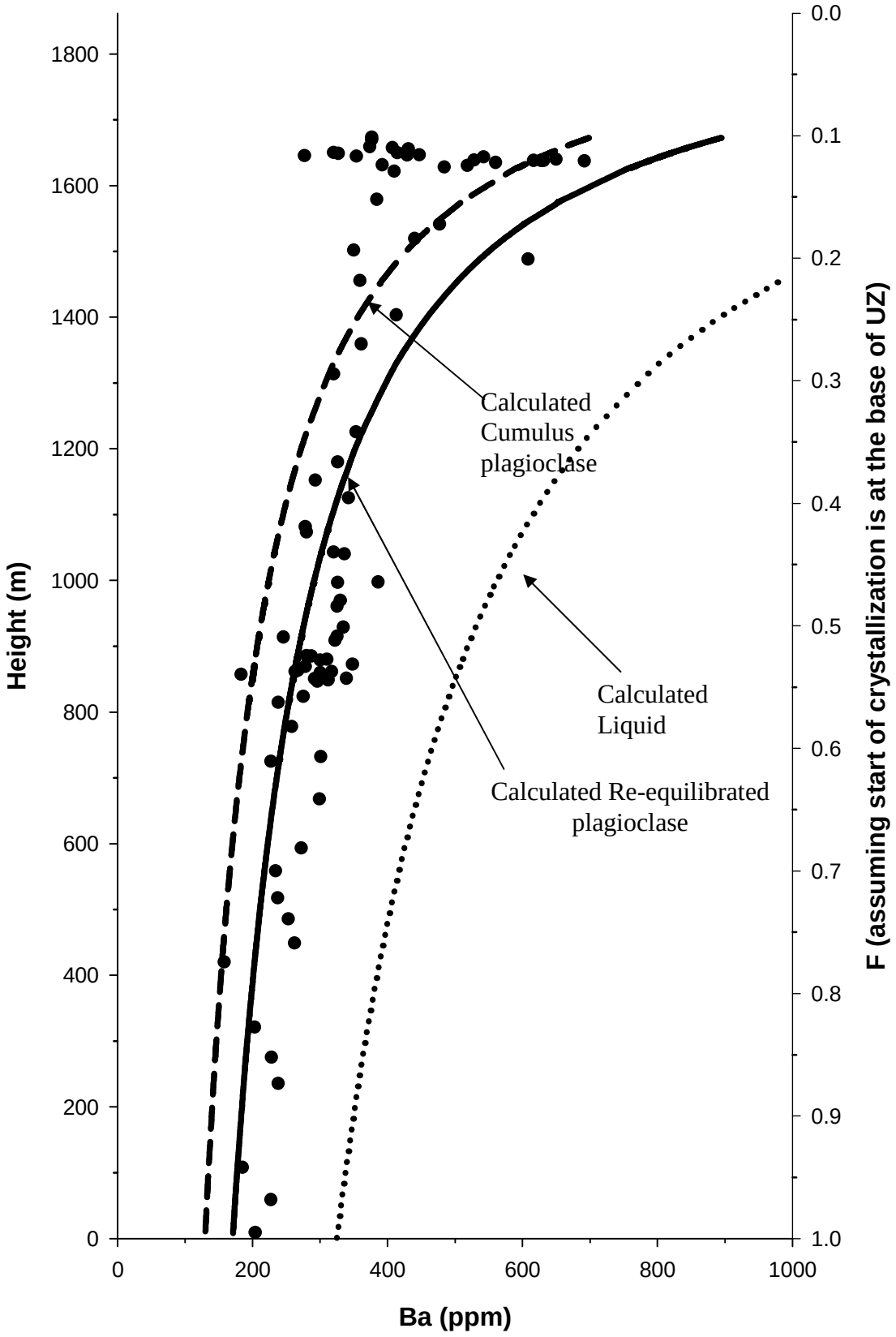


Fig. 6.1 Plots of Ba in liquid, original cumulus and re-equilibrated plagioclase vs. F (fraction of magma remaining) and height for the Upper Zone, Bushveld intrusion. Filled circles represent analytical data

6.4. Strontium in plagioclase

The Sr content of plagioclase increases slightly erratically from 400 to 650 ppm from base to top; with a number of outliers (Fig. 6.2), a trend similar to the Skaergaard intrusion. However, the rapid increase in Sr in plagioclase at top of the Skaergaard is not obvious in the Bushveld data.

Apatite appears as a minor cumulus phase in UZc and for which strontium has a high affinity; hence it becomes important to consider its effect on modeled compositions. The effect of apatite to the model is calculated from the level at which apatite appears to the end of the borehole, assuming a smooth modal change from 4.5% to 1%. D_{Sr} in apatite is kept constant at 2 throughout the interval. Because apatite is a minor phase, it has a negligible effect on the model. The minute effect of apatite is established by the following calculations.

In an average UZ succession with observed modes of 60% plagioclase, 5% apatite, and 35% other minerals which crystallized with 10% trapped liquid, this will lead to 55% cumulus plagioclase. The 10% trapped liquid crystallizes ½ (5%) plagioclase and ½ (5%) other minerals hence its contribution to apatite is negligible.

Bulk D, apatite present = ((55/100) * 1.5) + ((5/100)* 2) + ((30/100)* 0) + (10/100 *1)

=1.025

Bulk D, apatite absent = ((55/100) * 1.5) + ((30/100)* 0) + (10/100 *1)

= 0.92

The difference between Bulk Ds in the two situations is small and indicates that the presence of apatite would not have a significant effect on resulting modeled compositions in such rocks.

Initially, a constant D_{Sr} in plagioclase of 1.5 was used throughout the crystallization sequence (Fig. 6.2). However, it was noticed that increasing the D value with crystallization had a better fit (Fig. 6.3). This indicates that the Sr content of plagioclase is sensitive to variations in D_{Sr} in plagioclase. D_{Sr} in plagioclase is therefore set to vary

smoothly from 1.5 at the start to 2.1 at the end of crystallization. This leads to a bulk D that changes between 0.9 and 1; hence the Sr content of liquid remains fairly constant throughout crystallization (Fig. 6.3; Appendix D). The Sr content of starting liquid for UZ is calculated to be 273 ppm. The Sr contents of calculated re-equilibrated plagioclase increase slowly and steadily from 415 ppm at F=1 to 600 ppm at F= 0.09, similar to analytical data. This increase in Sr in plagioclase is not because of an increase in liquid but is due to an increase in the D_{Sr} value. Typical values for D_{Sr} in plagioclase in the literature exceed 2. If those values were used, then the bulk D would exceed 1 and the residual liquid would decrease in Sr, resulting in a decrease in Sr in plagioclase upward. Such a trend is not observed and so a smaller value for D for Sr in plagioclase has to apply. Due to the small contribution to the bulk D from pyroxene, olivine and magnetite, it is assumed that Sr is perfectly incompatible into these minerals.

The TLS effect for Sr is small as shown by the cumulus and re-equilibrated Sr contents, (Fig. 6.2 and 6.3; Appendix D). It is again emphasized that modeled compositions cannot fit all analytical values perfectly because the model assumes smooth changes in various parameters over the sequence whereas in nature, this condition hardly occurs.

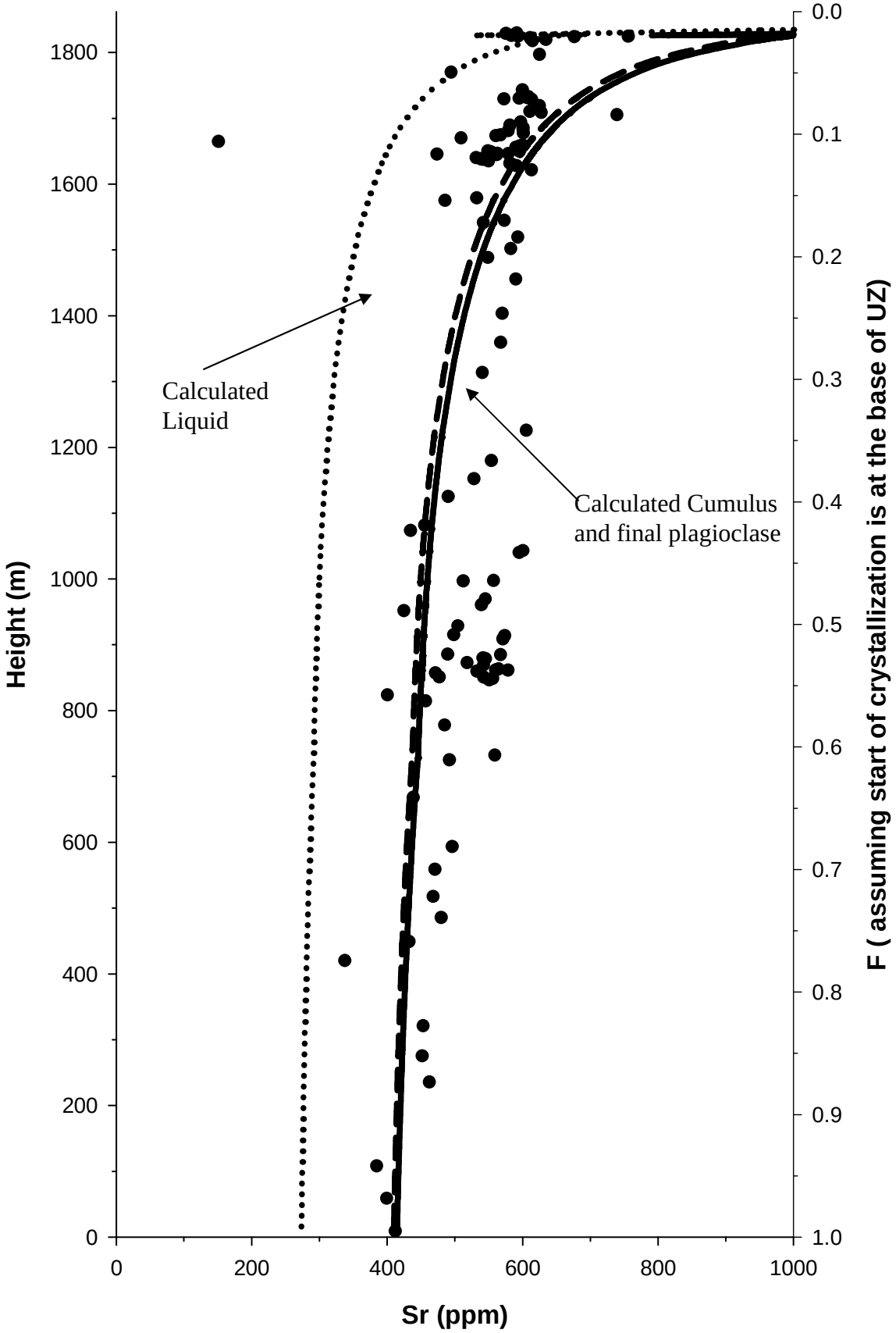


Fig. 6.2 Plots of Sr in liquid, original cumulus and re-equilibrated plagioclase vs. F(fraction of magma remaining) and height for the Upper Zone assuming a constant D_{Sr} in plagioclase of 1.5. The cumulus and final re-equilibrated plagioclase compositions do not differ significantly because the TLS effect is small for Sr .

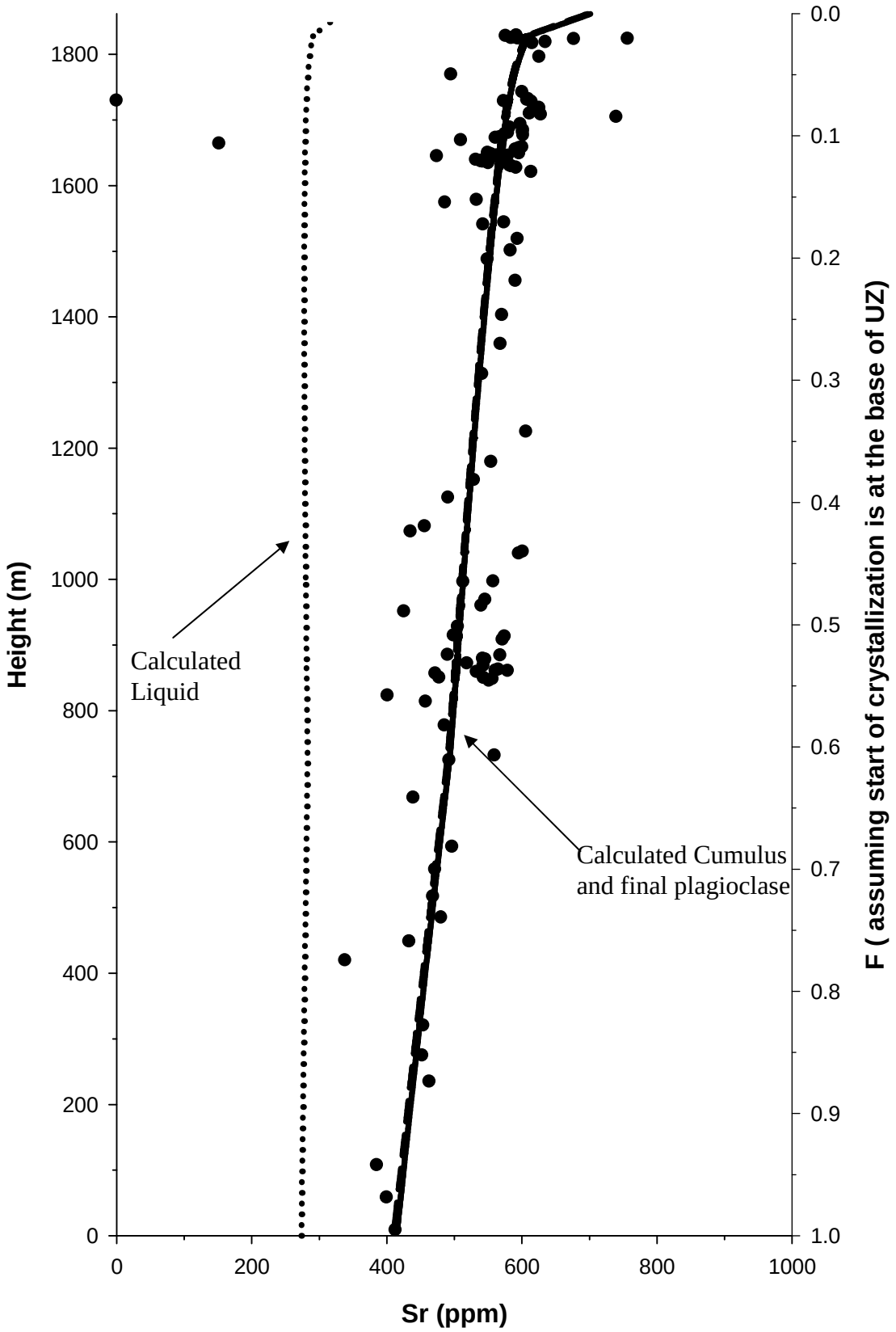


Fig. 6.3 Plots of Sr in liquid, original cumulus and re-equilibrated plagioclase vs. F(fraction of magma remaining) and height for the Upper Zone assuming a changing D_{Sr} value from 1.5 to 2.1 at the end of crystallization.

6.5. Relationship to previously published D values and Liquid Contents

The Ba and Sr models presented above imply that similar to the Skaergaard intrusion, the Bushveld Upper Zone can also be modeled as a single magma which evolved as an uninterrupted differentiated series. The data for plagioclase have been made to fit a single consistent model by using the Rayleigh law and allowing for the TLS effect.

Various D values proposed in other studies can be explored in order to investigate other means of modeling the crystallization of the Bushveld Upper Zone. For instance, the partition coefficients of Blundy and Wood, (1991) shown in equations 6.1 and 6.2 can be used to calculate the trace element content of the magma, and cumulus and re-equilibrated plagioclase contents.

$RT\ln D_{Sr}=26{,}800–26{,}700\ XAn$ ……6.1

$RT\ln D_{Ba}=10{,}200\text{-}38{,}200\ XAn$ ……....6.2

where R= A gas constant ($8.314 KJ^{-1}mol^{-1}$), T= temperature in Kelvin and XAn = the anorthite content of plagioclase expressed as a mole fraction

These two equations are used to calculate D for Sr and Ba in plagioclase using An_{60} at the base of UZ and An_{30} at the top and setting the An contents to vary smoothly within the sequence. The calculated D_{Sr} in plagioclase varies from 2.3 to 4 and D_{Ba} in plagioclase from 0.3 to 0.7 from bottom to top of the sequence. These D values are used to fractionate the Upper Zone magma using the same techniques employed in section 6.1. However, resulting modeled compositions vary greatly from analytical data (Fig. 6.4). Based on their model, calculated Ba contents of final re-equilibrated plagioclase increase from about 200 ppm at the bottom to over 1000 ppm at F=0.3 whereas analytical data only vary between 200 ppm to 500 ppm within the same interval. Modeled Sr contents decrease upwards whereas analytical data increase. Hence D values for plagioclase calculated from the two equations do not fit with trace element contents of the Upper Zone.

In order to fit the data for Sr in plagioclase, using the Blundy and Wood D values of greater than 2 would require decreasing the proportion of plagioclase in the cumulate to much less than 50%. However, to fit the data for Ba would require a very major increase in plagioclase proportion. Therefore, the Ds from these equations are considered unrealistic in the fractionation model presented. The fact that there are so many variables that can influence these calculations makes it impossible to test whether the D_{Ba} for plagioclase vary or remain constant for the range An_{60} to An_{30}. What does appear to be important is that the D value for Sr that give the best fit for these data are less than D values proposed by Blundy and Wood. (1991). The value for Ba used (0.4) is within the range which was proposed by Blundy and Wood; however, their D value of 0.7 at the top is much higher than several quoted values and does not conform with modeling in the present study. Using increasing D values for Sr in plagioclase with crystallization (decreasing An content) has a better fit for calculated re-equilibrated Sr in plagioclase in both the Skaergaard intrusion (Fig. 5.6) and the Upper Zone of the Bushveld Complex (Fig. 6.3). Hence, it appears Sr is more compatible in plagioclase at lower An contents as Blundy and Wood proposed.

Cawthorn (2006) computed Sr contents of the magma at the Pyroxenite Marker based on estimated values of Cawthorn and Davies (1984) and showed it to have 290ppm of Sr. It was also observed that the computed liquid contents of other levels were between 250 to 300 ppm Sr, similar to the liquid content of most basaltic magmas. Similarly, Vantongeren et al. (2010) proposed values between 200 and 300 ppm for the magma at the base of UZ by adding between 15-25% roof rock compositions in calculating the liquid content. The value of 273 ppm Sr calculated in this study for the base of UZ is therefore quite similar to the values proposed by Cawthorn (2006) and Vantongeren et al. (2010).

The estimate of Davies and Cawthorn for the Ba content of the magma at the PxMk is 176 ppm. Vantongeren et al. (2010) proposed Ba values in the range of 230 to 425 ppm for the magma at the PxMk in their modeling. In the present study, the Ba content of the magma at the base of UZ is calculated to be 325 ppm. The value calculated in this study is within the range of values proposed by Vantongeren et al. (2010). However, considering the Ba

estimates of 230 to 425 ppm for the parental magma and average Ba in plagioclase of 90 ppm of Vantongeren et al. with D_{Ba} in plagioclase between 0.3 and 0.6, a re-calculation to the Ba in plagioclase ought to be between 70 and 255 ppm. The upper value of 255 ppm differs enormously from their observed data for Ba in plagioclase, justifying the need to allow for the TLS effect. Using these D values and allowing for the TLS effect in the present study leads to values for Ba in plagioclase which agree fairly with observed data.

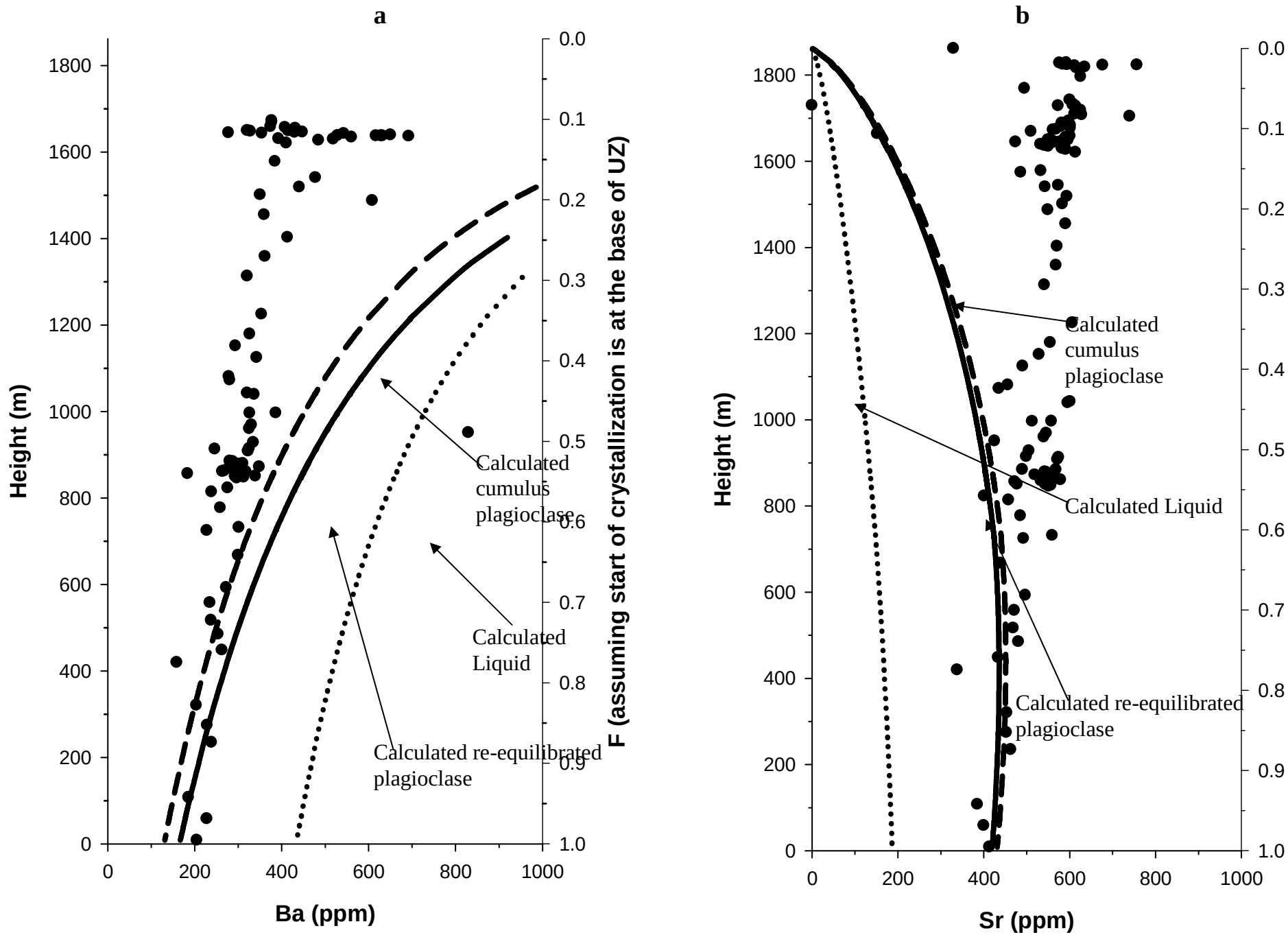


Fig. 6.4 Trends for Sr and Ba contents of liquid, cumulus and re-equilibrated plagioclase for the Bushveld intrusion calculated from equations by Blundy and Wood (1991)

6.6. Incorporation of lost Magma in the Upper Zone

In a model presented by Cawthorn and Walraven, (1998) for the crystallization of the entire Bushveld Complex, the UZ magma chamber was proposed to initially encompass 4000 m of magma. Of this amount, about 1500 m (35%) of evolved SiO_2 rich magma were considered to have escaped from the magma chamber. Their interpretations were based on Zr and K contents in UZ. Building on their proposal, a model was presented to show that the missing magma may be represented in the felsic roof rocks of the Bushveld Complex (Vantongeren et al., 2010).

The escape of this magma can be considered in terms of two extreme end members. One extreme model would be to suggest that all the magma is retained in the chamber until the last 1.5 km remained and that volume was then totally extruded. However, it is known that the Mg# of the mafic minerals decreases to essentially zero at the top of the Upper Zone (Tegner et al., 2006) and so indicates the very end of fractionation. Hence this extreme view cannot apply. The alternative model is to consider continual extrusion during the formation of the Upper Zone. Removal of some magma would not change the overall chemical evolutionary trend of the evolving magma relative to that calculated previously. However, it would affect the relative volumes, and so affect the value of F in the graphs. Incorporating the process of continual magma loss would mean that the rate of upward change in F would be overestimated near the base, and would be underestimated near the top relative to the present models. The numerous uncertainties make attempts at quantitative modeling too unconstrained.

6.7. Possible magmatic processes in the Upper Zone

In addition to the presence of at least 20 magnetitite layers in the Upper Zone and the intermittent occurrence of apatite, the general differentiation trend in the Bushveld Upper Zone is interrupted by reversals in mineral compositions (Molyneux, 1974; Ashwal et al, 2005; Tegner et al., 2006). Plagioclase An contents in the present study also decrease fairly regularly upward, showing normal upward fractionation. The most abrupt reversal in the An content which was recognized by Tegner et al. was examined in greater detail in the present study. In view of these reversals in mineral composition, the most likely anticipated mechanisms are magma addition and/or overturn. The possibility of major magma addition has been disputed due to constancy in Sr_o data (Kruger et al., 1987; Tegner et al., 2006). The model presented in section 6.1 therefore presupposes that the Upper Zone evolved from a single magma without major addition of magma. Although the Sr and Ba data in the present study have been made to fit a single homogeneous magma model, it is necessary to consider various mechanisms which have been proposed to occur in UZ in terms of these data. We therefore proceed to explore these mechanisms with specific emphasis to the effect they would have on Sr and Ba contents of plagioclase. The mechanisms presented in this section have been reviewed by Cawthorn and Ashwal (2009) based on the An content of plagioclase.

6.7.1. Re-examination of the single magma model

A fractionating magma in which the bulk D for Sr is very close to 1 would not change considerably in terms of the liquid and hence in plagioclase Sr content. Ba with bulk D far less than 1 throughout crystallization ought to increase in both the liquid and plagioclase. However, given the uncertainties initiated by trapped liquid variations and modal variation, small scale variation may exist in the plagioclase compositions and a uniformly smooth trend may not be observed. Data in the present study show a general steady upward increase in Sr and have been modeled as resulting from a single differentiating series. Ba contents of plagioclase remain fairly constant throughout and

only increase towards the end of crystallization; but modeling has shown this trend to be a consequence of the trapped liquid shift effect.

In the Skaergaard intrusion, data for the layered series show an increase in Sr contents of plagioclase (Wager and Mitchell, 1951; Jang and Naslund, 2001). In the Kiglapait intrusion, plagioclase Sr increases steadily with height and only decreases at the level where significant potassium feldspar starts to crystallize (Morse, 1982), probably changing the bulk D to greater than unity. These two intrusions have been shown to embody rocks which evolved as closed systems. However, their compositions have been modeled by various authors and some major additional processes have also been suggested such as magma addition (e.g. Stewart and De Paulo, 1990). It therefore becomes important to explore the possibility of such processes where data are available in order to raise understanding of magmatic processes in these layered intrusions. Generally, it is acknowledged that deviations in the general trend which are sustained over considerable vertical intervals could relate to some additional process occurring in the magma chamber.

6.7.2. The Possibility of fractionation Cycles

Tegner et al. (2006) identified cycles in the Upper Zone based on reversals to higher An content of plagioclase and the intermittent occurrence of apatite and olivine. The most prominent reversal observed in their study was also observed in the present study so it became necessary to infer if there were any fractionation cycles in the Sr and Ba data and whether they matched with those recognized by Tegner et al. It was shown in Chapter 4 (Fig. 4.12) that Sr seems to portray patterns which suggest breaks in differentiation. However, it seems implausible for a magma which fractionated with bulk Ds similar to those of the Bushveld Complex (that is, very close to unity) to portray such fractionation cycles. In view of Sr evolution, fractionation cycles are not likely to occur in the sequence because the liquid does not change significantly in Sr. For Ba, the TLS effect ought to mask the effect of any process such as overturn and mixing. Furthermore, not all the “cycles” seem to match with those recognized by Tegner et al. Although there is an

uncertainty in defining the cycle boundaries, the fact that the two do not co-inside suggests that the cycles are not related and do not necessarily represent breaks. Across the Lower- Upper Critical Zone boundary, Sr contents of plagioclase reported by Reichardt (1989) show similar variability (Fig. 6.5) even though they were analyzed by isotope dilution which is a very precise technique. Thus such variability seems inherent in the data.

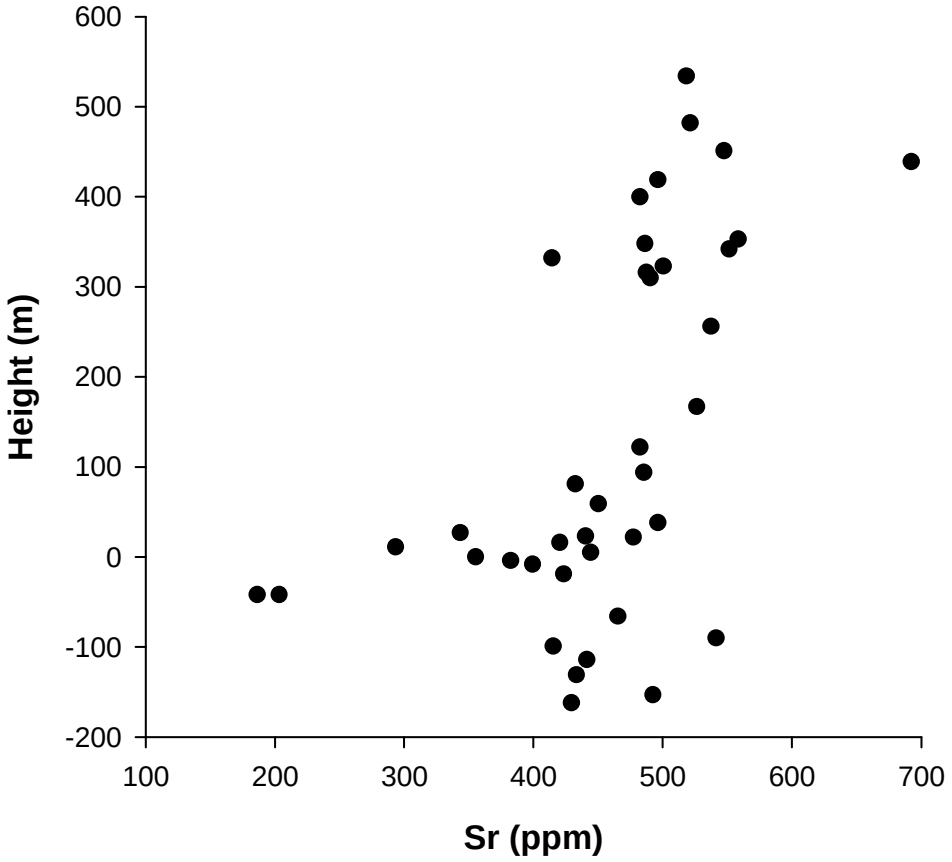


Fig. 6.5 Sr contents of plagioclase across the Lower- Upper Critical Zone boundary. Height is quoted relative to the base of the Upper Critical Zone (Reichardt, 1989)

6.7.3. Magma addition

Magma recharge has been used by various authors to explain the reversals in mineral composition and the origin of magnetitite and anorthosite layers in the Upper Zone of the Bushveld Complex. However, this possibility was refuted in the eastern and western

limbs based on constancy in Sr_o data (Kruger et al., 1987; Tegner et al., 2006) hence later studies focused mainly on internal mechanisms for the generation of this part of the Complex. However, Ashwal et al (2005) suggested that the reversals in plagioclase An content and pyroxene Mg# in UZ in the northern limb resulted from magma addition even though Sr_o ratios seemed more or less constant through the entire UZ sequence (Ashwal, Pers. Comm.). Harney et al. (1990) also suggested magma addition to be a cause for differences in Sr and Sr/Al_2O_3 ratios below and above MML. They proposed that if a very small volume of magma with a different Sr isotope ratio was added into the magma chamber, there will be no significant change in the Sr isotope ratio. These possibilities are discussed below.

The addition of magma can be considered in terms of two possibilities. One of the probabilities would be to suggest that the new magma added could be of the same genesis as the resident, but could be more primitive or more differentiated than the resident magma. The other model is to consider that the new and resident magmas are unrelated, and hence could either have more or less Sr and Ba contents than the resident. The two possibilities are discussed below.

6.7.3. a. Addition of New Magma of the same Genesis as Resident

Modeling has shown that there should to be very minimal change in the Sr content of liquid and hence in plagioclase with crystallization. This implies that any magma added, whether more primitive or more differentiated than resident will not induce trends different from that of a single homogeneous magma body. Therefore, Sr in plagioclase would not indicate magma addition in such an instance. On the other hand, Ba being incompatible in plagioclase with a bulk D far less than 1 would increase prominently in the liquid throughout crystallization and hence in plagioclase as shown in Fig. 6.6a if the fractionating magma evolved without further recharge during its crystallization. However, addition of a large proportion of magma to the magma chamber is expected to change the crystallization mode, depending on its composition.

In exploring the effect of this process, it is critical to consider the nature of the magma added (primitive or more differentiated) and the manner in which the added and residual magmas would further differentiate, depending on how it was added and its composition. The consequences of magma addition are shown in Fig. 6.6b to e. If the added magma is more primitive than resident and mixes upon addition, a new fractionation cycle may be initiated depending on whether there was rapid mixing (Fig. 6.6b) or slow mixing (Fig. 6.6c). If the added magma is denser than resident, it is unlikely for mixing to occur hence it would differentiate in a similar way to Fig. 6.6b. The added magma could also be more differentiated than resident and mix immediately or differentiate in a stratified magma chamber as shown in Fig. 6.6d or mix slowly (Fig. 6.6e). Modeling in the present study has shown that the increase in plagioclase Ba with crystallization may not be observed as a result of the trapped liquid shift effect. Therefore, in discussing the effects magma addition would have on the Ba contents of plagioclase, it is necessary to consider the TLS effect. The TLS would act by camouflaging any magma addition event, thus Ba may not indicate clearly if such a process has occurred.

6.7.3. b. Addition of New Magma with Unrelated Plagioclase Compositions

If the magma added to the chamber is unrelated to the resident magma, there is no idea of the trace element contents. If such magma were to be added to the magma chamber, there would be sudden changes in the Sr and Ba contents of liquid and hence plagioclase. However, because there are no sudden changes in the Sr and Ba contents of plagioclase, this is unlikely to have occurred.

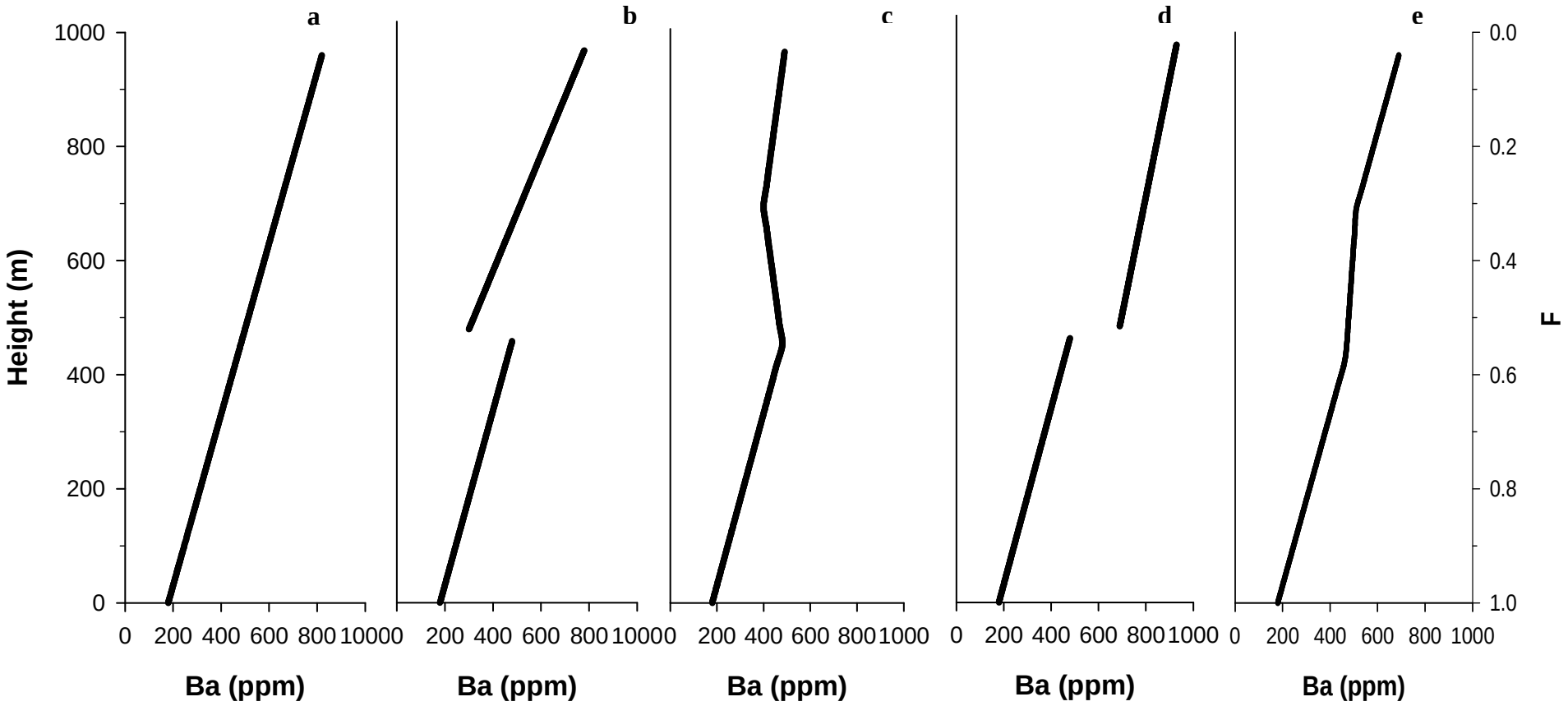


Fig. 6.6 Possible trends in the Ba contents of plagioclase plotted against height and fraction of magma remaining

6.7.3. c. Discussion

Magma recharge has been used by various authors to explain the reversals in mineral composition and the origin of magnetitite and anorthosite layers in the sequence. In the Upper Zone for which Sr_o ratios are constant throughout, it might be suggested that new magma with Sr_o identical to that in the UZ magma chamber, but more primitive was added and thorough mixing and homogenization led to progressive reversals in mineral compositions each time the new magma was added. This model stems from that proposed by Irvine (1977) for inducing the chromitite layers in the Muskox intrusion and analogous deposits. It should be noted that two isotopically identical magmas might differ chemically based on dissimilar degrees of fractionation. The model requires that the added magma mixes with the resident magma. However, it is not possible to resolve quantitative relations of new and resident magmas with the present data. For reasons discussed above, the Sr and Ba contents of plagioclase do not appear to be good indicators of such magma addition. Hence the possibility of magma recharge is not indicated in the Sr and Ba contents of plagioclase.

However, various problems exist with the application of this mechanism. It is generally believed that the magma added at the Pyroxenite Marker mixed and homogenized to form the uppermost rocks. This means that any magma which would have been added during UZ formation would have to have the same Sr_o as the resident (mixed) magma. It is improbable for such magma to be introduced into the chamber from a different locality but with the same Sr_o as that of UZ. The other issue with the model is that liquids with very minute density contrasts would not mix. In order for mixing to occur, the added and resident magmas ought to have equal densities and this situation seems highly implausible considering the inability of magmas to mix over huge horizontal distances. Furthermore, even if it is proposed that there was magma addition without mixing but stratification, it still remains difficult to explain the origin of the added magma and how it is possible for it to have the same Sr isotope ratio as that of UZ which obviously crystallized from mixing of residual MZ magma and added magma at the Pyroxenite Marker.

The model proposed by Harney et al. (1990) does not seem plausible in the present case because if a small volume of magma is added and mixes with the resident magma, its effect on plagioclase and other mineral compositions will also be negligible. In view of plagioclase Sr, such a process would progress in a similar way to that of a single magma fractionating hence fractionation cycles and reversals will not be observed. Taking into consideration the difficulty of magmas to mix, it might be suggested instead that a small proportion of magma was added and differentiated in a stratified magma chamber which should lead to dissimilar Sr_o at these levels. However, Sr_o studies done on 15 (Kruger et al., 1987) in addition to 8 (Tegner et al., 2006) and 10 (Sharpe, 1985) samples in the UZ sequence all give the same Sr_o, thus challenging the possibility of magma addition in UZ.

6.7.4. Crystal Settling and Sorting

After reviewing various proposed mechanisms which might have operated in the Upper Zone, Cawthorn and Ashwal (2009) showed crystal settling and sorting (previously suggested by Wager and Brown, 1968) augmented by pressure fluctuations as a more feasible mechanism to generate the anorthosite and magnetitite layers present. Their investigations were based on density measurements on modally graded units and ensued from the general absence of reversals in mineral compositions across these layers. The consequence of this process is discussed below in line with data for the present study.

Settling and sorting of crystals implies that during fractionation, several minerals crystallize at the same time (resulting in overall near constant bulk D) but settle at different rates due to density difference. The corollary of this process is that there ought to be no reversals or fractionation cycles in the intrusion. Therefore, the Sr and Ba in plagioclase would show a trend similar to normal differentiation. The Sr content of plagioclase generally follows this trend, apart from the small scale variation and a few odd values. This mechanism affects the trapped liquid contributions from the units in UZ with extremely different plagioclase proportions especially for incompatible elements as shown in section 6.3. The difference in contributions from trapped liquid and plagioclase proportion in these units show that there can be massive variation in the Ba contents of

plagioclase at very close stratigraphic levels. This process can therefore explain the small scale variation observed in the Ba contents of plagioclase. The effect is much less for a compatible element such as Sr in plagioclase so the variation observed in the Sr trend cannot also be explained by the same process. It is therefore proposed that the effects of crystal settling and sorting can be observed in the Sr and Ba contents of plagioclase in UZ. This mechanism also provides an explanation for the vertical changes in modal proportion and mineralogy in UZ.

6.7.5. Magma Overturn

Using mineral composition, whole rock and Sr isotope data, Tegner et al. (2006) showed the fractionation cycles observed in their study to be a result of bottom crystallization from a stratified magma which led to density inversion, magmatic overturn and possible mixing events in the magma chamber. They proposed that differentiation and crystallization occurred principally at the bottom of the magma chamber whereas the rest of the magma remained primitive and did not differentiate. Their model demonstrates how crystallization of gabbronorite in the Upper Main Zone would lead to an increased density in the residual liquid. This condition is interrupted in UZ by the crystallization of Fe-rich magnetite and olivine successions, leading to density inversion and periodic mixing with primitive overlying magma, thereby creating a more primitive composition at the crystallization front.

Modeling in section 6.4 has shown that the Sr content of liquid and plagioclase do not change considerably because the bulk D is close to 1 throughout crystallization. If density inversion and mixing are initiated due to the crystallization of magnetite and/or olivine rich rocks, the residual liquid with unchanged Sr contents mixes with an overlying layer with more primitive magma. However, mixing would not cause a significant change in the Sr content of the resultant liquid because the two liquids have similar Sr contents, due to the fact that the Sr content of liquid did not change (increase or decrease) prior to mixing. Therefore the Sr content of the mixed liquid does not change before it starts fractionating again. The next crystallization event is expected to start with Sr contents in liquid similar

to the one before magma mixing and the overall effect will be very similar to differentiation of a single homogenous magma. Hence the Sr contents of plagioclase will not indicate if a process such as overturn and consequent mixing has occurred.

The effect of this overturn and mixing ought to be much more pronounced for the Ba contents of liquid and likewise plagioclase because bulk D for Ba during crystallization remains < 1 and the Ba content of liquid increases significantly. Mixing with less differentiated magma, with obviously lower Ba contents should initiate a perceptible fractionation cycle. However, due to the TLS effect, original cumulus compositions would react with intercumulus component reducing the effect of any magma mixing event. This implies that Ba contents of plagioclase need not show the effect of overturn if it occurred in the magma chamber.

It can therefore be concluded that magma overturn, which was shown to result from the crystallization of Fe-rich rocks is not testable in the trends for Sr and Ba in plagioclase. The inability for plagioclase Sr and Ba to show the effect of magma overturn can be confirmed by observing the change in these trace elements in the interval over which a prominent reversal in plagioclase An such as the one revealed by Tegner et al. (2006) and the present study occurs. The reversal occurs from 846 to 888 m and the section is shown in Fig. 6.7. The ±30 m interval over which this reversal occurs contains about 6 magnetitite layers all adding up to about 1m in thickness. If magma overturn were to induce a significant change in the Sr (and Ba) trend, it would be expected that the trend at this level be significantly different due to mixing with primitive magma. However, this difference is not observed at the level of the reversal. Sr contents vary erratically between 401 and 559 ppm below the reversal. At the level of the reversal, they vary between 472 and 580 ppm and above the reversal between 490 and 575 ppm Sr. For Ba, the variation is again irregular, between 228 and 302 ppm below the reversal, between 264 and 349 ppm within the reversal and between 247 and 335 ppm above the reversal. Given the general variation in plagioclase Sr and Ba noticed in the present study, this difference does not represent a major change in Ba and Sr contents of plagioclase below, within and above the reversal. Hence the Sr and Ba contents of plagioclase are not good markers for testing the

occurrence of magma overturn and thus, the possibility of magma overturn cannot be resolved with data for these trace elements.

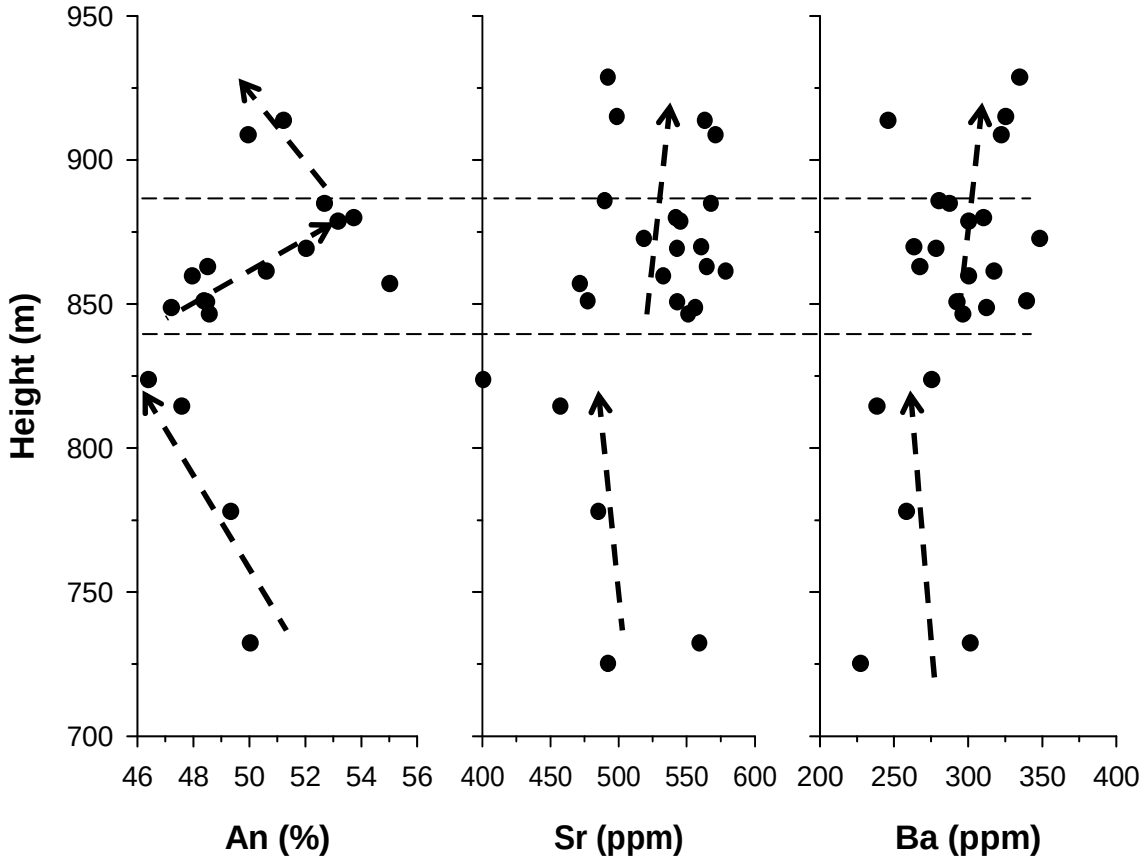


Fig. 6.7 Sr and Ba contents of the section over which the largest reversal in plagioclase An occurs in the Upper Zone of the Bushveld Complex

Data for Sr in plagioclase were also presented by Harney et al. (1990) for the lower part of UZ (Table 6.2). Sr was shown to increase above the Main Magnetitite Layer on account of mixing between density stratified layers. However, a reassessment of these data show that considering the internal scatter in the Sr contents of plagioclase in the present study, the ± 25 ppm change in the Sr content of plagioclase above the MML does not represent a significant change in the Sr content of plagioclase. The internal scatter observed in the Sr contents of plagioclase in the present study is more than the quoted 25 ppm change above the MML and can therefore not be attributed to a mixing event in the magma chamber.

Table 6.2.Data for Sr in plagioclase in the lower part of the Upper Zone of the Bushveld Complex. Height is quoted relative to the base of the MML. Data from Harney et al. (1990)

Height (m)	Sr (ppm)
210	440
195	440
125	448
35	455
10	451
5	442
-10	431
-20	414
-25	431
-45	433
-80	387
-110	458
-125	434
-295	432
-625	379
-825	437

A possible way to further investigate the occurrence of this model is to observe the behavior of Fe_2O_3 in the sequence. If the model predicts that the crystallization of Fe rich rocks led to density inversion and mixing, then it would be expected that an increase in the Fe content of whole rocks at each level be followed by a cycle in UZ. Fig 6.8 shows an identical section for which geochemical cycles were delineated based on the behavior of this Fe (Fig. 6.8a), compared with the cycles identified by Tegner et al, (2006) in Fig. 6.8b. The two profiles show that only 2 of the 9 cycles identified by Tegner et al are directly linked to an increase in Fe_2O_3 in the sequence. Investigations by Cawthorn and Ashwal, (2009) also showed that out of twenty magnetitite layers, only one shows a significant reversal in plagioclase An content. Thus they went further to challenge magma overturn as a mechanism which led to the formation of magnetitite layers in UZ.

It is clear from the above discussions that testing a model such as overturn and mixing requires a geochemical parameter which changes prominently with crystallization. The Sr and Ba contents of plagioclase do not do so. They will therefore not indicate if overturn and mixing have occurred in the magma chamber. The An content of plagioclase appears

to be more indicative of such processes because it ought to vary prominently with crystallization.

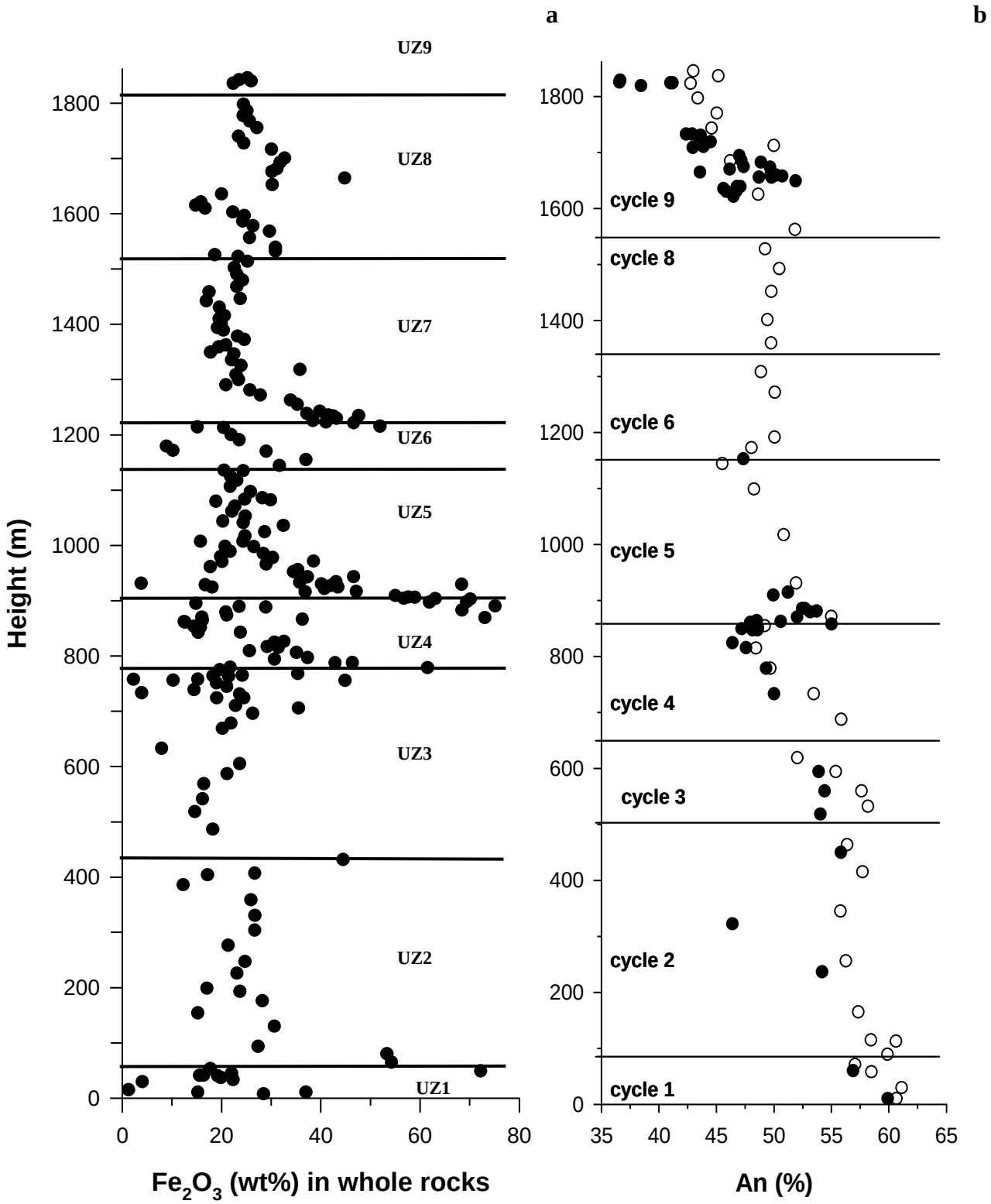


Fig. 6.8 Comparison of cycles based on increase in Fe_2O_3 in whole rocks with reversals in plagioclase An content identified by Tegner et al (2006). Filled circles are An contents from this study and empty circles are An contents from Tegner et al. Fe_2O_3 data are from Roberts (2005)

6.8. Summary

The evolution of the Upper Zone in the Bushveld Complex was examined with the use of major and trace element contents of plagioclase. A model was developed for the trace elements by building up a fractionation model for the Skaergaard intrusion, which is similar to the Bushveld Upper Zone and applying it to the later. Development and subsequent application of the Skaergaard model stems from the fact that it is well constrained in terms of starting liquid compositions, mineral proportions and trapped liquid fractions. Modeling of the Sr and Ba contents of plagioclase shows that the Upper Zone of the Bushveld Complex can be modeled as a single magma which evolved as an uninterrupted differentiated series

The fundamental importance of allowing for trapped liquid crystallization in modeling has also been demonstrated by showing the TLS effect especially for Ba which is incompatible into plagioclase. Due to the TLS effect, Ba can have up to three times higher Ba in the re-equilibrated plagioclase relative to the original cumulus plagioclase content. The TLS effect depends on the fraction of TL with which the mineral assemblage under consideration crystallized and the modal proportion. For example, the TLS effect is small for the Upper Zone of the Bushveld compared to the Skaergaard intrusion because in the former, smaller TL fractions (about 10%) are involved whereas TL fractions vary from 45 to 4% in the Skaergaard intrusion. The TLS effect is trivial for Sr which is compatible into plagioclase.

One reversal in the An content of plagioclase was examined in the sequence in addition to various reversals in mineral composition previously recognized. The two most quoted mechanisms which can induce these reversals appear to be magma recharge or overturn. Therefore, these and additional models which were proposed to have occurred in UZ have been examined in line with data in the present study. The possibility of these two mechanisms cannot be resolved with data in the present study because Sr and Ba contents of plagioclase do not appear to be good indicators of magma overturn and or addition. Therefore, the effects of these previously proposed hypotheses cannot be tested with Sr

and Ba data in the present study. It is emphasized that with the several uncertainties involved, none of the mechanisms which had previously been put forward for producing the features in UZ can be completely ruled out.

Chapter 7- Conclusions

The original thesis was designed to test various models for the evolution of the Upper Zone of the Bushveld Complex using trace elements. For the reason that the Skaergaard intrusion is much more constrained and available trace element data for plagioclase had not been quantitatively modeled before, the models were examined first in the Skaergaard intrusion. The project was eventually refocused to explain why previous models did not work, and the importance of the trapped liquid shift (TLS) effect became the main focus of this study. This aspect has been quantitatively modeled for both the Skaergaard and the Upper Zone of the Bushveld Complex, which has not been attempted or achieved before.

7.1. Differentiation Patterns

Plagioclase compositions in the Upper Zone of the Bushveld Complex generally show normal fractionation trends upwards in An, Sr and Ba contents. However, a reversal in the An content of plagioclase which has previously been identified (Tegner et al., 2006) was recognized in the present study. Possible causes for this and other reversals in mineral composition in the sequence are magma recharge and or internal overturn. However Sr_o data refute the possibility of major recharge in UZ. The small scale random variation in the Sr and Ba contents of plagioclase is a feature common to plagioclase at several different levels in the Bushveld Complex.

7.2. Rayleigh Fractionation and the trapped liquid shift effect

Rayleigh fractionation was tested in the Skaergaard intrusion by three different means. Initially, the equation, $D= C_M/C_L$ (equation 5.2) was used to calculate the Ba content of starting liquid (C_o) for the Skaergaard intrusion (at LZa, where the lowest analyzed sample was obtained) and the Rayleigh law was used to model the entire intrusion. However, the calculated value for C_o was more than two times higher than the range of typical Ba contents of Skaergaard parental liquid. In addition, the rate of increase in

calculated Ba contents of plagioclase did not fit the observed data of Jang and Naslund (2001). Secondly, a value within the range of typical Ba contents of starting liquid was used to model the Skaergaard intrusion using the Rayleigh law, but calculated Ba contents of plagioclase did not fit observed data as well. The inference of the lack of agreement is that there is a problem with the conventional modeling procedure. Lastly, the intrusion was modeled by using the value within the range of typical Ba contents of starting liquid, applying the Rayleigh law and allowing for the TLS effect. The model showed that due to the TLS effect, the original cumulus and re-equilibrated concentrations for Ba, an incompatible element can differ by a factor of nearly three in cumulus vs. re-equilibrated plagioclase. Furthermore, calculated Ba contents of re-equilibrated plagioclase were in much better agreement with observed data compared to the previous models in which allowance was not made for the TLS effect. Hence using the conventional Ba content of starting liquid and allowing for the TLS effect resolved the modeling for Ba in plagioclase in the Skaergaard intrusion.

The implications of the results of modeling for Ba in plagioclase are that equation 5.2 must not be used to calculate the starting liquid content of an element as it will lead to erroneous modeling especially for incompatible elements. Allowance must also be made for the TLS effect during modeling in order to account for the contribution from the intercumulus liquid to the mineral being considered. The classic starting liquid content of Sr was also used in modeling Sr in plagioclase for the Skaergaard intrusion and calculated Sr contents of plagioclase were also in good agreement with observed data for Sr in plagioclase. For Sr which is compatible into plagioclase, the TLS effect is trivial.

In the case of the Upper Zone of the Bushveld Complex, values for F, D_{Ba} in plagioclase, plagioclase mode and TL fraction were used to set up a calculation similar to the Skaergaard intrusion. Different starting liquid compositions were then tried into the built in calculation until values were obtained for which Ba and Sr contents of calculated re-equilibrated plagioclase were in agreement with analytical data. The calculated Ba contents of re-equilibrated plagioclase also differ from respective original cumulus contents due to the TLS effect. Therefore, applying the model to the Upper Zone of the

Bushveld Complex validates the importance of the TLS effect. This implies that using the Rayleigh Law without allowing for the TLS effect would lead to incorrect modeling and interpretations.

The model developed (which allows for the TLS effect) and applied to both intrusions validates the effect of trapped liquid equilibration on original cumulus compositions of minerals in large magmatic systems such as the Bushveld and Skaergaard intrusions. The effect of intercumulus component on original cumulus contents of minerals has been presented by Barnes (1986) and Cawthorn (1996) and it was noted that original cumulus compositions can be modified significantly by reaction with trapped intercumulus liquid. This effect has been shown for barium in plagioclase in the present study and also depicts the difference in trapped liquid contribution when a mineral such as plagioclase becomes a minor crystallizing phase in the sequence. The Bushveld Upper Zone is comprised of rocks which vary from pure anorthosites to nearly monominerallic magnetitite layers. Although the magnetite-rich successions which are poor in plagioclase constitute less than 30 m of the total UZ thickness, plagioclase compositions in such rocks result from a relatively large proportion of intercumulus component compared to cumulus plagioclase. It is therefore possible for two adjacent rocks to concentrate enormously different contents of trace elements in their plagioclase. The variation in the Ba content of plagioclase in both sequences is explained by this process.

The model shows clearly that the composition obtained from analyzing a mineral such as plagioclase is a bulk summation of cumulus an intercumulus component. Trace elements such as Sr and Ba diffuse very easily within an originally inhomogeneous plagioclase grain, thereby permitting rapid homogenization. Thus it is not possible to obtain values for Ba and Sr which only result from cumulus or intercumulus material by analyzing the bulk plagioclase grain. Contrarily, it has generally been assumed that plagioclase in UZ is purely cumulus; hence this assumption is incorrect. Modeling requires knowledge of precise mineral proportions, trapped liquid fractions and F values (fraction of magma remaining) for the entire intrusion. The evidence of the escape of evolved magma is not

observed in the An, Sr and Ba contents of plagioclase. However, the possible effect of magma loss has been introduced in terms of the model developed in the present study.

7.3. Partition Coefficients

The importance of trace element partitioning in modeling the evolution of magmatic systems has been demonstrated in various studies. However, available data show that a wide range of partitioning values can exist for a single element into a mineral depending on the experimental method or samples used. It therefore becomes difficult to choose what partitioning values to use in modeling.

However, modeling the Ba contents of plagioclase in the Skaergaard intrusion showed that the model developed and applied is relatively insensitive to varying partition coefficient values between reasonable published values; hence a constant D_{Ba} in plagioclase was used in modeling. The partition coefficient used for Ba in plagioclase in modeling is within the range quoted in several studies for plagioclase of Skaergaard composition (e.g. Blundy and Wood, 1991). However, with the number of uncertainties involved, it was impossible to infer if it changes or remains constant with crystallization. However, for Sr which is compatible into plagioclase the model is sensitive to variations in D_{Sr} in plagioclase. Therefore, D_{Sr} in plagioclase was varied smoothly from 1.7 at the start of fractionation to 1.9 at the end. These values used are much less than values quoted in previous studies. Using values from the literature (which are typically greater than 2) results in calculated Sr contents of re-equilibrated plagioclase which do not match with observed data. The fact that D_{Sr} in plagioclase increases with fractionation implies that Sr is more compatible in plagioclase at lower An content (end of crystallization) and less compatible at higher An content (start of crystallization), a behavior which has been predicted in many studies (Drake and Weill 1975; Blundy and Wood, 1991).

Modeling for the Upper Zone of the Bushveld Complex was based on the outcome of the Skaergaard model. Therefore, a constant D_{Ba} in plagioclase of 0.4 was used and D_{Sr} in plagioclase was set to vary from 1.5 to 2.1 in the built in calculation. These D values give

a reasonable fit for the model as calculated re-equilibrated plagioclase compositions are similar to analyses.

For both the Skaergaard intrusion and the Upper Zone of the Bushveld Complex, a constant D_{Sr} in plagioclase was tested in the model. However, it was noticed that a better fit could be obtained by increasing D_{Sr} in plagioclase with crystallization. The fact that different Ds for Sr were used for the two intrusions validates the fact that a realistic range of Ds can be used for trace elements and made to fit a single consistent model.

7.4. Calculated Liquid Contents

The different means by which Rayleigh fractionation was tested in the Skaergaard intrusion have been shown in section 7.2. In the first model, the value calculated for Ba in the starting liquid is 260 ppm. Contrarily, the value calculated at this level from the classic Ba content of starting liquid (80 ppm) is 100 ppm. The difference between the two calculated values is large, hence there has to be a problem with one of the approaches. However, because various authors have shown the Skaergaard starting liquid to have between 50-90 ppm Ba, the value of 260 ppm calculated at this level is considered quite large and is wrong. Thus a problem exists with the approach of calculating the starting liquid composition by using a D value and the observed mineral composition (equation 5.2). This method was therefore not applied.

Before this project was initiated, there had been no known attempt to calculate the trace element content of the liquid at the base of the Upper Zone of the Bushveld Complex. Hence a value was not available to put into the model as for the Skaergaard intrusion. The starting liquid contents of Sr and Ba were calculated at 273 ppm and 325 ppm respectively. The Sr content of liquid remains fairly constant with crystallization because the D values used and plagioclase proportion accumulating at the cotectic lead to a bulk D which is close to unity. The liquid concentration of Ba increases steadily with crystallization because the bulk D remains less than 1 throughout crystallization.

The calculated liquid content of Sr at the base of UZ is similar to the value computed by Cawthorn (2006) and Vantongeren et al. (2010) for the magma at the Pyroxenite Marker. Cawthorn (2006) also showed that the Sr content of liquid is near constant at different levels in the sequence, similar to most basaltic magmas. The computed starting liquid content of Ba falls within the ranges of values proposed by Vantongeren et al. (2010) for the magma above the PxMk.

7.6. Magma Chamber Processes

Various magmatic processes which have been proposed for the Upper Zone of the Bushveld Complex cannot be uniquely and conclusively resolved with the present data only. There are many uncertainties to be considered with the application of proposed magmatic processes in the present study. The fact that Sr and Ba contents of plagioclase do not appear to be good indices of processes such as addition and mixing limit the applicability of these processes. Therefore, none of the proposed magmatic processes can be eliminated and it appears no unique single process seems to have operated in UZ. However, the model developed for UZ is such that any new magmas can be put into the sequence manually by entering a new set of data at the specific value for F or height.

It is noted that no single mechanism seems to explain all the features noticed in UZ. While a single magma model is generally supported due to constancy in isotope ratio and its better applicability in UZ, the reversals in mineral composition need an additional mechanism such as magma overturn or addition. This issue has been emphasized by Cawthorn and Ashwal (2009) and the present study illustrates a similar outcome of modeling.

References

Ashwal, L. D., Webb, S. J. & Knoper, M. W. (2005). Magmatic stratigraphy in the Bushveld northern lobe: continuous geophysical and mineralogical data from the 2950m Bellevue drill core. *South African Journal of Geology* **108**, 199–232.

Barnes, S.J., (1986). The effect of trapped liquid crystallization on cumulus mineral compositions in layered intrusions. *Contributions to Mineralogy and Petrology* **93**, 524-531.

Bedard, J. H. (2006). Trace Element partitioning in plagioclase feldspar. *Geochimica et Cosmochimica* **70**, 3717-3742

Blundy, J., (1997). Experimental study of a Kiglapait marginal rock and implications for trace element partitioning in layered intrusions. *Chemical Geology* **141**, 73–92.

Blundy, J.D., Wood, B.J., (1991). Crystal-chemical controls on the partitioning of Sr and Ba between plagioclase feldspar, silicate melts, and hydrothermal solutions. *Geochimica et Cosmochimica* **55**, 193–209.

Brooks, C. K., Nielsen, T. F. D. (1978). Early stages in the differentiation of the Skaergaard magma as revealed by closely related suite of dike rocks. *Lithos* **11**, 1–14.

Cawthorn, R.G., (1996). Models for incompatible trace-element abundances in cumulus minerals and their application to plagioclase and pyroxenes in the Bushveld Complex. *Contributions to Mineralogy and Petrology* **123**, 109-l 15.

Cawthorn, R.G. (2006). Cr and Sr: Keys to parental magmas and processes in the Bushveld Complex, South Africa. *Lithos*. **95**, 381-398.

Cawthorn, R. G. & McCarthy, T. S. (1980). Variations in Cr content of magnetite from the Upper Zone of the Bushveld Complex-evidence for heterogeneity and convection currents in magma chambers. *Earth and Planetary Science Letters* **46**, 335–343.

Cawthorn, R.G., Davies, G., (1984). Experimental data at 3 kbars pressure on parental magma to the Bushveld Complex. *Contributions to Mineralogy and Petrology* **83**, 128–135.

Cawthorn, R. G. & McCarthy, T. S. (1985). Incompatible trace element behavior in the Bushveld Complex. *Economic Geology* **80**, 1016–1026.

Cawthorn, R. G. & Walsh, K. L. (1988). The use of phosphorus contents in yielding estimates of the proportion of trapped liquid in cumulates of the Upper Zone of the Bushveld Complex. *Mineralogical Magazine* **52**, 81–89.

Cawthorn, R. G., and Walraven, F. (1998). Emplacement and crystallization time for the Bushveld Complex. *Journal of Petrology* **39**, 1669–1687

Cawthorn, R. G., and Webb, S. J. (2001). Connectivity between the western and eastern limbs of the Bushveld Complex. *Tectonophysics* **330**, 195-209.

Cawthorn, R. G., and Meyer, P. S., Kruger, F.J. (1991). Major addition of magma at the Pyroxenite Marker in the Western Bushveld Complex South Africa. *Journal of Petrology* **32**, 739–763

Cawthorn, R. G., Ashwal L. D., (2009). Origin of Anorthosite and Magnetitite Layers in the Bushveld Complex, constrained by Major Element Compositions of plagioclase. *Journal of Petrology* **50**, 1607-1637

Cawthorn, R. G., Cooper, G. R. J. & Webb, S. J. (1998). Connectivity between the western and eastern limbs of the Bushveld Complex. *South African Journal of Geology* **101**, 291-298

Coertze, F. J. (1970). The geology of the western part of the Bushveld Complex. *South African Geological Survey*, Special Publication **1**, 5–22

Cox, K. G., Bell, D. and Pankhurst, R. J. (1979). Interpretation of Igneous rocks George Allen and Unwin, London, 450 p.

Drake, M. J. and Weill, D. F. (1975). The partition of Sr, Ba, Ca, Y, Eu2+, Eu+, and other REE between plagioclase feldspar and magmatic silicate liquid: an experimental study. *Geochimica et Cosmochimica*. **39,** 689-712.

Eales, H.V. & Reynolds, I.M. (1986). Cryptic Variations within Chromitites of the Upper Critical Zone, Northwestern Bushveld Complex. *Economic Geology,* **81,** 1056-1066.

Eales, H. V. and Cawthorn, R. G. (1996). The Bushveld complex. *in* Layered intrusions. R. G. Cawthorn, Ed., Elsevier Science B.V.**:** 181-229.

Hamilton, J. (1977). Strontium isotope and trace element studies of the Great Dyke and Bushveld mafic phase and their relation to the to early Proterozoic magma genesis in Southern Africa. *Journal of Petrology* **18**, 24-52

Harney, D.M.W. and von Gruenewaldt, G., (1995). Ore-forming processes in the upper part of the Bushveld complex, South Africa. *Journal of African Earth Sciences* **20**, 77– 89.

Harney, D. M. W., Merkle, R. K. W. and von Gruenewaldt, G. (1990). Plagioclase composition in the Upper Zone, Eastern Bushveld Complex- Support for Mixing at the Main Magnetite Layer. *Institute for Geological Research on the Bushveld Complex*, Research Report No **87**.

Harney, D. M. W., von Gruenewaldt, G. and Merkle, R. K. W. (1995). The use of Plagioclase composition as an indicator of magmatic processes in the Upper Zone of the Bushveld Complex. *Mineralogy and Petrology* **56**, 91-103

Henderson, P. (1970) The significance of the mesostasis of basic layered igneous rocks. *Journal of Petrology* **11**, 463-473

Irvine, T.N. (1977). Origin of chromitite layers in the Muskox intrusion and other stratiform intrusions: a new interpretation. *Geology* **5**, 273-277.

Irvine, T.N., (1980) Magmatic infiltration metasomatism, double diffusive fractional crystallization and adcumulus growth in the Muskox Intrusion and other layered

intrusions. In: Hargraves RB (ed) *Physics of magmatic processes*. Princeton Univ, Princeton, p 325-383

Jang, Y. D., Naslund, H. R., (2001). Major and Trace Element Composition of Skaergaard Plagioclase; Geochemical evidence for changes in magma dynamics during the final stage of crystallization of the Skaergaard Intrusion. *Contributions to Mineralogy and Petrology* **140**, 441-457

Jordan, G., Higgins, S.R., Eggleston, C.M., Swapp, S.M., Janney, D.E. and Knauss K.G. (1999) Acidic dissolution of plagioclase: in-situ observations by hydrothermal atomic force microscopy, *Geochimica et Cosmochimica Acta* **63**, pp. 3183–3191

Kruger, F.J. (1990). The Stratigraphy of the Bushveld Complex: a reappraisal and the relocation of the Main Zone boundaries. *South African Journal of Geology* **93**, 376–381

Kruger FJ (1994). The Sr-isotopic stratigraphy of the Western Bushveld Complex. *South African Journal of Geology* **97**, 393–398

Kruger, F. J. (2005). Filling the Bushveld Complex magma chamber: lateral expansion, roof and floor interaction, magmatic unconformities, and the formation of giant chromitite, PGE and Ti-V-magnetite deposits. *Mineralium Deposita* **40**, 451-472

Kruger, F.J., Marsh, J.S., (1985) The mineralogy, petrology and origin of the Merensky cyclic unit in the Western Bushveld Complex. *Economic Geology* **80**, 958-974

Kruger, F. J. & Smart, R. (1987). Diffusion of trace elements during bottom crystallization of double-diffusive convection systems: the magnetitite layers of the Bushveld Complex. *Journal of Volcanology and Geothermal Research* **34**, 133–142.

Kruger, F. J., Cawthorn, R. G. and Walsh, K. L. (1987). Strontium isotopic evidence against magma addition in the Upper Zone of the Bushveld Complex. *Earth and Planetary Science Letters* **84**, 51–58

Larsen, L. M., Watt, W. S. & Watt, M. (1989). Geology and petrology of the Lower Tertiary plateau basalts of the Scoreby Sund region, East Greenland. *Bulletin of Grùnlands Geologiske Undersùgelse* **157**, 164 pp.

Mathez, E. A. (1994). Magmatic metasomatism and formation of the Merensky Reef, Bushveld Complex. *Contributions to Mineralogy and Petrology* **119,** 277-286

McBirney, A. R. (1989). The Skaergaard Layered Series: I. Structure and average compositions. *Journal of Petrology* **30**, 363-397.

McBirney, A. R. (1996). The Skaergaard intrusion. In: Cawthorn, R. G. (ed.) Layered Intrusions. Amsterdam: Elsevier, pp. 147-180.

McBirney, A.R.,(2002). The Skaergaard Layered Series: Part VI. Excluded trace elements. *Journal of Petrology* **43**, 535–556.

Merkle, R.K.W. and von Gruenewaldt, G. (1986). Compositional variation of Co-rich pentlandite: relation to the evolution of the Upper Zone of the western Bushveld Complex, South Africa. *Canadian Mineralogist* **24**, 529-546.

Molyneux, T. G. (1974). A geological investigation of the Bushveld Complex in Sekhukhuneland and part of the Steelpoort Valley. *Transactions of the Geological Society of South Africa* **77**, 329–338

Morse S.A., (1982). Kiglapait geochemistry V: Strontium. *Geochimica et Cosmochimica* **46,** 223-234.

Morse, S.A., Nolan, K.M., (1984). Origin of strongly reversed rims on plagioclase in cumulates. *Earth and Planetary Science Letters* **68**, 485-498.

Morse SA, Lindsley DR, Williams RJ (1980) Concerning the intensive parameters in the Skaergaard intrusion. *American Journal of Science* **280**, 159-170.

Nielsen, T. F. D. (2004). The shape and volume of the Skaergaard Intrusion, East Greenland: implications for mass balance and bulk composition. *Journal of Petrology* **45**, 507-530.

Norrish, K., Hutton, J.T. (1969). An accurate X-ray spectrographic method for the analysis of a wide range of geological samples, *Geochimica et Cosmochimica* **33,** 431–453.

Reichardt, F. J. (1989).A petrological investigation of the transition from the lower to the upper critical zone in the central sector of the eastern Bushveld Complex, *Ph.D. Dissertation*, University of Pretoria, p. 238 unpublished.

Reynolds, I. M. (1985a). The nature and origin of titaniferous magnetite-rich layers in the Upper Zone of the Bushveld Complex: a review and synthesis. *Economic Geology* **80**, 1089–1108.

Reynolds, I. M. (1985b). Contrasted mineralogy and textural relationships in the uppermost titaniferous magnetite layers of the Bushveld Complex in the Bierkraal area north of Rustenburg. *Economic Geology* **80**, 1027–1048.

Roberts, R. J. (2005). Sulphide Saturation in the Upper Zone of the Bushveld Complex, South Africa. Thesis (MSc.) University of the Witwatersrand, Johannesburg

Rollinson, H.R. (1993). Using geochemical data: evaluation, presentation, interpretation. *Longman Group UK Ltd*, pp 352.

Scoates, J. S. & Friedman, R. M. (2008). Precise age of the platiniferous Merensky reef, Bushveld Complex, South Africa, by the U-Pb zircon chemical abrasion ID-TIMS technique. *Economic Geology* **103**, 465-471.

Sharpe, M.R. (1985). Strontium isotope evidence for preserved density stratification in the Main Zone of the Bushveld Complex, South Africa. *Nature*, **316**, 119-126

South African Committee for Stratigraphy(SACS) (1980). Stratigraphy of South Africa, Lithostratigraphy of the Republic of South Africa, South West Africa/Namibia and the Repubics of Bophuthatswana, Transkei and Venda. *Handbook of the Geological Survey of South Africa* **8**, 223-241.

Stewart, B.W., De Paolo, D.J., (1990). Isotopic studies of processes in mafic magma chambers: II. The Skaergaard intrusion, East Greenland. *Contributions to Mineralogy and Petrology* **104**, 125–141

Tegner, C., cawthorn, R. G., (2009). Iron in Plagioclase in the Bushveld and Skaergaard intrusions: implication for iron contents in evolving basic magmas. *Contributions to Mineralogy and Petrology* **159**, 719-730

Tegner, C., Cawthorn, R. G., Kruger, F. J. (2006). Cyclicity in the Main and Upper Zones of the Bushveld Complex, South Africa: Crystallization from a zoned magma sheet. *Journal of Petrology* **47**, 2257-2279.

Tegner, C., Thy, P., Holness, M. B., Jakobsen, J. K., Lesher, C. E. (2009). Differentiation and Compaction in the Skaergaard intrusion. *Journal of Petrology* **50**, 813–840

Thy, P., Tegner, C., Lesher, C. E. (2009). The Skaergaard liquid line of descent revisited. *Contributions to Mineralogy and Petrology*. **157**, 735-747.

Toplis M. J., Carroll, M. R. (1996). Differentiation of ferro-basaltic magmas under conditions open and closed to oxygen: implications for the Skaergaard intrusion and other natural systems. *Journal of Petrology* **37**:837–858

Vantongeren, J. A., Mathez, E. A., Kelemen, P. B. (2010). A Felsic End to Bushveld Differentiation. *Journal of Petrology* **online version**, 1-22.

von Gruenewaldt, G. (1970). On the phase change orthopyroxene– pigeonite and the resulting textures in the Main Zone and Upper Zones of the Bushveld Complex in the eastern Transvaal. In: Visser, D.J.L., von Gruenewaldt, G. (Eds.), Symposium on the Bushveld Igneous Complex and other layered intrusions. *Special Publication*, **1**. Geological Society of South Africa, 67–73.

von Gruenewaldt, G. (1973). The Main and Upper zones of the Bushveld Complex in the Roossenekal area, Eastern Transvaal. *Transactions of the Geological Society of South Africa* **76**, 207–227.

Von Gruenewaldt, G. (1976). Sulfides in the Upper Zone of the Eastern Bushveld Complex. *Economic Geology* **71**, 1324-1336.

Wager, L. R., Mitchell, R. L. (1951). The distribution of trace elements during strong fractionation of basic magma-A further study of the Skaergaard intrusion, East Greenland. *Geochimica et Cosmochimica* **l**, 129-208.

Wager, L.R., Brown, G.M. (1968). Layered Igneous Intrusions. Oliver & Boyd, Edinburgh & London, 588 pp.

Wager, L. R., Brown, G. M., Wadsworth, W. J. (1960). Types of igneous cumulates. *Journal of Petrology* **1**, 73- 85.

Walraven, F., Wolmarans, L. G. (1979). Stratigraphy of the upper part of the Rustenburg Layered Suite, Bushveld Complex, in the western Transvaal. *Annals of the Geological Survey of South Africa* **13**,109–114.

Walraven F., Armstrong, R. A., Kruger, F. J. (1990). A chronostratigraphic framework for the north central Kaapvaal craton the Bushveld Complex and the Vredefort Structure. *Tectonophysics* **171**, 23–48

Willemse, J. (1969). The geology of the Bushveld Igneous Complex, the largest repository of magmatic ore deposits in the world. *Economic Geology Monograph* 4, 1–22.

Appendices A – D

Appendix A- Analytical Techniques and Standards Used

Preparation of Plagioclase Separates

Samples from the Upper Zone of the Bushveld Complex were coarsely crushed in the jaw crusher. They were then milled for about 10 seconds and the material passed through two sieves (0.180 and 0.100 mm respectively). The remaining material in the coarser sieve was remilled for a few seconds and passed through the sieves. This was repeated until all the material had gone through the upper sieve. Milling was done for short time intervals so that the material is not crushed too fine. The material in the second sieve; between 0.105 and 0.180 um was cleaned repetitively with water to remove all the dust clinging to individual grains and left in the oven to dry. This was done in order to avoid clogging in the magnetic separator.

A hand magnet was used to remove magnetic material such as magnetite in samples from UZ before they were run through the magnetic separator. The dried samples were then run through the magnetic separator three times at a current of 0.5A, 0.9A and 1.5A. The non-magnetic fraction after the third pass is largely plagioclase. However, some plagioclase grains could still contain magnetic proportions either by virtue of included magnetite and pyroxenes or as composite grains with the magnetic proportion. In order to check for purity of plagioclase grains, all plagioclase separates were observed under the binocular microscope to ensure that there were no inclusions or composite grains of mafic minerals with the separates. About 10 of the samples had magnetite and pyroxene inclusions or composite grains. These samples were gently hand crushed and passed through the magnetic separator again. Apart from 3 samples which still had magnetite inclusions in them, the rest of the separates appeared to be free of dark minerals. However, samples collected within the apatite-bearing interval had variable proportions of apatite because it is not possible to separate plagioclase from apatite magnetically, because they are both non-magnetic and often the apatite occurred within the plagioclase grains. Each of the plagioclase separates for all samples was then milled finely to the

consistency of dust using an agate mortar and a portion was used to prepare pellets for XRF analyses. The method used for the preparation of pellets is from Norrish and Hutton (1969). After analyses on pellets were carried out, the same material was extracted from the pellets and used for XRF analyses on fusion discs (major elements) and ICP analyses (trace elements). Standards and analytical procedure for the various methods are detailed below.

Preparation of the pressed pellet and methodology for analytical procedures

Approximately 6g of sample is mixed with three drops of commercially purchased Mowiol (polyvinyl alcohol). This mixture is pressed under 10 ton pressure into an Al cup using a 40 ton press. The pressed pellet is allowed to dry for 24 hours prior to analysis.

Standards used for calibration of PW2404 XRFS for silicate analysis.

The X-Ray tube used is a Rhodium tube and is run at 50KV and 50 mA. The method used is from the paper "An accurate X-Ray spectrographic method for the analysis of a wide range of geological samples by K. Norrish and J.T. Hutton." Published in Geochimica et Cosmochimica Acta, 1969, Vol 33, pp. 431 to 453

Standard	%Fe2O3	%MnO	%TiO2	%CaO	%K2O	%P2O5	%SiO2	%Al2O3	%MgO	%Na2O	%LOI	%Total
NIM-G	2.02	0.02	0.00	0.79	5.03	0.01	76.31	12.18	0.06	3.39	0.45	100.42
NIM-S	1.41	0.01	0.00	0.68	15.40	0.12	63.85	17.40	0.46	0.43	0.28	99.70
NIM-N	8.96	0.18	0.20	11.49	0.25	0.03	52.57	16.48	7.49	2.46	-0.40	99.83
NIM-D	16.87	0.22	0.02	0.28	0.01	0.01	38.66	0.30	43.18	0.04	-0.93	99.42
NIM-P	12.77	0.22	0.20	2.67	0.09	0.02	51.39	4.20	25.47	0.37	-0.84	96.03
AN-G	3.39	0.04	0.22	16.03	0.13	0.01	46.67	30.04	1.81	1.64	0.65	99.84
AC-E	2.54	0.06	0.11	0.34	4.51	0.01	70.63	14.76	0.03	6.57	0.37	99.53
MA-N	0.47	0.04	0.01	0.59	3.19	1.40	66.86	17.69	0.04	5.86	1.82	97.60
AGV-2	6.69	0.10	1.05	5.20	2.88	0.48	59.30	16.91	1.79	4.19	1.59	100.18
FK-N	0.09	0.01	0.02	0.11	12.88	0.02	65.37	18.71	0.01	2.59	0.54	99.82
BHVO-2	12.30	0.17	2.73	11.40	0.52	0.27	49.90	13.50	7.23	2.22	-0.71	99.53
MICA-FE	25.65	0.35	2.50	0.43	8.75	0.45	34.40	19.50	4.55	0.30	2.00	98.88

Analytical precision for major element analysis.

The analysis is based on duplicate samples representing 5 calibrations.

Element	Standard deviation	Absolute % error	Relative Error - %	Standard Range %
Fe2O3	0.09	-0.03	-3.7	0.09 - 26.65
MnO	0.01	-0.009	4.8	0.01 – 0.35
TiO2	0.07	-0.04	13.7	0.00 – 2.69
CaO	0.04	0.003	0.2	0.11 – 16.03
K2O	0.07	0.005	-5.6	0.01 – 15.40
P2O5	0.02	-0.02	14.2	0.01 – 1.40
SiO2	0.36	0.06	-0.09	34.40 – 76.31
Al2O3	0.07	0.07	1.3	0.30 – 30.04
MgO	0.18	-0.05	-6.1	0.03 – 43.18
Na2O	0.13	-0.05	-6.8	0.04 – 6.57
LOI	0.26	-0.21	7.1	
Total	0.58	-0.18	0.2	

Standards used for calibration of PW2404 XRFS for trace element analysis.

Regression lines are calculated using SuperQ software with the De Jongh model for matrix correction (α-coefficients)and a rhodium x-ray tube (4KW) was used

Standard	ppm Rb	ppm Sr	ppm Y	ppm Zr	ppm Nb	ppm Co	ppm Ni	ppm Cu	ppm Zn	% TIO2	ppm V	ppm Cr	ppm Ba
AGV-1	67	662	21	225	15	15	17	60	88	1.06	123	12	1221
GA	175	310	21	150	12	5	7	16	80	0.38	38	12	840
GH	390	10	75	150	85	1	3	14	85	0.08	5	6	20
G-2	170	478	11	300	13	5	5	11	85	0.49	36	9	1880
NIM-G	325	10	143	300	53	0	8	12	50	0	2	12	120
NIM-S	530	62	1	20	0	3	7	19	10	0	10	12	2420
NIM-P	4	32	5	15	0	110	555	18	100	0.2	230	23950	46
NIM-N	5	260	7	14	0	58	120	14	68	0.2	220	30	102
NIM-D	0	3	0	8	0	208	2040	10	90	0.02	40	2870	10
PCC-1	0	0	0	0	1	110	2400	10	42	0.01	30	2730	1
BR	47	1320	30	250	98	52	260	72	160	2.6	235	380	1050
BHVO-1	11	403	28	179	19	45	121	136	105	2.71	317	289	139
MAG-1	149	146	28	126	12	20	53	30	130	0.75	140	97	479
SGR-1	83	420	13	53	5	12	29	66	74	0.26	128	30	290
SCO-1	112	174	26	160	11	11	27	29	103	0.63	131	68	570
QLO-1	74	336	24	185	10	7	6	29	61	0.62	54	3	1370
STM-1	118	700	46	1210	268	1	3	5	235	0.14	9	4	560
RGM-1	149	108	25	219	9	2	4	12	32	0.27	13	4	807
SDC-1	127	183	40	290	18	18	38	30	103	1.01	102	64	630
DR-N	73	400	28	125	8	35	15	50	145	1.09	220	42	385
GS-N	185	570	19	235	21	65	34	20	48	0.68	65	55	1400
MICA-FE	2200	5	50	800	270	23	35	5	1300	2.5	135	90	150
MICA-MG	1300	27	0	20	120	24	110	4	290	1.63	90	100	4000
FK-N	860	39	0	13	0	16	3	2	10	0.02	3	5	200
BX-N	10	110	114	520	58	35	190	18	75	2.37	310	290	34
DT-N	5	27	10	370	0	12	16	9	28	1.4	150	240	130
UB-N	6	10	3	8	0	100	2000	28	85	0.11	75	2300	30
GXR-1	14	259	0	38	1	8	41	1110	760	0.06	76	13	680
GXR-2	78	160	17	269	11	9	21	76	530	0.5	52	36	2240
GXR-3	92	950	15	63	2	43	60	15	207	0.17	42	19	5000
GXR-4	160	221	14	186	10	15	42	6520	73	0.48	87	64	1640
GXR-6	90	35	14	110	8	14	27	66	118	0.83	186	96	1300
GSP-1	254	234	29	530	26	7	10	34	103	0.66	53	13	1310
MA-N	3600	84	1	27	173	1	3	140	220	0.01	5	3	42
AN-G	0	76	8	15	2	25	35	19	20	0.22	70	50	34

Analytical precision for trace element analysis.

The analysis represents 5 calibrations.

Element	LLD-ppm	Standard deviation	Absolute error-ppm	Relative Error - %
Rb	3	2	1.0	-1.9
Sr	3	2	1.3	0.4
Y	3	2	-0.7	-3.7
Zr	8	3	4.3	1.2
Nb	3	1	-2.4	-8.5
V	12	9	-3.8	-12.7
Cr	12	7	0.7	5.2
Co	6	2	0.7	-10.7
Ni	6	2	0.6	-9.3
Cu	6	5	1.9	-0.3
Zn	6	2	2.8	-6.2
Ba	20	7	12.0	3.1
Pb	10	2	3.1	
As	15	2	4.7	

Summary of XRF Analysis on a Fusion Disc.

All major elements are analyzed for on an infinitely thick fused disk. Major elements were determined using the Norrish Fusion (Norrish & Hutton, 1969) technique using in-house correction procedures. Sample weight used was 0.35 gm and flux weight 2.5 gm. Calibration standards were primary International Reference Materials USGS series (USA) and NIM series (South Africa). Precision is taken as 1% for elements in abundance of greater than 5% by weight, and 5% for elements in abundance less than 5%. The instrument used was the Philips PW2404 x-ray spectrometer.

Standardization was carried out using International Reference Materials USGS series (USA) and NIM series (South Africa). Precision was determined on the basis of counting time and is taken as 5% for elements in abundance greater than 100 ppm, and 10% for elements in abundance between 10 and 100 ppm. The instrument used was the Philips PW2404 x-ray spectrometer.

Preparation of the fused disk:

1. All samples are ignited at 1000^{o}C for 40 minutes and the LOI is calculated.

2. The ignited sample is mixed with a commercially available pre-ignited flux (with composition $Li_2B_4O_7$ = 47%, Li_2CO_3 = 36.7%, La_2O_3 =16%) and fired for 40 minutes at 1000^{o}C.

3. This is then poured and pressed by a mechanical press into a fused disk.

Data Collection:
All data collection is performed on a PANalytical PW2404 WD XRF with a Rh tube set at 50kV and 50mA an analysis time of 40 sec per an element and 20 sec per a background (backgrounds are measured for Si, Al, Mg, Na and P only). See table 1 below for specific element data:

Table 1: Major element calibration instrument parameters

Element	Analysis Line	Crystal	Collimator	Detector
Ti	Ka	LiF200	150 µm	Flow
Ca	Ka	LiF200	150 µm	Flow
K	Ka	PE 002-C	550 µm	Flow
Si	Ka	PE 002-C	550 µm	Flow
Al	Ka	PE 002-C	550 µm	Flow
Mg	Ka	PX1	550 µm	Flow
Na	Ka	PX1	550 µm	Flow
P	Ka	Ge 111-C	550 µm	Flow
Ni	Ka	LiF 220	150 µm	Duplex
Fe	Kb	LiF 220	150 µm	Flow
Mn	Ka	LiF 220	150 µm	Duplex
Cr	Ka	LiF 220	150 µm	Duplex

The elemental concentrations are obtained by comparison to 13 known standards. The standards used are: W2, GSP1, BHVO2, AGV2, G2, DTS1, PCC1, BCR2, NIM N, NIM P, NIM S, NIM D, NIM G an their major element concentrations are listed above. A synthetic internal standard is run after every 5 analyses to monitor and compensate for instrumental drift.

In order to test for reliability of data, a subset of 20 samples was analyzed at an independent laboratory, SGS Lakefield. The graphs presented in Fig 1A compare the major element data from the two laboratories. The good correlation suggests that these results are accurate.

ICP Analyses

ICP analyses were carried out at the School of Geosciences, University of Cape Town. A plot comparing the Ba and Sr contents from the two methods (XRF and ICP) are presented in Fig 1B. Absolute values differ but it is more crucial to compare the relative changes. The linear correlation shows that relative changes in the Sr and Ba contents from the two methods are identical, hence the variation is real.

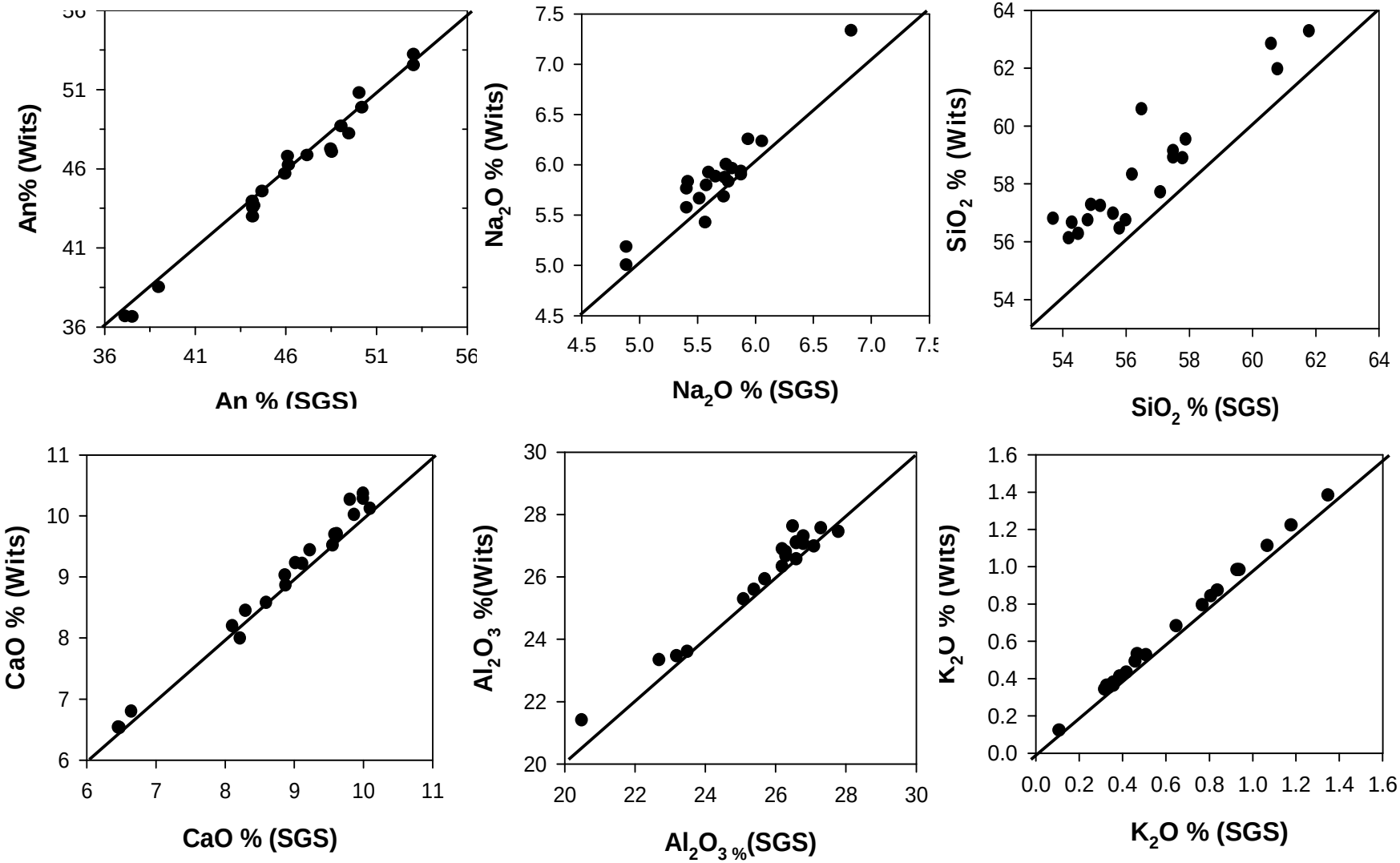


Fig 1A. Comparison of major element compositions for samples analyzed by both Wits University and SGS Lakefields

Appendix A

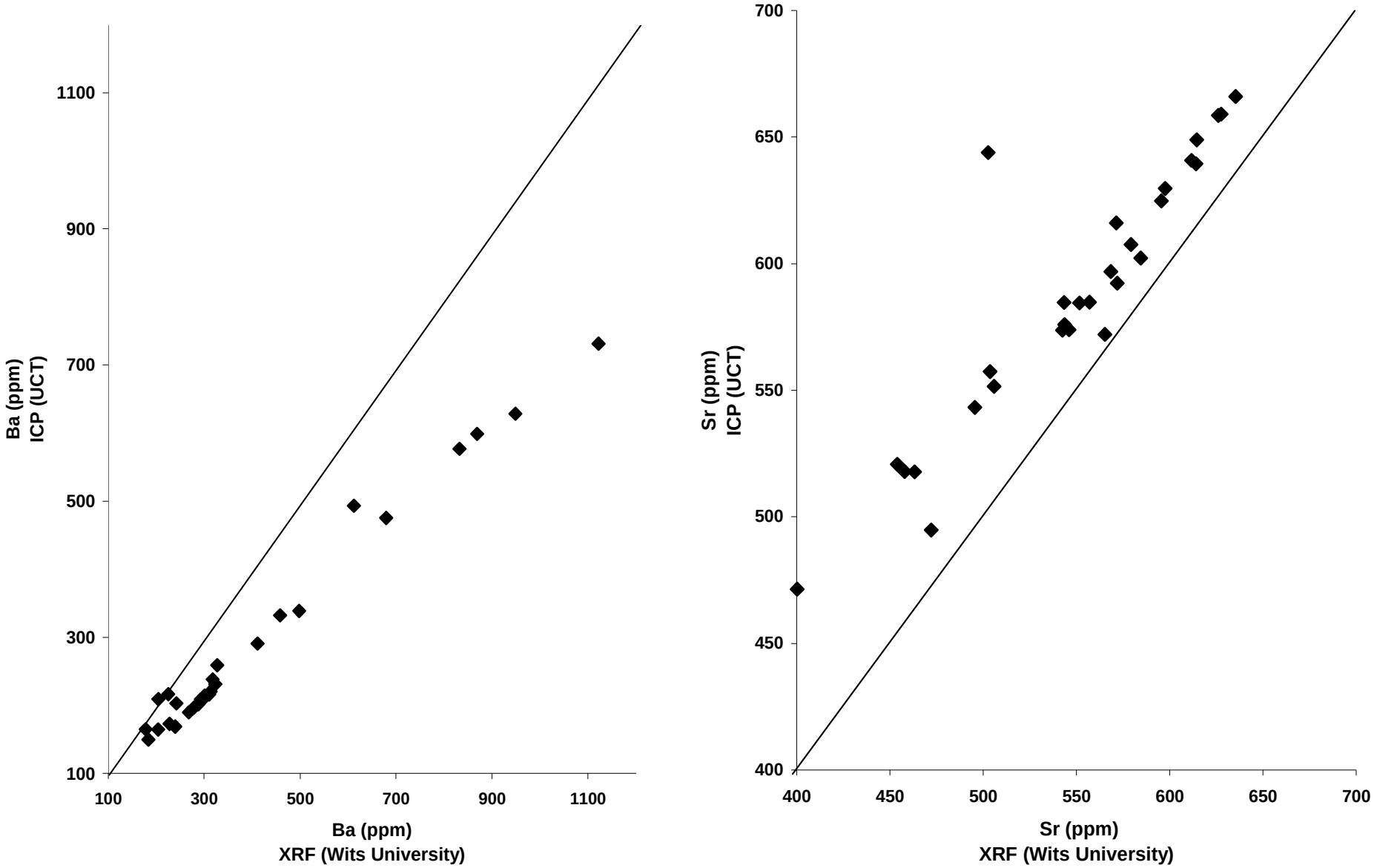


Fig. 1B. Comparison of Sr and Ba contents from analyses by both XRF at Wits University and the ICP at the University of Cape Town.

Appendix B. Dissolution Experiments

Preliminary analytical data indicated a serious problem, namely that many samples included apatite that was enclosed within plagioclase grains and so could not be separated by using dense liquids. Removing this apatite required the development of a leaching method and the most crucial aspect of this leaching process was that it should completely dissolve the apatite, not leaving any possible residue containing of the rare earth elements (which forms part of another study). It should also have no effect on the composition of the plagioclase. The first leaching experiments were conducted with HCl, based on data from the literature which have reported the range of behaviors of plagioclase feldspars in HCl (e.g. Hulburt 1959; Jordan et al., 1999). The experiments presented were conducted with both Critical Zone anorthosite and a Upper Zone anorthosite in order to explore different possible plagioclase dissolution behaviors since they range in composition from An_{80} to An_{40}.

LEACHING OF APATITE IN DILUTE HCl. 1

Aim:

To test if HCl dissolves apatite and to document the times and concentrations at which apatite dissolves in HCl.

Method:

Reagent grade HCl was diluted to different strengths (0.1 M, 0.25 M and 0.5 M) and 1 grain of apatite from Phalaborwa, about 3 mm in size, was placed in each of the three solutions. It took 1 day, 6 hours and 3 hours respectively for the apatite grains to dissolve in the solutions.

Result and Interpretation:

HCl dissolves apatite and the rate of dissolution is directly proportional to acid concentration.

LEACHING OF PLAGIOCLASE IN DILUTE HCl. 2

Aim:

To determine whether HCl dissolves plagioclase.

Method:

Three sets of solutions, each with 0.1 M (JL2, JL5, JL8), 0.25 M (JL3, JL6, JL9) and 0.5 M (JL4, JL7, JL10) HCl were prepared. 10 g of finely crushed Critical Zone pure plagioclase separate were added to each beaker. After one hour, three beakers, one from each of the different solution strengths was washed thoroughly with water and dried, the second batch of three was washed after 6 hours and the last batch of three after 1 day. The 9 dried samples, together with a 10 g batch of the unleached CZ plagioclase separate (JL1) were analyzed for major, trace and rare earth elements.

Results:

Results are presented in table 1. All analyses are within analytical error except for the weight percent of Na_2O which decreases even with the least concentration the samples were left in HCl (Table 1; JL 1 to 10). The unleached sample contains 1.7% Na_2O whereas all leached samples contain 1.0 to 1.3 % Na_2O. HCl does not appear to remove Sr or Rb.

Interpretation and Conclusion:

Na_2O which is a major constituent of plagioclase is being attacked by HCl and leached. It is rather intriguing that the reduction in Na_2O was virtually the same regardless of acid strength or dissolution time. This suggests that a very thin rim of Na_2O depleted plagioclase forms which shields the core of the grain from further attack. HCl would not be suitable for dissolving apatite from samples.

Table 1

Major, Trace and Rare Earth Elements

Sample No	**Acid Strength (Molar)**	**Dissolution time (hours)**	**SiO_2 %**	**AL_2O_3 %**	**Fe_2O_3 %**	**MgO %**	**CaO %**	**Na_2O %**	**K_2O %**	**LOI %**	**An %**	**Ba** ppm	**Sr** ppm	**Rb** ppm	**La** ppm	**Ce** ppm
JL1	Unleached	Unleached	49.1	32.4	0.79	0.7	15.5	**1.7**	0.19	0.22	84.8	24	596	9	3	41
JL2	0.1	1	49.4	32.5	0.73	0.7	15.4	**1.0**	0.17	0.26	90.3	I/S	I/S	I/S	I/S	I/S
JL3	0.25	1	49.5	32.6	0.75	0.7	15.6	**1.0**	0.16	0.24	90.4	I/S	I/S	I/S	I/S	I/S
JL4	0.5	1	49.9	33.0	0.72	0.7	15.7	**1.2**	0.18	0.23	89.1	<4	594	6	31	9
JL5	0.1	6	49.0	31.6	0.71	0.7	15.1	**1.3**	0.17	0.91	87.3	15	583	7	3	14
JL6	0.25	6	49.3	32.3	0.71	0.7	15.3	**1.1**	0.16	0.53	88.9	<4	592	6	<2	<5
JL7	0.5	6	49.3	32.3	0.72	0.9	15.5	**1.3**	0.26	0.29	88.2	41	591	7	<2	51
JL8	0.1	24	50.6	30.6	0.69	0.7	14.6	**1.0**	0.20	1.51	89.8	<4	568	7	9	<5
JL9	0.25	24	50.0	31.9	0.70	0.7	15.2	**1.0**	0.17	0.72	90.2	I/S	I/S	I/S	I/S	I/S
JL10	0.5	24	49.7	32.5	0.71	0.7	15.5	**1.2**	0.18	0.42	88.5	33	589	7	4	43

I/S: Insufficient sample for quantitative trace analysis.

LOI: Loss on ignition

LEACHING OF APATITE IN CITRIC ACID. 1

Aim:

To test if citric acid dissolves apatite and document the amount of time needed for apatite to dissolve in citric acid.

Method:

A solution of 50 g citric acid plus 50 ml of water was prepared and a grain of Phalaborwa apatite, about 3 mm in size, was added to the solution. After 21 hours, there was no change in size and so a further 80 g of citric acid were added to the solution in a bid to increase the concentration and speed up the dissolution process. However, 3 days later, there was still no change in size and the grain boundaries were still very sharp suggesting that there was no significant dissolution.

This same experiment was carried out again, but with grains of apatite hand crushed in a pestle and mortar to a size of about 0.8 mm (solution 1).

A new solution (50 ml water + 50 g citric acid) was prepared and hand crushed grains of apatite about 0.8 mm in size added to it (solution 2). In a bid to speed up the reaction process, the solution was left in a larger beaker of boiling water which was replaced every 30 to 45 minutes in order to maintain the heat of the boiling water.

One more solution was prepared with boiling water and apatite crystals, more finely hand crushed to a size of about 0.4 mm were added to it (solution 3).

On day 5, a solution of citric acid was prepared with cold water and finely hand crushed grains of apatite about 0.2 mm in size were immersed in the solution (solution 4)

After 24 hours, the water levels in solutions 2 and 3 had dropped due to evaporation and more boiling water was added to make up for this loss. There was also a marked decrease in grain size and number in apatite grains in the beakers carried out with hand crushed apatite grains.

Results:

After 9 days, the apatite grains which were hand crushed and left in all solutions had completely dissolved. However, the water level in the beakers left in boiling water had dropped due to evaporation and so the exact concentration of citric acid had not remained constant throughout the experiment.

Interpretation and Conclusion:

Apatite dissolves slowly in citric acid of strength greater than 50 g acid per 50 g water when grains are crushed fine to a size of 0.8 mm or less in both hot and cold water. However, more experiments need to be done to ensure that citric acid does not attack plagioclase.

PLAGIOCLASE AND APATITE LEACHING IN CITRIC ACID. 2

Aim:

This experiment was conducted in order to document the time and concentration needed for citric acid to dissolve apatite and to determine whether the acid attacks plagioclase. This was inferred by analyzing the residual powder for P, Na, Ca, Al, Sr and La by XRF after dissolution experiments were conducted.

Method:

A large number of experiments requiring large quantities of plagioclase had to be undertaken. Hence, virtually pure anorthosite (whole rock) rather than pure plagioclase separates was used.

A homogeneous mixture of apatite and plagioclase was prepared as follows. Apatite from Phalaborwa was finely crushed in a mortar and pestle. 7.5 g of this apatite were mixed with 150 g of pulverized Critical Zone (CZ) Bushveld anorthosite (with An_{85} as calculated from JL1, Table 1) in a large beaker of water and stirred to homogenize. This mixture was then left in the oven at 90 ºC to dry.

Four different sets of solutions were prepared each with 20, 50 and 100 g of citric acid per 100 ml of water giving a total of 12 solutions. 10 g of the mixture (CZ anorthosite + apatite) were added to three sets (9 solutions) and stirred frequently in order to expose all grains for dissolution. Upper Zone plagioclase was also used in the other 3 solutions for the leaching experiment in order to test if citric acid has any effect on plagioclase with an anorthite content (An_{50} as calculated from Tegner et al. (2006). The first set of four ended after 3 hours (sample Nos 1A, 2A and 3A), the next 1 full day (sample Nos 4A, 5A and 6A) and the last 3 full days (sample Nos 7A, 8A and 9A).

At the end time of each experiment, the citric acid was decanted and the remaining powder thoroughly washed in water several times while stirring to make sure that all the dissolved material was eliminated. The samples were then left in the oven at 90ºC until dry. 16 Pressed pellets were prepared for sample Nos 1A to 12A leached in citric acid, a reference standard GC2100 (13A), the unleached CZ anorthosite + apatite mixture (14A), unleached Upper Zone anorthosite (15A) and CZ anorthosite without apatite (16A).

Results:

Results of the dissolution are presented in Table 2 and based on these results, calculations of the amount of apatite dissolved and its effect on plagioclase are also presented (Tables 2, 3 and Fig. B.1)

Interpretation:

All of the P_2O_5, 10 % of CaO and 25 % of Sr is added to CZ anorthosite as apatite is mixed with it (Table 3, sample 14A). By the end of the third day, half the P_2O_5 and Sr added is dissolved (7A, 8A and 9A) even though acid concentrations differ. This suggests that concentration of citric acid is not as crucial to the rate of dissolution as time is. Sample No 16A contains 1.94 % Na_2O whereas the leached samples (1A to 9A) contain 1.5- 1.7 % Na_2O. This suggests that CZ plagioclase is being dissolved and the amount of dissolution also increases with time and acid concentration.

The amount of dissolution of apatite is directly proportional to time e.g. sets 1A,-4A,-7A; 2A,-5A,-8A; 3A,-6A,-9A.

In contrast, for the UZ anorthosite samples (10A, 11A, 12A and 15A), 54% of P_2O_5 and 20% of CaO present dissolves after day 3. A negligible amount of the Na_2O (4 %) dissolves after 3 days whereas there is no change in Sr. This suggests that unlike CZ anorthosite, citric acid does not attack the UZ anorthosite.

Conclusion:

The drop in CaO and P_2O_5 in samples 1A-9A reflects dissolution of the apatite which was added to the CZ anorthosite. It would be better to maintain the medium concentration and increase the time in order to successfully dissolve all the apatite in samples. Due to the significant drop in Na_2O in samples 1A to 9A, citric acid is probably dissolving the CZ anorthosite. Importantly, the attack on UZ anorthosite is much less and the reduction in UZ anorthosite CaO and P_2O_5 (10A, 11A and 12A) indicates that there is apatite in the UZ anorthosite.

Table 2. XRF results of analyzed samples.

SN	Sample Description	Na_2O	P_2O_5	CaO	Sr	La	Ce	Ba
		%	%	%	(ppm)	(ppm)	(ppm)	(ppm)
1A	CZ anorthosite+ apatite, 20 g 3hr diss	1.73	1.34	14.62	573	24	42	52
2A	CZ anorthosite+ apatite, 50 g 3hr diss	1.61	1.58	14.21	576	22	48	45
2B	CZ anorthosite+ apatite, 50 g 3hr diss	1.62	1.71	14.56	547	16	62	41
3A	CZ anorthosite+ apatite 100 g 3hr diss	1.72	1.59	14.96	592	15	60	51
3B	CZ anorthosite+ apatite 100 g 3hr diss	1.72	1.75	15.18	595	28	58	47
4A	CZ anorthosite+ apatite 20 g 1 day diss	1.72	1.20	14.45	563	8	35	50
5A	CZ anorthosite+ apatite 50 g 1 day diss	1.62	1.33	14.29	575	18	48	48
6A	CZ anorthosite+apatite 100 g 1 day diss	1.65	1.28	14.50	560	16	54	52
7A	CZ anorthosite+ apatite 20 g 3 day diss	1.69	0.80	14.03	523	4	21	58
8A	CZ anorthosite+ apatite 50 g 3 day diss	1.53	1.00	13.67	533	8	28	48
9A	CZ anorthosite+ apatite 100 g 3 day diss	1.48	0.85	13.68	525	7	32	51
10A	UZ anorthosite 3hrs diss	4.30	1.99	8.91	625	8	96	257
11A	UZ anorthosite 1 day diss	4.39	1.75	8.67	632	6	109	266
12A	UZ anorthosite 3 days diss	4.10	1.16	7.59	622	3	83	243
13A	GC2100 Reference Standard	2.21	0.04	13.57	398	13	10	72
13B	GC2100 Reference Standard	2.21	0.04	13.76	398	24	17	78
14A	CZ anorthosite + apatite	1.87	1.66	15.70	593	31	73	60
14B	Unleached CZ anorthosite + apatite	1.88	1.84	15.98	593	38	70	62
15A	Unleached UZ anorthosite+ apatite	4.26	2.53	9.46	608	26	124	254
16A	Unleached CZ anorthosite	1.94	0.08	14.14	448	-1	0	54
17 B	repeat of 10, 11, 12	4.47	2.50	9.49	629	24	117	392
18B	17 further diss of 10, 11, 12	4.49	0.06	7.08	684	9	74	417
19B	repeat 7, 8, 9	1.62	1.33	14.49	541	23	57	42
20B	19 further diss of 7, 8, 9	1.12	0.17	11.92	443	4	9	46
21B	Unleached CZ anorthosite + new apatite	1.65	4.04	17.16	752	74	199	52
22B	Unleached CZ anorthosite + new apatite	1.78	4.31	17.61	751	78	194	64
23B	Unleached CZ anorthosite + new apatite	1.74	4.48	17.75	762	83	193	59
24B	CZ anorthosite + apatite 7 days diss	1.19	0.46	12.22	469	15	19	55
25B	CZ anorthosite + apatite 7 days diss	1.15	0.34	12.14	458	2	9	53
26B	CZ anorthosite + apatite 7 days diss	1.10	0.29	11.72	458	1	1	35
27B	CZ anorthosite 7 days diss	1.18	0.02	12.08	439	11	4	50
28B	Pure apatite	0.15	52.34	50.44	2980	600	1579	91

A= first analyses results, B=second analyses results

CZ: Critical Zone, Bushveld

UZ: Upper Zone, Bushveld

Diss: Dissolution

SN = Sample Number

Table 3: Percentage of Components dissolved

SN		P2O5	% added	% dissolved	CaO	% added	% dissolved	Na2O	% added	% dissolved	Sr(ppm)	% added	% dissolved
16A	Unleached CZ anorthosite	0.08	0	0	14.14	0	0	1.94	0	0	448		0
14A	CZ anorthosite + apatite	1.66	95	0	15.70	10	0	1.87	0	0	593	25	0
1A	CZ anorthosite+ apatite, 20 g 3hr diss	1.34	95	19	14.62	10	7	1.73	0	7	573	25	3
2A	CZ anorthosite+ apatite, 50 g 3hr diss	1.58	95	5	14.21	10	10	1.61	0	14	576	25	3
3A	CZ anorthosite+ apatite 100 g 3hr diss	1.59	95	4	14.96	10	5	1.72	0	8	592	25	0
4A	CZ anorthosite+ apatite 50 g 1 day diss	1.20	95	28	14.45	10	8	1.72	0	8	563	25	5
5A	CZ anorthosite+ apatite 20 g 1 day diss	1.33	95	19	14.29	10	9	1.62	0	13	575	25	3
6A	CZ anorthosite+apatite 100 g 1 day diss	1.28	95	23	14.50	10	8	1.65	0	12	560	25	6
7A	CZ anorthosite+ apatite 20 g 3 day diss	0.80	95	52	14.03	10	11	1.69	0	9	523	25	12
8A	CZ anorthosite+ apatite 50 g 3 day diss	1.00	95	40	13.67	10	13	1.53	0	18	533	25	10
9A	CZ anorthosite+ apatite 100 g 3 day diss	0.85	95	48	13.68	10	13	1.48	0	21	525	25	12
15A	Unleached UZ anorthosite	2.53	0	0	9.46		0	4.26	0	0	608	0	0
10A	UZ anorthosite 3hrs diss	1.99	0	21	8.91		6	4.30	0	0	625	0	0
11A	UZ anorthosite 1 day diss	1.75	0	31	8.67		8	4.39	0	0	632	0	0
12A	UZ anorthosite 3 days diss	1.16	0	54	7.59		20	4.10	0	4	622	0	0
17 B	repeat of 10, 11, 12	2.50		1	9.49		0	4.47	0	0	629	0	0
18B	17 further diss of 10, 11, 12	0.06		98	7.08		25	4.49	0	0	684	0	0
19B	repeat 7, 8, 9	1.33	95	20	14.49	10	8	1.62	0	13	541		9
20B	19 further diss of 7, 8, 9	0.17	95	90	11.92	10	24	1.12	0	40	443		25
21B	Unleached CZ anorthosite + new apatite	4.04	98	0	17.16	20	0	1.65	0		752	40	
22B	Unleached CZ anorthosite + new apatite	4.31	98	0	17.61	20	0	1.78	0		751	40	
23B	Unleached CZ anorthosite + new apatite	4.48	98	0	17.75	20	0	1.74	0		762	40	
24B	CZ anorthosite + apatite 7 days diss	0.46	98	89	12.22	20	31	1.19	0	33	469	40	37
25B	CZ anorthosite + apatite 7 days diss	0.34	98	92	12.14	20	31	1.15	0	35	458	40	39
26B	CZ anorthosite + apatite 7 days diss	0.29	98	93	11.72	20	33	1.10	0	38	458	40	39
27B	CZ anorthosite 7 days diss	0.02			12.08			1.18	0		439		
28B	Pure apatite	52.34			50.44			0.15	0		3000		

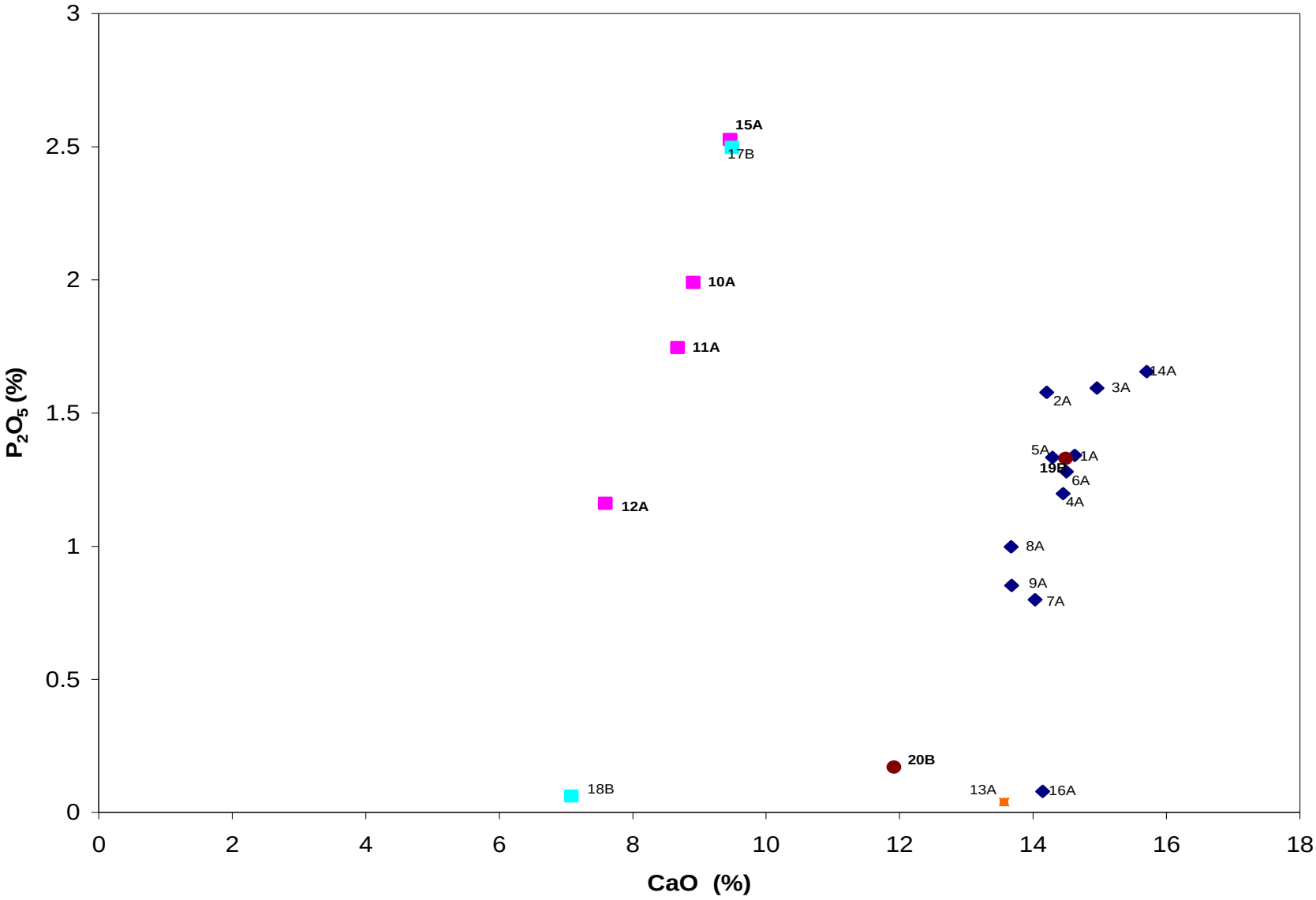


Fig. 1B:P_2O_5 change with CaO from Citric acid Leaching. 2

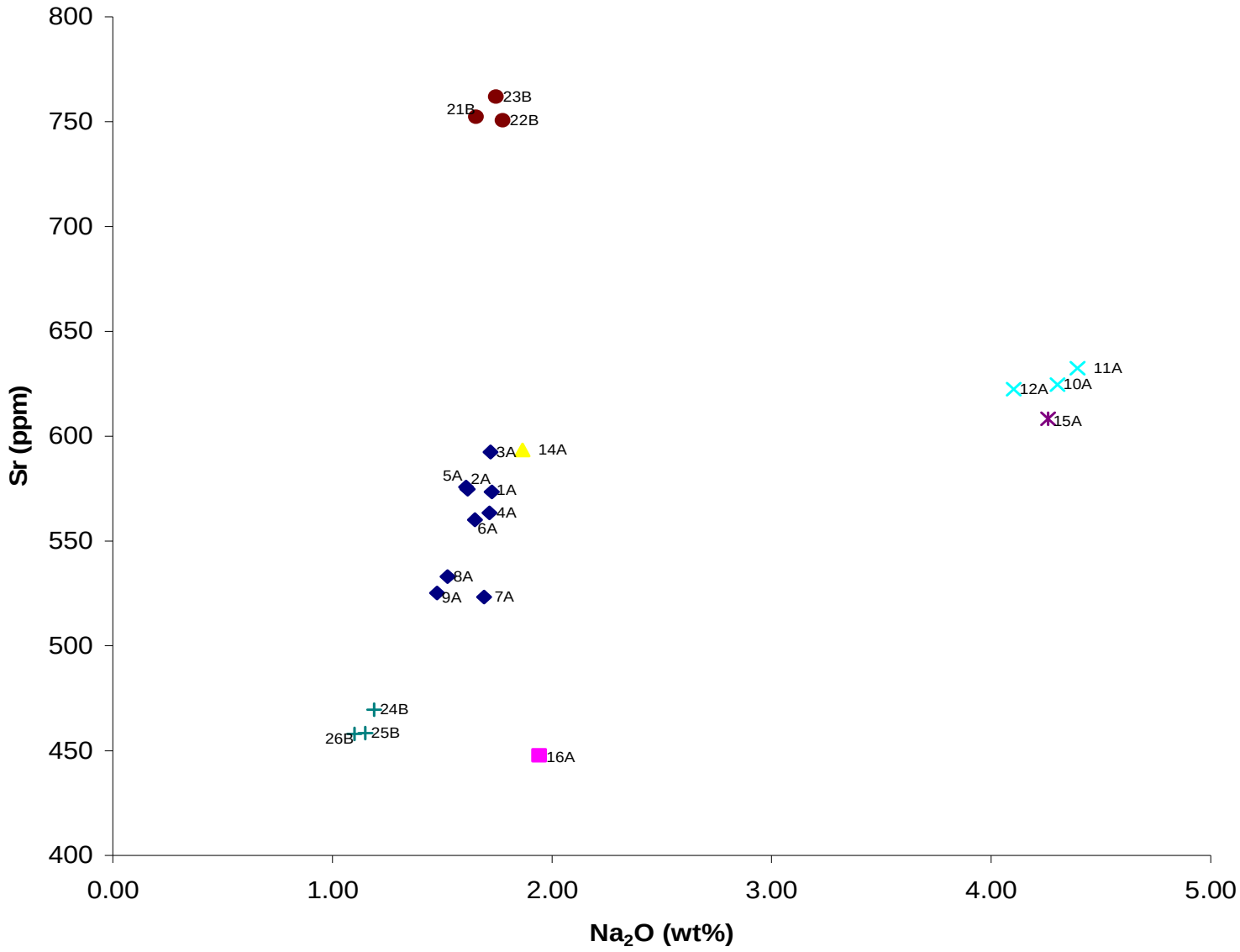


Fig.2B: Na_2O vs Sr decrease for Citric acid dissolution experiments

LEACHING OF APATITE IN CITRIC ACID. 3

Aim:

To determine the length of time needed to dissolve all the apatite.

Method:

Pellets from the 3 dissolutions done with UZ anorthosite (10A, 11A, and 12A) were all mixed together and crushed. Another pellet was prepared (17B) while the rest of the material was left in citric acid again for a further 7 full days. The sample was then washed, dried and the material used to prepare pellet 18B. This same procedure was followed for pellets 7A, 8A and 9A; making pellets 19B and 20B. These dissolutions were to test if complete dissolution of apatite had taken place.

3 g of different Phalaborwa apatite were crushed and mixed with 60 g of the CZ anorthosite and three pellets, 21B, 22B and 23B were prepared. Then three portions of 6g of the mixture (CZ anorthosite + new apatite) were left in citric acid for 7 days, washed and used to prepare pellets 24B, 25B and 26B. 3 pellets of the same material (21B, 22B and 23B) were prepared in order to test for analytical reproducibility. The original CZ anorthosite sample that made pellet 16A was also left in citric acid for 7 days and used to prepare pellet 27B. Four more pellets; 2A, 3A, 13A and 14A were reanalyzed to make samples 2B, 3B, 13B and 14B.

All these dissolution experiments were done with 50 g citric acid in 100 ml of water.

Results:

Results and calculations of these analyses are presented in Tables 2, 3 and 4. Figs. 1B, 2B and 3B show the calculated proportions of major, trace and rare earth elements in apatite which dissolve after leaching.

Interpretation:

Major Elements:

Of the P_2O_5 in the starting mix, 48% dissolved after 3days (9A) and about 90 % dissolved after the samples were left in citric acid for 7 more days (20B). The samples need to be left in citric acid for about 3 more days in order to dissolve all the apatite in them. With the dissolution experiments with new Phalaborwa apatite after 10 days, about 90% P_2O_5 which was added with apatite to the CZ anorthosite is dissolved (Table 3, 24B, 25B and 26B).

In the CZ anorthosite sample, there is a significant reduction by about 40% of Na_2O after the total 10 days leaching (Table 3, 20B). This indicates that plagioclase with this An content is attacked by citric acid and in order to dissolve apatite, the plagioclase separates need to be left in citric acid for this length of time. The Na_2O content also drops by 38% after the second dissolution (Table 3, 24B, 25B and 26B). On the contrary, UZ anorthosite results prove that citric acid has no effect on Na_2O with this An content as there is no reduction in the Na_2O content even after 10 days (Table 3, 10A, 11A, 12A, 17A and 18A).

It appears citric acid reduces the concentration of CaO in CZ anorthosite. This is because of the 10% CaO added to anorthosite with apatite, 25% CaO is leached out by the end of day 10 (20B) and this number exceeds the amount which was added as apatite. On Fig.1B, 20B plots way below 16A, indicating that the CaO content of the original CZ anorthosite is being reduced. With the second dissolution with new apatite, 20 % of CaO are added as apatite is mixed with anorthosite (21B, 22B and 23B). After 7 days dissolution with citric acid, about 31 % of CaO is dissolved (24B, 25B and 26B). This is an indication that citric acid is also dissolving the CaO component of pure plagioclase in CZ anorthosite.

After dissolving all the apatite added to CZ anorthosite (14A), the residual powder is expected to plot on 16A (Fig.1). But after 10 days dissolution, CaO contents plot lower than 16A, implying that some of the CaO originally present in 16A is being leached out

(e.g. on table 2, CaO content of 20B is less than that of 16A). 16A contains 1.73% Na_2O while 20B contains 1.12% Na_2O; this suggests that some Na_2O is also dissolving from the CZ anorthosite. The results illustrate that in trying to dissolve the P_2O_5 and CaO added to CZ anorthosite added as apatite, CaO in the anorthosite is also dissolved (Fig. 1B). On the contrary, UZ anorthosite is not attacked as the plagioclase compositions do not change after dissolution (Table 3, 10A, 11A, 12A, 17A and18A).

Trace and Rare Earth Elements:

With the CZ anorthosite, the 25 % Sr added as apatite is dissolved after 10 days. For the second dissolution with new apatite, all the Sr added as apatite is dissolved by day 7(Table 3, Fig. 2B. 24B, 25B and 26B). The Sr content of UZ anorthosite does not decrease even after 10 days dissolution (Table 3, 10A, 11A, 12A, 17A and18A) suggesting that dissolution with citric acid does not attack UZ anorthosite.

Calculations of La, Ce and Ba added and dissolved are presented in Table 4. All the La, Ce and Ba added to the CZ anorthosite as apatite are dissolved after 10 days. However, it appears some of the La, Ce and Ba initially present in the unleached CZ anorthosite dissolve as point 20B on Fig. 3B plots below 16A; which is the point where the unleached CZ anorthosite plots.

There is a very slight drop in La, Ce and Ba for the UZ anorthosite indicating that its trace and REEs are not leached out (Table 4 and Fig 3B; sample Nos 10A, 11A, 12A,17A and18A).

Conclusion:

Citric acid dissolves apatite but attacks also the CZ anorthosite. However, An contents from Tegner et al. (2006) reveal that samples used in this project on the UZ have An content between 40 and 50 by wt %. From the dissolutions done with UZ anorthosite, citric acid does not attack plagioclase with this UZ composition. Hence citric acid can be used to dissolve the apatite in the samples. This method was therefore used to dissolve apatite from the samples in the present study.

Table 4:Rare Earth Elements dissolved

SN		La(ppm)	% added	% dissolved	Ce(ppm)	% added	% dissolved	Ba(ppm)	% added	% dissolved
16A	Unleached CZ anorthosite	-1	0	0	0			54		
14A	CZ anorthosite + apatite	31	97	0	73	100		60	9	0
1A	CZ anorthosite+ apatite, 20 g 3hr diss	24	98	24	42	95	42	52	9	12
2A	CZ anorthosite+ apatite, 50 g 3hr diss	22	98	30	48	95	34	45	9	25
3A	CZ anorthosite+ apatite 100 g 3hr diss	15	98	52	60	95	18	51	9	15
4A	CZ anorthosite+ apatite 50 g 1 day diss	8	98	73	35	95	52	50	9	16
5A	CZ anorthosite+ apatite 20 g 1 day diss	18	98	41	48	95	34	48	9	20
6A	CZ anorthosite+apatite 100 g 1 day diss	16	98	47	54	95	26	52	9	14
7A	CZ anorthosite+ apatite 20 g 3 day diss	4	98	88	21	95	71	58	9	2
8A	CZ anorthosite+ apatite 50 g 3 day diss	8	98	75	28	95	62	48	9	19
9A	CZ anorthosite+ apatite 100 g 3 day diss	7	98	78	32	95	57	51	9	15
10A	UZ anorthosite 3hrs diss	8	0	69	96	0	22	257	0	0
11A	UZ anorthosite 1 day diss	6	0	77	109	0	12	266	0	0
12A	UZ anorthosite 3 days diss	3	0	89	83	0	33	243	0	5
15A	Unleached UZ anorthosite	26	0	0	124	0		254	0	0
17 B	repeat of 10, 11, 12	24	0	6	117	0	6	392		0
18B	17 further diss of 10, 11, 12	9	0	65	74	0	40	417		0
19B	repeat 7, 8, 9	23	98	27	57	95	22	42	9	29
20B	19 further diss of 7, 8, 9	4	98	86	9	95	88	46	9	12
21B	Unleached CZ anorthosite + new apatite	74	99	0	199	100		52	15	0
22B	Unleached CZ anorthosite + new apatite	78	100	0	194	99		64	15	0
23B	Unleached CZ anorthosite + new apatite	83	100	0	193	99		59	15	0
24B	CZ anorthosite + apatite 7 days diss	15	100	81	19	99	90	55	15	14
25B	CZ anorthosite + apatite 7 days diss	2	100	97	9	99	95	53	15	17
26B	CZ anorthosite + apatite 7 days diss	1	100	99	1	99	100	35	15	46
27B	CZ anorthosite 7 days diss	11			4			50		
28B	Pure apatite	600			1579			91		

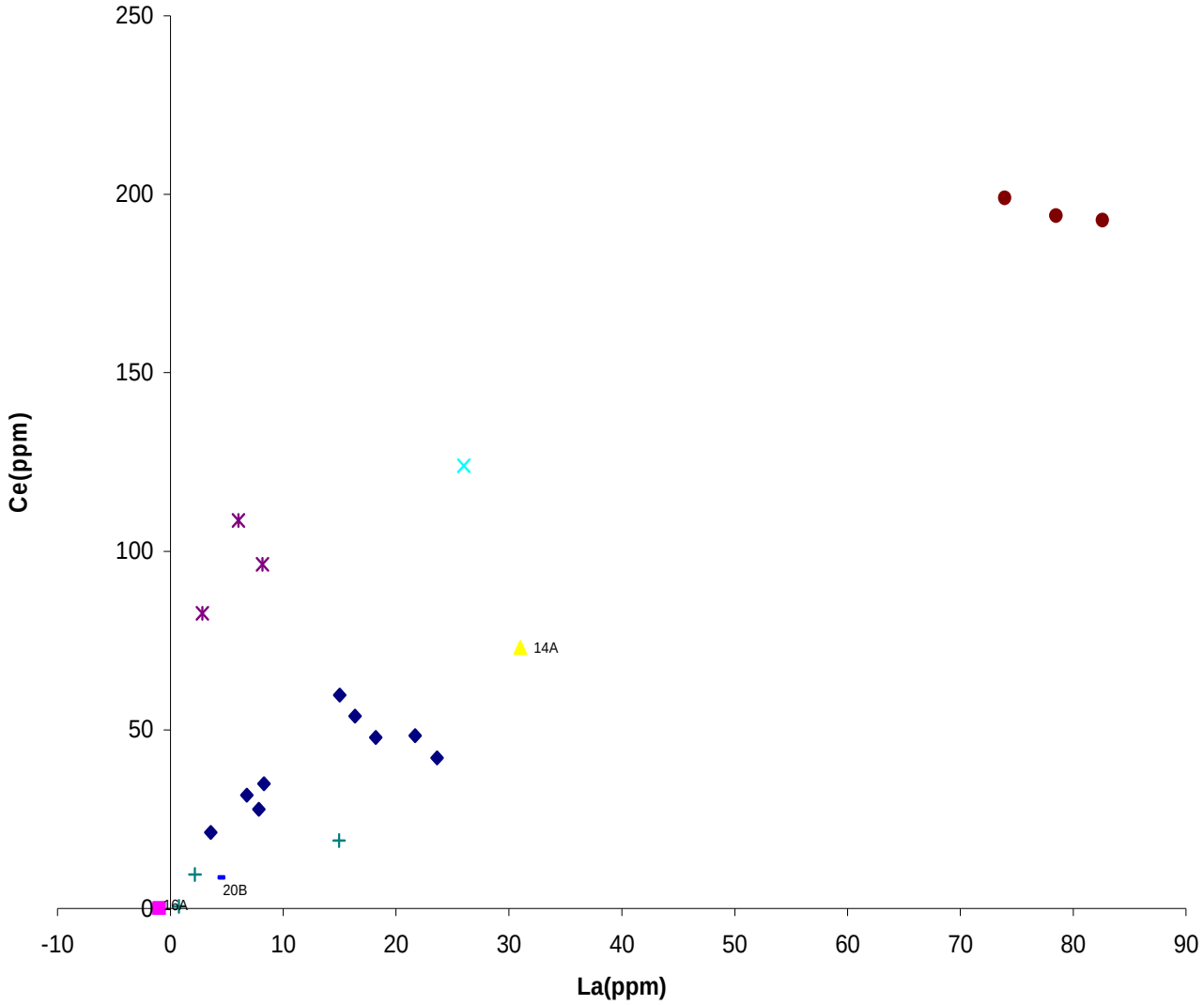


Fig. 3B :La change with Ce for Leaching experiments

Appendix C. Major and Trace Element Compositions

This section presents analytical data for major and trace element contents of plagioclase. Initially, plagioclase separates were analyzed on pellets at Wits University in order to obtain trace element contents of plagioclase and results of P, K, Sr, Ba, La and Ce were obtained. Analytical data indicated that a number of samples contained apatite (based on high P_2O_5, La and Ce contents) and or alkali feldspar (based on high K_2O). The presence of apatite was corrected by leaching samples in citric acid and calculating out the apatite fraction. The effect of alkali feldspar is too large to calculate out; hence all samples which contain significant alkali feldspar were excluded from subsequent modeling. In the ensuing tables, the samples which did not need to be corrected for and samples which were only corrected by calculating out the effect of apatite are presented as Sample Numbers + P and sample number +L represent samples which were leached in citric acid and reanalyzed. Analytical data for Sr and Ba were only corrected by the calculation method hence the XRF (pellet) data show Sr and Ba contents from analyses (uncorrected) and Sr and Ba contents for which the apatite proportion has been calculated out (corrected).

Major Element Data (XRF fusion , University of the Witwatersrand, 2009)

Height (m)	Sample #	SiO_2 (wt %)	Al_2O_3 (wt %)	Fe_2O_3 (wt %)	FeO (wt %)	MgO (wt %)	CaO (wt %)	Na_2O (wt %)	K_2O (wt %)	TiO_2 (wt %)	P_2O_5 (wt %)	TOTAL (wt %)	LOI (wt %)	An # (%)
1861.63	1W403.4P	73.27	15.77	0.08	0.67	0.04	3.87	4.96	0.46	0.03	0.06	99.25	0.78	30.14
1827.74	1W440.5P	60.18	23.15	0.10	0.79	0.11	7.18	6.12	1.40	0.05	0.59	99.69	0.51	39.35
1827.74	1W440.5L	61.95	23.59	0.03	0.25	0.08	6.52	6.23	1.38	0.04	0.02	100.09	0.52	36.66
1824.73	1W443.8L	63.27	23.45	0.02	0.13	0.07	6.53	6.25	1.22	0.03	0.03	101.00	0.81	36.62
1823.50	1W445.15P	56.80	25.88	0.10	0.77	0.10	8.59	6.46	0.61	0.08	0.35	99.76	0.21	42.37
1823.50	1W445.15L	57.90	25.99	0.03	0.29	0.07	8.28	6.53	0.61	0.08	0.01	99.80	0.75	41.22
1818.43	1W450.7L	62.83	23.32	0.02	0.18	0.06	6.79	6.00	1.11	0.03	0.01	100.34	1.35	38.49
1731.83	1W545.5P	57.88	24.98	0.09	0.71	0.11	8.56	5.90	0.97	0.05	0.54	99.79	0.29	44.51
1731.83	1W545.5L	59.52	25.27	0.03	0.21	0.07	7.99	5.87	0.98	0.04	0.02	100.00	0.79	42.94
1729.54	1W548L	61.32	24.80	0.02	0.14	0.07	7.88	5.62	0.99	0.03	0.01	100.89	0.81	43.67
1727.53	1W550.2L	58.90	25.58	0.02	0.13	0.07	8.19	5.88	0.98	0.04	0.01	99.81	1.15	43.51
1718.03	1W560.6L	58.88	26.32	0.02	0.16	0.07	8.57	5.90	0.84	0.04	0.01	100.81	0.76	44.54
1709.45	1W570L	59.13	25.91	0.05	0.39	0.12	8.44	5.96	0.87	0.06	0.02	100.95	0.79	43.92
1707.98	1W571.6L	58.71	25.87	0.03	0.25	0.09	8.13	5.96	0.73	0.04	0.01	99.83	0.70	43.00
1693.37	1W587.6L	56.73	26.97	0.03	0.24	0.09	9.51	5.92	0.49	0.05	0.02	100.04	0.72	47.04
1684.55	1W597.25L	57.23	26.65	0.04	0.34	0.10	9.43	5.83	0.53	0.08	0.02	100.26	1.81	47.21
1681.31	1W600.8L	56.80	27.23	0.02	0.16	0.07	9.63	5.56	0.42	0.04	0.02	99.96	1.53	48.92
1673.82	1W609L	57.21	26.77	0.02	0.18	0.08	9.46	5.80	0.42	0.08	0.31	100.32	1.50	47.42
1672.54	1W610.4L	56.12	26.69	0.05	0.38	0.10	9.98	5.58	0.43	0.08	0.60	100.00	0.99	49.72
1669.16	1W614.1L	56.96	27.05	0.02	0.17	0.06	9.21	5.93	0.35	0.06	0.03	99.84	0.98	46.20
1663.77	1W620L	60.57	21.39	0.04	0.33	0.08	10.26	7.33	0.12	0.08	0.02	100.23	2.89	43.63
1658.29	1W626L	56.34	27.63	0.03	0.27	0.09	9.99	5.47	0.44	0.05	0.02	100.33	0.59	50.25
1656.65	1W627.8L	56.45	27.43	0.03	0.20	0.10	10.11	5.42	0.38	0.05	0.02	100.20	1.12	50.77
1654.73	1W629.9P	49.20	24.78	0.07	0.55	0.15	14.99	5.29	0.32	0.06	4.53	99.94	0.25	61.04
1654.73	1W629.9L	56.73	27.55	0.02	0.19	0.08	10.01	5.57	0.34	0.05	0.04	100.58	0.59	49.84
1649.52	1W635.6L	54.76	25.30	0.02	0.16	0.08	12.81	4.99	0.25	0.06	2.59	101.00	1.97	58.67
1647.97	1W637.3L	56.32	26.78	0.02	0.19	0.08	10.41	5.33	0.31	0.10	0.52	100.08	0.00	51.93
1637.92	1W648.3P	52.06	25.12	0.09	0.70	0.12	12.90	5.43	0.51	0.05	3.19	100.18	1.01	56.78
1637.92	1W648.3L	57.27	26.88	0.02	0.15	0.08	9.22	5.79	0.52	0.05	0.02	100.00	0.56	46.82
1634.26	1W652.3L	57.70	26.56	0.03	0.21	0.10	8.86	5.83	0.79	0.04	0.02	100.12	0.56	45.66
1629.56	1W657.45P	56.09	26.20	0.07	0.56	0.12	10.00	5.77	0.70	0.05	0.88	100.45	0.34	48.94
1629.56	1W657.45L	58.31	26.79	0.02	0.17	0.08	9.02	5.68	0.68	0.04	0.01	100.80	2.31	46.76

Major Element Data (XRF fusion , University of the Witwatersrand, 2009)

Height (m)	Sample #	SiO_2 (wt %)	Al_2O_3 (wt %)	Fe_2O_3 (wt %)	FeO (wt %)	MgO (wt %)	CaO (wt %)	Na_2O (wt %)	K_2O (wt %)	TiO_2 (wt %)	P_2O_5 (wt %)	TOTAL (wt %)	LOI (wt %)	An # (%)
1620.74	1W667.1L	57.04	26.90	0.03	0.23	0.09	9.33	5.93	0.48	0.04	0.02	100.10	0.49	46.52
1215.06	1W1111.2P	48.00	24.38	0.10	0.78	0.17	14.04	4.52	2.45	0.05	5.21	99.71	2.85	63.20
1151.75	1W1180.5P	56.42	27.06	0.10	0.79	0.13	9.50	5.83	0.50	0.05	0.05	100.43	0.47	47.40
913.33	1W1441.5P	52.31	26.67	0.08	0.68	0.21	12.86	5.19	0.33	0.05	2.30	100.70	0.23	57.81
908.31	1W1447P	54.40	27.36	0.09	0.75	0.21	10.95	5.51	0.40	0.06	0.76	100.51	0.31	52.36
884.56	1W1473P	54.96	28.48	0.05	0.42	0.14	10.98	5.31	0.39	0.05	0.21	100.98	0.38	53.35
884.56	1W1473L	56.79	27.61	0.02	0.20	0.10	10.36	5.18	0.36	0.04	0.02	100.69	1.68	52.52
879.62	1W1478.4L	56.65	27.42	0.05	0.39	0.12	10.43	4.96	0.35	0.07	0.02	100.46	1.18	53.76
878.34	1W1479.8L	56.65	27.07	0.02	0.18	0.08	10.28	5.00	0.36	0.04	0.01	99.69	1.59	53.20
868.93	1w1490.1P	54.06	28.06	0.08	0.68	0.23	10.66	5.40	0.27	0.05	0.04	99.53	0.25	52.19
862.63	1W1497P	55.39	27.51	0.08	0.62	0.17	10.03	5.84	0.29	0.04	0.05	100.02	0.17	48.71
861.08	1W1498.7P	55.05	27.22	0.07	0.56	0.17	10.64	5.70	0.52	0.03	0.05	100.00	0.85	50.79
859.34	1W1500.6P	55.64	27.47	0.04	0.35	0.17	9.85	5.87	0.41	0.05	0.04	99.90	0.23	48.13
856.69	1W1503.5P	54.19	26.44	0.11	0.90	0.22	12.09	5.44	0.34	0.06	0.03	99.82	1.32	55.14
850.66	3W460.1P	55.47	27.16	0.16	1.33	0.15	9.63	5.65	0.47	0.18	0.03	100.26	0.48	48.52
850.39	1W1510.4P	56.24	27.77	0.05	0.40	0.09	10.01	5.83	0.45	0.05	0.06	100.95	0.15	48.70
850.39	1W1510.4L	56.26	27.29	0.02	0.18	0.08	9.70	5.66	0.43	0.05	0.02	99.69	3.96	48.66
848.38	1W1512.6L	55.46	27.05	0.03	0.23	0.10	9.80	6.05	0.45	0.04	0.03	99.25	0.52	47.25
846.19	1W1515P	56.06	27.85	0.06	0.48	0.08	9.98	5.76	0.42	0.04	0.10	100.82	0.20	48.93
846.19	1W1515L	56.11	27.10	0.02	0.18	0.08	9.69	5.76	0.41	0.03	0.02	99.39	3.70	48.19
823.35	3W490P	55.35	26.88	0.11	0.89	0.25	9.78	6.07	0.41	0.04	0.20	99.99	0.63	47.09
814.22	1W1550P	54.72	26.51	0.06	0.52	0.17	10.19	5.66	0.48	0.04	0.68	99.04	0.94	49.89
777.68	3W540P	53.91	26.83	0.31	2.50	0.52	9.58	5.41	0.41	0.32	0.03	99.85	0.60	49.47
732.00	3W590P	54.73	27.82	0.09	0.69	0.13	10.28	5.64	0.54	0.05	0.04	100.00	1.08	50.20
593.15	3W742P	53.94	28.29	0.07	0.57	0.15	10.88	5.12	0.35	0.05	0.03	99.45	0.33	54.02
558.44	3W780P	53.56	28.06	0.15	1.25	0.27	11.05	5.08	0.42	0.10	0.05	100.01	0.70	54.60
517.33	3W825P	53.54	27.89	0.21	1.72	0.41	10.51	4.92	0.37	0.11	0.02	99.70	0.73	54.15
448.82	3W900P	53.68	27.47	0.17	1.37	0.76	10.84	4.72	0.38	0.08	0.02	99.49	0.35	55.95
320.93	3W1040P	55.35	26.88	0.11	0.89	0.25	9.78	6.07	0.41	0.04	0.20	99.99	1.25	47.09
235.51	3W1133.5P	53.60	28.36	0.11	0.92	0.32	11.02	5.13	0.34	0.09	0.02	99.91	0.92	54.30
58.93	3W1326.8P	52.87	28.34	0.12	1.00	0.28	11.33	4.73	0.38	0.12	0.02	99.21	0.49	56.98
9.19	3W1381.25P	52.86	28.68	0.08	0.61	0.27	11.96	4.41	0.34	0.07	0.02	99.29	0.41	60.00

Major Element Data (XRF fusion, SGS Lakefields)

Height (m)	Sample #	SiO_2 (wt%)	Al_2O_3 (wt%)	CaO (wt%)	MgO (wt%)	Fe_2O_3 (wt%)	K_2O (wt%)	Na_2O (wt%)	TiO_2 (wt%)	P_2O_5 (wt%)	Total (wt%)	An # (%)
1827.74	1W 440.5L	60.8	23.5	6.48	0.07	0.42	1.35	6.06	0.04	<0.01	98.7	37.16
1824.73	1W 443.8L	61.8	23.2	6.46	<0.05	0.26	1.18	5.94	0.03	<0.01	98.9	37.55
1818.43	1W450.7L	60.6	22.7	6.65	<0.05	0.33	1.07	5.75	0.02	<0.01	97.2	39.01
1731.83	1W545.5L	57.9	25.1	8.22	0.07	0.4	0.94	5.74	0.05	<0.01	98.4	44.19
1727.53	1W550.2L	57.5	25.4	8.11	0.08	0.28	0.93	5.66	0.05	<0.01	97.9	44.21
1718.03	1W560.6L	57.8	26.2	8.6	<0.05	0.31	0.81	5.88	0.04	<0.01	99.7	44.71
1709.45	1W570L	57.5	25.7	8.3	0.08	0.51	0.84	5.8	0.07	<0.01	98.8	44.18
1693.37	1W587.6L	56	27.1	9.56	0.06	0.38	0.46	5.6	0.05	0.01	99.2	48.56
1684.55	1W597.25L	55.2	26.3	9.23	0.07	0.47	0.47	5.42	0.08	0.01	97.3	48.50
1669.16	1W 614.1	55.6	26.8	9.12	<0.05	0.31	0.34	5.88	0.06	0.02	98.2	46.17
1663.77	1W 620.0L	56.5	20.5	9.81	0.06	0.4	0.11	6.83	0.07	<0.01	94.3	44.27
1656.65	1W 627.8L	55.8	27.8	10.1	0.05	0.28	0.36	5.57	0.06	0.01	100	50.07
1654.73	1W 629.9L	54.8	27.3	9.87	<0.05	0.29	0.32	5.41	0.05	0.01	98.2	50.22
1637.92	1W 648.3L	54.9	26.2	9.02	<0.05	0.25	0.51	5.58	0.05	0.01	96.6	47.20
1634.26	1W 652.3L	57.1	26.6	8.88	0.06	0.32	0.77	5.77	0.04	<0.01	99.5	45.98
1629.56	1W 657.45L	56.2	26.3	8.87	<0.05	0.29	0.65	5.73	0.04	<0.01	98.1	46.12
884.56	1W 1473L	53.7	26.5	10	0.07	0.28	0.33	4.89	0.04	0.01	95.8	53.07
878.34	1W 1479.8L	54.3	26.6	10	<0.05	0.34	0.36	4.89	0.04	0.01	96.6	53.07
850.39	1W 1510.4L	54.5	26.8	9.62	0.06	0.24	0.42	5.52	0.04	<0.01	97.2	49.08
846.19	1W 1515L	54.2	26.6	9.59	<0.05	0.27	0.39	5.41	0.04	<0.01	96.6	49.50

XRF (pellet) data, University of the Witwatersrand, 2008

Height (m)	Sample #	P_2O_5 (%)	K_2O (%)	Sr (ppm)	Corrected Sr (ppm)	La (ppm)	Ce (ppm)	Ba (ppm)	Corrected Ba (ppm)
1861.63	1W 403.4P	0.00	0.33	329.9	329.9	9.3	28.6	481.0	481
1828.57	1W 439.6P	0.00	0.96	592.1	592.1	12.3	70.2	1269.5	1269
1827.74	1W 440.5P	0.00	1.03	576.5	576.5	7.0	68.9	1255.3	1255
1825.46	1W 443P	0.00	1.11	588.4	588.4	10.8	73.4	1342.3	1342
1824.73	1W 443.8P	0.00	0.87	584.5	584.5	13.0	61.3	1121.9	1122
1823.82	1W 444.8P	0.00	0.60	592.6	594.2	30.9	60.8	697.7	704
1823.50	1W 445.15P	0.00	0.47	756.9	756.9	10.3	44.8	755.2	755
1823.08	1W 445.6P	0.00	0.73	677.4	677.4	7.9	56.3	890.1	890
1821.26	1W 447.6P	0.00	0.75	612.1	612.1	7.6	37.7	658.6	659
1818.43	1W 450.7P	0.00	0.82	635.4	635.4	7.1	52.0	948.5	949
1816.87	1W 452.4P	0.00	0.65	615.5	615.5	9.1	47.4	879.4	879
1796.14	1W 475.1P	0.00	0.81	625.9	625.9	6.9	48.7	949.0	949
1769.10	1W 504.7P	0.00	0.82	495.3	495.3	6.8	38.3	898.0	898
1742.19	1W534.15P	0.00	0.73	600.7	600.7	9.1	52.9	901.8	902
1731.83	1W545.5P	0.00	0.71	609.5	609.5	11.5	50.4	841.5	841
1730.46	1W547P	0.00	0.72	607.7	607.7	5.0	46.3	791.9	792
1729.54	1W548P	0.00	0.71	595.6	596.0	8.4	48.5	869.0	869
1728.63	1W 549P	0.00	0.75	573.4	573.4	8.0	45.5	879.2	879
1727.53	1W550.2P	0.00	0.72	614.5	614.5	9.9	45.8	831.9	832
1718.03	1W560.6P	0.00	0.52	626.0	626.0	7.5	41.5	611.8	612
1709.45	1W570P	0.00	0.61	611.7	611.7	10.1	42.9	679.5	680
1707.98	1W571.6P	0.17	0.53	627.5	628.4	16.5	41.0	497.8	500
1704.42	1W575.5P	1.99	1.13	725.1	740.2	30.0	108.6	1455.9	1524
1693.37	1W587.6P	1.00	0.35	593.6	598.1	21.2	49.8	524.5	537
1688.44	1W593.0P	4.17	0.45	565.2	582.1	43.0	73.6	545.2	601
1684.55	1W597.25P	0.92	0.37	597.6	601.8	18.5	46.8	458.0	468
1681.31	1W 600.8P	4.69	0.30	580.5	601.6	47.0	69.7	375.6	420
1680.12	1W 602.1P	5.74	0.27	556.8	579.7	48.0	84.0	403.1	462
1676.74	1W 605.8P	9.95	0.45	557.4	602.1	84.9	117.0	353.5	453
1673.82	1W 609P	14.89	0.24	512.6	568.3	84.8	113.2	256.4	383
1672.54	1W 610.4P	10.19	0.28	524.9	561.5	48.2	82.9	291.6	378
1669.16	1W 614.1P	4.59	0.26	498.9	510.2	37.6	59.3	339.1	378
1663.77	1W 620.0P	4.10	0.11	174.7	152.0	46.0	103.2	932.2	1026
1658.29	1W 626.0P	2.13	0.31	591.3	600.9	27.0	47.1	356.7	375
1656.65	1W 627.8P	2.86	0.27	583.5	596.0	27.8	51.1	381.6	408
1654.73	1W 629.9P	3.31	0.24	576.7	590.8	31.8	60.7	400.0	432
1649.52	1W 635.6P	16.26	0.16	495.6	549.7	93.0	119.3	204.8	321
1648.97	1W 636.2P	3.84	0.35	579.6	596.4	25.2	58.5	379.6	416
1647.97	1W 637.3P	14.12	0.19	505.9	554.3	79.7	100.1	225.3	328
1645.87	1W 639.6P	1.19	0.53	559.2	563.6	18.1	44.1	435.6	448
1645.41	1W 640.1P	0.00	0.38	579.7	579.7	8.4	28.0	430.3	430
1644.68	1W 640.9P	0.00	0.28	474.5	474.5	0.3	16.1	278.3	278
1643.67	1W 642P	0.46	0.31	561.0	562.7	13.6	35.6	350.7	355
1642.49	1W 643.3P	0.50	0.48	549.1	550.8	9.5	41.1	537.3	543
1639.29	1W 646.8P	1.84	1.00	526.9	532.3	27.4	62.3	624.1	651
1637.92	1W 648.3P	2.03	0.38	536.1	542.5	20.7	52.4	504.8	529

XRF (pellet) data, University of the Witwatersrand, 2008

Height (m)	Sample #	P_2O_5 (%)	K_2O (%)	Sr (ppm)	corrected Sr (ppm)	La (ppm)	Ce (ppm)	Ba (ppm)	corrected Ba (ppm)
1637.28	1W 649.0P A	1.10	0.83	536.5	540.0	25.2	60.5	601.6	617
1637.28	1W 649.0P B	1.52	0.84	539.9	544.9	25.4	59.3	606.7	628
1637.28	1W 649.0P C	1.14	0.84	536.0	539.6	32.6	56.9	615.8	632
1636.46	1W 649.9P	0.87	1.11	539.8	542.6	24.3	53.1	679.1	693
1634.26	1W 652.3P	0.00	0.57	550.6	550.6	9.4	34.6	560.6	561
1630.61	1W 656.3P	0.00	0.37	582.2	582.2	12.7	27.8	392.8	393
1629.56	1W 657.45P	0.00	0.50	584.6	584.6	11.9	36.0	519.4	519
1627.23	1W 660P	0.00	0.49	591.7	591.7	4.3	28.1	485.0	485
1620.74	1W 667.1P	0.00	0.36	614.1	614.1	6.1	25.5	411.2	411
1578.18	1W 713.7P	0.00	0.37	533.3	533.3	3.5	18.8	384.9	385
1574.25	1W 718 P	0.00		486.5	486.5	1.5	17.9		
1544.01	1W 751.1P	0.00		573.9	573.9	0.3	24.1		
1540.63	1W 754.8P	0.00	0.36	543.0	543.0	2.3	20.8	477.5	478
1518.71	1W 778.8P	0.00	0.57	593.9	593.9	4.7	22.4	440.5	441
1500.98	1W 798.2P	0.00	0.33	583.6	583.6	8.3	21.4	351.2	351
1487.56	1W 812.9P	0.00	0.52	549.5	549.5	5.6	29.3	608.5	609
1454.85	1W 848.7P	0.00	0.33	591.0	591.0	-3.5	20.2	359.8	360
1402.69	1W 905.8P	0.00	0.55	570.9	570.9	2.1	25.6	413.5	414
1358.66	1W 954P	0.00	0.41	568.5	568.5	-0.6	18.6	362.3	362
1312.99	1W 1004P	0.00	0.39	541.5	541.5	4.8	17.8	320.9	321
1225.15	1W 1100.15 P	22.38	0.22	503.7	606.4	90.7	110.7	178.3	354
1179.16	1W 1150.5P	0.00	0.33	554.9	554.90	0.9	17.0	326.7	327
1151.75	1W 1180.5P	0.00	0.37	529.2	529.2	1.0	16.3	294.1	294
1124.81	1W 1210P	0.00	0.46	491.0	491.0	3.8	16.6	342.6	343
1081.05	3W 207.9P	0.00	0.28	456.4	456.4	4.4	16.7	278.6	279
1073.01	1W 1266.7P	0.00	0.38	435.5	435.5	2.0	14.5	280.7	281
1042.59	3W 250P	0.00	0.30	601.4	601.4	5.2	16.5	320.7	321
1039.67	1W 1303.2P	0.00	0.33	595.9	595.9	-2.9	17.7	336.7	337
996.92	3W 300 P	0.00	0.35	558.0	558.0	-0.2	22.9	387.5	387
996.55	1W 1350.4 P	0.00	0.31	513.2	513.2	1.3	19.2	327.0	327
960.28	3W 340.1 P	0.00	0.36	540.2	540.2	0.0	23.5	325.8	326
951.24	3W 350P	0.00	1.54	425.6	425.6	7.1	36.9	830.1	830
928.40	3W 375P	1.11	0.25	502.7	505.4	14.3	31.4	327.2	335
914.70	3W 390 P	0.00	0.32	499.4	499.4	3.0	16.2	325.8	326
913.33	1W 1441.5P	0.00	0.23	571.3	574.6	12.3	28.7	242.3	247
908.31	1W 1447P	0.00	0.29	571.8	571.8	8.0	22.7	323.5	323
885.24	1W 1472.25P	0.00	0.27	490.4	490.4	3.9	14.6	281.4	281
884.56	1W 1473P	0.00	0.29	568.4	568.4	4.3	19.8	287.9	288
879.62	1W 1478.4P	0.00	0.29	542.5	542.5	0.3	17.7	310.7	311
878.34	1W 1479.8P	0.00	0.30	546.0	546.0	4.1	19.5	300.7	301
872.31	1W 1486.4P	0.00	0.56	519.2	519.2	5.3	18.6	348.6	349
869.53	1W 1489.45P	0.00	0.43	561.2	561.0	6.9	19.6	263.9	279
868.93	1W 1490.1P	0.00	0.21	543.5	543.5	2.5	15.7	278.8	268
862.63	1W 1497P	0.00	0.22	565.3	565.3	3.4	14.4	267.9	264
861.08	1W 1498.7P	0.00	0.39	579.3	579.3	2.9	18.6	317.7	318
859.34	1W 1500.6 P	0.00	0.30	533.4	533.4	3.0	18.1	300.9	301

XRF (pellet) data, University of the Witwatersrand, 2008

Height (m)	Sample #	P_2O_5 (%)	K_2O (%)	Sr (ppm)	corrected Sr (ppm)	La (ppm)	Ce (ppm)	Ba (ppm)	corrected Ba (ppm)
856.69	1W 1503.5P	0.00	0.25	472.1	472.1	1.4	11.9	183.6	184
850.39	1W 1510.4P	0.00	0.33	543.7	543.7	1.6	17.9	293.0	293
848.38	1W 1512.6P	0.00	0.31	557.0	557.0	-0.2	18.2	313.5	313
846.19	1W 1515P	0.00	0.31	551.6	551.6	5.8	16.8	297.2	297
823.35	3W 490P	0.00	0.29	401.3	401.3	-1.9	13.6	276.2	276
814.22	1W 1550P	0.00	0.37	457.9	457.9	0.9	12.6	239.2	239
777.68	3W 540P	0.00	0.32	485.8	485.8	-1.8	15.4	259.5	259
732.00	3W 590P	0.00	0.39	560.0	560.0	2.0	18.4	302.1	302
724.88	1W 1647.8P	0.00	0.25	492.8	492.8	8.6	13.1	228.1	228
667.69	3W 660.4P	0.00	0.25	439.5	439.5	1.0	12.5	300.0	300
593.15	3W 742 P	0.00	0.25	497.1	497.1	-1.7	15.8	273.2	273
558.44	3W 780 P	0.00	0.31	471.6	471.6	2.3	14.5	234.6	235
517.33	3W 825P	0.00	0.28	468.8	468.8	2.5	14.5	237.8	238
485.36	3W 860P	0.00	0.33	480.8	480.8	-0.8	17.3	253.9	254
448.82	3W 900P	0.00	0.30	433.5	433.5	2.7	16.4	263.2	263
420.04	3W 931.5P	0.00	0.25	338.5	338.5	2.9	14.2	159.4	159
320.93	3W 1040P	0.00	0.27	454.1	454.1	0.8	12.7	204.1	204
275.25	3W 1090P	0.00	0.29	452.7	452.7	-1.5	13.9	228.5	229
235.51	3W 1133.5P	0.00	0.26	463.2	463.2	6.5	12.7	239.5	239
108.17	3W 1272.9P	0.00	0.26	385.4	385.4	2.4	14.6	185.9	186
58.93	3W 1326.8P	0.00	0.30	400.3	400.3	3.0	12.2	227.6	228
9.19	3W 1381.25 P	0.00	0.28	413.1	413.1	1.6	13.9	205.0	205

Trace Element data (ICP, University of Cape Town 2009)

Height (m)	sample #	Rb (ppm)	Sr (ppm)	Ba (ppm)	Pb (ppm)	Th (ppm)	U (ppm)
1824.7	1W443.8P	36.3	602.2	731.5	11.8	1.6	0.6
1824.7	1W443.8L	33.3	592.1	705.0	10.7	0.1	0.2
1818.4	1W450.7P	32.5	666.0	628.4	9.2	1.2	0.7
1818.4	1W450.7L	29.9	636.3	576.6	6.8	0.3	0.4
1729.5	1W548P	24.8	624.8	598.6	10.1	1.0	0.4
1729.5	1W548L	22.9	589.1	563.5	8.7	0.2	0.2
1727.5	1W550.2P	23.3	648.9	576.9	9.1	1.3	0.4
1727.5	1W550.2L	22.5	636.0	568.4	8.5	0.1	0.1
1718.0	1W560.6P	16.3	658.5	493.1	8.6	0.8	0.3
1718.0	1W560.6L	13.7	592.5	436.0	6.8	0.1	0.1
1709.4	1W570P	17.0	640.8	475.2	8.7	1.2	0.4
1709.4	1W570L	15.1	614.7	450.5	7.2	0.1	0.1
1708.0	1W571.6P	14.9	659.1	338.8	8.7	1.5	0.6
1708.0	1W571.6L	13.9	635.3	315.7	6.6	0.1	0.1
1684.6	1W597.25P	3.8	629.8	332.2	7.4	2.0	0.5
1684.6	1W597.25L	2.4	564.8	297.2	5.4	0.0	0.0
1650.1	1W635.6P	1.3	543.2	209.2	10.5	7.8	2.6
1650.1	1W635.6L	1.0	582.7	290.9	9.7	0.0	0.0
1648.2	1W637.3P	1.8	551.5	216.4	10.5	7.0	2.4
1648.2	1W637.3L	1.8	547.6	268.7	9.3	0.1	0.0
1629.6	1W657.45P	12.8	610.6	358.0	6.8	1.4	0.5
1629.6	1W657.45L	10.8	550.7	322.9	5.6	0.1	0.1
1620.7	1W667.1P	3.8	639.5	290.7	5.5	0.5	0.2
1620.7	1W667.1L	3.1	632.6	278.0	4.5	0.1	0.1
1225.2	1W1100.15P	1.8	557.4	164.7	4.2	4.7	2.5
1225.2	1W1100.15L	2.4	625.6	249.4	3.2	0.0	0.0
928.4	3W375P	2.6	643.9	259.0	3.4	0.8	0.3
928.4	3W375L	1.5	517.5	215.7	2.4	0.0	0.0
913.3	1W1441.5P	0.4	616.1	202.7	3.0	0.6	0.2
913.3	1W1441.5L	0.2	453.8	148.0	1.6	0.0	0.0
908.3	1W1447P	0.8	592.3	231.1	3.5	0.4	0.1
908.3	1W1447L	0.8	559.7	225.2	3.2	0.0	0.0
884.6	1W1473P	2.6	596.9	201.9	4.3	0.5	0.1
884.6	1W1473L	1.8	495.0	163.8	2.9	0.0	0.0
879.6	1W1478.4P	1.6	573.7	216.1	3.3	0.3	0.1
879.6	1W1478.4L	0.6	459.6	168.7	2.5	0.1	0.0
878.3	1W1479.8P	1.5	573.9	214.3	3.2	0.3	0.1
878.3	1W1479.8L	0.9	504.6	183.1	2.6	0.1	0.0
869.0	1W1490.1P	1.5	584.7	196.7	4.9	0.2	0.0
869.0	1W1490.1L	0.9	430.8	147.3	3.5	0.1	0.0
862.6	1W1497P	0.7	572.1	189.7	2.1	0.1	0.0
862.6	1W1497L	0.4	562.1	189.0	2.0	0.1	0.0
861.1	1W1498.7P	4.4	607.6	238.2	6.4	0.1	0.0
861.1	1W1498.7L	4.0	570.2	221.5	2.7	0.0	0.0
856.7	1W1503.4P	2.2	494.8	149.7	1.6	0.1	0.0
856.7	1W1503.4L	1.5	470.6	151.3	1.3	0.0	0.0

Trace Element data (ICP, University of Cape Town 2009)

Height (m)	sample #	Rb (ppm)	Sr (ppm)	Ba (ppm)	Pb (ppm)	Th (ppm)	U (ppm)
850.4	1W1510.4P	1.0	576.0	208.7	2.9	0.3	0.1
850.4	1W1510.4L	0.6	563.4	200.2	2.6	0.1	0.0
848.4	1W1512.6P	0.7	584.8	220.7	2.4	0.1	0.0
848.4	1W1512.6L	0.5	566.9	209.6	2.1	0.0	0.0
846.2	1W1515P	1.3	584.5	208.8	3.1	0.3	0.1
846.2	1W1515L	0.7	538.7	183.9	2.6	0.1	0.0
814.2	1W1550P	1.8	517.9	169.1	1.4	0.1	0.0
814.2	1W1550L	1.3	441.7	150.8	0.9	0.0	0.0
320.9	3W1040P	1.0	520.8	164.3	2.6	0.1	0.0
320.9	3W1040L	0.5	438.0	137.3	2.2	0.0	0.0
235.5	3W1133.5P	0.8	517.8	168.3	7.2	0.1	0.0
235.5	3W1133.5L	0.4	402.5	129.1	5.7	0.0	0.0
58.9	3W1326.8P	2.9	471.4	172.7	5.3	0.3	0.1
58.9	3W1326.8L	1.6	430.2	157.4	4.7	0.1	0.0

Appendix D. Variables used in modeling the Upper Zone of the Bushveld Complex and resulting calculated compositions

This section presents the variables used in modeling the Upper Zone of the Bushveld Complex and calculated bulk Ds, Sr and Ba contents of liquid, cumulus and re-equilibrated plagioclase. Values for F (fraction of magma remaining) were calculated from the height of each sample with respect to the base of the Upper Zone. The column- F for each step represent the vertical distance between adjacent samples relative to the vertical interval to the top such that for each step so that F values become extremely close to unity. D_{Ba} in plagioclase is constant at 0.4 throughout crystallization and D_{Sr} in plagioclase changes from 1.5 to 2.1. The cumulus plagioclase mode is estimated as follows:

Cumulus mode = observed mode – (TL %/2). Due to the effect of alkali feldspar on the analyses of Ba, modeling for Ba was terminated at F= 0.1.

Variables and resulting compositions of modeling (Ba)

F	Height (m)	Sample #	F for each step	DBa	TL (%)	plag mode	cumulus mode	Bulk D	C_L	Ba in cumulus plagioclase	Ba in re-equilibrated plagioclase	Observed Ba
0.09	1688.4	1W593.0P	1.0	0.4	10	45	42	0.24	1867	747	955	601
0.10	1684.6	1W597.25P	1.0	0.4	10	45	42	0.24	1835	734	940	468
0.10	1681.3	1W 600.8P	1.0	0.4	10	45	42	0.24	1810	724	927	420
0.10	1680.1	1W 602.1P	1.0	0.4	10	45	42	0.24	1801	720	922	462
0.10	1676.7	1W 605.8P	1.0	0.4	10	46	43	0.24	1776	710	909	453
0.10	1673.8	1W 609P	1.0	0.4	10	46	43	0.24	1755	702	899	383
0.10	1672.5	1W 610.4P	1.0	0.4	10	46	43	0.24	1746	698	894	378
0.10	1669.2	1W 614.1P	1.0	0.4	10	47	44	0.24	1723	689	882	378
0.11	1663.8	1W 620.0P	1.0	0.4	10	47	44	0.24	1687	675	864	1026
0.11	1658.3	1W 626.0P	1.0	0.4	10	47	44	0.24	1652	661	846	375
0.11	1656.6	1W 627.8P	1.0	0.4	10	47	44	0.24	1642	657	841	408
0.11	1654.7	1W 629.9P	1.0	0.4	10	47	44	0.24	1631	652	835	432
0.11	1649.5	1W 635.6P	1.0	0.4	10	47	44	0.24	1600	640	820	321
0.11	1649.0	1W 636.2P	1.0	0.4	10	47	44	0.24	1597	639	818	416
0.12	1648.0	1W 637.3P	1.0	0.4	10	47	44	0.24	1591	636	815	328
0.12	1645.9	1W 639.6P	1.0	0.4	10	47	44	0.24	1579	632	809	448
0.12	1645.4	1W 640.1P	1.0	0.4	10	47	44	0.24	1577	631	808	430
0.12	1644.7	1W 640.9P	1.0	0.4	10	47	44	0.24	1573	629	806	278
0.12	1643.7	1W 642P	1.0	0.4	10	47	44	0.24	1567	627	803	355
0.12	1642.5	1W 643.3P	1.0	0.4	10	47	44	0.24	1561	624	800	543
0.12	1639.3	1W 646.8P	1.0	0.4	10	47	44	0.24	1544	618	791	651
0.12	1637.9	1W 648.3P	1.0	0.4	10	47	44	0.24	1537	615	788	529
0.12	1637.3	1W 649.0P A	1.0	0.4	10	47	44	0.24	1533	613	786	617
0.12	1637.3	1W 649.0P B	1.0	0.4	10	47	44	0.24	1533	613	786	628
0.12	1637.3	1W 649.0P C	1.0	0.4	10	47	44	0.24	1533	613	786	632
0.12	1636.5	1W 649.9P	1.0	0.4	10	47	44	0.24	1529	612	784	693
0.12	1634.3	1W 652.3P	1.0	0.4	10	47	44	0.24	1518	607	778	561
0.12	1630.6	1W 656.3P	1.0	0.4	10	47	44	0.24	1500	600	769	393
0.13	1629.6	1W 657.45P	1.0	0.4	10	47	44	0.24	1494	598	766	519
0.13	1627.2	1W 660P	1.0	0.4	10	47	44	0.24	1483	593	760	485

Variables and resulting compositions of modeling (Ba)

F	Height (m)	Sample #	F for each step	DBa	TL (%)	plag mode	cumulus mode	Bulk D	C_L	Ba in cumulus plagioclase	Ba in re-equilibrated plagioclase	Observed Ba
0.13	1620.7	1W 667.1P	0.9	0.4	10	47	44	0.24	1453	581	745	411
0.15	1578.2	1W 713.7P	1.0	0.4	10	47	44	0.24	1284	514	659	385
0.17	1540.6	1W 754.8P	0.9	0.4	10	48	44	0.24	1169	468	601	478
0.19	1518.7	1W 778.8P	1.0	0.4	10	48	45	0.25	1112	445	572	441
0.19	1501.0	1W 798.2P	1.0	0.4	10	48	45	0.25	1071	428	551	351
0.20	1487.6	1W 812.9P	0.9	0.4	10	48	45	0.25	1042	417	536	609
0.22	1454.9	1W 848.7P	0.9	0.4	10	48	45	0.25	978	391	504	360
0.25	1402.7	1W 905.8P	0.9	0.4	10	49	45	0.25	893	357	460	414
0.27	1358.7	1W 954P	0.9	0.4	10	49	46	0.25	834	334	430	362
0.30	1313.0	1W 1004P	0.9	0.4	10	49	46	0.26	782	313	404	321
0.34	1225.2	1W 1100.15 P	1.0	0.4	10	50	46	0.26	700	280	362	354
0.37	1179.2	1W 1150.5P	1.0	0.4	10	51	47	0.26	665	266	344	327
0.38	1151.8	1W 1180.5P	1.0	0.4	10	51	47	0.26	646	258	335	294
0.40	1124.8	1W 1210P	0.9	0.4	10	51	47	0.26	628	251	326	343
0.42	1081.0	3W 207.9P	1.0	0.4	10	51	47	0.27	602	241	312	279
0.43	1073.0	1W 1266.7P	1.0	0.4	10	51	47	0.27	598	239	310	281
0.44	1042.6	3W 250P	1.0	0.4	10	52	48	0.27	581	232	302	321
0.44	1039.7	1W 1303.2P	1.0	0.4	10	52	48	0.27	580	232	301	337
0.47	996.9	3W 300 P	1.0	0.4	10	52	48	0.27	559	223	290	387
0.47	996.6	1W 1350.4 P	1.0	0.4	10	52	48	0.27	558	223	290	327
0.48	969.1	1W 1380.4 1416.5P	1.0	0.4	10	52	48	0.27	546	218	284	331
0.49	960.3	3W 340.1 P	1.0	0.4	10	52	48	0.27	542	217	282	326
0.50	951.2	3W 350P	1.0	0.4	10	53	48	0.27	528	211	275	335
0.51	928.4	3W 375P	1.0	0.4	10	53	48	0.27	523	209	272	326
0.51	914.7	3W 390 P	1.0	0.4	10	53	48	0.27	522	209	272	247
0.51	913.3	1W 1441.5P	1.0	0.4	10	53	48	0.27	520	208	271	323
0.53	908.3	1W 1447P	1.0	0.4	10	53	49	0.28	511	205	266	281
0.53	885.2	1W 1472.25P	1.0	0.4	10	53	49	0.28	511	204	266	288
0.53	884.6	1W 1473P	1.0	0.4	10	53	49	0.28	509	204	265	311
0.53	879.6	1W 1478.4P	1.0	0.4	10	53	49	0.28	509	203	265	301

Variables and resulting compositions of modeling (Ba)

F	Height (m)	Sample #	F for each step	DBa	TL (%)	plag mode	cumulus mode	Bulk D	C_L	Ba in cumulus plagioclase	Ba in re-equilibrated plagioclase	Observed Ba
0.53	878.3	1W 1479.8P	1.0	0.4	10	53	49	0.28	506	203	264	349
0.54	869.5	1W 1489.45P	1.0	0.4	10	53	49	0.28	505	202	263	279
0.54	868.9	1W 1490.1P	1.0	0.4	10	53	49	0.28	503	201	262	268
0.54	862.6	1W 1497P	1.0	0.4	10	53	49	0.28	502	201	262	264
0.54	861.1	1W 1498.7P	1.0	0.4	10	53	49	0.28	502	201	262	318
0.54	859.3	1W 1500.6 P	1.0	0.4	10	53	49	0.28	502	201	261	301
0.54	856.7	1W 1503.5P	1.0	0.4	10	53	49	0.28	501	200	261	184
0.55	850.7	3W 460.1P	1.0	0.4	10	53	49	0.28	499	199	260	340
0.55	850.4	1W 1510.4P	1.0	0.4	10	53	49	0.28	499	199	260	293
0.55	848.4	1W 1512.6P	1.0	0.4	10	53	49	0.28	498	199	259	313
0.55	846.2	1W 1515P	1.0	0.4	10	53	49	0.28	497	199	259	297
0.56	823.4	3W 490P	1.0	0.4	10	53	49	0.28	489	196	255	276
0.57	814.2	1W 1550P	1.0	0.4	10	53	49	0.28	486	194	253	239
0.59	777.7	3W 540P	1.0	0.4	10	54	49	0.28	474	190	247	259
0.61	732.0	3W 590P	1.0	0.4	10	54	50	0.28	460	184	240	302
0.61	724.9	1W 1647.8P	1.0	0.4	10	54	50	0.28	458	183	239	228
0.64	667.7	3W 660.4P	0.9	0.4	10	55	50	0.29	442	177	231	300
0.68	593.1	3W 742 P	1.0	0.4	10	55	50	0.29	424	169	222	273
0.70	558.4	3W 780 P	1.0	0.4	10	56	51	0.29	416	166	217	235
0.73	517.3	3W 825P	1.0	0.4	10	56	51	0.29	407	163	213	238
0.74	485.4	3W 860P	1.0	0.4	10	56	51	0.29	400	160	209	254
0.76	448.8	3W 900P	1.0	0.4	10	56	51	0.30	392	157	206	263
0.78	420.0	3W 931.5P	0.9	0.4	10	57	51	0.30	387	155	203	159
0.83	320.9	3W 1040P	1.0	0.4	10	57	52	0.30	369	148	194	204
0.86	275.3	3W 1090P	1.0	0.4	10	58	53	0.30	362	145	190	229
0.88	235.5	3W 1133.5P	0.9	0.4	10	58	53	0.31	356	142	187	239
0.95	108.2	3W 1272.9P	1.0	0.4	10	59	54	0.31	338	135	178	186
0.97	58.9	3W 1326.8P	1.0	0.4	10	60	55	0.31	331	132	174	228
1.00	9.2	3W 1381.25 P	1.0	0.4	10	60	55	0.32	325	130	171	205

Variables and resulting compositions of modeling (Sr)

F	Height (m)	sample #	F for each step	$D_{Sr\ in}$ Plag	Plagioclase mode	TL (%)	cumulus mode	Apatite mode	$D_{Sr\ in}$ Apatite	Bulk D	C_L	Sr in cumulus plagioclase	Sr in re-equilibrated plagioclase	Observed Sr
0.00	1861.6	1W 403.4P	0.0	2.1	45	10	42	1	2	0.92	484	968	974	330
0.02	1828.6	1W 439.6P	1.0	2.1	45	10	42	1	2	0.92	337	671	676	592
0.02	1827.7	1W 440.5P	0.9	2.1	45	10	42	1	2	0.92	337	670	675	576
0.02	1825.5	1W 443P	1.0	2.1	45	10	42	1	2	0.92	335	667	671	588
0.02	1824.7	1W 443.8P	1.0	2.1	45	10	42	1	2	0.92	334	666	670	585
0.02	1823.8	1W 444.8P	1.0	2.1	45	10	42	1	2	0.92	334	664	669	594
0.02	1823.5	1W 445.15P	1.0	2.1	45	10	42	1	2	0.92	334	664	668	757
0.02	1823.1	1W 445.6P	1.0	2.1	45	10	42	1	2	0.92	333	663	668	677
0.02	1821.3	1W 447.6P	0.9	2.1	45	10	42	1	2	0.92	332	661	665	612
0.02	1818.4	1W 450.7P	1.0	2.1	45	10	42	1	2	0.92	330	657	662	635
0.02	1816.9	1W 452.4P	0.7	2.1	45	10	42	1	2	0.93	330	655	660	616
0.04	1796.1	1W 475.1P	0.7	2.1	46	10	42	1	2	0.93	320	635	639	626
0.05	1769.1	1W 504.7P	0.8	2.1	46	10	43	1	2	0.93	312	617	621	495
0.06	1742.2	1W534.15P	0.9	2.1	46	10	43	1	2	0.93	307	604	608	601
0.07	1731.8	1W545.5P	1.0	2.1	46	10	43	1	2	0.93	305	599	603	609
0.07	1730.5	1W547P	1.0	2.1	46	10	43	1	2	0.93	305	599	603	608
0.07	1729.5	1W548P	1.0	2.1	46	10	43	1	2	0.93	305	599	602	596
0.07	1728.6	1W 549P	1.0	2.1	46	10	43	1	2	0.93	305	598	602	573
0.07	1727.5	1W550.2P	0.9	2.1	46	10	43	1	2	0.94	304	598	602	615
0.08	1718.0	1W560.6P	0.9	2.1	46	10	43	1	2	0.94	303	594	598	626
0.08	1709.4	1W570P	1.0	2.1	46	10	43	1	2	0.94	302	591	595	612
0.08	1708.0	1W571.6P	1.0	2.1	46	10	43	2	2	0.94	302	591	595	628
0.09	1704.4	1W575.5P	0.9	2.0	46	10	43	2	2	0.94	301	590	594	740
0.09	1693.4	1W587.6P	1.0	2.0	46	10	43	2	2	0.94	300	586	590	598
0.09	1688.4	1W593.0P	1.0	2.0	46	10	43	2	2	0.94	299	585	589	582
0.10	1684.6	1W597.25P	1.0	2.0	46	10	43	2	2	0.94	299	584	588	602
0.10	1681.3	1W 600.8P	1.0	2.0	46	10	43	2	2	0.94	299	583	587	602
0.10	1680.1	1W 602.1P	1.0	2.0	46	10	43	2	2	0.94	299	583	587	580
0.10	1676.7	1W 605.8P	1.0	2.0	46	10	43	2	2	0.94	298	582	586	602
0.10	1673.8	1W 609P	1.0	2.0	47	10	43	2	2	0.94	298	581	585	568

Variables and resulting compositions of modeling (Sr)

F	Height (m)	sample #	F for each step	$D_{Sr\ in}$ Plag	Plagioclase mode	TL (%)	cumulus mode	Apatite mode	$D_{Sr\ in}$ Apatite	Bulk D	C_L	Sr in cumulus plagioclase	Sr in re-equilibrated plagioclase	Observed Sr
0.10	1672.5	1W 610.4P	1.0	2.0	47	10	43	2	2	0.94	298	581	584	562
0.10	1669.2	1W 614.1P	1.0	2.0	47	10	43	2	2	0.94	298	580	584	510
0.11	1663.8	1W 620.0P	1.0	2.0	47	10	43	2	2	0.94	297	578	582	152
0.11	1658.3	1W 626.0P	1.0	2.0	47	10	43	2	2	0.94	297	577	581	601
0.11	1656.6	1W 627.8P	1.0	2.0	47	10	43	2	2	0.94	296	577	580	596
0.11	1654.7	1W 629.9P	1.0	2.0	47	10	43	2	2	0.94	296	576	580	591
0.11	1649.5	1W 635.6P	1.0	2.0	47	10	43	2	2	0.94	296	575	579	550
0.11	1649.0	1W 636.2P	1.0	2.0	47	10	43	2	2	0.94	296	575	579	596
0.12	1648.0	1W 637.3P	1.0	2.0	47	10	43	2	2	0.94	296	575	578	554
0.12	1645.9	1W 639.6P	1.0	2.0	47	10	44	2	2	0.94	296	574	578	564
0.12	1645.4	1W 640.1P	1.0	2.0	47	10	44	2	2	0.94	296	574	578	580
0.12	1644.7	1W 640.9P	1.0	2.0	47	10	44	2	2	0.94	296	574	578	474
0.12	1643.7	1W 642P	1.0	2.0	47	10	44	2	2	0.94	295	574	577	563
0.12	1642.5	1W 643.3P	1.0	2.0	47	10	44	2	2	0.94	295	573	577	551
0.12	1639.3	1W 646.8P	1.0	2.0	47	10	44	2	2	0.94	295	573	576	532
0.12	1637.9	1W 648.3P	1.0	2.0	47	10	44	2	2	0.94	295	572	576	543
0.12	1637.3	1W 649.0P A	1.0	2.0	47	10	44	2	2	0.94	295	572	576	540
0.12	1637.3	1W 649.0P B	1.0	2.0	47	10	44	2	2	0.94	295	572	576	545
0.12	1637.3	1W 649.0P C	1.0	2.0	47	10	44	2	2	0.94	295	572	576	540
0.12	1636.5	1W 649.9P	1.0	2.0	47	10	44	2	2	0.94	295	572	576	543
0.12	1634.3	1W 652.3P	1.0	2.0	47	10	44	2	2	0.95	295	572	575	551
0.12	1630.6	1W 656.3P	1.0	2.0	47	10	44	2	2	0.95	295	571	574	582
0.13	1629.6	1W 657.45P	1.0	2.0	47	10	44	2	2	0.95	294	570	574	585
0.13	1627.2	1W 660P	1.0	2.0	47	10	44	2	2	0.95	294	570	574	592
0.13	1620.7	1W 667.1P	0.9	2.0	47	10	44	2	2	0.95	294	569	572	614
0.15	1578.2	1W 713.7P	1.0	2.0	47	10	44	2	2	0.95	291	560	564	533
0.16	1574.2	1W 718 P	0.9	2.0	47	10	44	2	2	0.95	291	560	563	487
0.17	1544.0	1W 751.1P	1.0	2.0	48	10	44	2	2	0.95	290	555	558	574
0.17	1540.6	1W 754.8P	0.9	2.0	48	10	44	2	2	0.95	290	554	558	543
0.19	1518.7	1W 778.8P	1.0	2.0	48	10	44	2	2	0.96	289	551	554	594
0.19	1501.0	1W 798.2P	1.0	2.0	48	10	45	2	2	0.96	288	548	552	584

Variables and resulting compositions of modeling (Sr)

F	Height (m)	sample #	F for each step	$D_{Sr\ in}$ Plag	Plagioclase mode	TL (%)	cumulus mode	Apatite mode	$D_{Sr\ in}$ Apatite	Bulk D	C_L	Sr in cumulus plagioclase	Sr in re-equilibrated plagioclase	Observed Sr
0.20	1487.6	1W 812.9P	0.9	2.0	48	10	45	2	2	0.96	288	546	550	549
0.22	1454.9	1W 848.7P	0.9	1.9	48	10	45	2	2	0.96	287	542	545	591
0.25	1402.7	1W 905.8P	0.9	1.9	49	10	45	2	2	0.97	285	535	539	571
0.27	1358.7	1W 954P	0.9	1.9	49	10	46	3	2	0.97	284	530	534	569
0.30	1313.0	1W 1004P	0.9	1.9	49	10	46	3	2	0.97	284	525	529	542
0.34	1225.2	1W 1100.15 P	1.0	1.9	50	10	46	3	2	0.98	283	517	520	606
0.35	1215.1	1W 1111.2P	0.9	1.9	50	10	47	3	2	0.99	282	516	519	
0.37	1179.2	1W 1150.5P	1.0	1.9	51	10	47	3	2	0.99	282	513	516	555
0.38	1151.8	1W 1180.5P	1.0	2.0	51	10	47	3	2	0.99	282	510	514	529
0.40	1124.8	1W 1210P	0.9	1.8	51	10	47	3	2	0.99	282	508	512	491
0.42	1081.0	3W 207.9P	1.0	1.8	51	10	47	3	2	1.00	282	505	508	456
0.43	1073.0	1W 1266.7P	1.0	1.8	51	10	48	4	2	1.00	282	504	507	436
0.44	1042.6	3W 250P	1.0	1.8	52	10	48	4	2	1.00	282	502	505	601
0.44	1039.7	1W 1303.2P	1.0	1.8	52	10	48	4	2	1.00	282	501	505	596
0.47	996.9	3W 300 P	1.0	1.8	52	10	48	4	2	1.00	282	498	502	558
0.47	996.6	1W 1486.4P	1.0	1.8	52	10	48	4	2	1.01	282	498	502	513
0.48	996.6	1W 1350.4 P	1.0	1.8	52	10	48	4	2	1.01	282	496	500	546
0.49	969.1	1W 1380.4	1.0	1.8	52	10	48	4	2	1.01	282	496	499	540
0.49	960.3	3W 340.1 P	1.0	1.8	52	10	48	4	2	1.01	282	495	498	426
0.50	951.2	3W 350P	1.0	1.8	53	10	49	4	2	1.01	282	493	497	505
0.51	928.4	3W 375P	1.0	1.8	53	10	49	4	2	1.01	282	492	496	499
0.51	914.7	3W 390 P	1.0	1.8	53	10	49	4	2	1.01	282	492	496	575
0.51	913.3	1W 1441.5P	1.0	1.8	53	10	49	4	2	1.01	282	492	495	572
0.53	908.3	1W 1447P	1.0	1.8	53	10	49	4	2	1.01	282	490	494	490
0.53	885.2	1W 1472.25P	1.0	1.8	53	10	49	4	2	1.01	282	490	494	568
0.53	884.6	1W 1473P	1.0	1.8	53	10	49	4	2	1.01	282	490	493	542
0.53	879.6	1W 1478.4P	1.0	1.8	53	10	49	4	2	1.02	282	490	493	546
0.53	878.3	1W 1479.8P	1.0	1.9	53	10	49	4	2	1.02	282	489	493	519
0.54	869.5	1W 1489.45P	1.0	1.9	53	10	49	4	2	1.02	282	489	493	543
0.54	868.9	1W 1490.1P	1.0	1.9	53	10	49	4	2	1.02	282	489	492	565

Variables and resulting compositions of modeling (Sr)

F	Height (m)	sample #	F for each step	$D_{Sr\ in}$ Plag	Plagioclase mode	TL (%)	cumulus mode	Apatite mode	$D_{Sr\ in}$ Apatite	Bulk D	C_L	Sr in cumulus plagioclase	Sr in re-equilibrated plagioclase	Observed Sr
0.54	862.6	1W 1497P	1.0	1.8	53	10	49	4	2	1.02	282	489	492	561
0.54	861.1	1W 1498.7P	1.0	1.8	53	10	49	4	2	1.02	282	489	492	579
0.54	859.3	1W 1500.6 P	1.0	1.8	53	10	49	4	2	1.02	282	489	492	533
0.54	856.7	1W 1503.5P	1.0	1.8	53	10	49	4	2	1.02	282	488	492	472
0.55	850.7	3W 460.1P	1.0	1.8	53	10	49	4	2	1.02	282	488	492	478
0.55	850.4	1W 1510.4P	1.0	1.8	53	10	49	4	2	1.02	282	488	492	544
0.55	848.4	1W 1512.6P	1.0	1.8	53	10	49	4	2	1.02	282	488	491	557
0.55	846.2	1W 1515P	1.0	1.8	53	10	49	4	2	1.02	282	488	491	552
0.56	823.4	3W 490P	1.0	1.8	53	10	49	4	2	1.02	282	486	490	401
0.57	814.2	1W 1550P	1.0	1.8	53	10	49	4	2	1.02	283	486	489	458
0.59	777.7	3W 540P	1.0	1.8	54	10	50	5	2	1.02	283	483	487	486
0.61	732.0	3W 590P	1.0	1.8	54	10	50	0	2	0.93	283	480	484	560
0.61	724.9	1W 1647.8P	1.0	1.7	54	10	50	0	2	0.93	283	479	483	493
0.64	667.7	3W 660.4P	0.9	1.7	55	10	50	0	2	0.93	282	473	477	440
0.68	593.1	3W 742 P	1.0	1.7	55	10	51	0	2	0.93	281	466	469	497
0.70	558.4	3W 780 P	1.0	1.7	56	10	51	0	2	0.93	280	462	466	472
0.73	517.3	3W 825P	1.0	1.7	56	10	51	0	2	0.93	280	458	462	469
0.74	485.4	3W 860P	1.0	1.7	56	10	52	0	2	0.93	279	455	459	481
0.76	448.8	3W 900P	1.0	1.7	56	10	52	0	2	0.93	279	451	455	434
0.78	420.0	3W 931.5P	0.9	1.6	57	10	52	0	2	0.93	278	449	453	338
0.83	320.9	3W 1040P	1.0	1.6	57	10	53	0	2	0.93	277	439	443	454
0.86	275.3	3W 1090P	1.0	1.6	58	10	53	0	2	0.93	276	435	439	453
0.88	235.5	3W 1133.5P	0.9	1.6	58	10	53	0	2	0.93	276	431	435	463
0.95	108.2	3W 1272.9P	1.0	1.6	59	10	54	0	2	0.93	274	420	424	385
0.97	58.9	3W 1326.8P	1.0	1.5	60	10	55	0	2	0.93	274	415	419	400
1	9.2	3W 1381.25 P	1.0	1.5	60	10	55	0	2	0.93	273	411	415	413